MEASUREMENT OF FIBER SUSPENSION FLOW AND FORMING JET VELOCITY PROFILE BY PULSED ULTRASONIC DOPPLER VELOCIMETRY

A THESIS SUBMITTED BY

HANJIANG XU

IN PARTIAL FULFILLMENT OF THE REQUIREMENTS

FOR THE DEGREE OF DOCTOR OF PHILOSOPHY

FROM THE INSTITUTE OF PAPER SCIENCE AND TECHNOLOGY

ATLANTA, GEORGIA

May 8, 2003

TABLE OF CONTENTS

LIST OF FIGURES

LIST OF TABLES

ABSTRACT

The flow of wood fiber suspensions plays an important role during the pulp and paper manufacture process. Considerable research has been carried out in the past 50 years to characterize the fiber suspension flow behavior and to monitor the fiber suspension flow during paper manufacture. However, the above research has been hampered by the lack of techniques to directly characterize fiber suspension flow fields because fibers and fiber flocs tend to interfere with instruments inserted into the flow.

The fundamental studies in this thesis concentrated on three parts: (1) examine the feasibility of measuring wood fiber suspension flow by Pulsed Ultrasonic Doppler Velocimetry (PUDV), (2) apply PUDV to characterize fiber suspension flow behavior in a rectangular channel, (3) apply PUDV to measure the forming jet velocity profile along the jet thickness direction (ZD). In the first part, it is demonstrated that PUDV is an accurate technique for the velocity profile measurement of fiber suspension flow. The measurement has high repeatability and sensitivity. Suitable parameters should be selected in order to obtain the optimum measuring results.

The research goal in the second part focuses on the characteristics and mechanisms of fiber suspension flow. Velocity profiles of fiber suspension flow in a rectangular channel are measured by PUDV under different flow rates and fiber concentrations. Five types of flow behaviors have been observed and the flow behavior differs at different fiber concentrations and Reynolds numbers. The velocity profiles at different fiber

concentrations and Reynolds numbers can be fit into the following mathematical model: $\frac{u}{U_{\max}} = 1-(1-A)(1-\frac{y}{b/2})^2 - A(1-\frac{y}{b/2})^N$. For the turbulent fiber suspension flow, the velocity profile can be described by $u^+ = \frac{1}{0.41}\ln(y^+) + 4.69 + \frac{\Pi}{0.41}\sin^2(\frac{y}{0.9b}\pi)$, where b is the height of the channel, Π is the wake constant, a function of fiber concentration nl^3 and Reynolds number Re ($\Pi = 0.98\exp(0.14nl^3 - 1.9*10^{-5}*\mathrm{Re})$).

The change of velocity profiles with fiber concentration and flow rate can be explained by the different momentum transfer mechanisms. Addition of fiber to the suspension will affect the momentum transfer in two different ways. It will reduce the turbulence and thus reduce the momentum transfer. On the other hand, the fibers will interlock with each other and increase the momentum transfer. The velocity profile shape change under different flow conditions is determined by a combination of the above two momentum transfer mechanisms. Experiment shows that the turbulence intensity decreases with increasing fiber concentration.

Drag reduction occurs in fiber suspension flow. In the mixed flow, the suspension friction factor increases with increasing fiber concentration; in the turbulent flow, the suspension friction factor decreases with increasing fiber concentration. At low flow rate and high fiber concentration, a coherent plug forms in the center of the channel. The size of the plug will increase with increasing fiber concentration and decreasing flow rate. There is a progressive increase in the shear stress disrupting the fiber plug as the plug radius decreases.

In the third part of the thesis, PUDV is applied to measure the forming jet velocity profile along jet thickness direction (ZD). By installing an ultrasonic transducer underneath the apron, forming jet ZD velocity profiles are obtained through two measurements with different inclination angles. The accuracy of the velocity profile measurement can be within two percent if the jet thickness is high enough.

1 INTRODUCTION

The flow behavior of fiber suspension has been widely studied in the past 50 years because of its important applications in the manufacture of many products such as pulp, paper, food, beverage and polymer materials. Among all of the experimental techniques, velocity profile measurement is one of the most practical methods to characterize fiber suspension flow behavior. However, because fibers tend to staple on the probe surface and fiber suspension is normally opaque, techniques developed for velocity measurements in single-phase system are generally unsuitable for use in fiber suspension. It has been found that there are significant discrepancies in the velocity profile data reported in the literature, partially because of the difficulty of measuring velocity profile of fiber suspension flow.

Some early experiments by Daily and Bugliarello (1958), using a special impact probe with a wide, flat-faced tip to prevent clogging of fibers, indicated that velocity profiles became sharper with an increase in flow rate. Also, for a specified fiber and velocity, the velocity profiles became blunter as the concentration increased. Using an annular purge impact tube, Mih and Parker (1967) measured the local mean velocities for the turbulent fiber suspension flow in the pipe and found that, at low turbulent flow rates, a central plug region will be presented and it shrinks as flow rate increases and perhaps finally vanishes. The turbulent portions of these profiles appear to obey logarithmic distribution law as that of Newtonian fluids. The apparent von Kármán constant is lower for these suspensions than for Newtonian fluids and varies with fiber concentration and type. In contradiction to results obtained by Mih and Parker (1967), Seely (1968) found that the von Kármán constant increased in a systematic manner throughout the damped turbulent regime and approached the Newtonian value at very high flow rate although both of them used the same measuring technique. Sanders and Meyer (1971) reported that the von Kármán constant is a function of both fiber concentration and flow rate. It decreases with increasing concentration and with decreasing flow rate. Using a similar purge impact tube, Lee and Duffy (1976) investigated the velocity profiles of fiber suspension over wide ranges of bulk velocity. It was found that the fully turbulent velocity profiles become steeper as stock concentration increases. The reduced local velocities for fiber suspension in regions of turbulent shear were greater than those for water under the same conditions. At low flow rates, the deviation of local reduced velocities from those for water increased as flow rate was increased. At higher flow rates, this trend was reversed and the deviation of local reduced velocities from those for water decreased as flow rate was increased.

In the last twenty years, the flow behavior of fiber suspension has been studied theoretically and experimentally. In the experimental studies, noninvasive techniques have been applied to the velocity profile and turbulence measurement. Li et al. (1994) applied NMR imaging technique to the velocity profile and turbulent velocity fluctuations measurement for suspension of cellulose pulp fibers in water. It should be noted that this technique could only be used to measure the velocity profile at low flow rates. Using Laser Doppler Anemometry (LDA), Steen (1989) measured mean velocities, fluctuating velocities, and turbulent spectra of pipe flow for glass fibers in a mixture of ethanol and benzyl alcohol. Higher turbulent energy was found at low concentrations and short fibers, compared to higher concentrations and/or long fibers. With the same index-matching technique, Andersson and Rasmuson (2000) studied the flow and transition of fiber suspensions to turbulence in a rotary shear tester and found that the fluctuation velocity approached those of single-phase flow with increasing rotational speed until they were nearly equal. However, even in the dilute wood fiber suspensions, it was found that the penetration depth of LDA measurements is severely limited because of the light-scattering properties of wood fibers (Kerkes and Garner 1982).

In the theoretical studies, the rheology of fiber suspension including the orientation distribution of fibers (Shaqfeh and Koch 1988; Rahnama et al. 1995), the bulk stress in a suspension of rigid rods (Batchelor 1970; Batchelor 1971; Hinch and Leal 1976; Shaqfeh and Fredrickson 1990), the effective viscosity of the fiber suspension (Batchelor, 1971; Hinch and Leal 1976; Shaqfeh and Fredrickson 1990; Yamamoto and Matsuoka 1994), and the particle concentration profile in the flow (Kallio and Reeks 1989; Kroger and Drossinos 2000; Dong et al. 2003) have been investigated. However, the above analyses of the rheology of suspensions of slender rods are limited to infinite dilution or semi-dilute concentrations. The former completely neglect interactions and, therefore, requires $nl^3 \ll 1$, where n is fiber number density and l is fiber half-length. The latter accounts for interactions among the fibers and assumes $nl^3 \gg 1$ and $\phi \ll 1$, where ϕ is the volume fraction of the fiber materials. Although some of the simple properties of fiber suspension (e.g., viscosity) can be predicted from theoretical analyses, it is very difficult to model the velocity profile of fiber suspension flow, especially in the concentrated fiber suspension when the forming of fiber network, the nonuniform distribution of fibers in the flow field, the change of effective viscosity, and the flexibility of fibers are considered. Therefore, it is necessary to measure the velocity profile of fiber suspension flow through experimental investigations.

As we just reviewed, because of the entanglement of fiber and subsequent floc formation in the wood fiber suspension floc, it is difficult to obtain the velocity profile of wood fiber suspension flow with existing traditional techniques. On the other hand, different authors obtained inconsistent results on how fibers affect the velocity profile of fiber suspension flow. To clarify the discrepancies in the velocity profile data reported in the literature, Pulsed Doppler Ultrasonic Velocimetry (PUDV) was proposed to measure the velocity profile of fiber suspension flow in a rectangular channel and to measure forming jet velocity profile in a pilot headbox. The objectives of this study include:

- *Evaluation of the feasibility of measuring wood fiber suspension flow by PUDV.*
- *Investigation of the fiber suspension flow behavior using PUDV.*
- *Application PUDV to the ZD velocity profile measurement for forming jet.*

A general literature review is presented in Chapter 2. It begins with the definition of different categories and the general rheological properties of fiber suspension flow. Three regimes of fiber suspension flow defined in the previous investigations, the velocity profile of fiber suspension flow measured by different researchers, and the turbulence and drag reduction of fiber suspension flow are introduced. Next, different methods are reported in the literature for the velocity profile measurement. The last section of the chapter presents a brief review of the fundamentals of ultrasound and Pulsed Ultrasonic Doppler Velocimetry. The applications of the PUDV to the velocity measurement for other fluids are introduced as well.

Chapter 3 introduces the flow loop, the apparatus used in the experiments and the experimental procedures. The major components of the experimental setup are illustrated in Section 3.1 and Section 3.2. Section 3.3 presents the transducer and procedures for pressure drop measurement in the channel flow. Section 3.4 introduces the Pulsed Ultrasonic Doppler Velocimetry and the procedures for velocity profile measurement.

The evaluation of PUDV for velocity profile measurement of fiber suspension flow is presented in Chapter 4. The ultrasound echo signals, the accuracy, the repeatability and the sensitivity of PUDV measurements are evaluated. In order to optimize the PUDV measurement, the effect of different measuring parameters on the measurement is studied. The characteristics of PUDV measurement, the relationship between the maximum measurable depth and the maximum measurable velocity are also discussed in this chapter.

Chapter 5 investigates the behavior and mechanisms of fiber suspension flow through the velocity profile and friction loss measurement under different fiber concentrations and flow rates. First, the velocity profiles and turbulent intensity data for fiber suspension flow at different flow rates and fiber concentrations are presented. Based on the velocity profile measurement results, five different types of flow behaviors and the characterization of fiber suspension flow at different fiber concentrations and Reynolds numbers are discussed. Next, a mathematical model is used to describe the velocity profiles at various flow conditions. An empirical equation is obtained to describe the velocity profile of turbulent fiber suspension flow. The effect of fiber flocculation on the momentum transfer of suspension flow is proposed to explain the shape changes of velocity profiles. In the final part of this chapter, the friction factor data of fiber suspension flow at different concentrations are presented. The changing of plug size with the flow rate and the disruptive shear stress acting on the surface of the plug are analyzed.

In Chapter 6, PUDV is applied to ZD velocity profile measurement for a forming jet issued from a pilot paper-machine headbox. A theoretical analysis is provided to obtain the local velocities and flow directions at the measuring point by performing two PUDV measurements with different inclination angles. An example is given to demonstrate how to obtain the jet velocity profile through two PUDV measurements at different inclination angles. Finally, the jet velocity profiles at different slice openings and flow rates are presented. The accuracy of the measurement is analyzed.

Chapter 7 summarizes the major findings of this study. The recommendations for future work are illustrated in Chapter 8.

It should be noted that although this project is focused on the characterizations of wood fiber suspension flow, the results and theories obtained from this study could also be applied to other types of fiber suspension flow.

2 REVIEW OF THE LITERATURE

The study of the flow properties of fiber suspension is interesting from both scientific and technological considerations. The practical significance of such studies is due to the fact that the flow characteristics of fiber suspension and the state of dispersion of the fibers in suspension play important roles in almost every facet of pulp and paper manufacture. In order to better understand the background of this research project, the literature related to wood fiber suspension flow and its measurement is presented in this chapter. The topics discussed in this chapter include the definition of different categories of fiber suspension, the general rheological properties of fiber suspensions, the characteristics of wood fiber suspension flow, the technique used for fiber suspension flow measurement, and the fundamentals of ultrasound and Pulsed Ultrasonic Doppler Velocimetry (PUDV).

2.1 Fundamental of Fiber Suspension Flow

2.1.1 Categories of fiber suspension flow

A fiber interacts with all other fibers within approximately one fiber length L of its center. Thus, the most important measure of fiber concentration is $n\mathrm{L}^3$, where n is the number of fibers per unit volume. In experimental studies, the full fiber length L is typically used, while the fiber half-length l = L/2 is used in theoretical derivations. Most rheological studies of suspensions of rod-like particles have divided the suspensions into three categories based on the value of nl^3 and the volume fraction of the fiber materials ϕ: dilute suspension, semi-dilute suspension and concentrated suspension (Batchelor 1970;

Koch and Shaqfeh 1990; Shaqfeh and Fredrickson 1990; Rahnama, Koch and Shaqfeh 1995, Shauly et al. 1996). Under different categories, the addition of asymmetric solids such as fibers or rod-shaped particles has a different effect on the viscosity and flow behavior of the suspending fluid.

In a dilute suspension, there are occasionally two-particle interactions and the dilute limit is $nl^3 << 1$. In this type of suspension, particles are sufficiently far apart from each other. The relative motion of the fluid near one particle is unaffected by the presence of the others. In a semi-dilute suspension, each fiber interacts with many surrounding particles at any given time. In this concentration regime $nl^3 >> 1$ and $\phi << 1$, where ϕ is the volume fraction of the fiber materials. There is no strict definition for concentrated suspension in the literature. However, it is generally believed that in this category of suspension ϕ is larger than 0.1.

The categories of low particle concentration, intermediate particle concentrations and concentrated particle concentration are also reported in the literature. The upper limit of low particle concentration is commonly defined by following criterion for the 'critical concentration' for free rotation of rod-shaped particles (Nawab and Mason 1958):

$$\phi \, \mathrm{r}^2 < 1.5 \tag{2. 1}$$

where ϕ is the volume concentration of the particle and r is the aspect ratio of the particle.

Since r = L/d (d is diameter of the fiber) and $n = \phi / (\frac{\pi}{4} Ld^2)$, where n is the number of the particle per unit volume, Equation 2.1 can be expressed as follows:

$$\frac{\pi}{6}(nL^3) < 1.5 \tag{2. 2}$$

Since the volume of a sphere swept out by a fiber is $\frac{\pi}{6}L^3$, Equation 2.2 then represents a suspension concentration at which there is less than one particle in the volume swept out by one fiber length. Accordingly, Equation 2.1 represents conditions at which particle collisions, particularly rotational collisions, are negligible. Blakeney (1966) showed that a sharp increase in suspension effective viscosity occurs at this limit, while at lower concentrations the suspension exhibits a Newtonian increase in viscosity.

In a study of the rheological properties of suspensions of rigid, rod-shaped glass particles in intermediate particle concentrations, Carter (1967) found the suspension viscosity to increase in a slightly non-Newtonian manner according to a function of ϕ (concentration) and r (aspect ratio). Moreover, he established an approximate upper limit for intermediate particle concentration in terms of ϕ and r:

$$\frac{\phi\ r}{3(\mathrm{Ln}(2r) - 1.80)} \approx 0.18 \tag{2.3}$$

and

$$\mathrm{Ln}(2r) >> 1.80 \tag{2.4}$$

Beyond this limit, the suspension viscosity increased considerably in an abrupt 'anomalous' fashion to a value corresponding to the category of large particle concentrations.

Table 2.1 summarized the concentration ranges for different categories of fiber suspensions.

Table 2.1 Fiber concentration ranges for different categories of fiber suspensions.

Dilute/low particle concentration	Semi-dilute/intermediate particle concentration	Concentrated/large particle concentration
$nl^3 << 1$	$nl^3 >> 1$ and $\phi << 1$	$\phi \geq 0.1$
$\frac{\pi}{6}(\mathrm{nL}^3) < 1.5$	$\frac{\phi\ \mathrm{r}}{3(\mathrm{Ln}(2\mathrm{r}) - 1.80)} \approx 0.18$ and $\mathrm{Ln}(2\mathrm{r}) >> 1.80$	$\frac{\phi\ \mathrm{r}}{3(\mathrm{Ln}(2\mathrm{r}) - 1.80)} > 0.18$

2.1.2 The rheological properties of fiber suspensions

The bulk properties of suspensions of elongated particles are of direct interest, since some natural particles, such as paper-pulp fibers, are of these forms. These types of suspensions in Newtonian liquids exhibit an interesting variety of rheological phenomena, including finite normal stresses in steady laminar shearing flows and a viscosity function which decreases with increasing shear rate. The rheological properties of suspensions in extensional flows are also of significance in a number of areas, including the spinning of multiphase synthetic textile fibers, the papermaking process, and possibly, turbulent drag-reduction processes.

A suspension of straight elongated rigid particles has the striking property that, when subjected to steady pure straining motion, all the particles take up the orientation in which they individually make their greatest contribution to the bulk stress (Batchelor 1970). If the suspension is dilute, each particle of length $2l$ makes a contribution to the bulk stress which is of roughly the same order of magnitude as that due to a rigid sphere of radius l. The fractional increase in the bulk stress due to the presence of the fiber is thus equal to the concentration by volume multiplied by a factor of order l^2/r^2, where r is the radius of particle. This suggests that the stress due to the particles might be relatively larger, although the volume fractions of particle are still small. However, the above theory is not applicable to the semi-dilute suspension. In the semi-dilute suspension, it is assumed that when the average lateral spacing of particles (h) satisfies the conditions $r << h << l$, the disturbance velocity vector is parallel to the particles and varies only in the cross-sectional plane. The expression for the contribution to the bulk stress due to the particles differs from that for a dilute suspension only in a minor way (by the replacement of $\log 2l/r$ with $\log h/r$ (Batchelor 1971)).

The bulk stress generated in fiber suspension has strong influence on the other properties of fiber suspensions. It was found that in a pure straining motion, elongated rigid particles in suspension are aligned parallel to the direction of the greatest principal rate of extension, provided the effect of Brownian motion is weak (Batchelor 1971). The orientation of any given fiber in the suspension is influenced by the fluid velocity disturbance caused by the surrounding fibers as well as the average flow, which can often be considered a linear shear flow on the fiber length. Rahnama et al. (1995) have visualized the orientation of an opaque tracer fiber in the midst of an index of refraction and density-matched fiber suspension in a four-roll mill and determined that the mean squares of the components of the fiber orientation in Newtonian fluids with $nL^3 = 5 – 17$ are qualitatively consistent with the dilute limit of the theory of Shaqfeh and Koch (1988). Measurement of orientation dispersion in polyacrylamide solutions indicated that the non-Newtonian stresses increase fiber alignment, as predicted by Harlen and Koch (1992). In a recent study, Rahnama, Koch and Shaqfeh (1995) investigated the hydrodynamic interactions in dilute and semi-dilute suspensions using slender-body theory. The effect of hydrodynamic interactions on the orientation of large aspect ratio fibers undergoing simple shear flow was analyzed. The theoretically predicted orientation distribution for the semi-dilute suspensions were in good agreement with the experimentally observed results of Stover et al. (1992), and the steady-state orbit distributions are quite similar in the dilute and semi-dilute regimes.

The addition of particles to the suspension will also affect the velocity profile and turbulence intensity of suspension flow. Nearly all experiments found that the stream-wise particle mean velocity profile is flatter than the corresponding fluid velocity profile, with particles leading the flow near the wall and lagging the flow in the core. This effect has been attributed to the transverse mixing of particles that, owing to their greater inertia, retain longer memories of their streamwise velocity than do fluid elements. Many of these experiments showed that particle velocity fluctuation intensities were higher than the turbulence intensity, while others found the opposite case. Particles have been found both to raise and to lower the pressure drop, and there are no reliable means of predicting either the direction or the magnitude of the change based on particle and flow properties. The model development of Sommerfeld (1992) has shown that very small changes in the modeling of particle-wall collision dynamics can affect profound changes in particle velocity statistics elsewhere in the flow, which may account for the variations between experiments using different particle and pipe materials. Gore and Crowe (1991) showed that whether given particles increase or decrease turbulence intensity depends on the ratio of particle diameter to a characteristic eddy diameter of the turbulence.

Kulick et al. (1994) studied the particle response and turbulence modification in fully developed channel flow. It was found that the streamwise mean particle velocity profiles were flatter than the mean fluid velocity profile, which was unmodified by particle loading. Particle velocity fluctuation intensities were larger than the unladen-fluid turbulence intensity in the streamwise direction but were smaller in the transverse direction. Fluid turbulence was attenuated by the addition of particles; the degree of attenuation increased with particle Stokes number, particle mass loading, and distance from the wall. Turbulence was more strongly attenuated in the transverse than in the streamwise direction because the turbulence energy is at higher frequencies in the transverse direction. To measure the local velocity accurately, Laser Doppler Anemometry (LDA) was used to measure velocity profile of fiber suspension flow using an index-matching technique. Steen (1989) used glass fibers in a mixture of ethanol and benzyl alcohol, which then had the same refractive index as the fibers. He measured mean velocities, fluctuating velocities, and turbulent spectra of 1.2 and 12 g/L glass fiber suspension flowing in a pipe. It was found that turbulent energy is higher at low concentrations and short fibers than at higher concentrations and/or long fibers. With the same index-matching technique, Andersson and Rasmuson (2000) studied the flow and transition of fiber suspensions to turbulence in a rotary shear tester. It was found that the flow of fiber suspension underwent two transitions: the first one coincided with complete agitation, a sharp increase in torque, and fluctuating velocities close to zero. The mean velocities were similar to those of single-phase flow above this transition. The fluctuation velocities approached those of single-phase flow with increasing rotational speed, until they were nearly equal. This second transition was interpreted as fully developed turbulent flow. The presence of the fibers also flattened the profiles, indicating an increased momentum transfer. McComb (1991) discusses turbulence modification in drag-reducing asbestos fiber suspension at fiber concentration of 0.03%, for which turbulence spectra have been measured by LDA. He concludes that there is an increase in turbulence intensity at low and high wave numbers, but that turbulence is suppressed by resonant absorption of turbulent energy by the fibers in a region comparable to the fiber length.

Another interesting phenomenon in the particle-laden suspension flow is the nonuniform concentration distributions. Hookham (1986) and Koh et al. (1994) used a modified laser-Doppler technique to measure the velocity and concentration profiles for the flow of concentrated suspensions in a rectangular channel. It was found that the flow of concentrated suspensions in a rectangular channel is characterized by a blunting of the particle velocity profile. The magnitude of this blunting increases with increase of either the bulk particle concentration of the suspension or the ratio of the particle size to the gap width of the channel. The local particle concentration is not uniform across the flow channel. In general, the particles tend to concentrate near the center of the flow channel. Using NMR techniques, Sinton and Chow (1991) and Abbott et al. (1991) measured the velocity profile of suspension flow. The former authors report velocity blunting, but no measurable non-uniformity of particle concentration. On the other hand, the measurement of Abbott et al. (1991) show a definite migration of particles toward the outer cylinder, namely, from the region of highest shear-rates toward the lowest shear-rates in the flow system.

2.2 Characteristics of Wood Fiber Suspension Flow

2.2.1 Regimes of fiber suspension flow

Investigations of the flow characteristics of fiber suspension were carried out by the M.I.T. Hydrodynamic Laboratory under TAPPI sponsorship in the late 1950s (Daily and Bugliarello 1958). The M.I.T. report contains a large amount of friction factor-Reynolds number correlation for both synthetic and wood fibers. The friction factor-Reynolds number correlation indicated the existence of two different turbulent flow regimes as previously reported by Robertson and Mason (1957) and Forgacs et al. (1958). The friction loss behavior found by these investigations, which is typical for a large number of fiber suspensions, is shown in Figure 2.1, illustrating three separate flow regimes: plug flow, mixed flow, and turbulent flow. The representations of these three basic flow

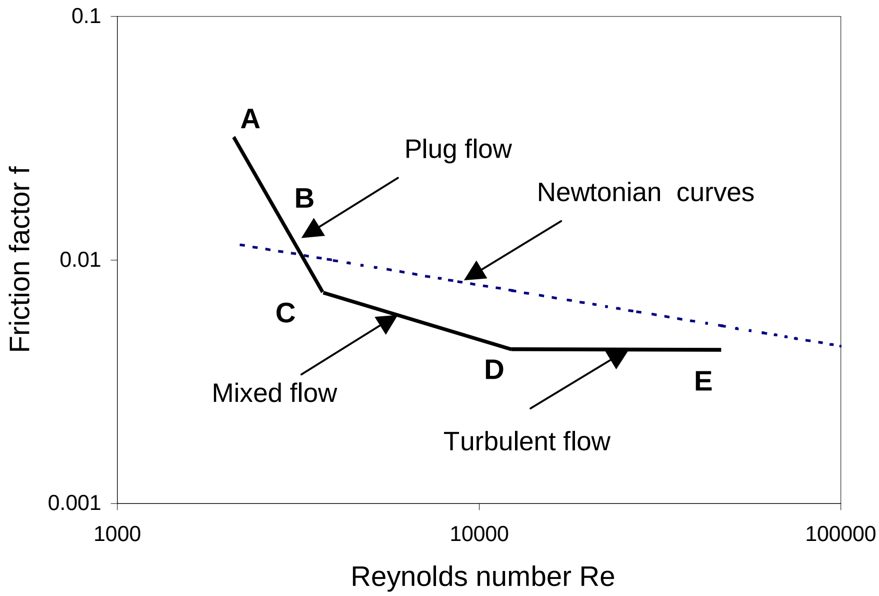

Figure 2.1 Schematic representation of friction loss curve with fiber suspension flow (Robertson and Mason 1957).

mechanisms of fiber suspensions are shown schematically in Figure 2.2. Here the fractional factor f is defined by:

$$f = \frac{D\Delta P}{2\rho U^2 x} \tag{2.5}$$

where

D = hydrodynamic diameter of channel, m

P = pressure, Psi

x = length in channel length direction, m

U = bulk flow velocity, m/s

ρ = fluid density, kg/m^3

Plug flow. At low flow rates (BC, Figure 2.1) a plug region exists in which the core is a coherent plug of fiber networks. There is no movement of fibers relative to one another within the networks, and the velocity gradient is confined to an essentially fiber-free water annulus near the wall. The thickness of the water annulus increases with flow rate and varies with fiber properties and concentrations. In this flow regime, pressure losses in pipe flow are greater than that for water flow at comparable rates. At very low velocities (AB), pressure losses become much higher than that of water flow at the same flow rates.

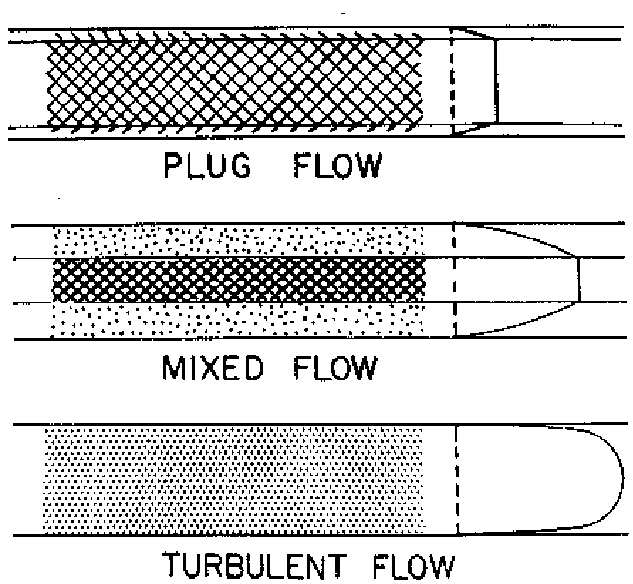

Figure 2.2 Schematic representations of the three basic flow mechanisms of pulp suspensions in pipes. Cross-hatching represents a plug; dots represent turbulent shear flow (Forgacs et al. 1958).

Mixed flow. At the first transition point (C), flow in the water annulus becomes unstable and an increasingly turbulent water layer forms around the plug. Further increases in flow rate produce turbulent stresses in excess of the yield stress of the fiber networks, which cause progressive disintegration of the plug until it apparently disappears at point D. The pressure loss in pipe flow becomes less than that of water flow in this flow regime.

Turbulent flow. At velocity above the second transition velocity D, the flow is turbulent across the entire cross section except for the boundary, and the friction factor is practically constant over a considerable range of velocities. Results for a range of pulp types showed that the higher the coherence of a fiber network the greater the suppression of the turbulence and hence the lower the pressure gradient. An inconsistency exists in the data of Robertson and Mason (1957) with respect to the location of the transition point C. Point C in their curve of friction factor versus velocity is shown to correspond to a lower pressure drop than for water at the same velocity. Point C in the plot of head loss versus velocity for the same suspension, however, corresponded to a greater pressure drop than for water.

In later investigations, Daily et al. (1961) obtained extensive friction-loss data, which confirmed that the value of friction loss at point C is greater than the corresponding friction loss for water. They also found that representation of the dependence of friction factor on flow rate by a series of straight lines was only approximate and suggested a better representation of the transition regime was a series of lines rather than a single line.

The above three broad classifications were introduced by Mason and Daily (1959) in their comprehensive fundamental studies of fiber suspension flow. Since their pioneering research works in fiber suspension flow, many investigations have continued in these areas. Because the fiber suspension flow in the headbox is a turbulent flow, it is our purpose in the next few sections to review the fiber suspension flow mechanism with an emphasis in the mixed and turbulent flow regimes.

2.2.2 The velocity profile of fiber suspension flow

Mih and Parker (1967) used an annular purge impact probe to measure velocity profiles for turbulent flow of aqueous suspensions of papermaking fibers (average length 2.7 mm, average fiber diameter 0.03 mm) in a 50- and 100-mm-diameter hydraulically smooth pipe at bulk velocities up to 9.17 m/s. At low flow rates and high concentrations, they found a region near the pipe axis where local velocity was independent of position. The region corresponded to a central plug of fibers. The size of the plug decreased with increasing bulk velocity and with decreasing fiber concentration. At high flow rates and low concentrations, no plug was detected, although an apparent flattening of profiles near the pipe axis was reported. Velocity profiles for regions of turbulent shear were linear when plotted on the reduced velocity (U^+) versus the logarithm of distance from the wall ($\ln y^+$) coordinates. U^+ is defined as:

$$U^+ = \frac{u}{U\tau} \tag{2.6}$$

where

$$U\tau = \sqrt{\tau_w / \rho} \tag{2.7}$$

U_τ is referred to as the frictional velocity, τ_w is the wall shear stress, and ρ is the fluid density.

The slope of the velocity profile in the coordinate of U^+ and $\ln y^+$ appeared to be independent of flow rate and was a function of fiber type and concentration. Moreover, they found that at high flow rates velocity profiles for a given suspension in both diameter pipes could be approximately represented by a single line on these coordinates. They associated this behavior with a regime of turbulent flow characterized by values of friction factor independent of flow rate (Lee and Duffy 1976b).

Seely (1968), who studied softwood sulfite pulp fibers, confirmed that velocity profiles in regions of turbulent shear were linear when plotting the reduced velocity U^+ versus the logarithm of dimensionless distance from the wall y^+ defined by:

$$y^+ = \frac{yU\tau}{\nu} \tag{2.8}$$

where ν is the kinematic viscosity of water at the same temperature as the suspension. Seely extrapolated the reduced velocity profiles and found that most profiles intersected the water curve somewhere near the coordinates $y^+ = 30$, $U^+ = 14$. The gradient of these profiles increased with bulk velocity (conflicting with the Mih and Parker (1967) results). Seely (1968) was unable to distinguish the velocity profiles he obtained for dilute fiber suspensions at high flow rates from those he obtained for water. This apparent Newtonian behavior at high flow rates was also observed in measurements of flow resistance, which has the same value as that of water flow.

Lee and Duffy (1976a; 1976c) also found that y^+ and U^+ intersected near the coordinates $y^+ = 30$, $U^+ = 14$. These coordinates correspond with the outer layer of the buffer zone in turbulent Newtonian fluids. They suggested that the addition of fibers to water did not modify the wall layer in flow through smooth pipes, and the cause of drag reduction was attributed to the turbulent core region. Drag reduction occurred as a result of fibers reducing momentum transfer in the turbulent core. In addition, there was no significant dependence of the values for U^+ at $y^+ = 30$ on fiber concentration, fiber aspect ratio, bulk velocity, or pipe diameter (Lee and Duffy 1975).

The expression for a linear, reduced-velocity profile that passes through the point $U^+ = 14$, $y^+ = 30$ is given by:

$$U^+ = \frac{1}{K}\ln y^+ + [14 - \frac{3.4}{K}] \tag{2.9}$$

where K is the apparent von Kármán constant. In the turbulent regime, the value of K was found to be constant for a particular suspension concentration.

Equation 2.8 can also be used to calculate the von Kármán constant K for a suspension from flow-resistance data (Lee and Duffy 1976b):

$$\frac{1}{\sqrt{f}} = \frac{1}{K}\ln(\mathrm{Re}\sqrt{f}) + \left[14 - \frac{5.6}{K}\right] \tag{2.10}$$

where Re is Reynolds number, f is defined by Equation 2.5.

Equation 2.9 can reduce to the Kármán-Prandtl law for water in a smooth pipe if K = 0.4. Lee and Duffy also showed that values of K characterizing a turbulent suspension can be predicted from data for the torque resistance measured with a rotational disk apparatus based on an analysis performed by Goldstein (1935).

Lee and Duffy (1976b) further postulated that variations of K could be explained in terms of the relationship between intensity of turbulence and the scale of fiber agglomeration in a suspension. In fully developed turbulent flow, two regimes could be recognized from the variations of K with bulk velocity. At low turbulence intensities, values of K for a particular suspension increase with increases in bulk velocity. The behavior corresponds to the regime in which friction factor is largely independent of flow rate. At high-turbulence intensities, there is a regime in which K is independent of flow rate. As concentration decreases in this regime, the lower bulk velocity limit decreases, and the limiting value of K increases to approach that for water. This corresponds to a regime in which the flow-resistance curves are approximately parallel to the water curve.

They suggested that a significant portion of the momentum transfer in turbulent fiber suspension is the result of radial movement of fiber flocs. Shear in turbulent fiber suspensions is restricted to a small volume of water between adjacent flocs. Consequently, the relative velocity between adjacent eddies in a fiber suspension is less than that for pure water. In addition, there is the probability of direct contact between flocs that further restricts relative motion. The three-dimensional fiber network that comprises a floc possesses properties similar to those normally encountered in solid materials. Fiber networks can transmit forces from one point to another within their structures and can enhance momentum transfer by providing a solid link between adjacent fluid layers. The larger the fiber floc, the greater is the distance over which it can transfer momentum. Thus, fiber flocs affect momentum transfer in two opposing ways: they tend to lower it by damping the turbulence of the suspending phase and also tend to enhance the momentum transfer by providing a solid link between adjacent fluid layers. The concept of two opposing mechanisms to control the momentum transfer was presented to explain the variation of K with bulk velocity and distance from the pipe axis.

After Duffy and coworkers proposed the above momentum transfer mechanism in the 1970s, the debate on the influence of fibers on the momentum transfer has continued. Gore and Crowe (1989) performed an analytical review of the literature to describe the conflicting conclusions dealing with various particle flows in gas streams. Gore discovered that a critical parameter appears to be the ratio of particle diameter to a turbulent length scale, d_p/l_c. The length scale associated with the fluid phase, l_c, was the integral length scale or the characteristic length of the most energetic eddy when only one phase is present. Hutchinson et al. (1971) demonstrated that the l_c/r ratio across a pipe in fully developed flow was approximately constant ($l_c/r \approx 0.2$) except near the pipe wall. A critical demarcation value of $d_p/l_c \approx 0.1$ caused the turbulent intensity of the carrier phase to either increase or decrease with the addition of particles. For a value greater than 0.1, the addition of particles caused an increase in the carrier-phase turbulence intensity.

2.2.3 Turbulent intensity of fiber suspension flow

Daily et al. (1959) performed the first turbulence measurements in pulp suspensions using an impact probe mounted in a pipe. They concluded that turbulence is strongly suppressed by the addition of fibers to water. Although this result has been verified, their measurements were not conclusive. A closer study of their reported turbulence spectrum by Norman et al. (1977) revealed that practically all the turbulence energy fell within a frequency range below (thus, a wavelength range above) that corresponding to the pipe diameter.

Laser Doppler Velocimetry (LDV) was used to determine the influence of particles on turbulent flows. Ek (1979) measured the turbulence intensity of fiber suspension flows at fiber concentration of 0.5%. When compared to pure water flow, the longitudinal turbulent intensity was higher than that of water at locations close to a wall ($0.5<r/R<1$) and decreased near the center.

McComb and Chan (1985) made single-component laser-Doppler measurements in drag-reducing suspensions of asbestos fiber with extremely high l/d ratios (ca. 10^5). Tangential and longitudinal components were measured. At the lowest Reynolds number examined, $Re = 1.4 \times 10^4$, 70 percent drag reduction was observed. The longitudinal fluctuating component, u', decreased compared to the fiber-free turbulent flow, but the tangential component, w', increased. Similar results were reported for $Re = 9.0 \times 10^3$. This represents a profound modification of the turbulent structure, much more than simply suppression of turbulence. (The decrease in u' is the opposite effect seen in drag-reducing polymer flows, where u' increased dramatically, and radial component, v', is decreased.)

As the same solution was repeatedly passed through the flow system, there was a transition from "fiber-like" drag reduction to "polymer-like" drag reduction, with u' increasing and then decreasing back to that of the pure carrier fluid, and with drag reduction also decreasing. Examination of energy spectra, however, showed no evidence of a transition from one kind of drag reduction to another. Drag reduction magnitude also showed no obvious transition. These findings suggested that fibers affect turbulence in complex ways.

At higher Reynolds numbers (3.2×10^4 and 5.3×10^4), u' was higher than in the carrier fluid alone even at high levels of drag reduction. Energy spectra showed a dip at length scales on the same order as the fiber length, suggesting resonant energy adsorption by the fibers.

Counter to the work of Gore and Crowe (1989), Steen (1990) measured the turbulence intensity in a fiber suspension with a concentration of 12 g/L and found that long fibers (length of 3 mm) decreased and short fibers (1 mm) increased the turbulence levels when compared to water flows. Radial profiles of axial velocity and turbulence spectra were recorded using an LDV technique on vertical upward pipe flow. An increase in velocity and turbulent energy when compared with a pure fluid could be observed for the short fibers at a low concentration level of 1.2 g/L. Near the wall the turbulence levels were found to be higher than those for pure fluid. Steen (1989) cites qualitative comparisons with the results of Ek (1979).

At present, a great deal of research has involved the aspects of turbulent suspension flows, particularly the causes of drag reduction. Unfortunately, the results often do not lend themselves to quantitative analysis. The complexity of turbulent suspensions of fibers has continued to challenge researchers and further work is required on the fundamental nature of momentum transfer and turbulent fiber flows.

2.2.4 Drag reduction of fiber suspension flow

The addition of fiber to water produces a lowering of the longitudinal pressure gradient at the same flow rate when turbulent flow exists. This phenomenon is termed drag reduction. The ability of certain particulate additives to reduce turbulent flow resistance has been reported in numerous publications (Bobkowicz and Gauvin 1965; Lee and Duffy 1976a; Kerekes 1970; Radin and Patterson 1975). It has been established that the effectiveness of particulates as drag-reducing additives increases as their aspect ratio increases and is appreciable only for fibrous additives. Radin and Patterson (1975) established that drag reduction could always be obtained with fibrous additives having aspect ratios about 30. Vaseleski and Metzner (1974) measured flow-resistance data for fiber suspensions in pipes with different diameters and inferred that the presence of fibers in the turbulent core region of flow was important for drag reduction. This is in contrast to drag-reducing polymer solutions, in which the mechanism of drag reduction has been shown to occur near the wall (Virk 1975).

Figure 2.3 shows typical curves of friction factor versus velocity for wood fiber suspensions. Lee and Duffy (1976) suggested a continuous curve in the plot of friction factor versus velocity. They considered the mixed flow to begin at bulk velocities lower than A. The drag reduction develops to a maximum at B. In the regime BC, the values of friction factor are approximately independent of bulk velocity, and suspension friction curves approach the water curve. The friction factor decreases as the bulk velocity is increased in the regime CD. The flow resistance is less than that of water, and the difference between the pulp and water curves increases with an increase in fiber concentration. This disagrees with the assumption made by Seely (1968) that, in the regime CD, the flow-resistance curves could not be distinguished from that of water at all concentrations.

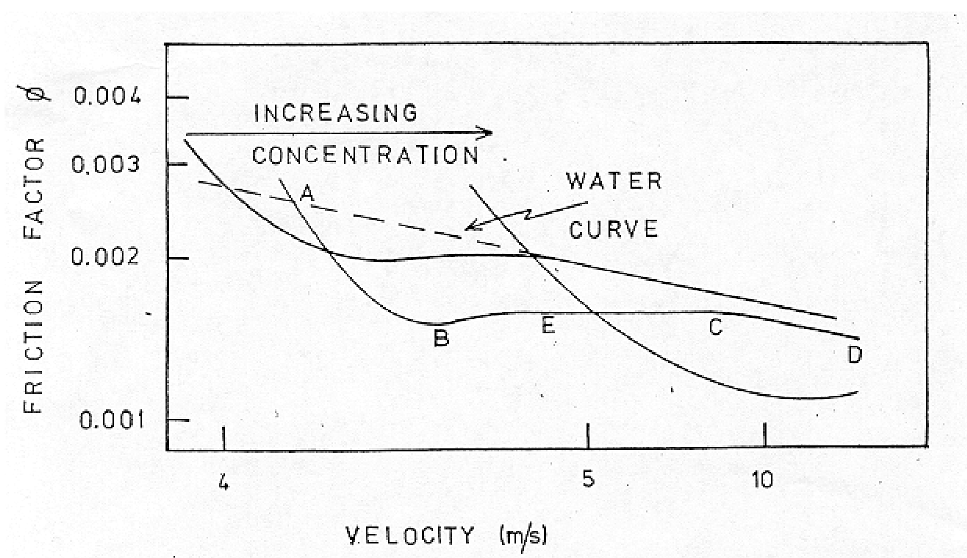

Figure 2.3 Typical curves of friction factor versus velocity for wood fiber suspensions (Lee and Duffy 1976).

Lee and Duffy (1976b) proposed a mechanism to explain the drag reduction in the mixed flow regime of Figure 2.3. They based their assumption on the concept that at any flow rate there is a state of equilibrium in which both the formation and disruption of flocs are occurring simultaneously (Roberston and Mason 1957). Also, there is a distribution of floc sizes from the surface of the plug to the region near the wall (Mih and Parker 1967). Fibers and flocs affect the momentum transfer in two opposite ways as suggested by Daily and Bugliarello (1959). At low intensities of turbulence the predominant effect in momentum transfer in the turbulent fiber-water annulus is due to large flocs providing solid links between adjacent fluid layers. Under these conditions increasing the intensity of turbulence by increasing the flow rate decreases the average floc size in the turbulent annulus. Consequently, momentum transfer decreases, local mean velocity gradients increase, and drag reduction continues to increase. At bulk velocity greater than that at maximum drag reduction, the average floc size is sufficiently small that the effect of flocs in suppressing radial turbulence predominates. Therefore, the decrease in floc size accompanying an increase in flow rate results in an increase in momentum transfer and hence drag reduction decreases. The magnitude of maximum drag reduction is expected to be a function of the fiber and suspension properties that offer fiber flocculation.

Lee and Duffy (1977) obtained the maximum values of drag reduction of different pulp suspensions. They found that both stone groundwood and refined mechanical pulps gave greater values of drag reduction (approximately 40 percent) than chemical pulps. An NSSC hardwood pulp produced the lowest maximum drag reduction (approximately 18 percent) apparently due to the increased stiffness of fiber from this process. It appears that fiber stiffness, the presence of fibers, and a wider fiber-length distribution could have significant effects on suspension behavior at high flow rates. In contrast to Bobkowicz and Gauvin (1972), Kerekes and Douglas (1972) found that drag reduction for suspensions of synthetic fibers increased with an increase in fiber aspect ratio.

2.3 Methods of Measuring the Velocity Profile of Fiber Suspension Flow

The unique fiber suspension flow behaviors have been widely investigated through the study of pipe flow mainly with two different techniques: friction loss measurement and velocity profile measurement. The main practical problem encountered in the measurement of local velocities in fiber suspensions is the tendency of fibers to staple on any sharp-edged surface of an inserted probe. Therefore, techniques which have been developed for velocity measurements in the single-phase system are generally unsuitable for use in fiber suspension. In this section, a brief review of the methods reported in the literature for fiber suspension flow measurement will be presented.

2.3.1 Impact tube

Brecht and Heller (1950) attempted to prevent the stapling of fibers on the probe by using a countercurrent Pitot tube with a large entrance diameter (8 mm). To keep a countercurrent purge tube free from stapling, it was necessary for the purge flow velocity to be greater than the approach velocity being measured. At these high velocities in a small impact tube, the fraction head loss amounted to a significant part of the stagnation pressure sought. Hence, the measured back-pressure was always appreciably greater than the approach flow stagnation pressure and it was very sensitive to the purge flow rate.

Readings obtained from this type of probe were not accurate. Nevertheless, velocity profiles were obtained at low flow rates.

Daily and Bugliarello (1958) attempted to design a probe in which clogging of fibers would be automatically prevented by the shape of the tip. Experimentation with various types of impact tubes indicated that good results could be obtained with flat-faced tips. However, subsequent research by Mih and Parker (1967) showed that the flat-faced tips of rods as large as 0.5 inch in diameter will momentarily build up or arrest fiber bundles in long-fiber furnishes used in papermaking when the velocity is too low to generate a high level of turbulence at the tip of the probe. For tips of greater diameter, the stream distortion is too excessive for reliable measurements.

A special probe for measuring stagnation pressure of the fiber suspension flow was developed by Mih and Parker (1967). Termed annular purge impact tube, this probe consists of two concentric tubes (Figure 2.4). The enclosed annulus provides a continuous purge of water to keep the projecting tip of the inner sensing tube free from fiber stapling. The water-filled inner tube sensing the impact pressure is connected to a manometer. A piezometer ring located one pipe diameter upstream provides the static pressure tap. The local mean velocities are therefore determined without interference from fiber-probe interaction.

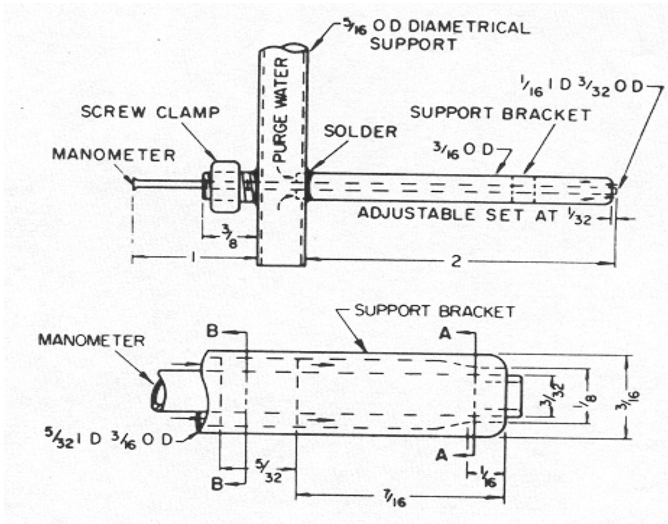

Figure 2.4 Construction of the annular purge impact tube.

Since the introduction of the purge impact tube, several researchers have applied this device to measure the local velocity of fiber suspension flow. Mih and Parker (1967) measured the local mean velocities for the flow of turbulent fiber suspension through both 50- and 100-mm-diameter pipes at bulk velocities up to approximately 3.5 m/s. Seely (1968) used the same type of probe to measure local mean velocities in 36- and 48-mm- diameter pipes for suspensions of softwood sulfite fiber. Velocity profiles were obtained for suspensions with concentrations up to 0.6% and flowing at bulk velocities up to 3.5 m/s. Using a similar purge impact tube, Lee and Duffy (1976) investigated the velocity profiles of fiber suspensions over wide ranges of bulk velocity (up to 9 m/s) and fiber concentration for chemical fiber flowing in a 100-mm-diameter pipe.

Although the annular purge impact tube is the most popular method so far developed for local velocity measurement of fiber suspension flow, several problems still exist. First of all, it is an intrusive method. The stream may be distorted by the tube and thus give inaccurate measurements. Because of the size of the tube, the velocity near the wall is usually not available. Secondly, in order to prevent the fibers from stapling on the tube, purge water must be used. At low purge rates, the probe tip tends to block partially with fibers and the measured pressure differential is too low. At high purge rates, the annular jet extends into the approach flow and can completely close over and isolate the impact tube. Although the purge at a suitable purge rate may not affect the velocity measurement, it has to be adjusted with the changing of approaching fiber suspension flow rate. Usually, a single purge rate could not be used to obtain all the local velocity measurements required in an investigation. Since the purge water will reduce the local fiber concentration at measuring point, the measured results may not reflect the flow behavior of the fiber suspension at desired concentrations. Therefore, the velocity profile obtained has no accuracy, and a new technique is desirable to measure the fiber suspension flow velocity profile.

2.3.2 Nuclear magnetic resonance imaging (NMRI) method

NMRI is based on the nuclear magnetic resonance frequency being proportional to the magnitude of the magnetic field acting on the nucleus. By combining a main homogeneous polarizing magnetic field with magnetic field gradients so that the total magnetic field crossing the entire sample varies in a well-defined way, the resonance of the nuclear spins at different spatial locations will be a function of position. The spectrum of the resonance frequency can be recorded to map the position of the nuclear spins in the real space. Furthermore, the phase information of the nuclear magnetic resonance signal can also be recorded and used to encode either the spatial coordinate or transnational motions of the nuclear spins. By applying differently shaped fields gradient pulses, such as dipolar sine wave, the phase of the NMR signal can be made to be sensitive to different flow components of the fluids. Recent technical developments have greatly increased the temporal resolution of NMRI. This makes it a powerful tool for rapid-flow studies in opaque and multiphase systems. The NMRI technique can visualize directly both the time-averaged mean velocity profile and the turbulent intensity. Furthermore, this technique is noninvasive and requires no tracer particles in the fluid.

By the nuclear magnetic resonance imaging technique, Li et al. (1994, 1995) measured the mean velocity profile of wood fiber suspensions flowing through a horizontal circular pipe and a 4:1 continuous conical contraction. Suspensions of hardwood and softwood kraft pulps at different consistencies were studied at mean flow rates up to 1 m/s. Maneval and McCarthy (1991) applied an NMR time-of-flight method to measure velocity profiles for 1% and 3% fiber suspensions. The velocity profiles obtained confirmed plug flow behavior at plug velocities of around 0.54 and 1.12 feet per second. Actual plug velocities were calculated by dividing the length of pipe over which the plug of fiber traveled by the time required for the plug to travel along that length. These values were compared to those velocities measured by the NMR method. For all experimental runs, the velocity determined by NMR measurement was within 10% of the actual velocity of the fiber suspension.

Both of the above studies indicated that NMR imaging was able to measure the flow field in low-to-medium concentrations of fiber suspensions. The limitation of NMR is that it cannot be used in the presence of ferromagnetic or paramagnetic materials and the volume under study must be confined entirely in a precisely controlled magnetic field. The high-intensity magnets that are available generally have a rather small internal bore, limiting the size of industrial equipment which may be studied (at present to about 100 mm in diameter) (Li et al. 1995). The more serious limitation is that the maximum velocity it can measure is in the order of 1 m/s.

2.3.3 Laser Doppler Velocimetry (LDV)

Limited studies have been conducted using LDV for fiber suspension flow measurement. Ek (1979) applied laser Doppler velocimetry (LDV) to a 0.5% sulfate pulp suspension flowing through a 10-mm-diameter glass pipe. The LDV measurements, based on scattering from fibers, were made in the longitudinal direction only. The objective of Ek's experiment was to measure velocity profile and turbulence intensity of fiber fluctuations in the radial direction.

Although Ek achieved good resolution (less than 1 mm) during his experiments, the employment of such a small pipe diameter surely limited the industrial relevance of his measurements. Moller (1976) warned that the use of pipe diameter of 75 mm or less may significantly change the flow behavior of fiber suspensions in ways that would not be observed in industrial flows. The sensitivity of LDV to fines and other small particulates further limited the applicability of Ek's results to industrial fiber suspension flows. Ek assumed that only the long-fiber fraction of the fiber suspension controlled the mechanisms of pulp flow and friction loss. Based on this assumption, he used only long fibers during his experiment. The data of Raij and Wahren (1964), however, indicated that pulps consisting of shorter fibers exhibit significantly different flow behavior in pipes than pulps consisting of long fibers.

Further studies by Kerekes and Garner (1982) indicated that LDV signals may result from both the fibers and tracing particles, which were observed later by Hand (1982), but not Chuang (1982). Steen (1989) used refractive index matching to conduct LDV measurements in a Pyrex glass fiber suspension in a mixture of benzyl and ethyl alcohol. The measurements of fiber velocity and fluid velocity were achieved using the signal visibility technique (Borner et al. 1986) to differentiate the two phases in a fiber suspension flow with a concentration of 1.2%.

Several issues remain to be resolved in order to apply LDV for flow measurements in wood pulp suspension flows (Zhu 1996). First, the ability to transmit light decreases significantly when the concentration of fiber suspension increases, which creates a very difficult problem for LDV measurements. The effect of wood fiber concentration on the Doppler signal quality needs to be quantified. Second, the difference in the refractive index of fiber and water is very large, which can affect the measurement significantly. The effect of using refractive index matching fluid for fiber suspension flow velocity measurements needs to be quantified as the shape of fibers can be easily changed in fluids. And finally, the effectiveness of the visibility technique to differentiate between signals from fibers and signals from tracing particles needs to be studied. This technique may be in question under low signal-to-noise conditions.

2.3.4 Other methods for fiber suspension flow measurement.

Diffusion methods were reported to measure the turbulence intensity of fiber suspension flow. Andersson (1966) injected a narrow stream of dye-stuff into a fiber suspension flowing in a straight channel. The distribution of dye-stuff was evaluated from photographs taken in transmitted light and scanned in a microdensitometer. The turbulence intensity was calculated from the rate of dye-stuff diffusion in a direction perpendicular to the mean flow direction. Bobkowicz and Gauvin (1967) injected a stream of hot fluid into a pulp suspension flowing in a pipe and measured the temperature profile downstream using a thermistor probe. The turbulence intensity was calculated from the heat diffusion characteristics.

Ogawa (1990) reported a method to measure the local velocity of fiber suspension flow through an electrode probe. The electrode is 25 mm in diameter and 2 mm in length. Pulp fibers flow along the blunt nose tip, and the belt-shaped electrode is scarcely covered with wood fibers. With this device, local velocity is measured at four radial points at different Reynolds number and fiber concentrations. By the ultrasonic echo correlation method, Hirsimaki (1978, 1982) measured the velocity profile of fiber suspension flow. The correlation delay between two ultrasound echoes was used to measure the transit time of flow and hence the speed of flowing fiber suspensions as a function of distance from the wall.

Ricker and Forster (1985) investigated the application of pulsed ultrasonic techniques to the velocity profile measurement in a fiber suspension with a concentration of 3%. It was found that measurements of local velocity can be made to depths of 8 cm with an average accuracy of 0.8%. However, in their measurement, the transducer had to be immersed in a water-filled tank to increase the transmitting of ultrasound. The sample volume position is determined by the position of the transducer.

2.4 Direct Measurement of Forming Jet Velocity

The function of the headbox is to take the stock delivered by the fan pump and transform the pipeline flow into an even, rectangular discharge equal in width to the paper machine and at uniform velocity in the machine direction. Since the formation and uniformity of the final paper product are dependent on the even dispersion of fibers and fillers, the characteristics of the forming jet leaving the headbox is absolutely critical to a successful papermaking system.

However, because of the shape of the headbox and hydraulic conditions (for example, uneven configuration of the flow path, the lip opening adjustment, side wall effects, and deformation of slice lip), uneven forming jet velocity will happen (Shimizu 1992). As a result, the basic weight variation, fiber orientation strip pattern, and sheet formation will be affected by the properties of the forming jet.

Several techniques have been developed to measure jet velocity as an aid to papermaking. Nielsen (1997) reported a headbox jet-speed profiling system which provides rapid, real-time velocity readings with high accuracy and repeatability independent from the composition of the pulp or hydrodynamic properties inside the headbox. Combined with a computer-controlled scanning beam, the sensor system provides complete headbox jet-speed profiling. Similar techniques for jet-velocity measurement were also reported by Franzen (1987) and Loewen (1991). Figure 2.5 shows the jet-velocity measurement system developed by Franzen (1987). The system is based on the principle that the average velocity of a stock jet can be computed by measuring the time it takes the jet to traverse a fixed distance between two probes, A and B, as shown in Figure 2.5. The transit time is determined by computing the cross-correlation of optical signals measured at two probe locations. The optical signals record random irregularities on the surface of the jet. Over short distances, these surface irregularities are sufficiently stable so that a pattern of surface irregularities noted by the upstream probe is still recognizable at the downstream probe. The shift in time between these signals is the transit time.

The high-speed imaging technique has been applied to diagnose and to optimize the headbox jet and the sheet forming process (Aidun 1996, 1997). Based on the high-speed imaging technique, the Surface-Pattern Image Velocimeter (SPIV) was developed to measure the surface velocity profile for a section of the forming jet (Ono et al. 2000). This technique takes advantage of the nonuniform patterns on the surface of the forming jet, recording the positions of the patterned structures using a high-speed digital camera, and using cross-correlation techniques to produce the jet-velocity profile. By measuring the velocity field over the entire imaged area, the SPIV technique provides valuable information on small-scale local nonuniformity in the forming jet velocity and,

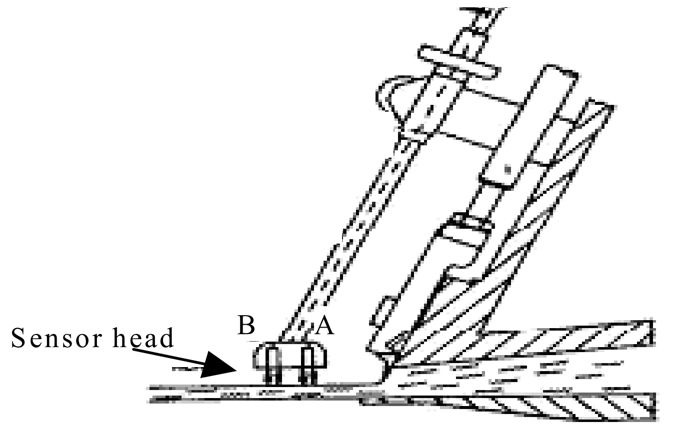

Figure 2.5 Jet-velocity measurement system (Franzen 1987).

consequently, the sheet properties. This method has been shown to produce results accurate enough to identify and diagnose commercial headbox flows.

All of these systems, however, take advantage of the nonuniformity pattern on the forming jet surface and can only be used to measure forming jet surface velocity. Local velocity measurement inside the forming jet has been hampered by the opaque properties of fiber suspension which makes the optical methods inapplicable in this case. In fact, no current technique is available to measure this type of velocity profile for a jet involving an opaque two-phase flow.

2.5 Fundamentals of Ultrasound and Pulsed Doppler Ultrasonic Flowmeter

2.5.1 Piezoelectric effect

The piezoelectric effect, which was first discovered by the Curie brothers in 1880, occurs in crystals, which have axes of nonsymmetry. In a piezoelectric material, the application of an electric field causes a change in physical dimensions. The electric charges bound within the crystal lattice of the material interact with the applied electric field to produce a mechanical stress (Woodcock 1979). The converse effect leads to a potential difference across the end-faces of the transducer in response to an applied stress (Figure 2.6).

In the application of ultrasound in fluid velocity measurement, the generation and detection of ultrasound depend on the piezoelectric effect, in which mechanical energy is

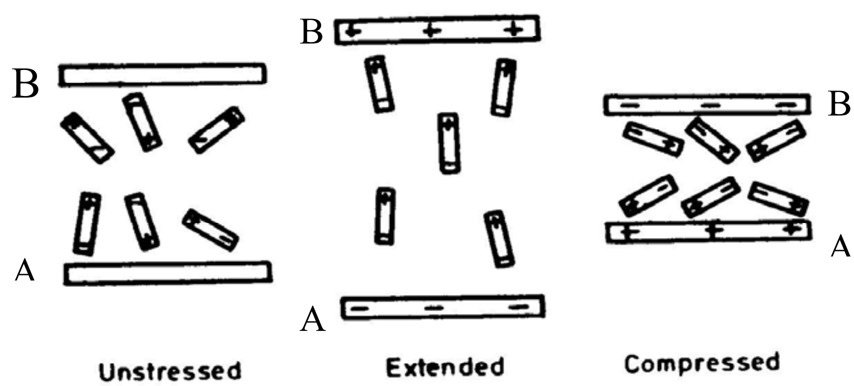

Figure 2.6 Interaction between force and electric charge in piezoelectric materials (Woodcock 1979).

converted to electrical energy and vice versa. The electric field is usually applied to the piezoelectric ceramic by two electrodes on surface A and B (Figure 2.6). A stress applied to a solid in any direction can be resolved into six components, three of tensile stress and three of shear stress, each acting along one of three orthogonal axes.

The strain produced in a piezoelectric material by the application of unit electric field is called the piezoelectric coefficient d, usually known as the transmitting constant of the material. A second piezoelectric coefficient g, known as the receiving constant, is defined as the electric field produced, in open-circuit conditions, for unit applied stress. These two coefficients are related to the dielectric constant ε of the material of the transducer by:

$$d / g = \varepsilon \tag{2.12}$$

In general, a large value of the transmitting constant d is desirable for a transmitter, and a large value of g is necessary for a sensitive receiver. If a transducer is to operate both as a transmitter and as a receiver, it is desirable for both d and g to be large.

2.5.2 Generation of an ultrasound

From the point of view of Sonics, the distinction between audible and inaudible frequencies is arbitrary. The frequency of ultrasound covers a large range from 20KHz to $2*10^9$ Hz, as shown in Table 2.2 (Hueter and Bolt 1955)

Table 2.2 Frequency range of different types of sound

Frequency

10^{-2}	1	10^{2}	10^{4}	10^{6}	10^{8}	10^{10}	10^{12}

<--INFRAAUIBLE--><-------- AUDIBLE ------><------------------------ULTRAAUDIBLE-------------------->

<------------ Ultrasonic --- ----------><---Hypersonic--->

The mechanical vibration based on piezoelectric effect can generate ultrasound. As shown in Figure 2.7 (a), the application of a potential difference across the ends of a piezoelectric ceramic results in a change in thickness. The movement of the faces of the transducer radiates energy into the media in contact with both the front and back faces. This mechanical oscillation can be used to set up an ultrasonic wave in material coupled to the transducer, producing the energy transfer:

electrical pulse $\rightarrow$ mechanical oscillation $\rightarrow$ ultrasonic wave

If this process is energy efficient, the "ringing" of the transducer will be heavily damped and the oscillation will decay after a few cycles (Figure 2.7 (b)).

The application of a sinusoidal electrical driving signal to a transducer results in a corresponding variation in the thickness of the transducer. The energy reflected at each face of the transducer travels back across the transducer toward the opposite face. When the crystal vibrates, its two surfaces will move periodically toward and away from each other. If the distance between the surfaces is equal to half the wavelength of the internal

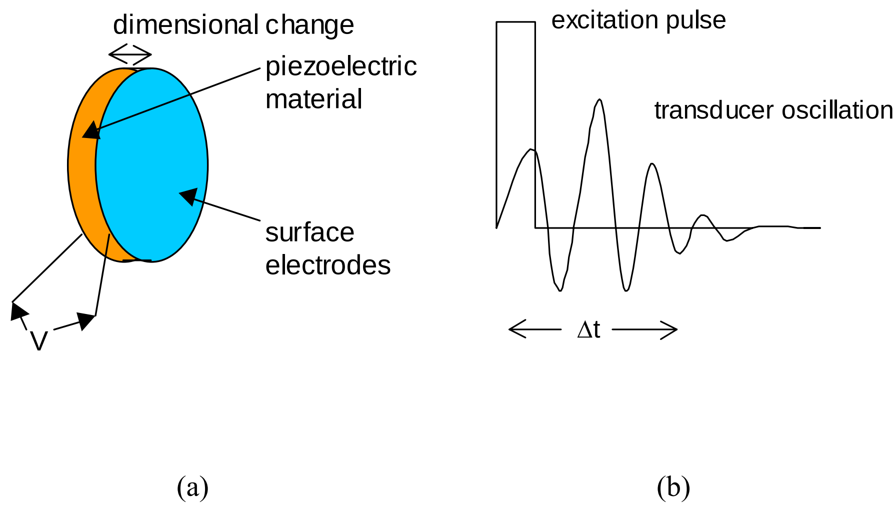

Figure 2.7 Generation of ultrasound based on piezoelectric effect. (a) Dimensional change of transducer, (b) oscillation damped after a few cycles.

sound waves, the waves from the two surfaces will coincide in phase and reinforce each other. The two surfaces will vibrate in synchrony, i.e., in resonance. The so-called "fundamental resonant frequency" of an ultrasound transducer is the transmit frequency that corresponds to the half-wavelength crystal thickness.

2.5.3 The Doppler effect

The Doppler effect is the change in frequency of an acoustic or electromagnetic wave resulting from the physical movement of either the emitter or receptor. Consider an ultrasonic transducer which emits waves of frequency f_o and remains fixed in a medium where the speed of sound is given by c (Figure 2.8). A receptor, or target, in the medium moves with a velocity v. By convention, v is considered negative when the target is moving toward the transducer. If the trajectory of the target forms an angle θ with respect to the propagation direction of the ultrasonic wave, the frequency of the waves perceived by the target will be:

$$f_g = f_0 + \frac{f_0 \mathrm{v} \cos \theta}{c} \tag{2.13}$$

If the acoustic impedance of the target is different from that of the surrounding medium, the waves will be partially reflected. In this way, the target acts as a moving source of ultrasonic signals. The frequency of the waves reflected by the target, as measured by a stationary transducer, is:

$$f_r = \frac{c}{c - \mathrm{v} \cos \theta} f_g \tag{2.14}$$

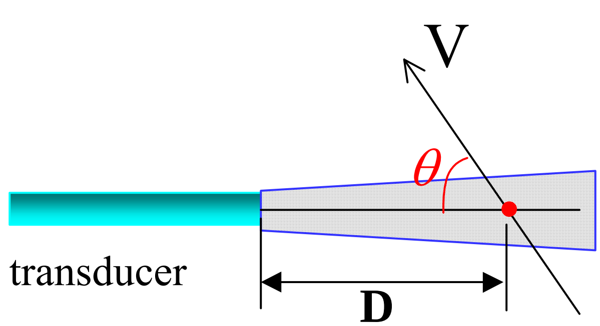

Figure 2.8 Schematic of a particle passing through the ultrasound field.

By combining the two above equations, the frequency of the signal received by the transducer is:

$$f_r = \frac{c + \mathrm{v}\cos\theta}{c - \mathrm{v}\cos\theta} f_e \tag{2.15}$$

The frequency shift, called the Doppler frequency, is given by:

$$f_d = f_r - f_0 = \frac{2\mathrm{v}\cos\theta}{c - \mathrm{v}\cos\theta} f_0 \tag{2.16}$$

This equation may be simplified by knowing that the velocity of the target is much smaller than the speed of sound (v<<c):

$$f_d = \pm \frac{2\mathrm{v}\cos\theta}{c} f_0 \tag{2.17}$$

2.5.4 Pulsed Doppler flowmeter

Simple continuous-wave Doppler systems are unable to measure the distance between the probe and the moving structure. Techniques were developed many years ago in radar detection by which the transmitted signal could be time-coded so that range information could be obtained by measuring time delays, while velocity information could be simultaneously extracted in the form of Doppler frequency shift. Analogous techniques were applied in medical ultrasonic diagnostics in the late 1960s.

Baker and Watkins (1967) were the first to realize the possibility that range-selective Doppler information could be obtained by gating the output of a continuously running oscillator to transmit pulses. The phases of the echoes could be compared with that of the oscillator to give velocity information about targets lying within any chosen range interval. Two years later, other investigators independently developed the pulsed Doppler system (Flaherty 1969; Peronneau and Leger 1969).

Figure 2.9 illustrates the basic components of a pulsed Doppler flow detector developed by Baker (1973). The master oscillator generates a reference frequency of 1 to 10 MHz. This reference frequency is the input to a gating circuit which transmits just a few cycles of the reference frequency at preset intervals. This produces a train of pulses at a

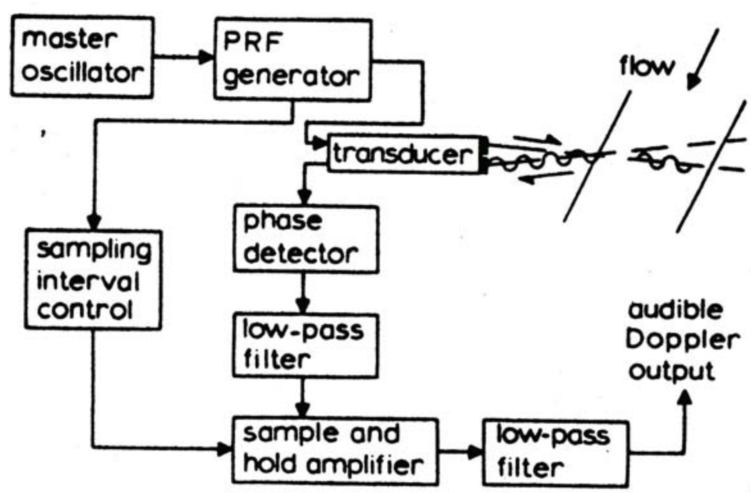

Figure 2.9 Pulsed Doppler ultrasonic flowmeter (Baker 1973).

frequency called the ‘pulse repetition frequency’ or PRF. A typical PRF is 30 kHz (or a period 33 μs), with each pulse having a duration of 0.4 μs, i.e., the pulse train is on for only a short time during each period. The pulse train is the input to the transmitting piezocrystal to produce acoustic pulses. As the acoustic burst leaves the crystal and propagates through the flow field, a continuous train of echoes is produced. Since these echoes are produced by a single acoustic burst, range information can be obtained. This is accomplished by ‘range gating’ the receiver crystal. The receiver is turned off while a burst is transmitted. Since the acoustic burst propagates at a known acoustic velocity through the medium, the distance it travels corresponds to a particular time delay. Thus, if the receiver is turned on for an instant after a given time delay from the instant of pulse transmission, the echoes reaching the receiver crystals at that instant will correspond to a particular range distance. At this instant, the phase of received signal is compared in a phase detector with reference frequency. The phase-detector output is a voltage pulse proportional in magnitude to the phase difference between the echo and the reference frequency. Repeating the comparison over many PRF cycles results in a train of phase-detector output voltages with each pulse proportional to an instantaneous phase difference. The envelope curve of the phase pulse train is the Doppler shift frequency.

2.5.5 Spatial resolution

In a pulsed Doppler system, short bursts of acoustic energy are transmitted by amplitude modulation of a carrier frequency. The returning signal is sampled at a specific delay time from transmission of each pulse. As a consequence, the sampled portions of the returning signal correspond to a back-scattered acoustic energy originating from a specific region of space called the sample volume, whose range from the transducer is determined by the delay time (Figure 2.10(a)).

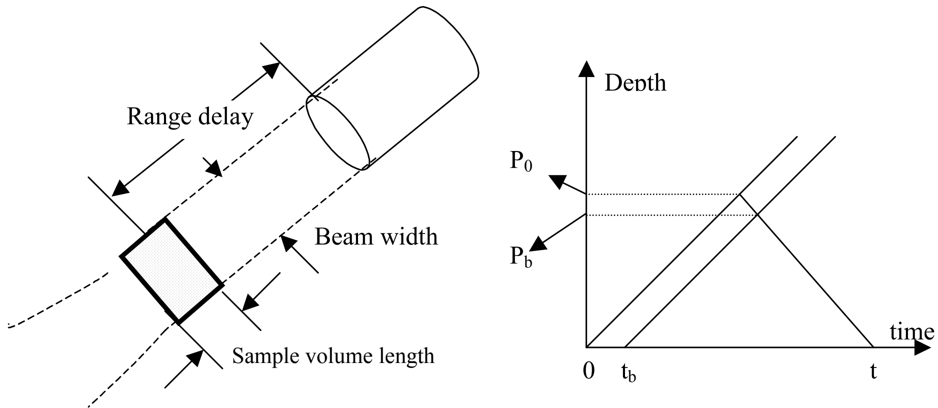

(a) (b)

Figure 2.10 The acoustic sample volume for a pulsed Doppler system.

The spatial resolution of a Doppler system is determined by the size of the sample volume. The lateral size of the sample volume is determined by the ultrasonic beam size. The length of the sample volume corresponds to the distance sound travels as demonstrated in Figure 2.10 (b). Here, we assume an ultrasound burst with duration of t_b that was transmitted at time 0. At time t, the received signals include the echoes not only from the ultrasound transmitted at time 0 and travel to Position P_0, but also from those transmitted at time between 0 and t_b and travel to positions between P_0 and P_b. Since the position of P_0 and P_b is $0.5c*t$ and $0.5c*(t-t_b)$, respectively, the sample volume length will be the distance from P_b to P_0, which can be expressed as:

$$S_l = 0.5c*(t-t_b)-0.5c*t = 0.5c*t_b \quad . \tag{2.18}$$

where S_l is the sample volume length and c is the sound velocity at the medium.

2.6 Pulsed Ultrasonic Doppler Velocimetry (PUDV)

The pulsed ultrasonic flowmeter was initially developed to measure the flow in a blood vessel (Fry 1978). However, due to various constraints arising from its direct application to the human body, the measurement method never realized its full potential. Takeda (1986, 1995) subsequently extended this method to nonmedical flow measurements and developed a monitor system (PUDV) for the velocity profile measurement of general fluids.

PUDV utilizes a pulsed echo-graphic technique of ultrasound. It can provide a velocity profile directly so that the measurement of the spatial information is very efficient, and thus extension to multidimensional and multi-component measurements is practicable. This also makes possible a comparison of the spatial structure of velocity fields between experiments and numerical calculations. Further, this method can be applied not only to transparent but also to opaque liquids. It is also feasible to set a detecting probe outside a container or at a position remote from the measured region in a fluid so that noninvasive measurements can be made.

2.6.1 The principle of PUDV

Figure 2.11 shows the configuration of the ultrasound beam and liquid flow. An ultrasound pulse is emitted from the transducer along the measuring line and the same

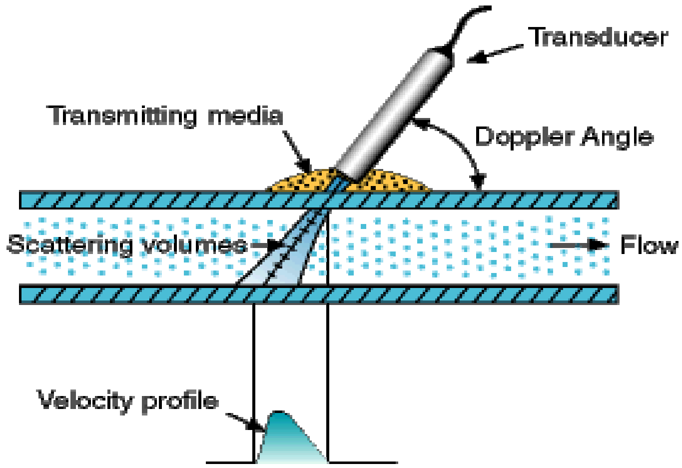

Figure 2.11 Measuring principle of PUDV.

transducers receive the echo reflected from the surface of microparticles suspended in the liquid. All velocity profile information is contained in the echo. Information on the position from which the ultrasound is reflected is extracted from the time delay t between the start of the pulse burst and its receptions as:

$$R = ct/2 \tag{2.29}$$

At the same time, the velocity information is derived from the Doppler shift frequency at that instant:

$$u = \frac{f_D c}{2 f_0 \cos\theta} \tag{2.30}$$

Thus a velocity profile can be obtained by analyzing the echo signal to derive instantaneous frequencies at each instant. In practice, the echo signal is processed at 128 instants in parallel, and thus we obtain a data set $\{2\pi f_D(\tau_i)\}$ which can be converted to the velocity profile $\{V(x_I)\}$ by Equation 2.19 and 2.20.

2.6.2 Detection of instantaneous Doppler shift frequency

The essential point of PUDV is to detect the Doppler shift frequency as a function of time (the elapsed time after the emission of an ultrasound pulse). For the measurement of instantaneous frequency, information theory gives several analytical tools that require high-speed electronics and sophisticated algorithms for signal processing. Since a Doppler shift generally occurs in much less time than the time period corresponding to the required spatial resolution, it is difficult to obtain these frequencies with high resolution from a single echo. The method adopted by Takeda uses repetition of the pulse emission as illustrated in Figure 2.12. The procedure can be divided into five steps.

(1) The echo signal is decomposed into two components of basic frequency and Doppler-shifted frequency, and then the basic frequency is filtered out, resulting in the expression:

$$F(t) = D(t)*\cos[2\pi f_D(\tau)] \qquad (2.24)$$

(2) The decomposed echo signal is sampled into channels.

(3) For the signal of Equation 2.17, the reception of repeated echoes would construct a waveform (for each channel i) as shown in Figure 2.12, with PRF corresponding to the sampling frequency. This waveform can be expressed as:

$$F_I(t) = D(\tau_I)\cos[2\pi f_D(\tau_I)t] \quad (2.25)$$

(4) By counting zero crossing or detecting the phase of this reconstructed wave, a Doppler shift frequency at time instant τ_I can be obtained.

(5) By performing the above procedure for all channels in parallel, a set of instantaneous frequencies is obtained and then converted to a velocity profile.

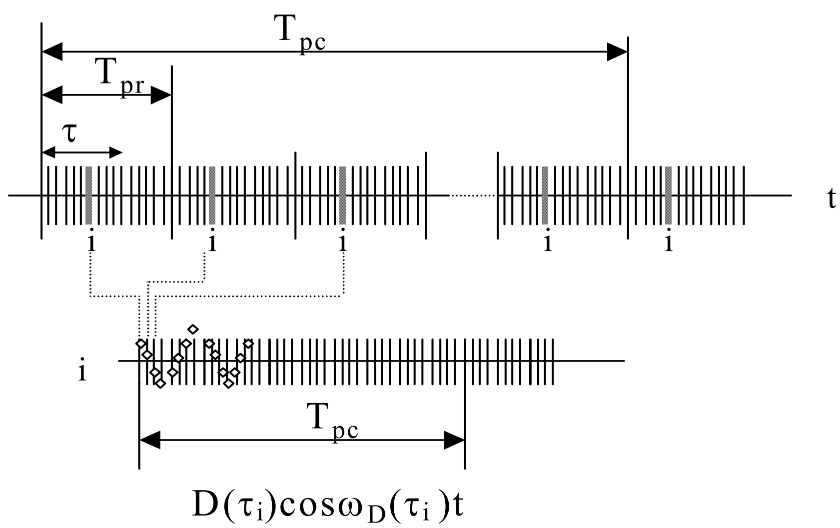

Figure 2.12 Detection of an instantaneous frequency. T_{pr} is pulse repetition period. T_{pc} is total profile measuring time (Takeda 1986).

2.6.3 The advantages of PUDV measurement

In contrast to other measurement methods, PUDV has the following advantages:

(1) It obtains spatial information about the flow field. The velocity field described in an Eulerian frame is a function of both space and time. In conventional measurement techniques, except for particle image velocimetry (PIV) and other image-recording schemes, only the velocity field at one instant or velocity values at one spatial point as a time series can be obtained. In a PUDV measurement, by collecting data along its ultrasound beam line, the velocity field as a function of time can be obtained.

(2) It is applicable to opaque liquids. Until recently it was practically impossible to make velocity measurements of opaque fluids. Flow visualization techniques by optical means are obviously impossible and other measurements such as pressure or torque measurements do not give spatially local information. In addition, many of these fluids show non-Newtonian behavior and are highly viscous so that immersing any velocity-sensing probe disturbs the flow field. By employing the PUDV method, it is possible to measure flow field in opaque, non-Newtonian viscous liquids as if they were ordinary liquids.

(3) It can be used for online measurement. PUDV is a nonintrusive method and the only requirement for this method to be effective is that a sufficiently large number of particles are suspended in the fluid as an ultrasound reflector (Takeda 1995). In addition, the ultrasound transducer can be made as small as several millimeters in diameter and length.

It is convenient to install in existing equipment and to monitor flow structures in real environments.

2.6.4 Application of PUDV

Because of the unique characteristics, PUDV has been applied to the flow measurement in different fluids. Takeda (1990) studied liquid metal flow by PUDV, where the ultrasonic transducer was immersed directly into mercury and the flow in a T-branch of a pipe was measured to confirm the method. A group at the Swiss Federal Institute of Technology in Zurich is working on the application to flow of food materials (Uriev et al. 1998). Uriev and coworkers have succeeded in measuring velocity of chocolate flow from which a flow rate was estimated. They evaluate such velocity profiles together with pressure difference to obtain various parameters such as shear rate and viscosity, both of which can be used as parameters in process control. Sawada et al. (1996) have been investigating the flow of magnetic fluids. The magnetic fluid is composed of tiny magnetic particles (diameter range of 5 to 15 nm) suspended in the oil. They are mostly black liquid and no optical method can be used.

PUDV can also be used for flow mapping. Takeda (1991, 1995) measured the flow field in a square cavity attached to a parallel channel and a circular jet emanating into a tank of the same liquid. An extensive study was made by Wachter et al. (1996) for a flow in the stirrer of a water tank. The measured field was 40*40*50 cm^3 with a rotating stirrer located centrally at the bottom. Using a traversing system for a single transducer, they measured velocity profiles at 8*8*9 positions. In the field of hydraulics, DeCesare and

Boilalt (1997) at Ecole Polytechnique Federale de Lausanne used flow mapping in order to investigate flow with sedimentation. They investigated flow using a model flume and also behind a dam (Beyer-Portner et al. 1998). A flow map was obtained at various times after starting the flow, especially along the bottom region near the flow bed. These results were compared with numerical computations.

In the area of experimental gas-liquid flows, the PUDV method can be applied to a moving interface such as bubbles and free surfaces. Aritomi et al. (1996) investigated a water-air bubbles two-phase flow. At present the application is limited to a bubbly flow with low void fraction, since the ultrasonic beam is totally reflected or deflected by large bubbles in certain flow regimes. Rolland and Lemmin (1996, 1997) applied this method to open-channel turbulent flows. They obtained mean vertical water velocity distributions and several turbulent characteristics. The instantaneous measurement of one or two components of the velocity vector allows one to determine time-, space- and space-time correlations. They verified that the local mean velocity and the convection velocity coincide. Using a modified PUDV, Cellino and Graf (2000) studied the influence of bed forms in open-channel flow on the suspended sediment concentration distribution. The longitudinal and vertical mean velocity profiles are measured with PUDV. In addition, they were able to obtain the longitudinal and vertical components of the turbulence intensity as well as the Reynolds-stress profiles. By measuring the echo strength, the vertical mean concentration profiles could be obtained. Nakamura et al. (1996) made simultaneous measurements of velocity profile and interfacial profile in a horizontal duct containing free-surface wavy flow. The position of the free surface appears on the velocity profile as a sudden and discontinuous change of the velocity values. A time change of the water level was compared with results from a level-detector probe and showed good agreement. The velocity profile in the liquid also showed agreement with results taken by Particle Tracking Velocimetry.

3. EXPERIMENTAL SETUP

3.1 Pulp Suspension Flow Loop

In order to evaluate the PUDV for fiber suspension flow measurement, a pulp suspension flow loop was built, as shown in Figure 3.1. Storage tank 1 and storage tank 2 were used to store the pulp fiber suspensions. Valves 1 to 6 are installed for the purpose of transporting the pulp suspension from the storage tank to the flow loop or from the flow loop to the storage tank. Under normal conditions, these valves are closed. A Moyno pump, manufactured by Robbins & Myers, is used for pumping the pulp suspension from the discharge tank to the flow loop; it then flows through a rectangular channel back to the discharge tank. The suspension is circulated in the flow loop during all the experiments. If a small flow rate, less than the minimum capacity of the pulp, is desired, the valve at the bypass line adjacent to the pump (valve 11) can be opened to reduce the net flow rate in the flow loop. In this case, part of the pulp suspension will flow through the bypass line and then be discharged directly to the discharge tank through a flexible pipe. The pump rate of the Moyno pump is controlled by the attached mechanical drive and the flow rate is measured by a Micro Motion DS300S155SU mass flow meter (Figure 3.2b).

To reduce the pressure fluctuation in the flow loop, two surge suppressors are installed as depicted in Figure 3.2. Surge suppressor 1 is installed at a point two meters away from the pulp exit; surge suppressor 2 is installed right before the entrance of the channel.

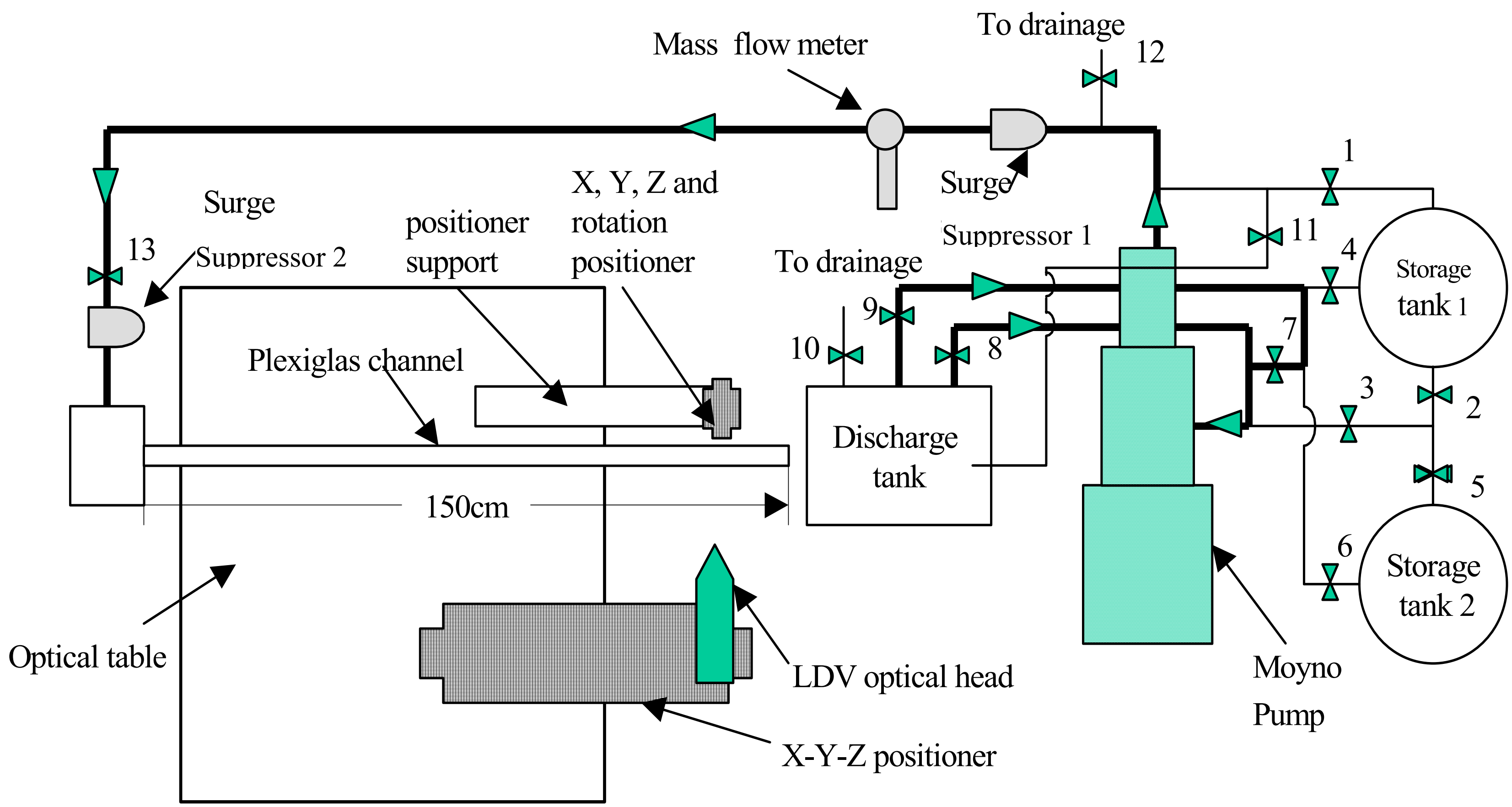

Figure 3.1 Flow loop layout.

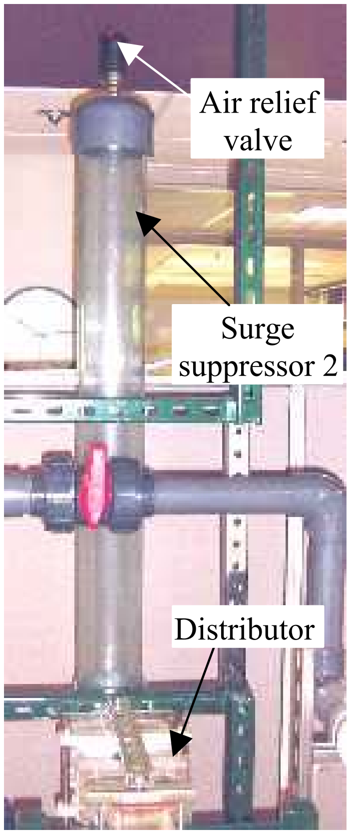

(a)

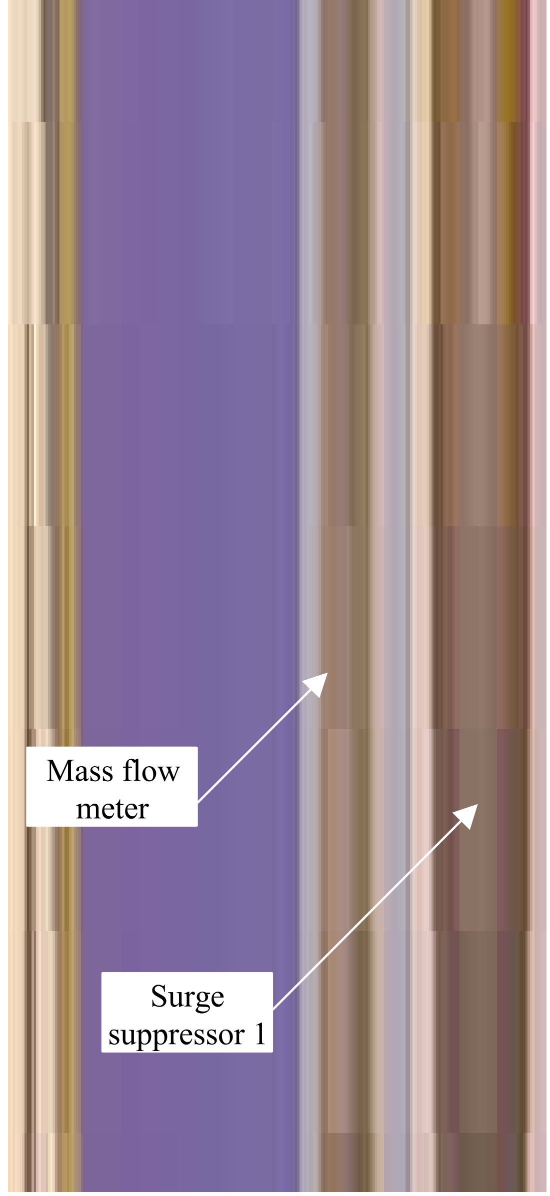

(b)

Figure 3.2 Photographs showing the configuration of the surge suppressor and Micro Motion mass flow meter. (a) suppressor 2, (b) suppressor 1 and mass flow meter.

Both suppressors are made of transparent [illegible] can be monitored. An air relief is mounted on t[illegible]a). By adjusting this valve, a proper water level i[illegible]h may help to catch the big air bubbles in the flo[illegible]e flow system.

3.2 Setup of Distributor and Channel

The experiments were conducted in a rectangular Plexiglas channel which is schematically shown in Figure 3.3. One end of the channel is connected to a Plexiglas box which is 20 cm long, 12.7 cm wide, and 5.7 cm high. This Plexiglas box serves as a distributor to connect the circular pipe with the rectangular channel. Pulp suspension flows into the distributor from the bottom of the box and flows out through one side of the box and then into the channel.

The Plexiglas channel is 150 cm long, 5.08 cm wide, and 1.75 cm high. At the end of the channel, as shown in Figure 3.3, a 2-cm-diameter hole is cut in the center so that the wall thickness in this area is only 2 mm. During the velocity profile measurement, the ultrasonic transducer is inserted into the hole. Its position and inclination angle can be

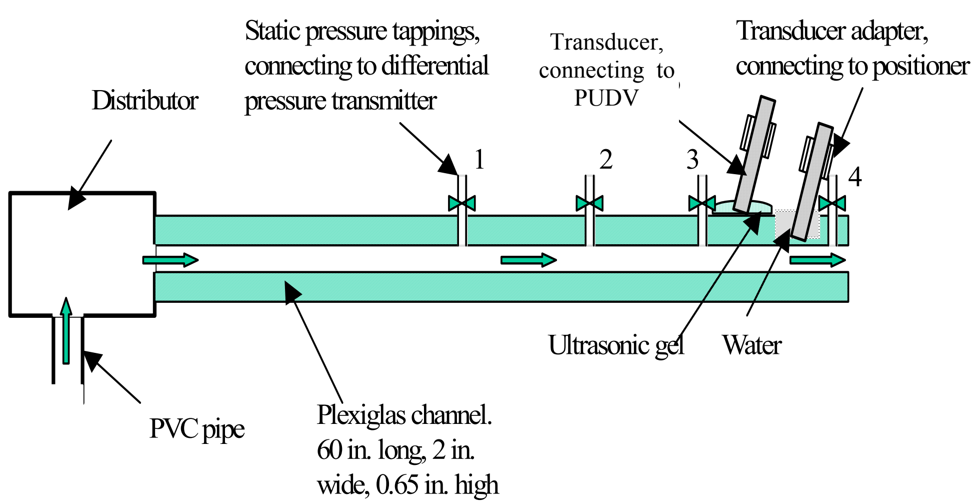

Figure 3.3 Layout and details of channel.

adjusted by an X-Y-Z-rotation positioner through the attached transducer adapter (Figure 3.4). In order to reduce the ultrasound reflection at the interface between air and Plexiglas surface, the hole is filled with water, which acts as a coupling medium between transducer and Plexiglas. In some other measurements, the transducer is simply installed directly on the top wall of the channel. In this case, an ultrasonic gel is used as coupling medium. Some additional measurements are also made in a small channel which is 60 cm long, 3.3 cm wide, and 1 cm high.

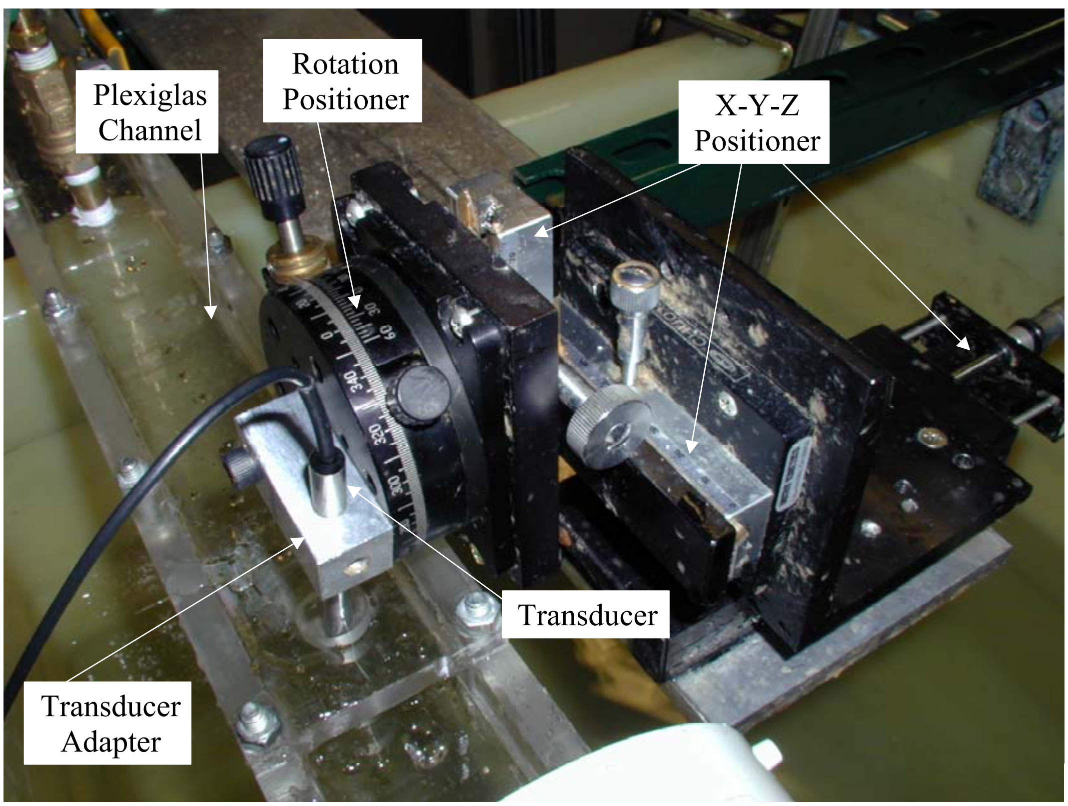

Figure 3.4 Photograph showing the installation of ultrasound transducer.

Figure 3.5 is the photograph of the setup of channel, transducer, PUDV, and transducer positioner. The detailed structure of the channel and distributor is included in Appendix I.

The wood fibers used in this thesis were unbleached softwood pulp with an average length of about 2.3 mm. The detailed dimensions and properties of the fibers were tested with FQA and the results are shown in Table 3.1. When an increase in fiber concentration is desired during the experiment, a certain amount of wood fiber is added to the discharge tank and the suspension is circulated at least 30 minutes before any measurements are taken.

Table 3.1. FQA analysis results for unbleached softwood fibers used in the experiment.

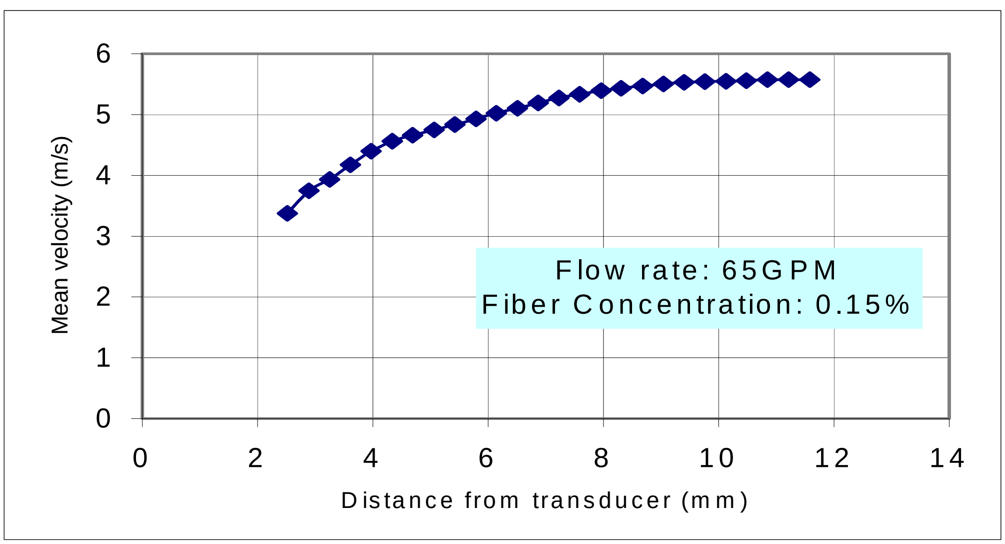

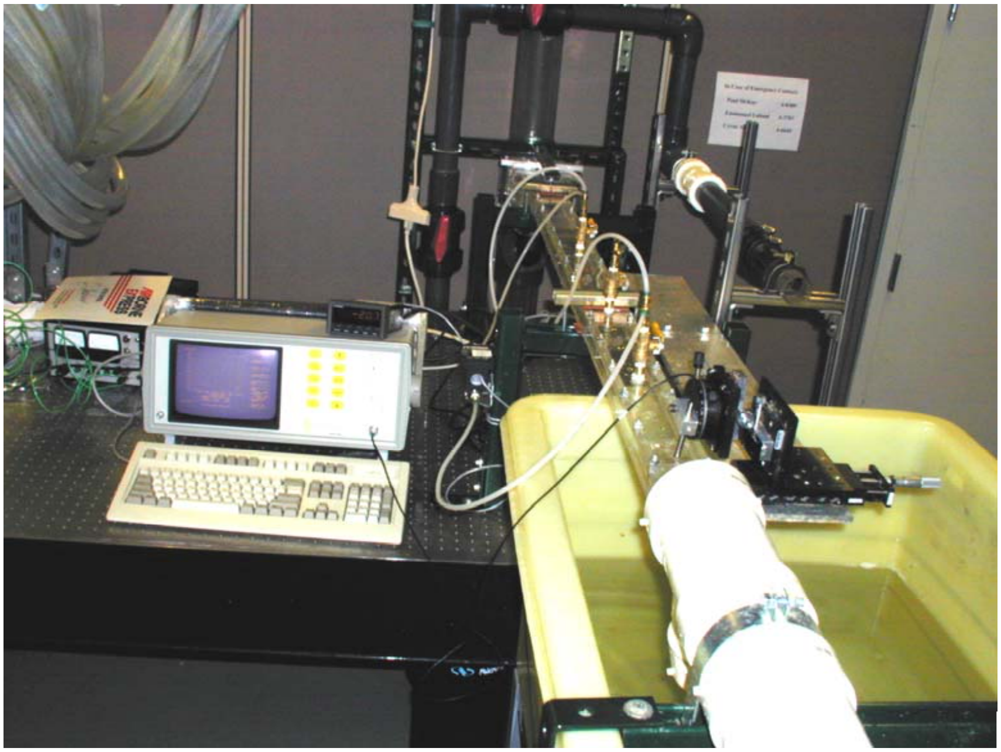

Figure 3.5 Photograph showing the setup of channel, transducer, PUDV, and transducer positioner.

3.3 Measurement of Channel Flow Resistance

3.3.1 Installation of differential pressure transducer

The pulp suspension flow resistance in the channel is obtained by measuring the pressure differentials over the test sections. Four static pressure taps were drilled in the center of the channel with a distance of 22 cm between the adjacent taps (Figure 3.3). In order to measure the pressure drop at the fully developed region, tap 3 and tap 4 were used when average velocity of the flow was larger than 0.91m/s, while at a low flow rate (≤0.91m/s), tap 1 and tap 4 were used. Here, the entrance length (L) of the flow is calculated based on the channel height (b) and Reynolds number (Re): L/b >0.05 Re for laminar flow, L/b>50 for turbulent flow.

An OMEGA PX 2300 differential pressure transducer, with a maximum measurable pressure of 5 psi and accuracy of ± 0.25%, was used to measure the pressure drop between the different taps. The high-pressure and low-pressure ports of the transducer were connected to the taps through ¼ `` -18NPT internal fittings (Figure 3.6). In order to prevent pressure shock on the transducer, the pressure sensor was installed with a valve in each line, with a shunt valve across the high and low pressure ports (Figure 3.6 B).

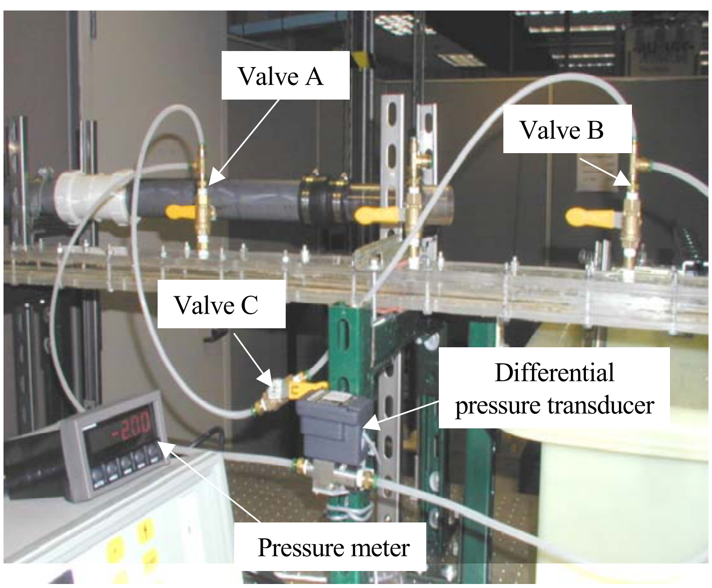

(A)

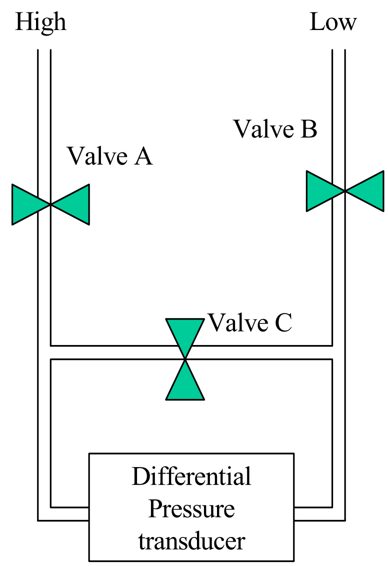

(B)

Figure 3.6 Installation of differential pressure transducer and pressure meters. (A) Photograph of experiment setup; (B) Flow diagram.

Valve C will be open and valves A and B closed whenever the system is first being wetted or pressurized. Valves A and B should be opened slowly to avoid hammering. Valve C can then be closed and the system will be operating.

The transducer is connected to a OMEGA DP41-E process indicator from which the pressure difference between the high and low pressure ports can be read directly.

3.3.2 Procedure for measuring pressure drop

The measurements of flow resistance and the velocity profiles are obtained during each flow rate of a concentration run. For simplicity, the procedure of measuring the velocity profiles is introduced in Section 3.4.2

The following procedure is adopted for each concentration run:

(1) Close valve 1, 3, 4, and 6 and leave all other valves opened. Fill storage tank 1 and storage tank 2 with water.

(2) After closing valves 8, 9, 10, 11, and 12, open valves 3, 4, and 6; and then turn on the pump. When 100 gallons of water are pumped to the discharge tank and flow system, open valve 8 and 9; close valve 3, 4, and 6.

(3) After adding a calculated amount of wood fiber to the discharge tank, adjust the flow rate to 40 gpm and circulate the suspension for at least 30 minutes.

(4) After opening valve C in the flow loop for differential pressure transmitters, open valves A and B. Back off the bleed screw in the transmitter until liquid begins to flow

out. After only bubble-free liquid flows out, retighten the bleed screw and then close valve C.

(5) After turning on the pressure meter, adjust the flow rate to the desired level. When readings in the pressure meter and mass flow meter are stabilized, record the pressure drop reading and flow rate.

(6) Repeat step (5) to obtain the pressure drop at another flow rate.

(7) Add a calculated amount of fiber to the discharge tank. After circulating 30 minutes, repeat step (5) and (6) to obtain the pressure drop at other fiber concentrations and flow rates.

3.4 Determination of Velocity Profile

3.4.1 DOP 1000 Pulsed Ultrasonic Doppler Velocimetry

The basic function of pulsed ultrasonic Doppler velocimetry (PUDV) is to measure the Doppler shifter frequency and time delay between emission and reception of ultrasound scattered back by small particles which are moving with the fluid. The information on velocity and sample volume position is included in the ultrasound echoes. In this study, a commercially available ultrasonic velocity profile monitor (DOP 1000, Model 1032) manufactured by Signal Processing S.A., Switzerland, is used for the velocity profile measurement of pulp suspension flow.

Table 3.2 lists part of the specifications of the UVP. Except specified elsewhere, the parameters used in this study are listed as follows:

Transducer. Two transducers with different size and frequency were used in this study. One of them is 2 MHz, 8 mm in diameter; another is 4 MHz, 5 mm in diameter.

Frequency of ultrasound. The basic frequencies of ultrasound are determined by the transducer. They are 2 MHz and 4 MHz respectively for 8-mm and 5-mm transducer.

Pulse repetition frequency (PRF). The pulse repetition was adjusted according to the different maximum measurable velocity desired. The maximum PRF used is 15.6 kHz (64 μs).

Number of emissions per profile. The measurement of the Doppler frequency needs many ultrasonic emissions. 256 emissions were used in one profile.

Number of profiles. The number of profiles used to calculate the mean velocity profile in each measurement is 256 profiles.

Inclination angle. The angle between the flow direction and ultrasound is 75 degrees.

Ultrasound emitting power: 0.5 watt.

Number of emitted ultrasound cycles: 2 cycles.

Pulse duration: 0.5 μs for 4-MHz transducer; 1 μs for 2-MHz transducer.

Amplification (TGC). The strength of the received Doppler signal depends on the signal attenuation in the liquid. The TGC was adjusted according to the experiment conditions (such as flow rate, consistency) so that the strength of the received signal increases exponentially between two defined depth values.

The PUDV records data values in a binary format. This format ensures a minimum space requirement. The stored data will be converted to ASCII format by the application software SIMUL (provided by Signal Processing S.A., Switzerland) after each measurement. Besides analyzing velocity profile data, SIMUL can also allow computation of the mean profile, the standard deviations and the maximum and minimum values of local velocity values.

Table 3.2. Specifications of DOP 1000 Pulsed Ultrasonic Doppler Velocimetry.

Basic frequency	8 MHz, 4 MHz, 2 MHz, and 1 Mhz
Emission power	0.5 watt, 5 watt, and 35 watt
Number of emitted cycles	2, 4, or 8 cycles
Pulse repetition frequency	64 μs to 2040 μs, step of 8 μs
Lateral resolution	defined by the size of transducer
Longitudinal resolution	0.9 mm
Display resolution	0.375 mm
Velocity resolution	minimum: 0.056 mm/s; maximum: 45.77 mm/s
Acquisition time / profile	minimum: 3 ms
Maximum velocity	11.72 m/s in ultrasound direction

3.4.2 Procedure for measuring velocity profile

The following procedure is used to determine the velocity profile for fiber suspension flow at different concentration runs:

(1) Close valves 1, 3, 4, and 6 and leave all other valves opened. Fill storage tank 1 and storage tank 2 with water.

(2) After closing valves 8, 9, 10, 11, and 12, open valves 3, 4, and 6 and then turn on pump. When 100 gallons of water are pumped to the discharge tank and flow system, open valves 8 and 9, close valves 3, 4, and 6.

(3) After adding a calculated amount of wood fiber to the discharge tank, adjust the flow rate to 40 gpm and circulate the suspension for at least 30 minutes.

(4) Adjust the flow rate to the desired level. Turn on Pulsed Ultrasonic Doppler Velocimetry (PUDV) and adjust the different parameters until the optimal velocity profile displays in the monitor.

(5) Record the velocity profile and save the data to a floppy disk.

(6) Repeat steps (4) and (5) to obtain the velocity profiles at other flow rates.

(7) Add a calculated amount of fiber to the discharge tank. After circulating 30 minutes, repeat steps (4), (5), and (6) to obtain the velocity profiles at other fiber concentrations and flow rates.

4. EVALUATION OF PULSED ULTRASONIC DOPPLER VELOCIMETRY FOR FIBER SUSPENSION FLOW MEASUREMENT

4.1 Introduction

As reviewed in Section 2.2, the main problem encountered when measuring the local velocities in fiber suspensions is the tendency of fibers to staple on the probe inserted into the suspension. Several disadvantages exist in the current methods for fiber suspension flow measurements. In addition, no nonintrusive methods exist for fiber suspension flow measurement in a flow rate range comparable to the papermaking process.

The objective of this chapter is to evaluate the feasibility of measuring wood fiber suspension flow by Pulsed Ultrasonic Doppler Velocimetry. Section 4.2 analyzes the ultrasound echo signals received by the transducer and the effect of fiber concentration on echo strength. Section 4.3 evaluates the accuracy of the PUDV measurements, where the velocity profiles of water flow measured by PUDV are compared with the theoretical velocity profile of water flow between infinite parallel planes and with the results from LDA measurements. In order to avoid the statistical errors caused by velocity fluctuation, the optimum number of repeat measurements are also analyzed in this section. The repeatability and sensitivity of PUDV measurements to the flow rate changes are presented in Section 4.4 and Section 4.5, respectively. To optimize the PUDV measurement, the effect of different measuring parameters including pulse repeat frequency, sampling time, sensitivity, and transducer inclination angles are studied in

Section 4.6. Finally, the characteristics of PUDV measurement are presented in Section 4.7. The relationship between the maximum measurable depth and the maximum measurable velocity are also discussed in this section.

4.2 Evaluate the Ultrasound Echo Signals and Feasibility of Measuring Velocity Profile by PUDV

During the PUDV measurements, the sample volume positions and velocity information at different measuring points are extracted from the ultrasound echo signals. Therefore, the most important requirement for a successful PUDV measurement is that the fibers in the suspensions can act as an effective ultrasound reflector. In order to evaluate the ultrasound reflecting ability of wood fibers, changes in the strength of received ultrasound echoes are measured with fiber concentrations at average velocity of 4.6 m/s. Figure 4.1 shows the average modulus of the received echo signals as a function of the distance between the transducer and the measuring positions at four different fiber concentrations. In this experiment, a 4 MHz, 5 mm transducer was used, and it was installed outside of the channel wall. All of the four measurements at different fiber concentrations are carried out at the same ultrasound amplification level.

As shown in Figure 4.1, two peaks of ultrasound echoes appear at different locations. Position A and Position C correspond to the positions where the sample volume begins to touch the top and bottom inner wall of the channel, respectively. At Position A, most of the sample volume is located in the channel wall material. With the increased distance from the transducer, more and more volume in the fluid will be included in the sample volume. Because of different acoustic impedance between channel material (Plexiglas, Z_I = 3.26) and fluid (water, Z_I = 1.483), there will be a strong reflection of ultrasound at the interface between Plexiglas and fiber suspensions. Therefore, an ultrasound echo peak will appear at Position B. The peak at location D is formed for the same reason. The distance between Position A and Position C is 17.62 mm. Considering the position resolution of 0.37 mm (the minimum distance between two adjacent measuring points), this value is in agreement with the channel height of 17.5 mm.

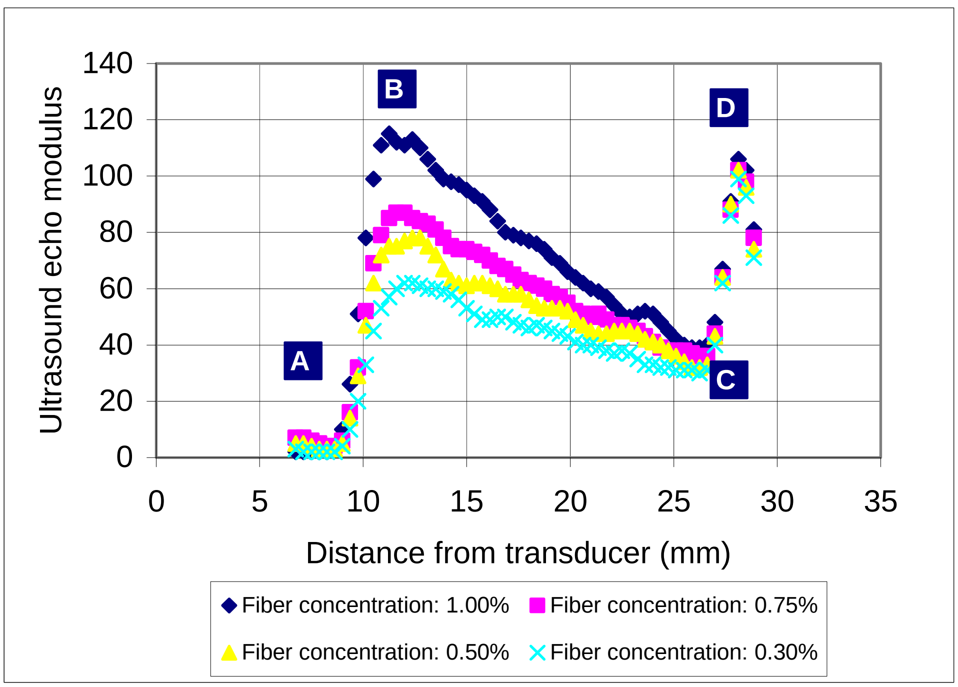

Figure 4.1 The strength of ultrasound echoes as a function of the distance between the transducer and the measuring positions.

In PUDV measurement, the position information is determined by the time delay between the emission and receiving of the ultrasound signal. The location of each sample volume is located in the center of the sample. However, when part of the sample volume is located inside the channel wall, this position will not reflect the actual measuring position. In this case, position correction is needed for these data points. Appendix II provides the position correction values for these points when part of the sample volume is located inside the channel wall. All velocity profiles measured in this paper are subject to the position correction using the value listed in Appendix II.

The fiber concentration effects on the strength of ultrasound echoes are shown in Figure 4.1. With increasing fiber concentrations, the strength of ultrasound echoes increases accordingly. It was found that the strong ultrasound echo signals are beneficial to the measurement because low ultrasound power and amplification are needed, which will effectively reduce the wall reflection and second reflection from the emitting burst.

Figure 4.2 shows the typical velocity profile of fiber suspensions at different mean flow rates. Because of symmetry, only velocity profiles from the channel centerline to the near wall surface are shown here (the interaction between ultrasound and channel wall is shown in Appendix III). As expected, the fiber suspension exhibits three basic types of shear flow as mean flow rate is increased: plug flow, mixed flow, and turbulent flow. These basic flow patterns are consistent with observations by other authors (Robertson and Mason 1958, Lee and Duffy 1976). Based on the above preliminary study, it can be concluded that wood fiber is an ideal reflector for ultrasound and it is possible to measure the velocity profile of fiber suspension flow by Pulsed Ultrasonic Doppler Velocimetry.

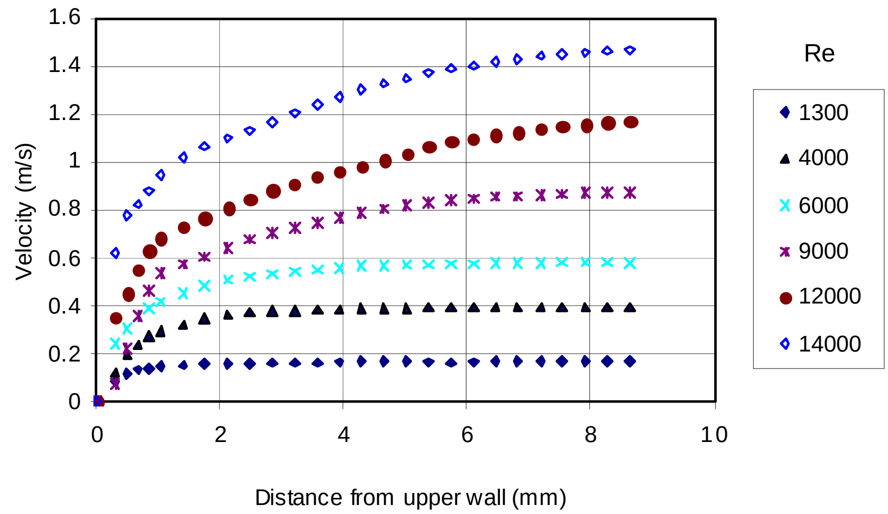

(A)

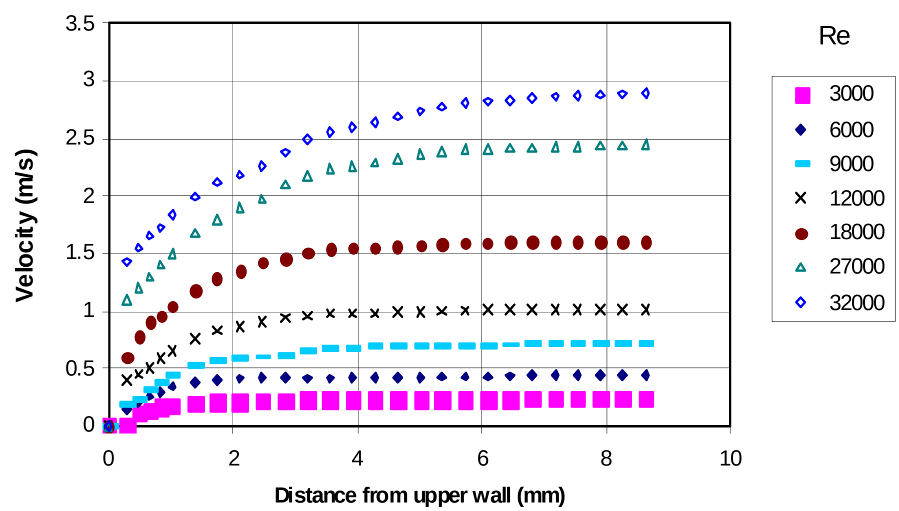

(B)

Figure 4.2 Typical velocity profiles of fiber suspensions at different Reynolds numbers. (A) concentration: 0.3%, (B) concentration: 0.75%.

4.3 The Accuracy of the PUDV Measurement

4.3.1 Compare PUDV measurement results with velocity profiles of water flow between infinite parallel planes

As a test of the accuracy of the PUDV measurement, mean velocity profiles of pure water flow in the turbulent region were determined. The results are shown in Figure 4.3 on a linear scale and in Figure 4.4 in the nondimensional wall-layer coordinates $U^+ = u/U_\tau$ and $y^+ = y\, U_\tau/\nu$. Here, y is the distance from the wall, b is the distance between the wall, u is the mean streamwise velocity, the wall shear velocity U_τ is defined as $(\tau_w/\rho)^{1/2}$, ρ is the fluid density, and ν is the kinematic viscosity. The wall shear stress τ_w is obtained

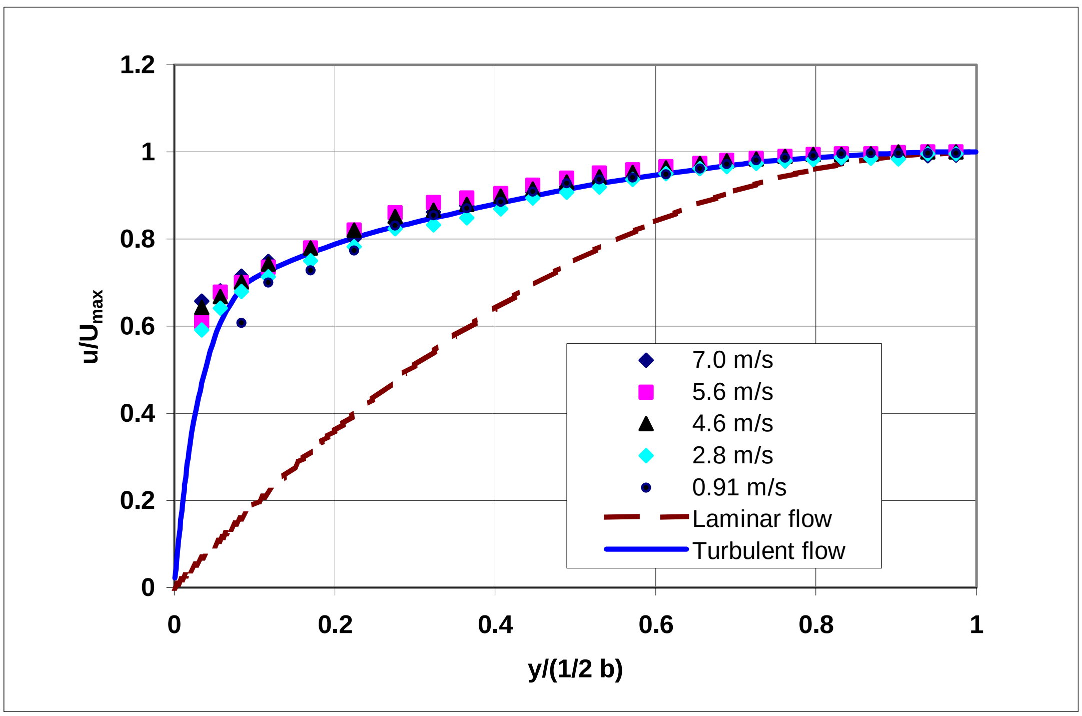

Figure 4.3 Dimensionless velocity profiles of water at mean velocity of 0.98 m/s to 7.0 m/s corresponding to Re = 11880 and Re = 91510, respectively.

through the measurement of pressure drop. For comparison purposes, the velocity distribution equations (Equation 4.1 (Pai 1957) and Equation 4.2 (Schlinger and Sage 1953)) for turbulent flow between infinite parallel planes are also shown in Figure 4.3 and Figure 4.4, respectively. The measurements made by PUDV are in fair agreement with the velocity profile reported in the literature (Pai 1957).

$$\frac{u}{U_{max}} = 1 - 0.3293(1 - \frac{y}{b/2})^2 - 0.6707(1 - \frac{y}{b/2})^{32} \tag{4.1}$$

$$U^+ = 6.2\log y^+ + 3.6 \tag{4.2}$$

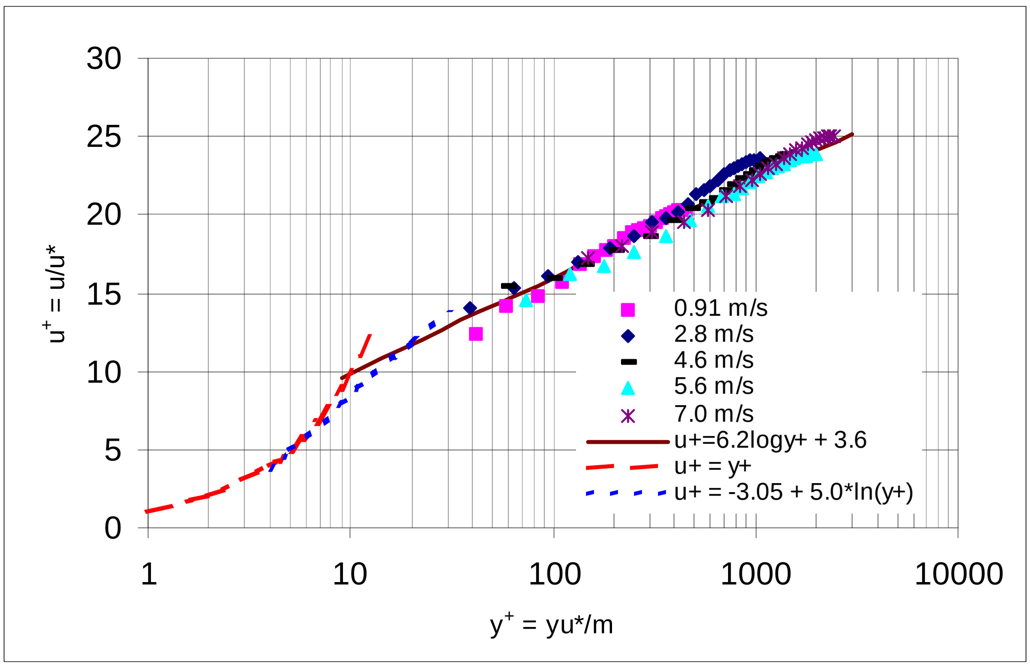

Figure 4.4 Reduced velocity profiles of water at mean velocity of 0.98 m/s to 7.0 m/s corresponding to Re = 11880 and Re = 91510, respectively.

4.3.2 Compare PUDV measurement with LDA measurement

As a further test of the accuracy of velocity profile measurements, a number of profiles of pure water were measured by LDA in the same location as that of the PUDV measurements. During the LDA measurements, seeding particles with different sizes (0.3 micron and 3 micron) are used. These profiles, together with the results measured by PUDV under the same flow rates, are shown in Figures 4.5 (A), (B), and (C). Once again, the profiles measured by these two different methods are in good agreement.

By integrating the area under the velocity profile, the relative difference between PUDV and LDA can be obtained. For velocity profiles shown in Figure 4.5, the relative errors between PUDV measurement and the average of two LDA measurements are -1.55%, -0.14%, and +0.13% at mean velocity of 0.12 m/s, 0.91 m/s and 2.8 m/s, respectively.

4.3.3 Avoid statistical errors

During the PUDV measurements, a certain number of “instantaneous velocity profiles” were used to calculate the mean velocity profile as defined by an equipment parameter "number of profiles". Because of the turbulence, there will be a small difference between different instantaneous profiles. To avoid the statistical error caused by local velocity fluctuation, it is necessary to determine the mean velocity profile based on enough instantaneous velocity profiles. In this section, we will evaluate the statistical error caused by the turbulence fluctuation and try to find the optimum parameter: “number of profiles”. The following equation was used to check the statistical error and decide the parameter "number of profiles":

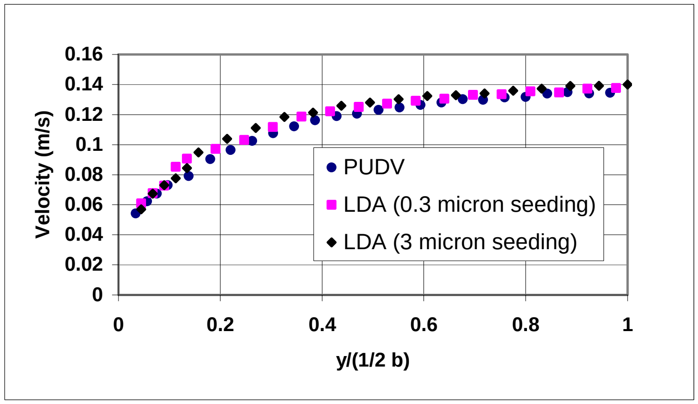

(A)

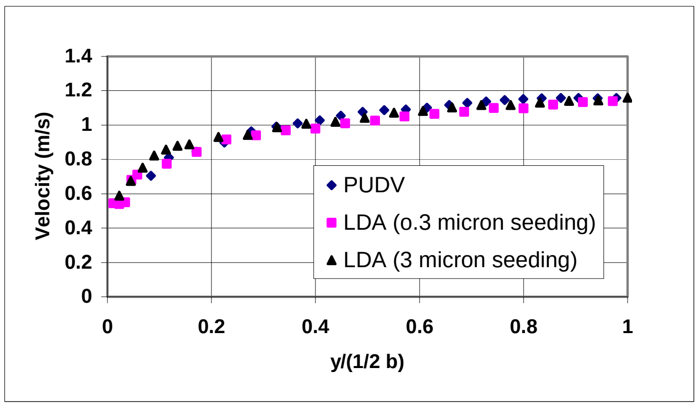

(B)

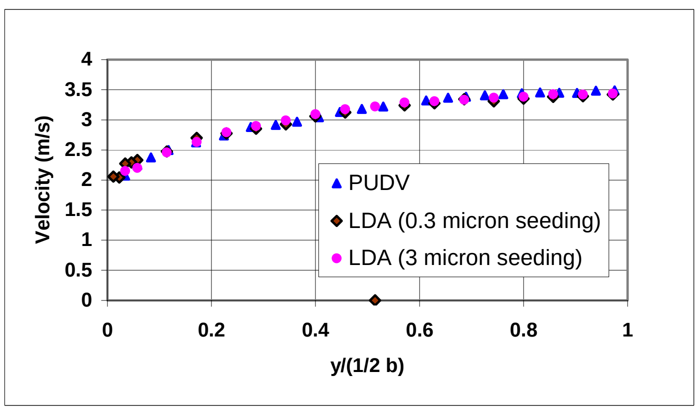

(C)

Figure 4.5 Velocity profiles of pure water measured by PUDV and LDA at different mean velocities. (A) 0.12 m/s, (B) 0.91 m/s, (C) 2.8 m/s.

$$\varepsilon = \sqrt{\frac{z^2 \cdot \sigma_x^2}{N}} \tag{4.3}$$

Here, σ_x^2 is the standard deviation of measurement, which is obtained from the RMS values; N is the number of measuring data points; z is a factor that characterizes the confidence interval.

With a confidence interval of 96% (z = 2) and an RMS value measured in the center of the channel, the statistical error and relative error is listed in Table 4.1 for different numbers of instantaneous velocity profiles. As shown in Table 4.1, when the number of instantaneous velocity profiles is larger than 256, the relative error caused by velocity fluctuation will be less than 0.5%. In this thesis, unless specified elsewhere, the number of instantaneous velocity profiles used to calculate the mean velocity profile is 256.

Table 4.1 Relation between statistical error and measurement points

Velocity (m/s)	Concentrations (%)	Statistical / relatival error	Number of instantaneous velocity profiles				
			10	20	50	100	256
7.0	0	ε (mm/s)	182	104	71.9	53.2	31.2
		ε/Uavg (%)	2.1	1.2	0.84	0.62	0.36
7.0	0.5	ε (mm/s)	150	98.7	68.1	45.7	26.4
		ε/Uavg (%)	1.8	1.2	0.83	0.56	0.32
7.0	1	ε (mm/s)	164	92.8	59.9	39.9	23.6
		ε/Uavg (%)	2	1.1	0.73	0.49	0.29
4.6	0	ε (mm/s)	124	103	61.2	42.2	27.9
		ε/Uavg (%)	2.3	1.9	1.1	0.77	0.5

Beside the errors caused by the velocity fluctuation, another measurement error may come from the instrument itself (accuracy of the instrument) and or measurement itself. According to Equation 2.3, the accuracy of the measured velocity is determined by the accuracy of following variables: Doppler shift frequency, ultrasound velocity in the fiber suspension, basic frequency of the ultrasound, inclination angle of ultrasound transducer. Among these four variables, basic frequency of the ultrasound is determined by the ultrasound transducer and it is calibrated by the manufacture. The error from this variable is very small and can be neglected. The Doppler shift frequency is the only variable measured by PUDV, It is the average of multiple (> 256) measurements and the error is normally less than 0.5%. The ultrasound velocity in the fiber suspension will be affected by suspension temperature and the fiber concentration. At room temperature (20 ^{0}C ~ 25 ^{0}C), the speed of sound in the water is between 1482 m/s and 1496 m/s. When fiber was added to the suspension, the sound speed will go up, but the change won't be significantly. In this project, the speed of sound is set at the default value of PUDV, which is 1500 m/s. consider the temperature and fiber concentration changes, the error caused by ultrasound will be less than 1%. Finally, the accuracy of the inclination angle of transducer is controlled by the rotation positioner which has a resolution of 0.5^0. At the inclination angle of 60^0, the error is about 1.5%. Adding these errors together, the total relative error caused by these variables will be 1.87%. The magnitude of the relative error is consistent with the accuracy of the specification of the PUDV, which is about 2%.

4.4 The Repeatability of the PUDV Measurement

The repeatability of the PUDV measurement is presented in Figure 4.6. Here, velocity profiles of fiber suspensions at concentration 0.5%, flow rate 80 gpm, and concentration 1.0%, flow rate 100 gpm are used as an example to demonstrate the repeatability of two independent measurements. As shown in Figure 4.6, the repeatability of PUDV is extremely high. The difference between the mean velocity profiles for two repeat measurements is almost invisible, although there may be small differences within the instant profiles.

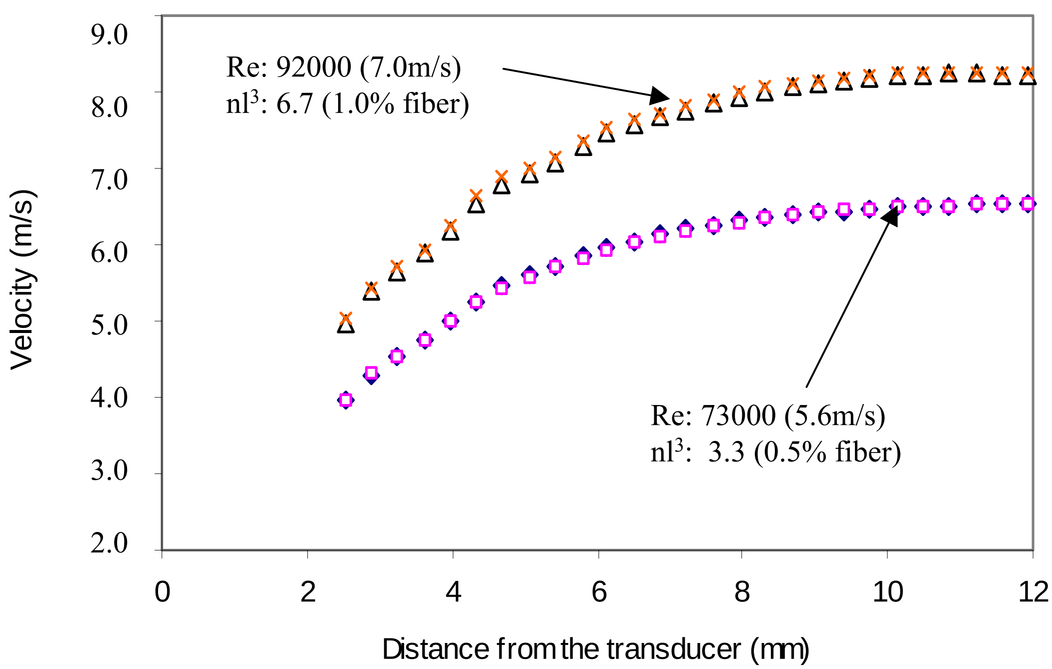

Figure 4.6 Repeatability of PUDV measurement.

4.5 The Sensitivity of PUDV Measurement to the Flow Rate Changes

As a further test of the velocity profile measurement, the sensitivity of the PUDV measurement to the small bulk flow rate changes is investigated. After measuring the velocity profile at mean velocity of 5.6 m/s, the flow rate is changed by ±1%, and the velocity profile is measured again. Figure 4.7 gives an example of how velocity profile changes after about 1% change in bulk flow rate for a fiber suspension at concentration of 0.5%. By integrating the area under the velocity profile, the measured mean velocity changes can be obtained. Table 4.2 gives a comparison between the changes from the reading of the flow meter and changes measured by integrating the area under the velocity profiles. It is obvious from Table 4.2 that flow rate changes obtained through PUDV measurement are consistent with the flow rate changes calculated from the mass flow meter reading. In addition, PUDV measurement is very sensitive to the bulk flow rate changes, and changes less than 1% can be detected easily.

Table 4.2 The sensitivity of PUDV to the bulk flow rate changes

Fiber concentrations (%)	Bulk flow rate changes (%)	Measured velocity changes (%)	Difference (%)
0.3	-1.33	-1.35	-0.02
	+1.03	+0.82	-0.21
0.5	-1.03	-1.05	-0.02
	+1.08	+1.14	0.06
0.75	-1.18	-1.27	-0.09
	+1.03	+0.89	-0.14
1.0	-1.32	-1.56	-0.24
	+1.18	+1.04	-0.14

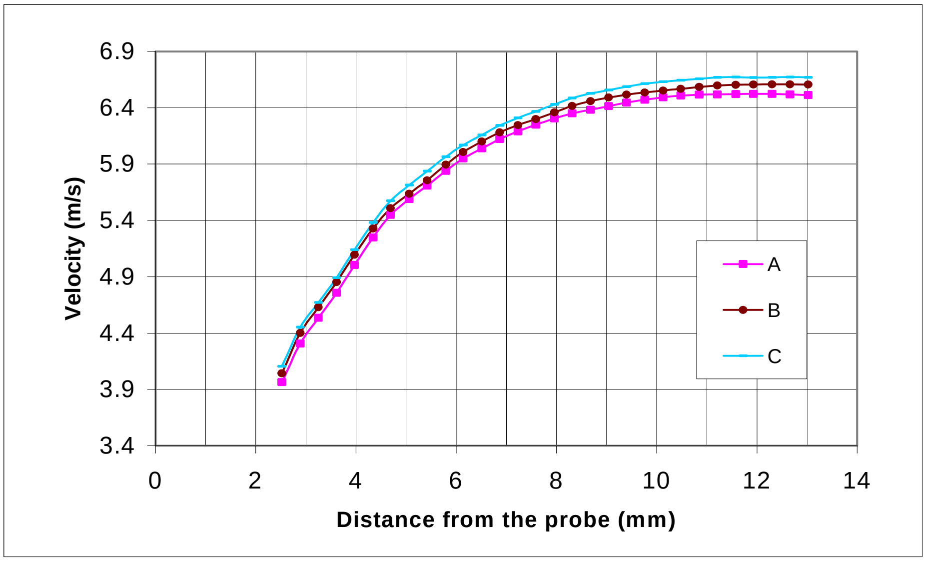

Figure 4.7 The sensitivity of PUDV to the bulk flow rate changes measured at mean velocity of 5.6m/s and concentration of 0.5%. A: flow rate decreases by 1.03%; B: 5.6 m/s; C: flow rate increases by 1.18%.

4.6 Optimize PUDV Measurement

In order to optimize the PUDV measurement, the selection of different measuring parameters was investigated. These parameters include PRF (pulse repeat frequency), sampling time, sensitivity, and inclination angle.

Figure 4.8 shows the velocity profile of fiber suspension at concentration of 0.3% and mean velocity of 0.23 m/s (Figure 4.8 (A)) and 2.8 m/s (Figure 4.8 (B)) when different PRF were used during the measurement. As will be discussed in Section 4.7, the maximum measurable velocity of PUDV depended upon the value of PRF. The higher the PRF, the larger the measurable velocity ranges. In Figure 4.8, most of the measurements fit very well, except the one measured at 15.6 KHz (64 μs), where there is a small difference in the area near the wall. This small difference may be caused by measurement errors when trying to measure a small velocity on a very large scale. Therefore, it is recommended that a suitable PRF be selected so that the measured velocity is comparable with the maximum measurable velocity.

During velocity measurement, ultrasound pulses are emitted at a fixed frequency and then reflect back. The instantaneous velocity profile is obtained by analyzing a certain number of pulse echoes. Therefore, the time used to get an instantaneous velocity profile will depend on the number of echoes and the emission frequency (PRF). Here, we define this time as sampling time.

To investigate the effect of sampling time on PUDV measurement, the velocity profiles of a fiber suspension at concentration of 0.3% and flow rate of 40 gpm are measured at different pulse numbers and fixed PRF. It was found that the sampling time has no significant effect on the velocity profile (Figure 4.9 (A)). However, the effect of sampling time on the rms value is obvious (Figure 4.9 (B)). With the increase of sampling time, the rms value decreases.

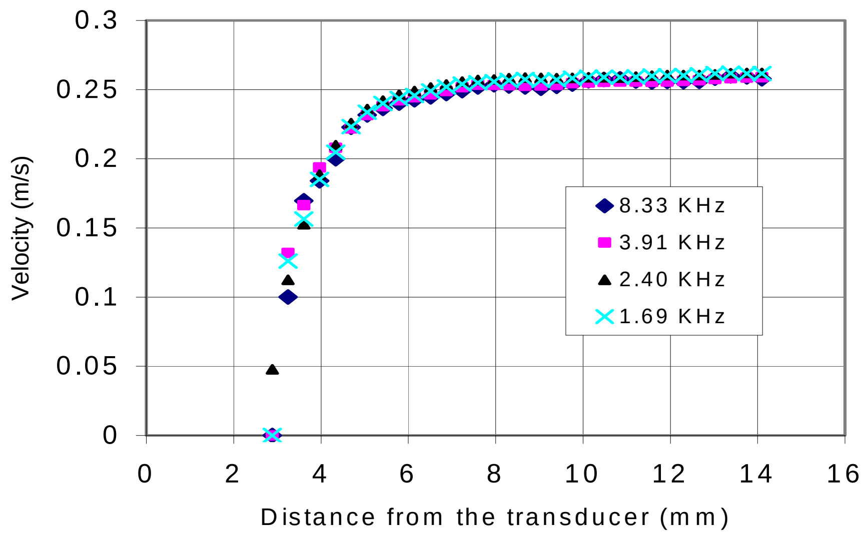

(A)

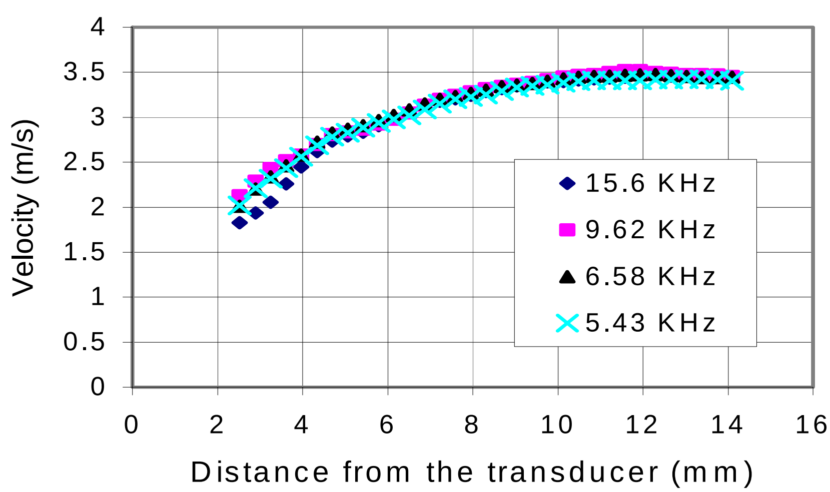

(B)

Figure 4.8 Effect of pulse repeat frequency on the PUDV measurement.
(A) mean velocity: 0.23 m/s; (B) mean velocity: 2.8 m/s

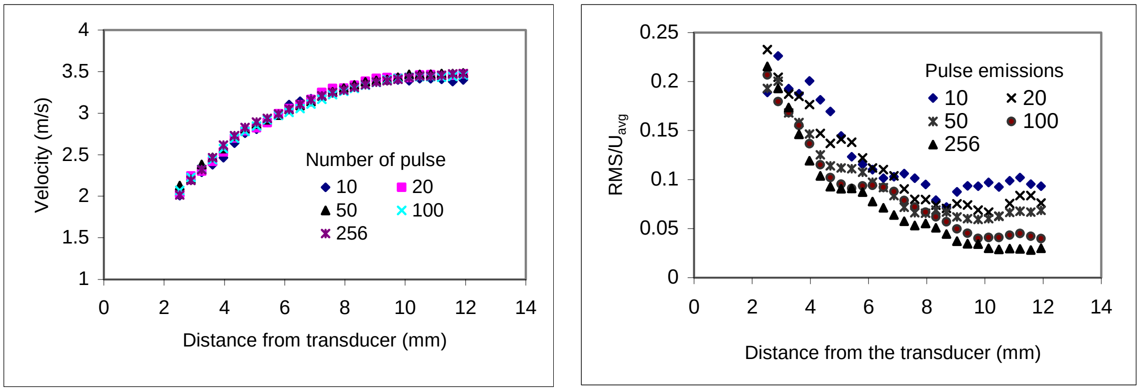

(A) (B)

Figure 4.9 The effect of pulse emissions number on velocity profile and rms values.

Another important parameter we will discuss here is sensitivity. The algorithm used to measure the Doppler frequency allows the results to be nullified when the Doppler energy is below a defined level so that the noise signal can be removed by using different levels of sensitivity. The PUDV used in this study has five levels for sensitivity parameter: "very low", "low", "medium", "high" and "very high". When “very low” is used, there is the possibility that some low Doppler energy signal will be removed; if “ very high” is used, noise signals may be collected. Figure 4.10 shows an example of how sensitivity affects the measuring results. At low flow rate (Figure 10 (A)), the low velocity value will be nullified if sensitivity is not high enough to measure the low energy Doppler signal. However, sensitivity does not have any significant effect on the measurement when velocity is larger, where there are enough particles to reflect the ultrasound (Figure 10 (B)).

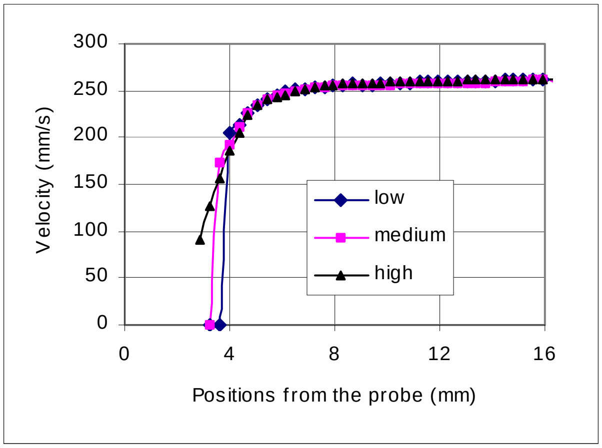

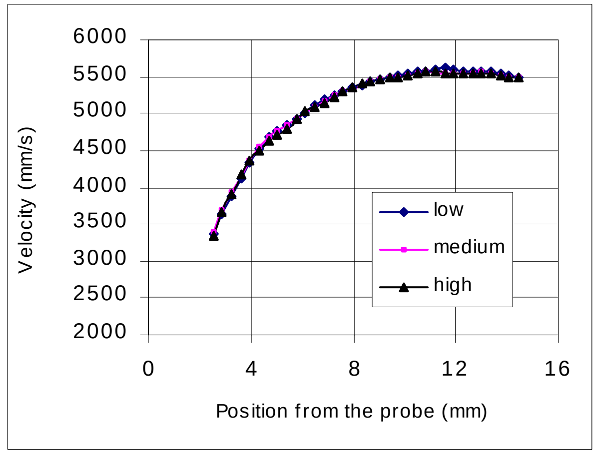

(A) (B)

Figure 4.10 The effect of sensitivity on PUDV measurement. (A) Concentration: 0.3%, mean velocity: 0.23 m/s; (B) Concentration: 0.3%, mean velocity: 4.6 m/s.

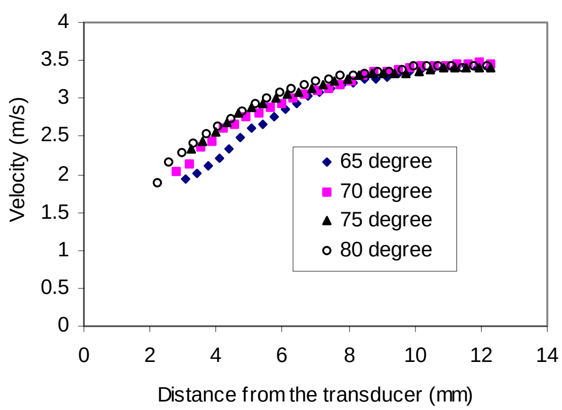

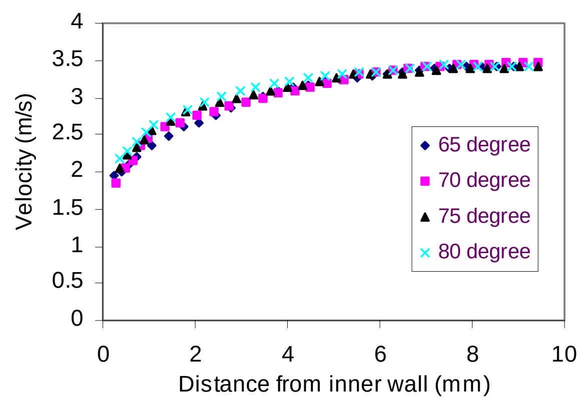

(A) (B)

Figure 4.11 Velocity profiles measured at different inclination angles. (A) raw data; (B) position adjusted.

Figure 4.11 presents the effects of transducer inclination angle on the measurement. Theoretically, the inclination angle should not have any effect on the measurement results. However, it should be noted that there is a small difference between the distances from the center of the transducer front end to the inner surface of the wall when different inclination angles are used (Figure 4.11(A)). For example, the distance will decrease about 1 mm when inclination angle changes from 65 degrees to 80 degrees for a transducer with an outer diameter of 8 mm. After position adjustment, the velocity profiles measured at different inclination angles are comparable to each other (Figure 4.11(B)).

4.7 Characteristics of PUDV

We have shown that the PUDV system can be used for noninvasive measurement of velocity profiles for fiber suspension flows. One of our concerns, when considering the potential application of PUDV in the pulp and paper industry, is the maximum measurable velocity and depth that can be detected.

First, consider the maximum measurable depth that can be detected by PUDV. This is determined by the pulse repeat frequency because the PRF period must be long enough so that each transmitted burst occurs after the reception of the echo from the previous burst. The following expression shows the relationship between the pulse repetition rate, PRF, and the depth (Fry 1978):

$$PRF_{max} = \frac{c}{2R_{max}} \tag{4.4}$$

Here, PRF_{max} is the maximum pulse repetition frequency; c is the ultrasound speed in the medium; R_{max} is the maximum depth that can be detected.

The maximum detectable velocity is determined by the maximum measurable Doppler shift frequency. According to Nyquist sampling theory, to adequately describe a signal, it must be sampled at a frequency equal to, or higher than, twice the highest frequency present. This requirement places a restriction on the maximum detectable Doppler frequency:

$$f_{max}^{D} < PRF_{max}/2 \tag{4.5}$$

Substitute this equation into the Doppler shift Equation 2.13, the maximum detectable velocity will be:

$$V_{max} = \frac{c \cdot PRF}{4 f_0 \cos\theta} \tag{4.6}$$

Combing this equation with Equation 4.4, we have the relation between the maximum measurable velocity and maximum detectable depth:

$$V_{max} = \frac{c^2}{8 f_0 R_{max} \cos\theta} \tag{4.7}$$

This shows that the larger the velocity to be measured, the smaller the maximum detectable depth. Table 4.3 shows the maximum measurable streamwise velocity and detectable depth for Model 1032 PUDV when different inclination angles were used. By using a suitable combination of basic ultrasound frequency, measuring depth, and inclination angles, the PUDV can be used to monitor the pulp suspension flow (e.g., forming jet) during the papermaking process.

Table 4.3 The maximum measurable velocity and depth for Model 1032 PUDV.

Maximum measurable distance (mm)	Doppler angle (degree)	Maximum velocity (m/s)	
		4MHz	2MHz
20	70	8.2	16.5
	75	11	22
	80	16.4	32.8
	82	20.4	40.4
30	70	5.47	11.00
	75	7.33	14.67
	80	10.93	21.87
	82	13.60	26.93

In order to verify that PUDV can be used to measure fiber suspension at higher velocity, additional measurements are carried out in a small channel 60 cm long, 3.3 cm wide and 1 cm high. This is an open channel and it is inserted directly into the channel described in Section 3.2. A 2 MHz transducer is installed outside of the top wall with an inclination angle of 75° to the flow direction. An ultrasonic gel is used as a coupling medium. Figure 4.12 shows the measured velocity profile of fiber suspension flowing at the maximum capacity of the flow system. The maximum velocity detected in this experiment is about 14.5 m/s. In addition, it is surprising to find that at such velocity, there is no significant difference among the velocity profiles for fiber suspensions at different concentrations. This flow behavior at high flow rate will be discussed in detail in Chapter 5.

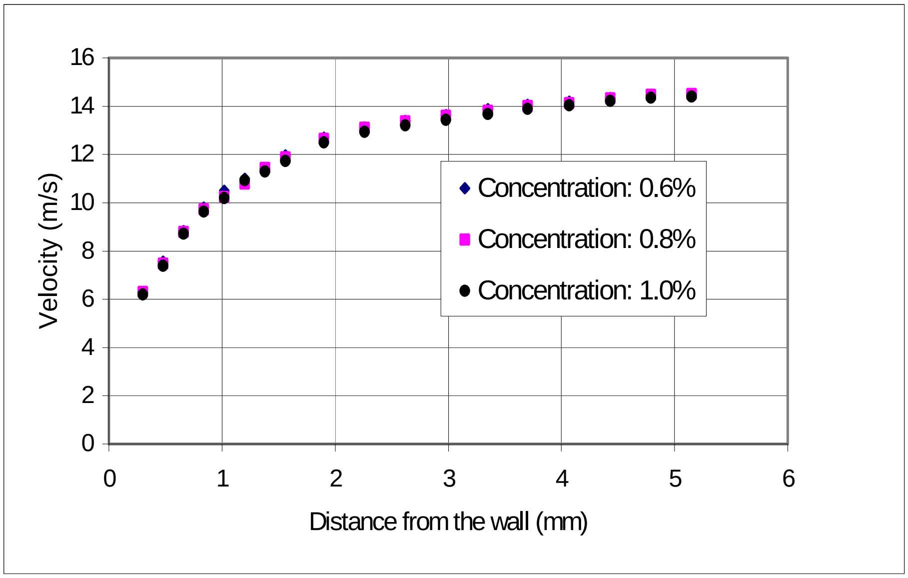

Figure 4.12 Velocity profile of fiber suspensions in a channel of 3.3 cm wide and 1cm high.

Another important characteristic of PUDV is its spatial resolution. In a pulsed Doppler system, short bursts of acoustic energy are transmitted by amplitude modulation of a carrier frequency. The returning signal is sampled at a specific delay time from the transmission of each pulse. As a consequence, the sampled portions of the returning signal corresponding to a backscattered acoustic energy originating from a specific region of space is called sample volume. The spatial resolution of a Doppler system is determined by the size of the sample volume. The lateral size of the sample volume is determined by the ultrasonic beam size. The length of the sample volume corresponds to the distance ultrasound travels in one-half the transmitted burst duration:

$$S_l = \frac{c \cdot t_b}{2} \tag{4.8}$$

where S_l is the sample volume length, c is the sound velocity at the medium, and t_b is the burst duration. For the 4 MHz transducer used in this study, the theoretical sample volume is 5 mm in diameter, 0.375 mm in length. However, the time for the integration of the signal will reduce the depth resolution. The actual resolution in the depth direction is 0.9 mm.

4.8 Summary

The investigation in this chapter demonstrates that Pulsed Ultrasonic Doppler Velocimetry is an effective technique for the velocity profile measurement of fiber suspension flows. By measuring the mean velocity of pure water flow in the turbulent region, it was found that the measured results fit very well with the theoretical values and LDA measuring results. To avoid the static error caused by local velocity fluctuation during the measurement, it is recommended that a sampling number higher than 256 be used. When applied to pulp fiber suspension flow measurements at different flow rates and different fiber concentrations, the experiments show that PUDV has a high repeatability and it also has high sensitivity for detecting small velocity changes.

The selection of several measuring parameters may have effects on the velocity profile. The most important parameter during velocity profile measurement is pulse repetition frequency (PRF), which has a significant effect on the maximum measurable velocity. To reduce the measurement errors, it is recommended that a suitable PRF be selected so that the measured velocity is comparable to the scale of maximum measurable velocity. The sampling time does not have a significant effect on the mean velocity profile measurement. However, experiments show that with increased sampling time, the rms values will decrease. The parameter of "sensitivity" is used to control the signal noise ratio. At low flow rate, where the signal strength is weak, high sensitivity of PUDV should be selected so that the low strength signal will not be nullified. When the transducer is set up at different inclination angles, there will be a small difference between the distance from the center of the transducer to the fluid surface. After position adjustments, however, the velocity profiles measured at different inclination angles are comparable to each other.

The maximum depth and the maximum velocity that PUDV can detect are determined by pulse repetition frequency, inclination angles, and ultrasound frequency. Although higher measurable velocity can only be obtained at the cost of the maximum detectable depth, by adjusting the measuring parameters it can become a useful tool for measuring fiber suspension flow up to a velocity comparable to the papermaking process.

5. CHARACTERIZATIONS OF FIBER SUSPENSION FLOW

5.1 Introduction

In the pulp and paper industry, the flow of fiber suspensions occurs at various velocities and various concentrations through pumps, pipes, valves, tanks, cleaners, screens, and headboxes. The knowledge of flow mechanisms is of fundamental importance, yet the understanding of those mechanisms is only superficial. This is because the experimental results differ and the sources of differences are unknown (Duffy 1976, Bodenheimer 1969, Brecht 1950, Robertson 1957). The understanding of fiber suspension flow behavior is obscured by contradictory conclusions that have been drawn by different investigations.

The objective of this chapter is to investigate the behavior of fiber suspension flow through the velocity profile and friction loss measurements under different fiber concentrations and flow rates. In addition, it is hoped to resolve contradictions in the literature on how fiber concentration and flow rate affect velocity profiles.

Section 5.2 presents the velocity profile results at different flow rates and fiber concentrations. The effect of fiber concentration and flow rates on the velocity profiles are analyzed as well. Section 5.3 provides the turbulence intensity data of fiber suspension flow at mean velocity ranging from 0.91 m/s to 7.0 m/s. The characterizations of fiber suspension flow at different flow rates and fiber concentrations are summarized in Section 5.4. In addition, a mathematical model is used to describe the velocity profiles measured at different flow conditions. A schematic diagram is presented to illustrate the different flow regions in the fiber concentration-Reynolds number space. In Section 5.5, a mathematical model based on log-law and wake function was proposed to predict the velocity profiles in terms of the Reynolds number (Re) and fiber concentration (nl^3) in the turbulent flow regime. The flow mechanism in different flow regimes is discussed in Section 5.6. Here, the effect of fiber flocculation on the momentum transfer of suspension flow is proposed to explain the shape changes of velocity profiles. Section 5.7 gives the friction factor data of fiber suspension flow at different concentrations. Section 5.8 analyzes how plug size changes with the flow rate and the disruptive shear stress acting on the surface of the plug.

5.2 Velocity Profile of Fiber Suspension in Rectangular Channel

In order to study the characterization of fiber suspension flow, velocity profile measurements are carried out at seven concentrations ranging from 0.05% to 1.0% and eight mean velocities ranging from 0.15 m/s to 7.0 m/s. The detailed test conditions at different mean velocities and fiber concentrations are shown in Table 1. In Table 1, the corresponding flow rate, the Reynolds numbers based on water density and viscosity, and calculated nl^3 based on average fiber length of 2.3 mm and aspect ratio of 60 are listed. In this chapter, fiber concentration will be expressed in either volume percentage or nl^3. The measured velocity profile results at each flow condition are attached in Appendix II. Figure 5.1 to Figure 5.7 provide the dimensionless velocity profiles at different fiber concentrations.

Table 5.1 Experiment conditions for velocity profile measurements.

Flow rate (gpm)	Uavg (m/s)	Re	Concentration (%)/nl^3						
			0.05/ 0.33	0.1/ 0.67	0.15/ 1.0	0.3/ 2.0	0.5/ 3.3	0.75/ 5.0	1.0/ 6.7
2.2	0.15	2000		X	X	X	X	X	
3.3	0.23	3000		X	X	X	X	X	X
6.5	0.45	6000		X	X	X	X	X	X
13	0.91	12000	X	X	X	X	X	X	X
40	2.80	37000	X	X	X	X	X	X	X
65	4.60	60000	X	X	X	X	X	X	X
80	5.60	73000	X	X	X	X	X	X	X
100	7.00	92000	X	X	X	X	X	X	X

According to the value of nl^3, the fiber suspensions belong to dilute suspension category if fiber concentration is equal to or less than 0.15% (nl^3<1). On the other hand, when fiber concentration increases to 0.3% (nl^3 = 2), the suspension belongs to semi-dilute suspension category. It is expected that the fiber suspension in different categories will exhibit different flow behaviors.

First, we examine how velocity profiles change with the flow rate at the same fiber concentration. Figure 5.1, Figure 5.2, and Figure 5.3 show the velocity profiles of fiber suspensions in the low particle category. At this concentration range, the fiber concentration has less effect on the flow behavior and velocity profiles are similar to that of water. With the increase of flow rates, the velocity profile changes from laminar flow to fully developed turbulent flow. Under these low fiber concentrations, fibers cannot form a coherent network in the suspension even at low flow rates.

When fiber concentration increases to 0.3% ($nl^3 = 2$, Figure 5.4), the flow pattern changes significantly and the flow rate has a large effect on the shape of the measured velocity profiles. When Re ≥ 12000, the entire velocity profile becomes sharper with the decrease of Reynolds number. When Reynolds number is reduced to 6000, the center part of the profile becomes blunter gradually while the outside part of the profile becomes sharper. With the further decrease of Reynolds number, at Reynolds number of 3000 and 2000, fibers interlock with each other and a coherent network forms in the center of the channel. This phenomenon has been observed by many other researchers and is widely reported in the literature. Such networks have well-defined mechanical strength properties. For example, if a fiber network is subjected to a shear stress, it deforms in a manner similar to that of a viscoelastic solid provided the yield value is not exceeded (Norman 1977).

At higher fiber concentrations, the effect of flow rate on the velocity profiles remains similar to that of fiber concentration at 0.3% ($nl^3 = 2.0$). The only difference is that the flow rate at which plug begins to form increases and the size of the central plug becomes larger at the same flow rate (Figure 5.5, Figure 5.6, and Figure 5.7).

As has been observed, fiber concentration has a significant effect on the shape of the velocity profile. To further study the effect of fiber concentrations on the flow behavior, the dimensionless velocity profiles are grouped by fiber concentrations and redrawn in Figure 5.8 to Figure 5.15. The effect of fiber concentrations on the shape of the velocity profiles can be characterized according to the different Reynolds numbers.

At low Reynolds number (Re ≤ 12000), the center part of the velocity profile becomes flat and a central plug is formed if fiber concentration is higher than 0.3% ($nl^3 = 2.0$). At the same Reynolds numbers, the plug size increases with the fiber concentrations (Figure 5.8 to Figure 5.11).

At higher Reynolds number (Re ≥ 37000), fiber concentration does not have any significant effect on the shape of the velocity profile (Figure 5.12 to Figure 5.15). The only effect is that the velocity profiles of the fiber suspension become sharper when compared with the velocity profile of water flow. The deviation from the velocity profile of water flow becomes larger as the fiber concentration increases. However, this deviation becomes smaller with the increase of Reynolds number. Finally, at Reynolds number of 92000, fiber concentration has almost no effect on the velocity profiles and all the velocity profiles tend to be the same as that of water (Figure 5.15).

5.3 The Turbulence Intensity of Fiber Suspension Flow

There have been several attempts to measure turbulence in fiber suspension using impact probes and various diffusion techniques. However, because of the low frequency response of the measuring system and heavy fiber buildup on the probe tip, this kind of probe can only measure large-scale variations.

Pulsed Ultrasonic Doppler Velocimetry can measure local velocity at a relatively short sampling time. Therefore, the fluctuation of local instantaneous velocities will be reflected in the measuring results. It is possible to calculate the turbulence intensity based on the variation of all local velocity measurements. Figure 5.16 shows the turbulence intensity $\sqrt{\overline{u'^2}}/U$ plotted versus the distance from the probe for fiber suspension flow at different fiber concentrations. As shown in Figure 5.16, the effect of different factors on turbulence intensity can be summarized as follows:

(1) From the center of the channel to the wall region, turbulence intensity increased gradually.

(2) With an increase of fiber concentration, turbulence intensity was reduced.

(3) With an increase of Reynolds number, the effect of fiber concentration on the turbulence intensity decreases gradually and finally, if the Reynolds number is high enough, fiber concentration has almost no effect on turbulence intensity.

(4) If a plug forms in the center of the channel (Figure 5.16A), the turbulence intensity decreases significantly in the plug region and is almost uniform in all these regions. In the region outside the plug, the flow is still turbulent and the intensity is much higher than that of the plug region.

It should be noted that, because of the limitations of the measuring method, different sampling times were used when measuring velocity profiles at different Reynolds numbers. For example, the sampling time at Reynolds number of 12000 and 92000 is 51.2 and 18.4 ms, respectively. On the other hand, because of the large sample volume used during measurement (5 mm in diameter, 0.9 mm in length), the turbulence intensity is actually the velocity fluctuation in the sample volume. However, the information we get here is still valuable. It confirms the results reported by Daily and Bugliarello (1958) and provides an insight in understanding the turbulent structure and flow mechanisms of fiber suspensions. Section 5.6 will provide further explanation of how turbulence affects the momentum transfer and flow mechanisms in the fiber suspension flow.

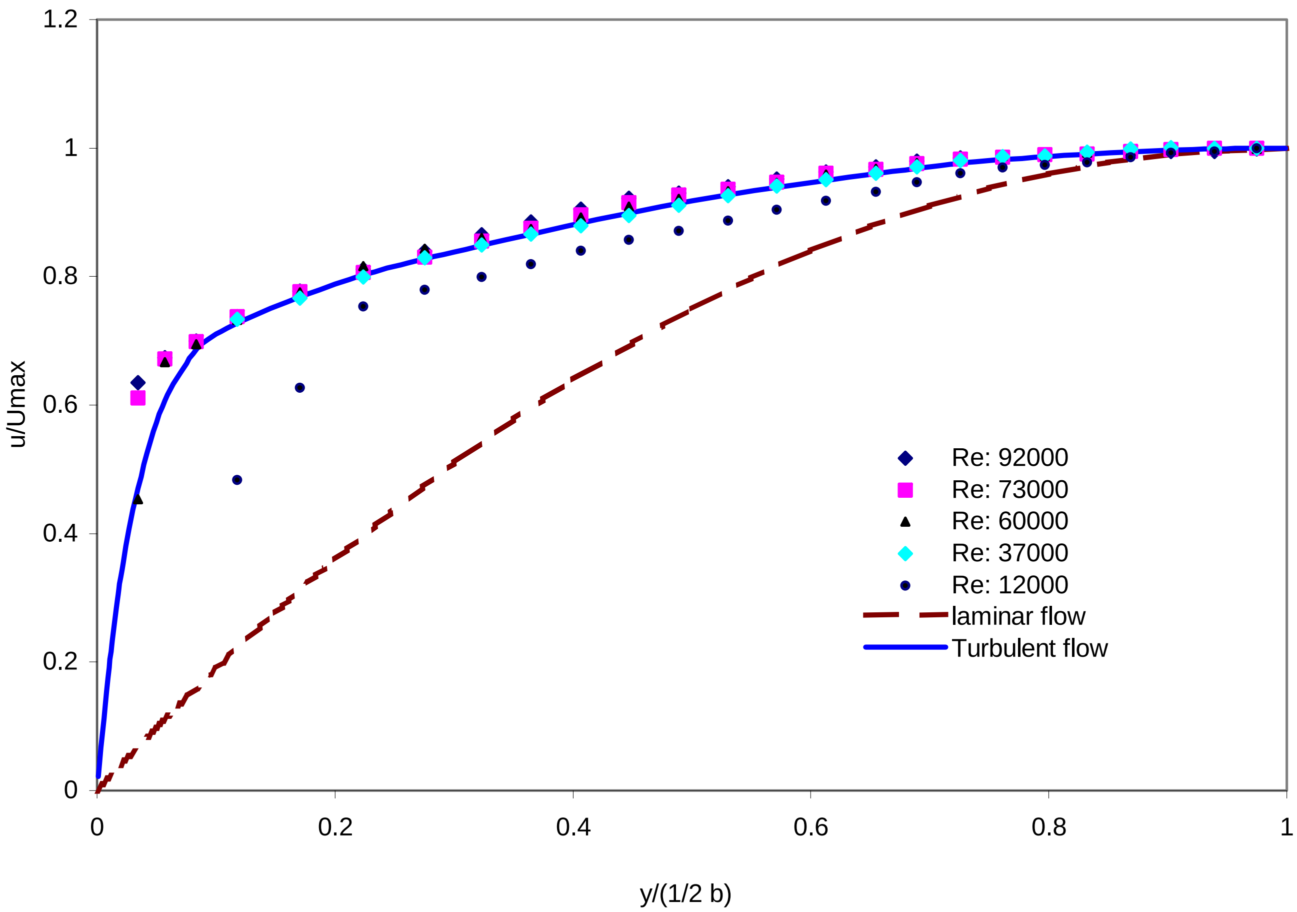

Figure 5.1 Velocity profiles of fiber suspensions at fiber concentration of 0.05% (nl^3 = 0.33).

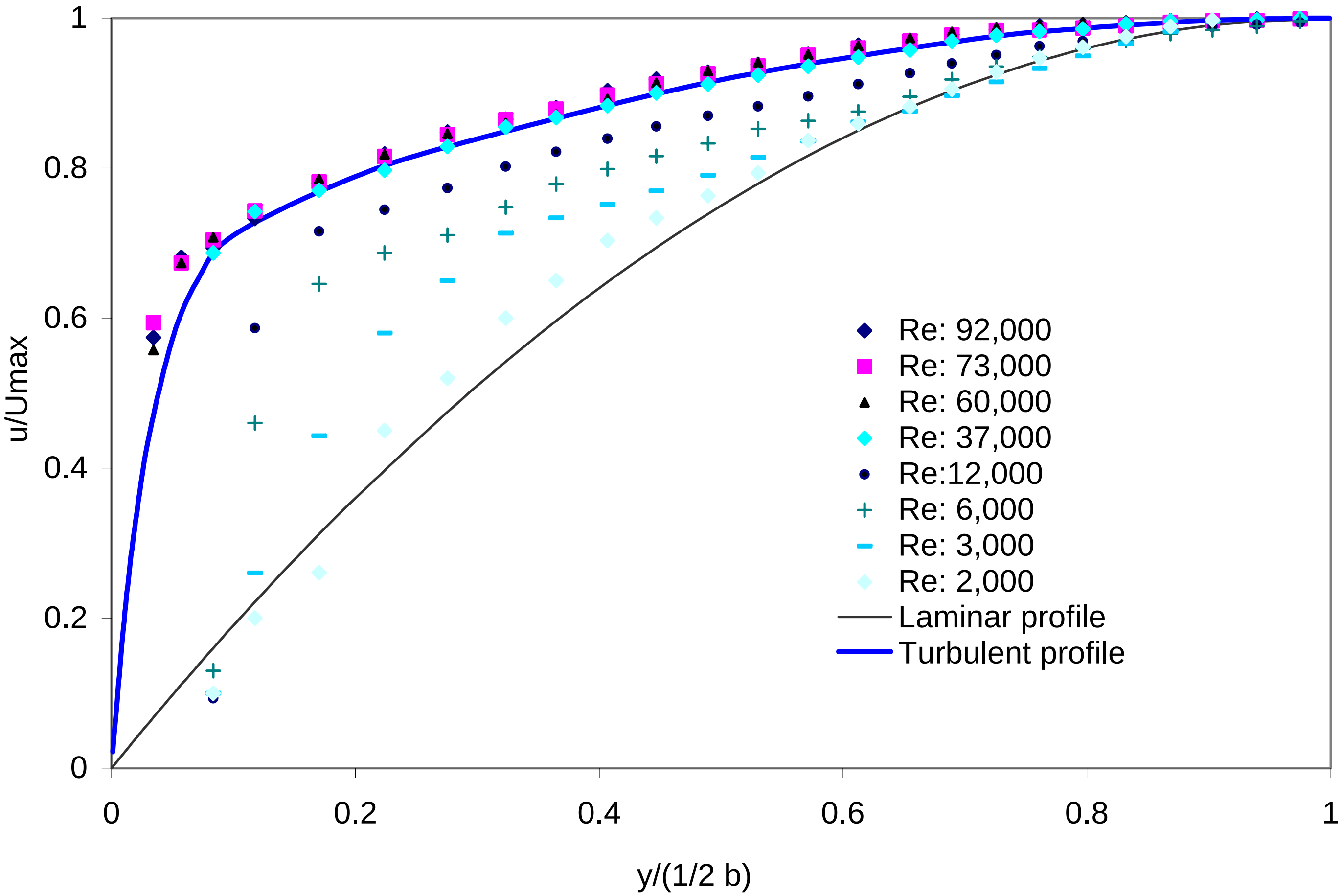

Figure 5.2 Velocity profiles of fiber suspensions at fiber concentration of 0.10% ($nl^3 = 0.67$).

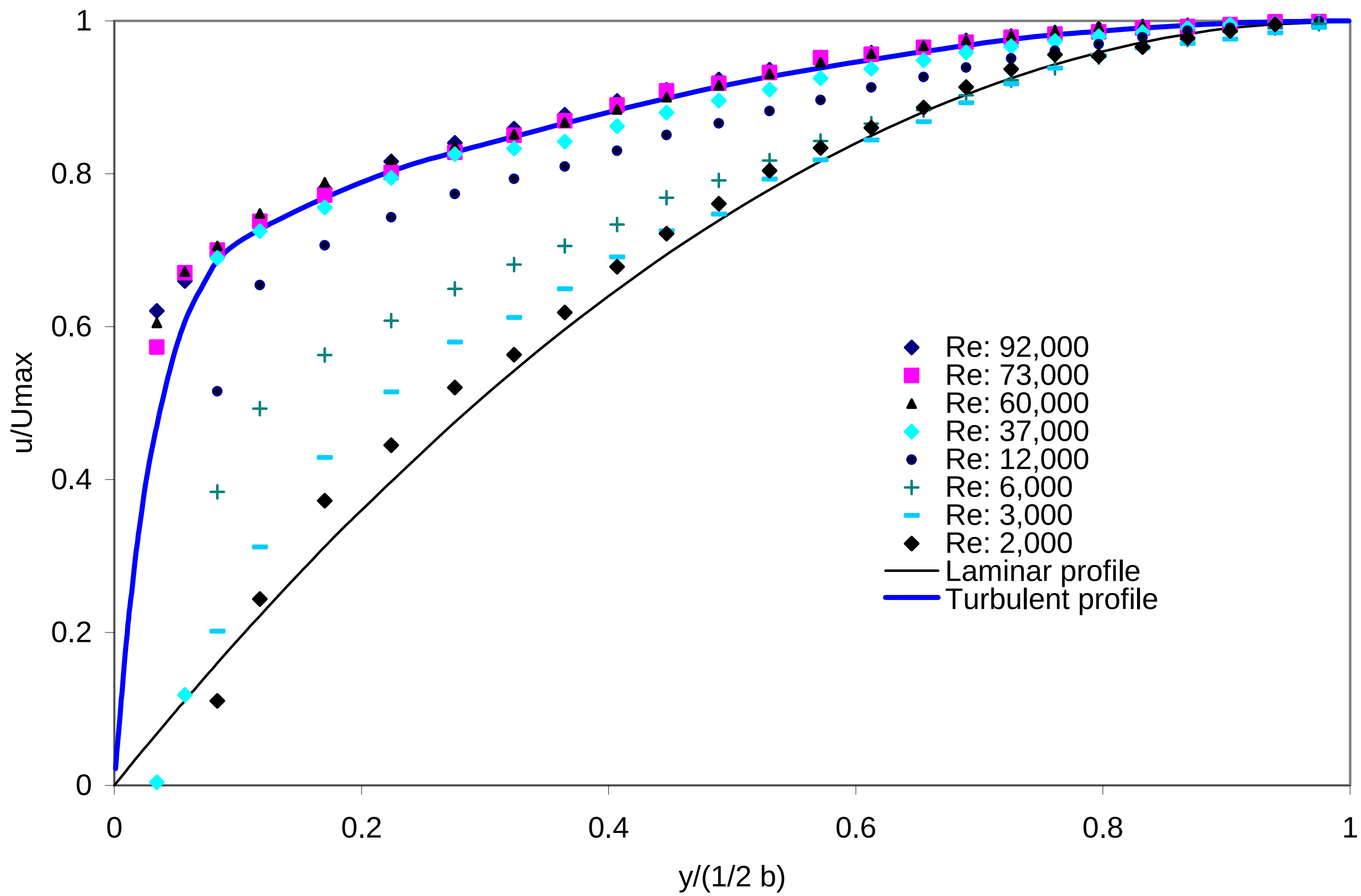

Figure 5.3 Velocity profiles of fiber suspensions at fiber concentration of 0.15% (nl^3 =1.0).

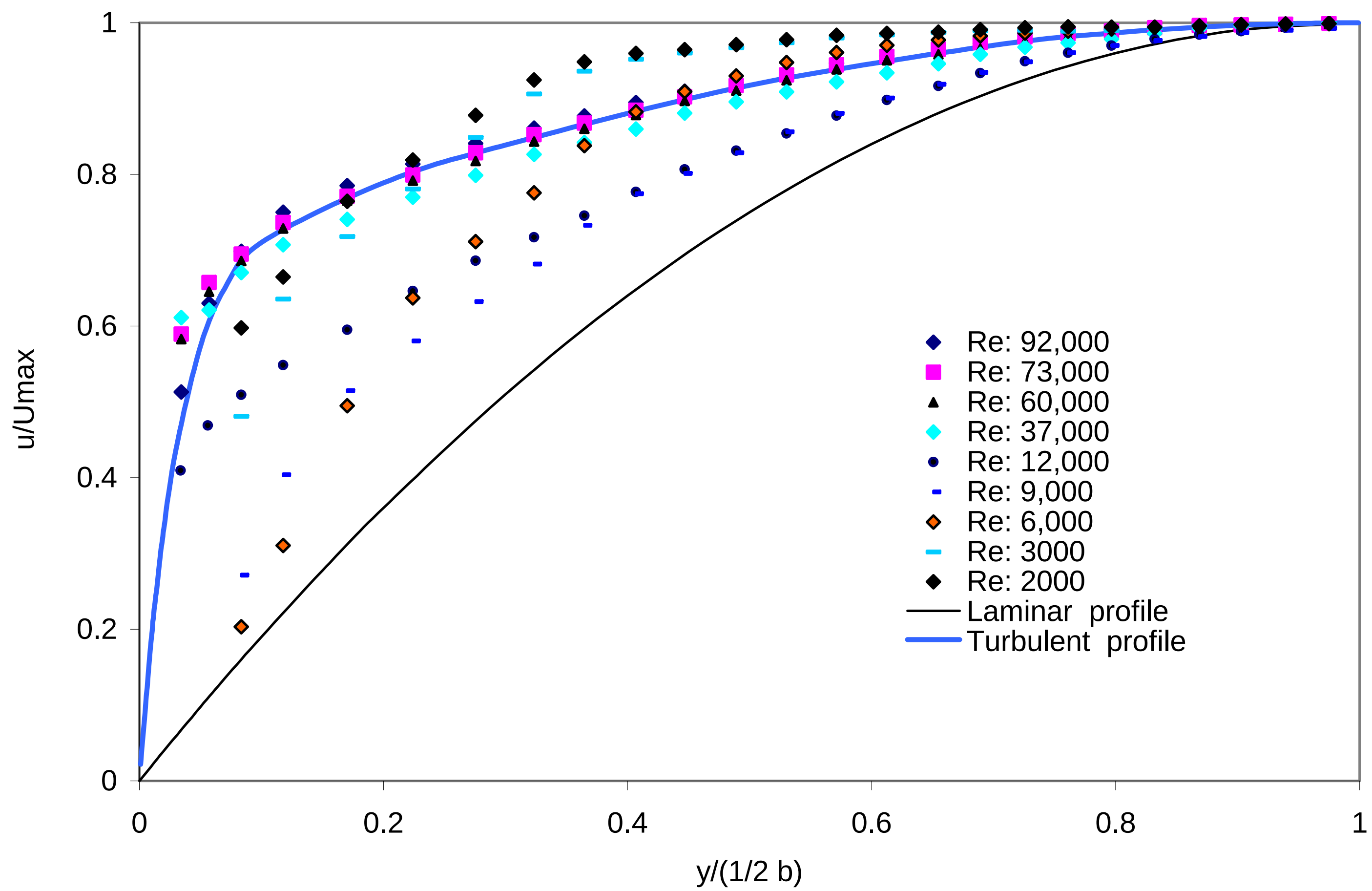

Figure 5.4 Velocity profiles of fiber suspensions at fiber concentration of 0.30% ($nl^3 = 2.0$).

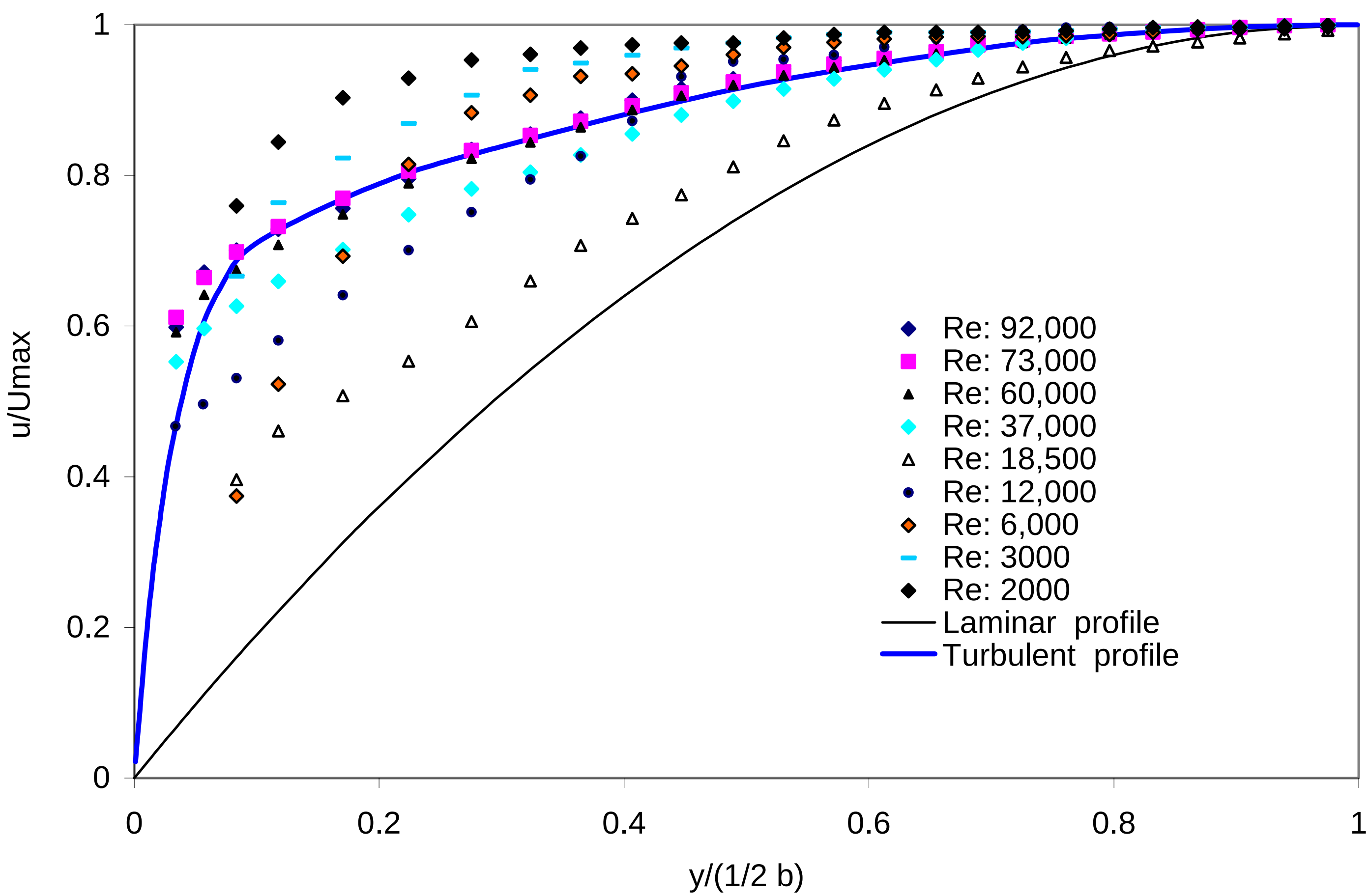

Figure 5.5 Velocity profiles of fiber suspensions at fiber concentration of 0.50% (nl^3 = 3.3).

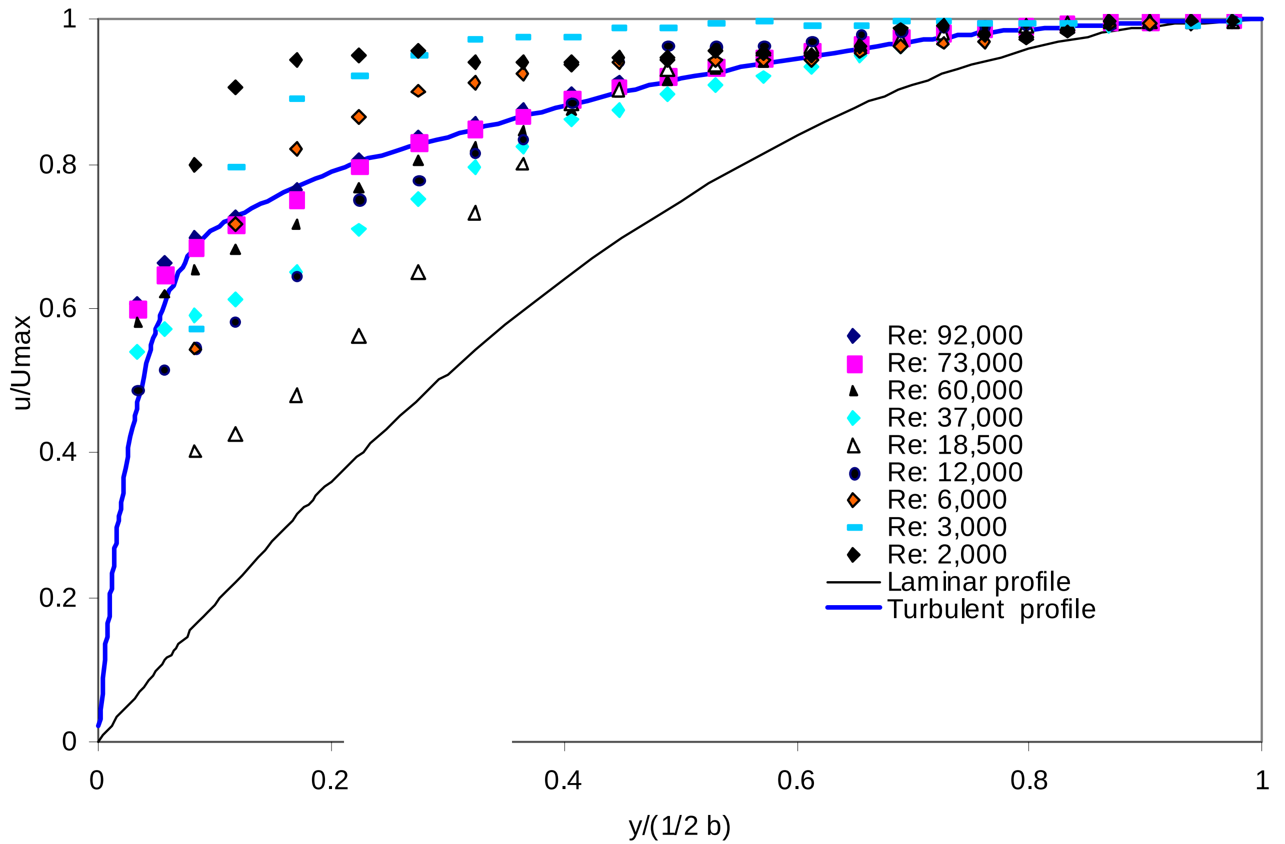

Figure 5.6 Velocity Profiles of fiber suspensions with concentration of 0.75% ($nl^3 = 5.0$).

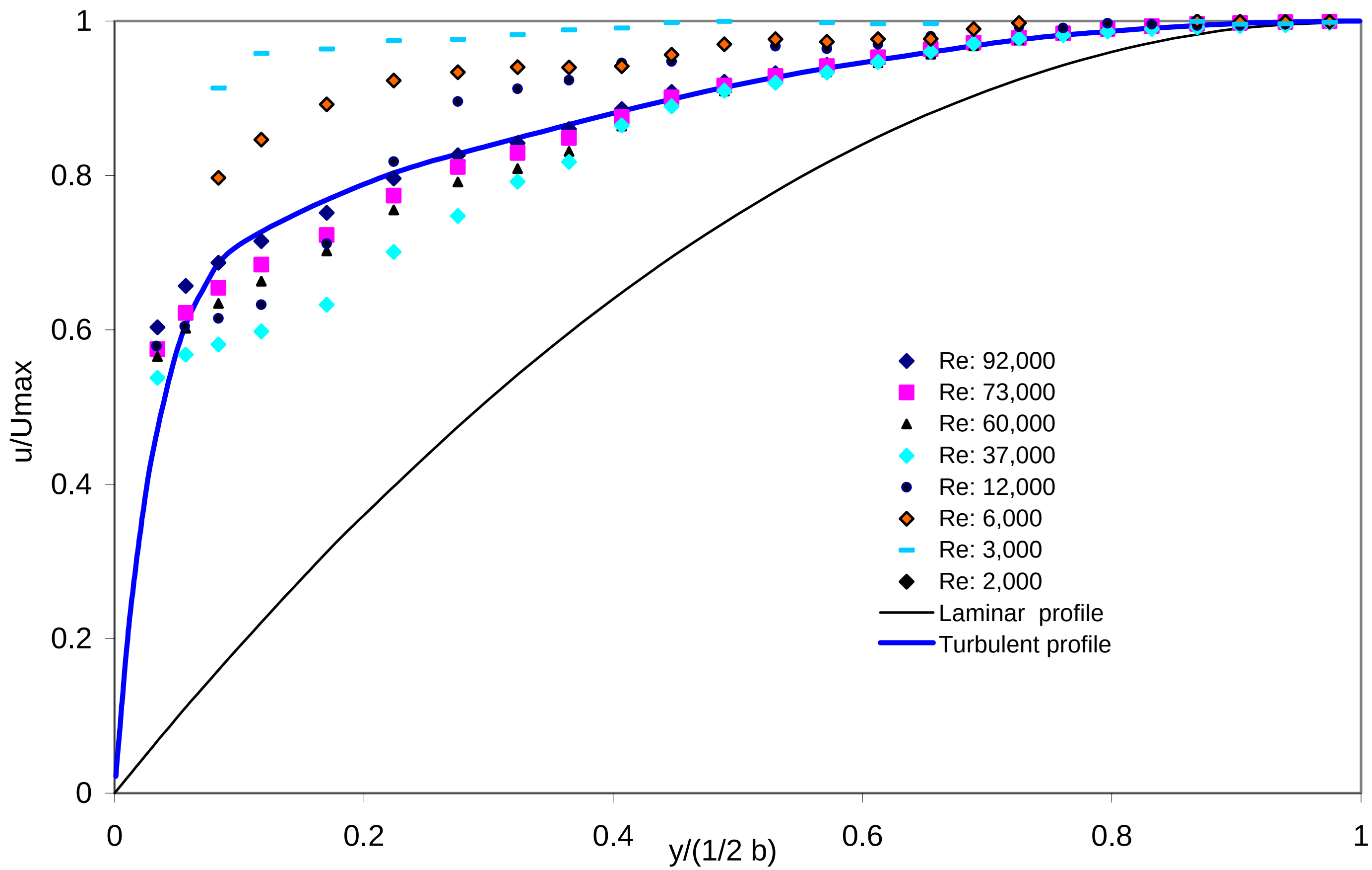

Figure 5.7 Velocity profiles of fiber suspensions with concentration of 1.0% ($nl^3 = 6.7$).

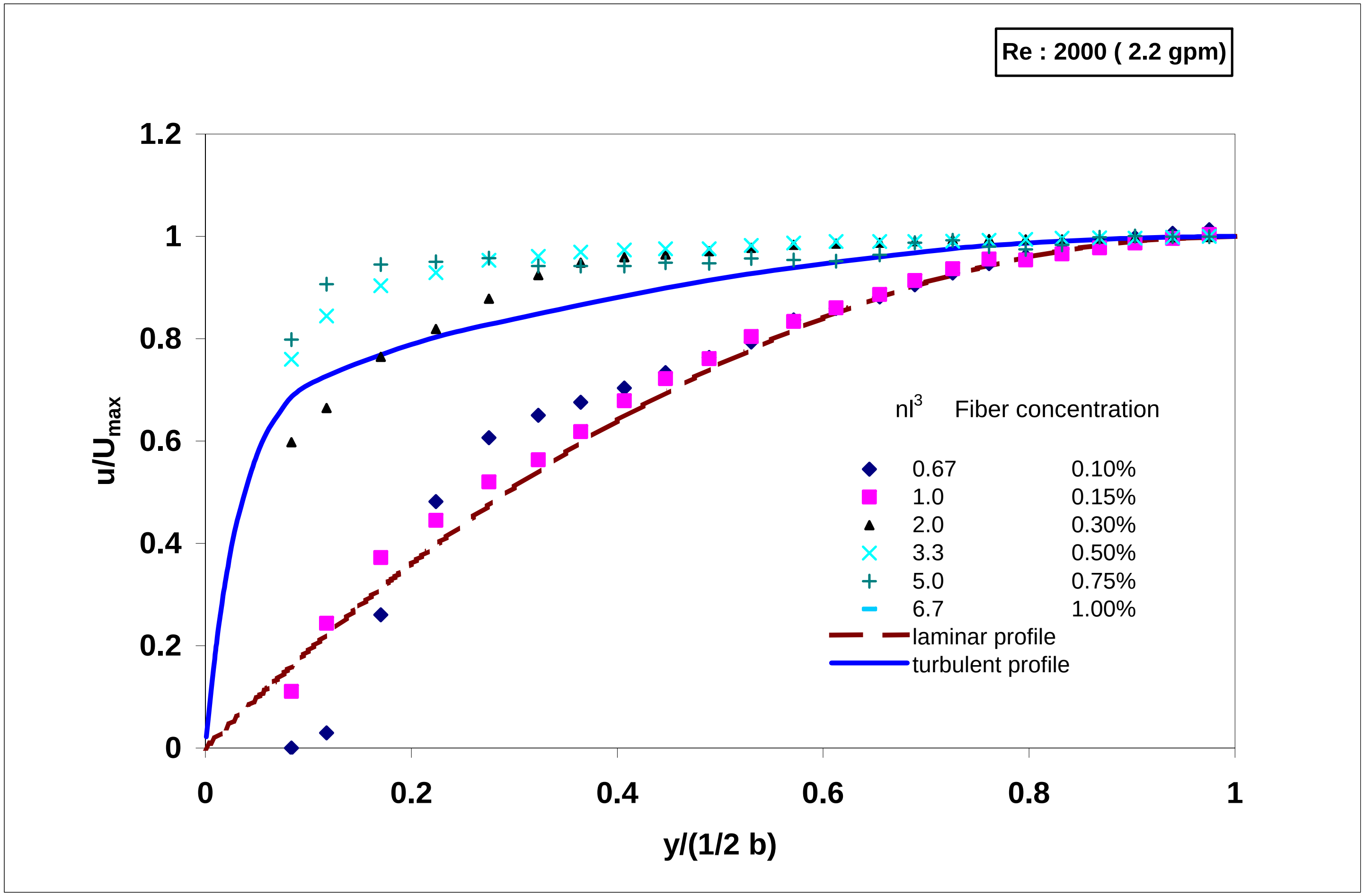

Figure 5.8 Velocity profiles of fiber suspensions at Reynolds number of 2000.

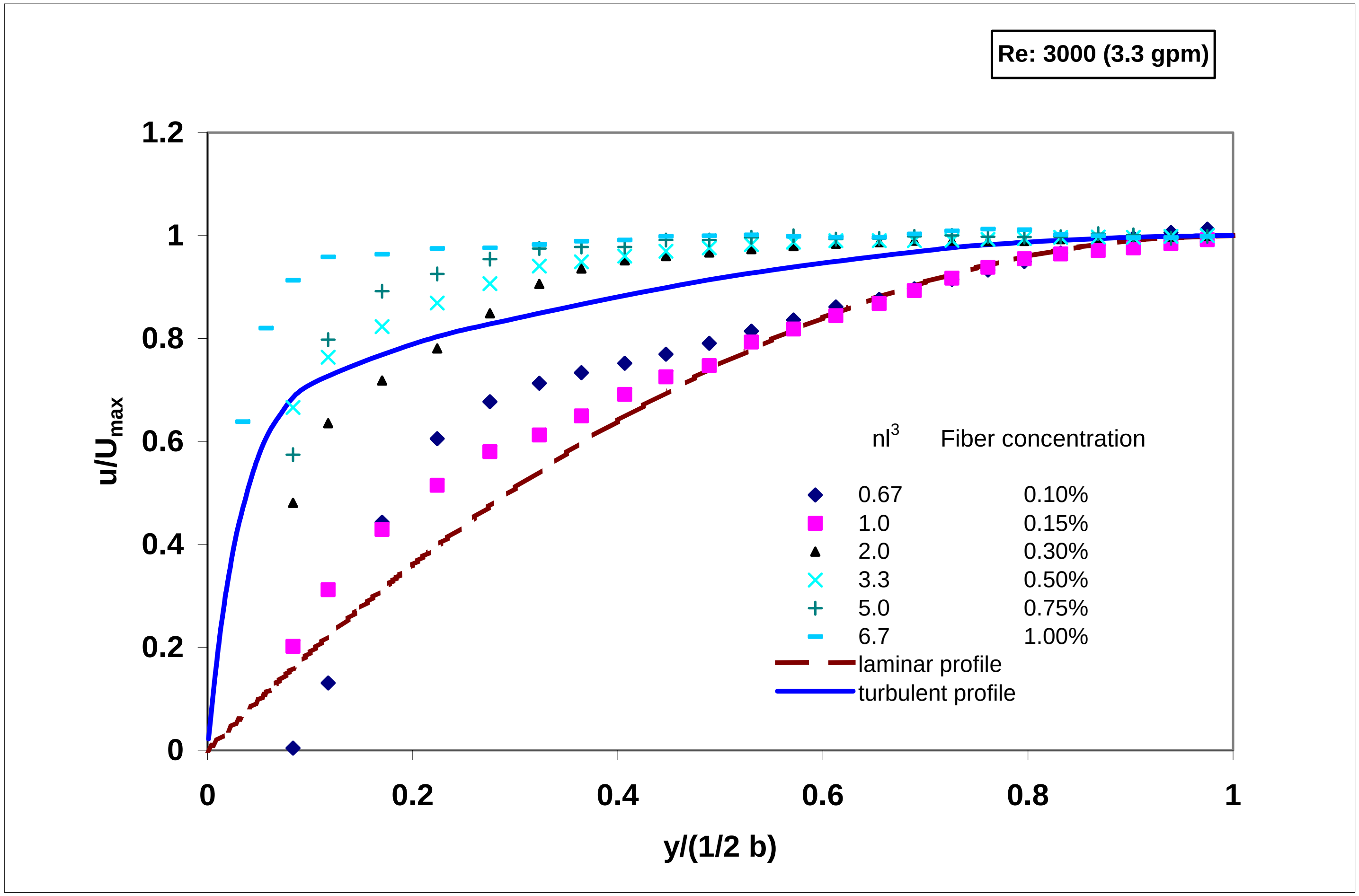

Figure 5.9 Velocity profiles of fiber suspensions at Reynolds number of 3000.

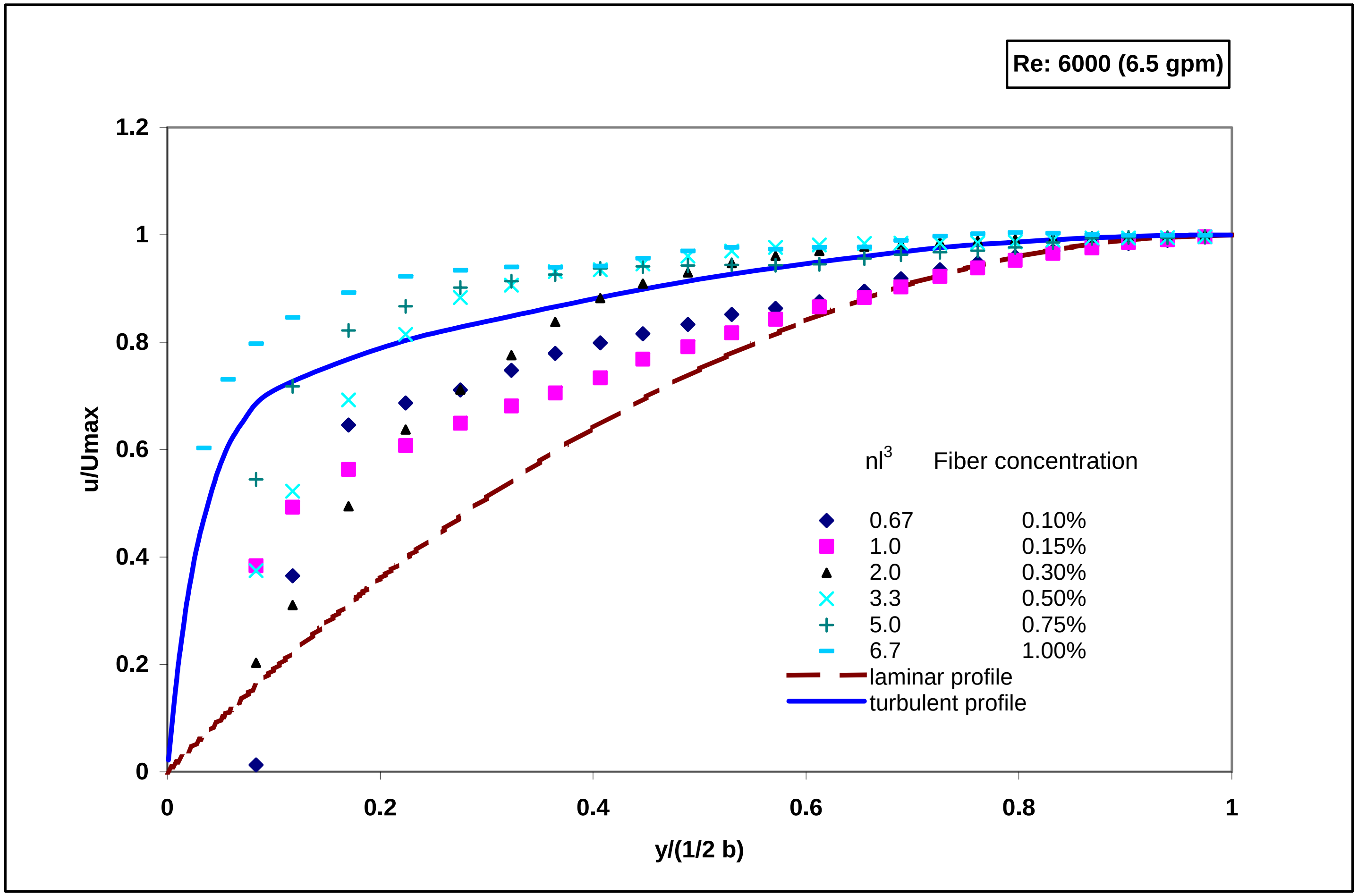

Figure 5.10 Velocity profiles of fiber suspensions at Reynolds number of 6000.

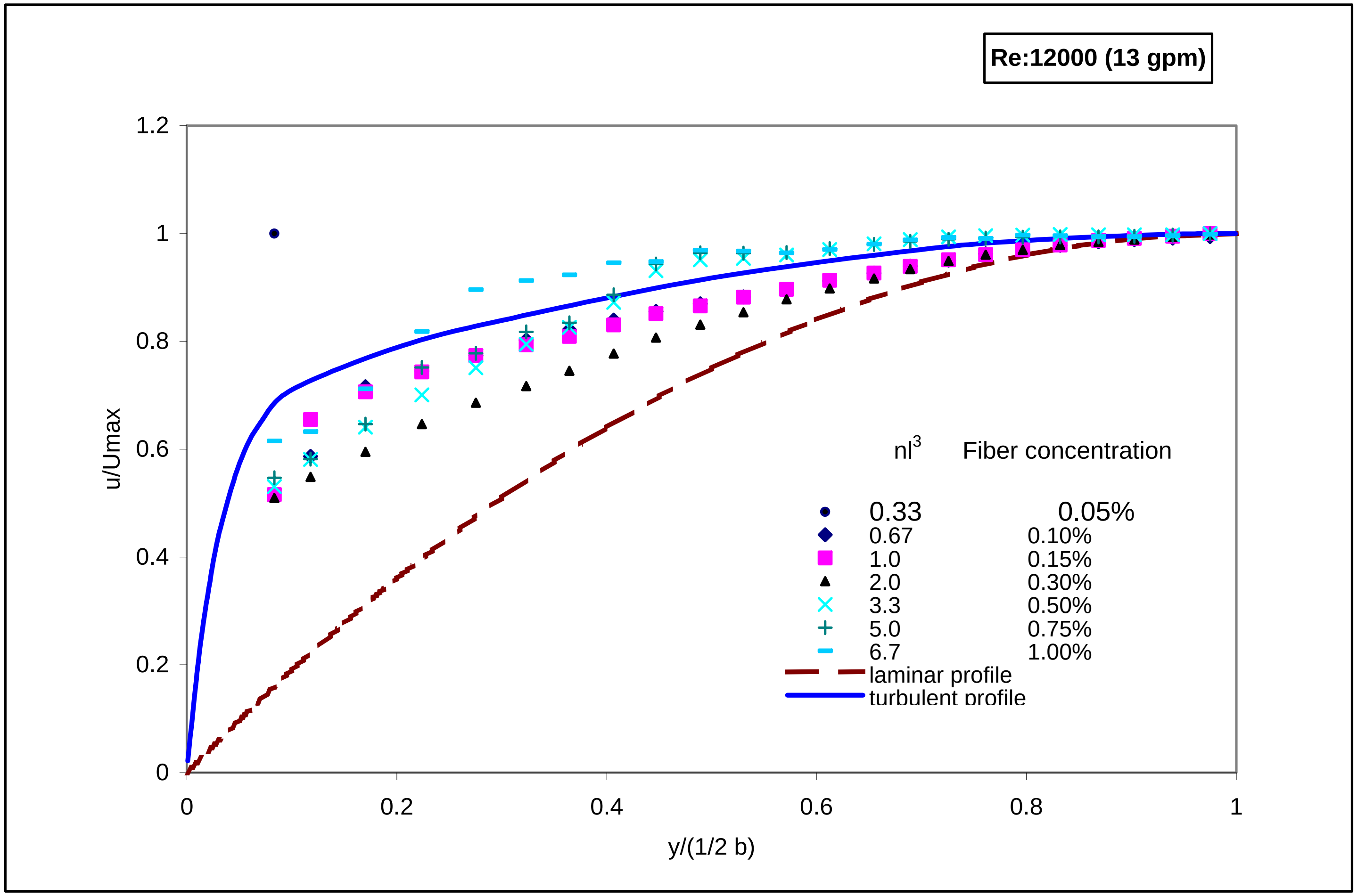

Figure 5.11 Velocity profiles of fiber suspensions at Reynolds number of 12000.

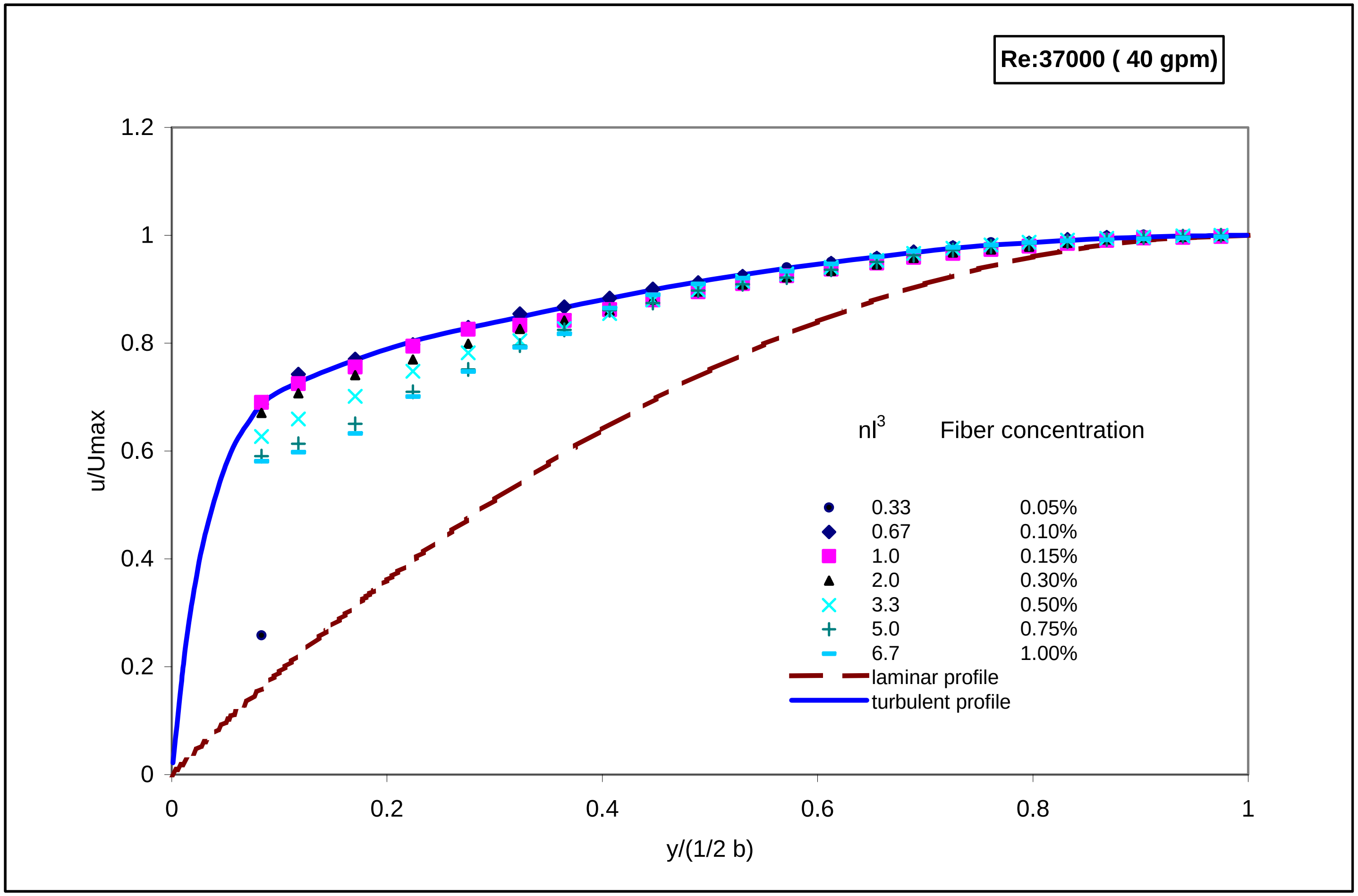

Figure 5.12 Velocity profiles of fiber suspensions at Reynolds number of 37000.

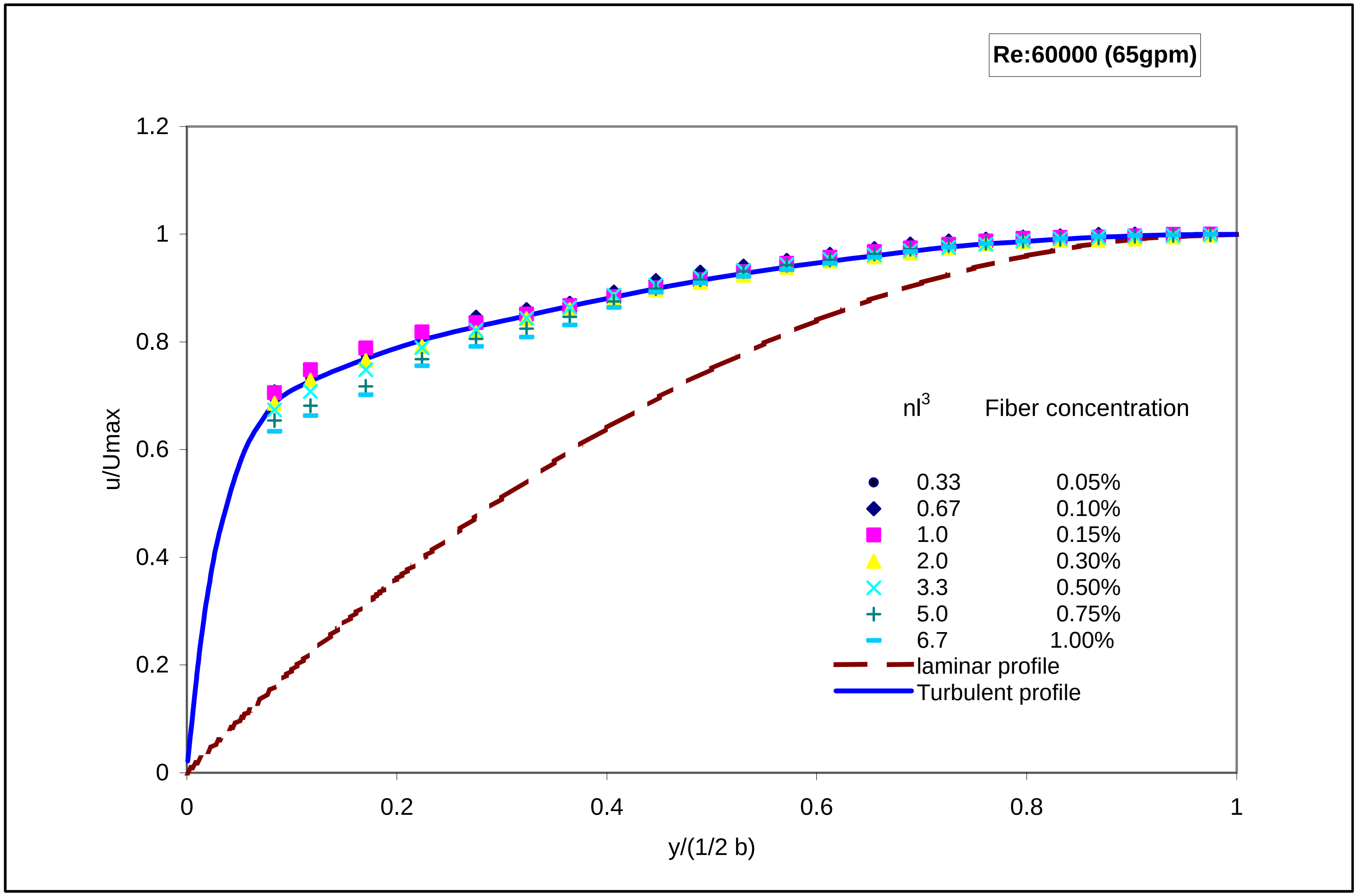

Figure 5.13 Velocity profiles of fiber suspensions at Reynolds number of 60000.

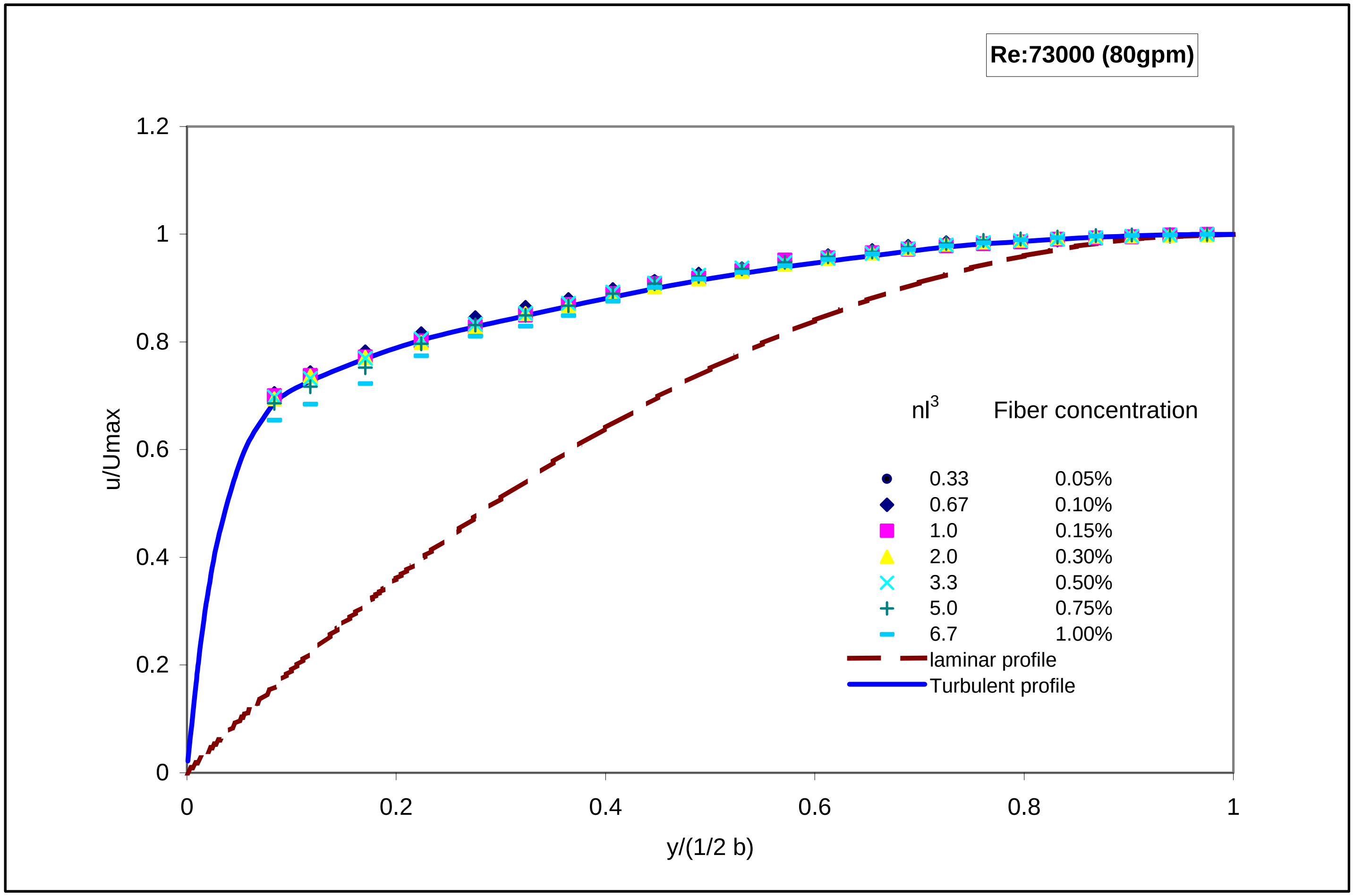

Figure 5.14 Velocity profiles of fiber suspensions at Reynolds number of 73000.

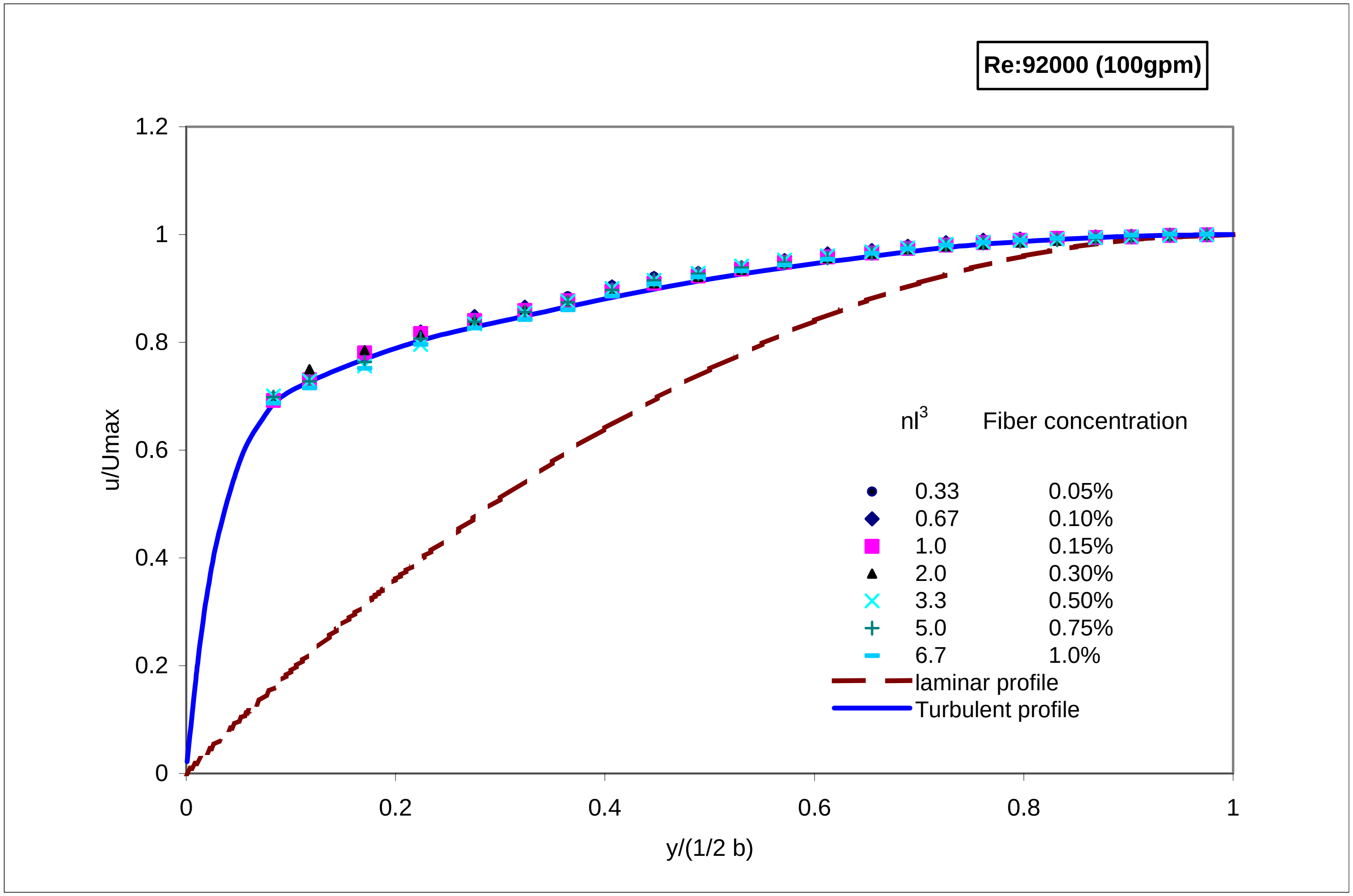

Figure 5.15 Velocity profiles of fiber suspensions at Reynolds number of 92000.

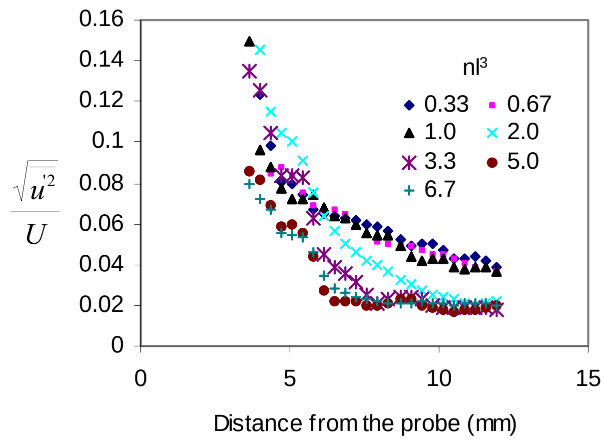

(A)

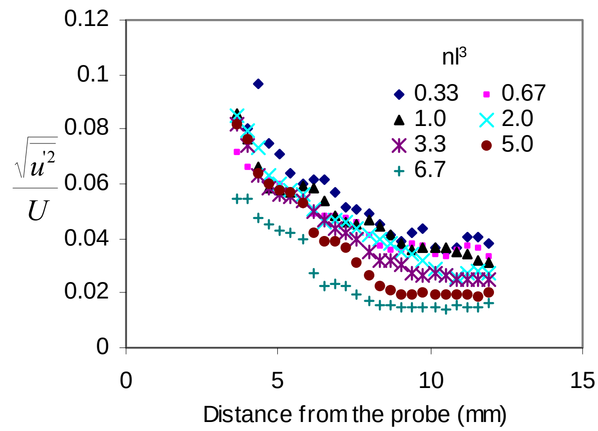

(B)

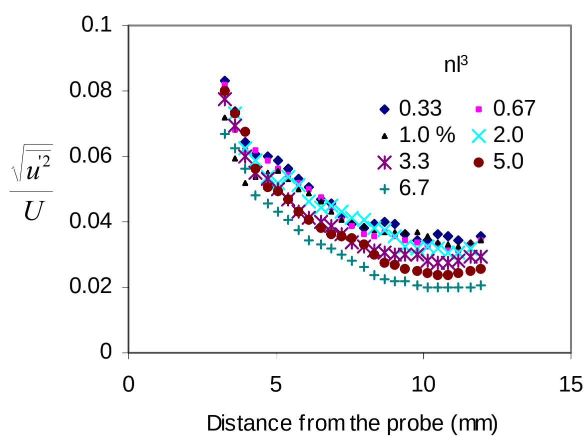

(C)

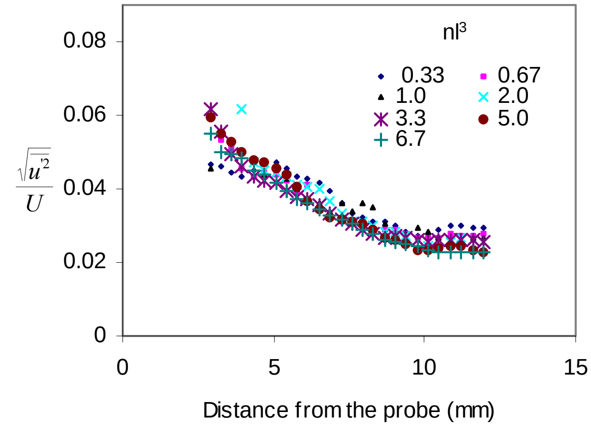

(D)

Figure 5.16 Turbulence intensity of fiber suspension flow at different Reynolds numbers. (A) 12000, (B) 37000, (C) 60000, (D) 92000.

5.4 Characterizations of Fiber Suspension Flow

In their fundamental studies of fiber suspension flow, Forgacs, Robertson and Mason (1958) and Daily and Bugliarello (1958) showed that fiber suspensions exhibit three basic types of shear flow: turbulent flow, mixed flow, and plug flow. In another study, Seely (1968) was unable to distinguish the velocity profiles he obtained for dilute fiber suspensions at high Reynolds numbers from those he obtained for water. He further divided the fully turbulent regime into two sub-regimes: damped turbulent flow and Newtonian turbulent flow. In this experiment, five types of velocity profiles under different Reynolds numbers and fiber concentrations have been observed. These five types of flow are schematically shown in Figure 5.17 and their characteristics are described below.

Type 1. At high Reynolds number and low fiber concentration, the velocity profile is almost the same as the turbulent velocity profile of single-phase Newtonian fluid. The shape of the velocity profile will not change with the changes of Reynolds numbers and fiber concentrations. This type of flow behavior has been suggested previously and experimentally verified by Seely (1968).

Type 2. With the increase of fiber concentration or decrease of Reynolds number, the velocity profile moves towards the laminar velocity profile. The velocity gradient becomes larger and the velocity profile gradually becomes sharper.

Type 3. When fiber concentration increases to a certain level or Reynolds number decreases beyond a point, the velocity profile becomes blunter (for fiber

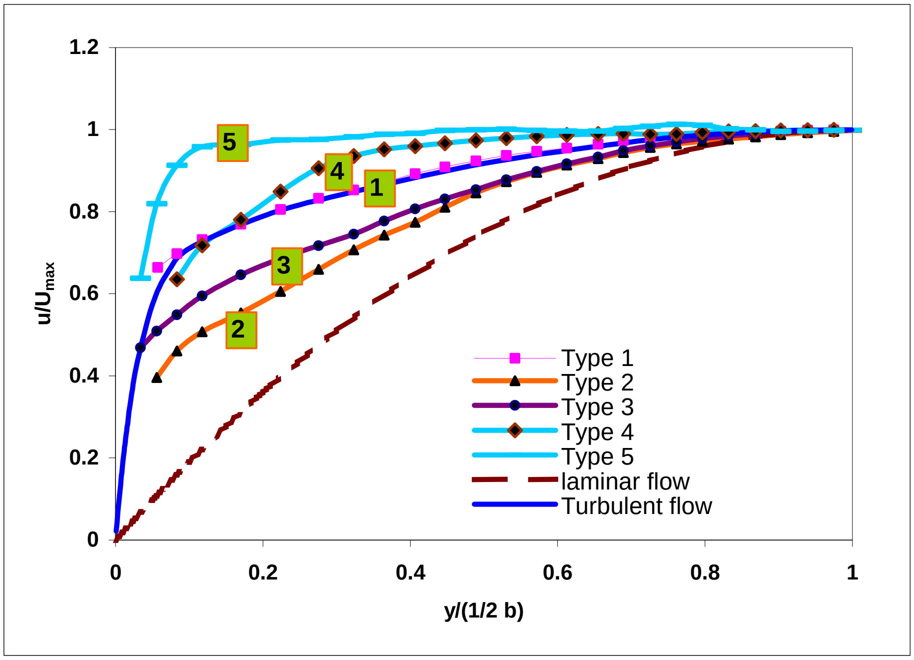

Figure 5.17 Different types of flow observed in the experiments.

concentration ≥0.3%) with the increase of fiber concentrations or decrease of Reynolds numbers. The actual transition point is dependent on the Reynolds numbers and fiber concentrations. However, the maximum deflection of velocity profiles from the Newtonian turbulent velocity profile at the transition point decreases with the increase of fiber concentrations. It should be noted that the difference between Type 2 and Type 3 flow is that both fiber concentration and Reynolds number have similar but opposite effects on the shape of the velocity profile.

<u>Type 4.</u> This type of flow pattern is termed mixed flow in the literature and is used to describe the transition regime between plug flow (Type 5) and turbulent flow. It is simply

the flow of a central plug region at uniform velocity with a turbulent flow region between the plug boundary and channel wall. The plug region may be thought of as a more or less continuous fiber network with included water, the network being capable of supporting the shear stress applied to it. The transition from Type 3 flow to this type of flow is so smooth that it is impossible to discern visually in the experiments when the plug begins to form.

Type 5. This type of flow only happens at low Reynolds number and fiber concentration over a certain minimum value. The fibers in the suspension form interlocking, coherent networks. Such networks have well-defined mechanical strength properties. Between the plug and wall, a thin water layer exists. It is possible that slip happens between the fiber network and water (e.g., water velocity is higher than that of fiber network in the central flow region). However, we have not found any experiment in the literature to support this hypothesis.

It should be noted that we have distinguished the above five different types of flow according to the shape of velocity profiles. There is no obvious sharp transition point between different types of flow. However, different flow mechanisms existed in the different types of flow. These mechanisms will be discussed in more detail in Section 5.4.

To further characterize these five types of flow, especially to find the transition point between different types of flow, a nonlinear regression was performed for all the velocity profiles measured under different flow conditions. Because the velocity profile of water flow in the channel flow can be expressed by Equation 4.1, the following mathematical model was used for the curve fitting:

$$\frac{u}{U_{max}} = 1 - (1 - A)(1 - \frac{y}{b/2})^2 - A(1 - \frac{y}{b/2})^N \qquad (5.5)$$

where y is the distance from the wall, b is the distance between the walls, u is the mean streamwise velocity, U_{max} is the velocity at the center of the channel, A and N are two parameters which can be obtained through the nonlinear regression.

The nonlinear regression was carried out using a commercial computation program (NCSS 97). The dimensionless coefficient A and the value of N obtained through regressions are listed in Table 5.2. The experimental data fitted to the above

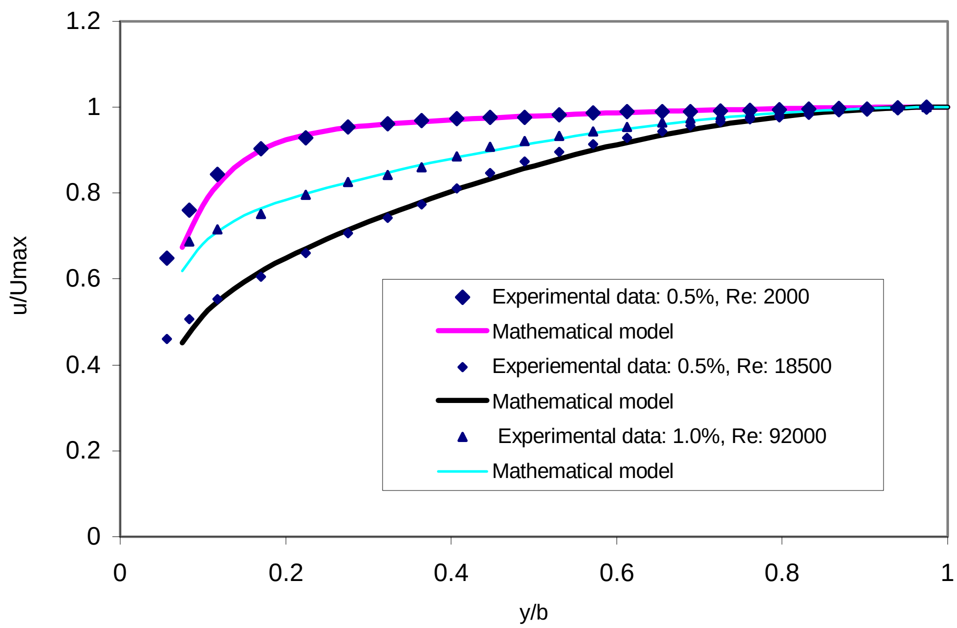

Figure 5.18 Some examples of curve fitting using Equation 5.5.

mathematical model fairly well, which is evident in that most of the regression coefficients is higher than 0.98 (Table 5.2). Figure 5.18 gives an example of how the experimental data fit with the regression curves.

Table 5.2. Nonlinear regression results.

Re	Parameter	Fiber Concentration (%)					
		0.1	0.15	0.3	0.5	0.75	1
2000	A	0.1808	0.0832	0.8766	0.9177	0.8823	
	N	5.357	9.136	9.59	16.41	56.56	
	Regression coefficient						
3000	A	0.318	0.1592	0.8589	0.8938	0.9472	
	N	6.03	18.82	8.56	10.96	13.84	
	Regression coefficient						
6000	A	0.4414	0.3036	0.7345	0.8773	0.8	0.8665
	N	11.24	42.5	38.5	7.822	15.23	22.72
	Regression coefficient						
9000	A			0.5206	0.791	0.6813	0.8673
	N			12.94	4.09	8.169	7.5
	Regression coefficient						
12000	A	0.5561	0.548	0.3902	0.705	0.7352	0.8546
	N	19.46	38.4	36.7	7	8.567	9.029
	Regression coefficient						
18500	A				0.4553	0.839	0.8351
	N				22	6.975	8.8436
	Regression coefficient						
37000	A	0.6687	0.6388	0.6157	0.5847	0.5521	0.5672
	N	33.4	35.3	43.1	36.4	18.68	14.28
	Regression coefficient						
60000	A	0.704	0.6878	0.6564	0.6638	0.6314	0.6673
	N	26.39	35.64	41.73	23.43	22.17	24.73
	Regression coefficient						
73000	A	0.7027	0.6783	0.6746	0.6851	0.6771	0.639
	N	25.62	31.69	32.88	26.3	22.95	21.73
	Regression coefficient						
92000	A	0.712	0.6987	0.696	0.6875	0.692	0.6673
	N	21.68	23.58	31.24	23.48	23.05	24.73
	Regression coefficient						

The most important parameter in Equation 5.5 is the value of coefficient A. It has a significant effect on the shape of the velocity profile and may represent a measure of the momentum transfer capacity of the suspensions. Figure 5.19 shows how coefficient A and N change with the Reynolds number for fiber suspensions at different concentrations. It is obvious from Figure 5.19 that fiber concentration has a significant effect on the value of coefficient A.

At low fiber concentration ($\leq 0.15\%$), coefficient A increases gradually with the Reynolds number until Reynolds number reaches about 60,000, and then it remains at a

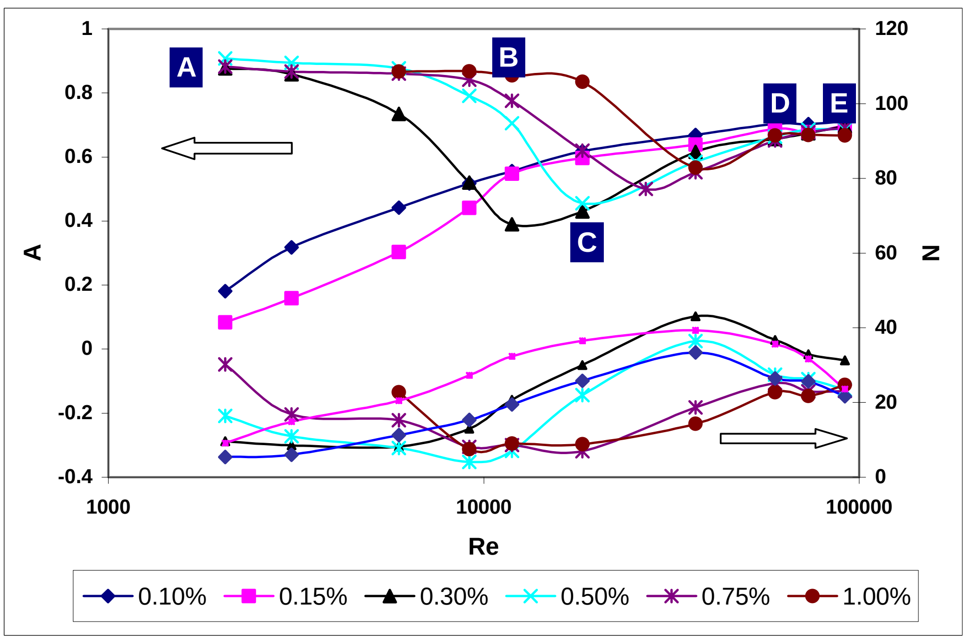

Figure 5.19 Change of coefficient A with the Reynolds number.

stable value. From the velocity profiles in Figure 5.1 to Figure 5.3, it can be found that the velocity profile changes from laminar flow to transition turbulent flow and finally to fully developed turbulent flow.

At high fiber concentration (≥ 0.3%), the change of coefficient A with Reynolds number can be divided into several regions as shown in Figure 5.19. At low Reynolds number (region AB), the coefficient A has a high value and it is not sensitive to the change of Reynolds number. With the increase of Reynolds number, at region BC, the coefficient A decreases with the increase of Reynolds number, and then after transition point C, it increases with the Reynolds number. When Reynolds number increases to a suitable value, coefficient A does not change with the Reynolds number and remains at a relatively stable value.

By checking the velocity profiles (Figure 5.1 to Figure 5.15) and Figure 5.19, it is found that the higher value of coefficient A corresponds to the flat velocity profiles, and on the other hand, the low value of coefficient A corresponds to the sharp velocity profiles. The four regions in Figure 5.19 are also related to the different types of velocity flows described in this session. For example, at region AB, the flow behavior are similar to that of Type 4 and Type 5 flow; at regions BC, CD and DE, the flow behaviors are similar to that of Type 3, Type 2 and Type 1, respectively.

In summary, the flow behavior of fiber suspension is completely different from that of water. Different types of velocity profiles exist under different fiber concentrations and Reynolds numbers. Figure 5.20 shows schematically the different types of velocity profiles observed under different fiber concentrations and Reynolds numbers.

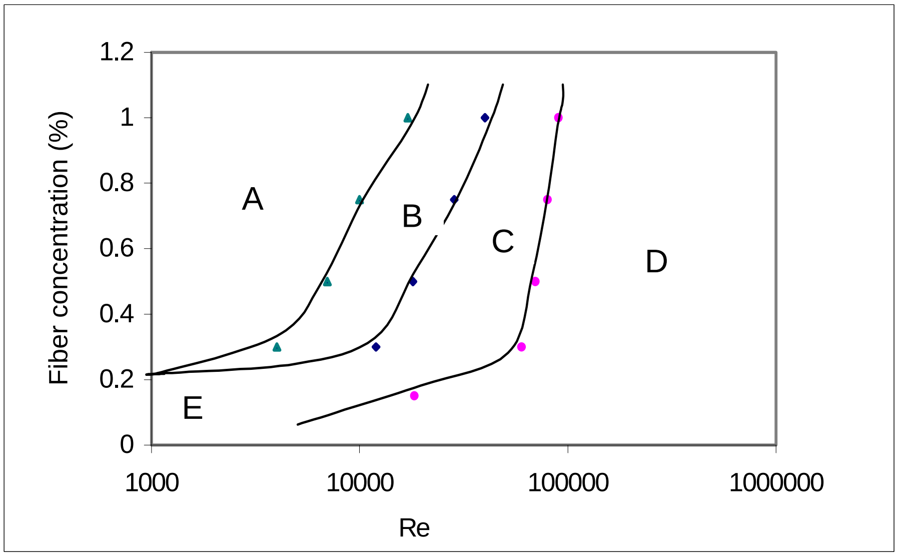

Figure 5.20 Different regimes of fiber suspension flow. (A) Plug flow + mixed flow; (B) Fiber-floc enhanced turbulent flow; (C) Fiber-floc damped turbulent flow; (D) Newtonian turbulent flow; (E) Laminar flow.

In the literature, most of the researchers only observed part of the flow behaviors observed in the current study. In addition, because of the small range of fiber concentrations or small range of Reynolds numbers used in their studies, their results were usually not consistent with each other. The different types of flow regimes observed in this study can explain these inconsistent results very well. For example, the Type 3 flow observed in the current study is in agreement with Daily and Bugliarello's (1958) observation that velocity profiles become blunter as fiber concentration is increased.

Type 1 and type 2 flow are consistent with Seely's (1968) observation that von Kármán constant increases in a systematic manner throughout the damped turbulent regime and approaches the Newtonian value at a very high Reynolds number. Type 3 flow explains Lee and Duffy's (1976) observation that the deviation of local reduced velocities from those for water increases as the Reynolds number is increased at a low Reynolds number, while Type 2 flow can explain their observation that the deviation of local reduced velocities from those for water decreases as Reynolds number is increased at a high Reynolds number.

The changes of suspension velocity profiles with the Reynolds numbers and fiber concentrations can assist considerably in understanding the complex internal flow mechanism of fiber suspension. In the next section, we will explain the velocity profile changes at different flow conditions and study the flow mechanism in the different flow regimes.

5.5 Velocity Profiles of Turbulent Fiber Suspension Flow

Although the effect of fiber concentration and Reynolds number on velocity profile has been widely reported in the literature, quantified descriptions of this effect are rare. In order to quantify the effect of fiber concentrations and Reynolds numbers on fiber suspension flow, velocity profiles (Type 1 and Type 2) are redrawn in the non-dimensional wall-layer coordinates $u^+ = U/U_\tau$ and $y^+ = y\, U_\tau/\nu$ and shown in Figure 5.21. Here, y is the distance from the wall, b is the distance between the wall, U is the mean streamwise velocity, the wall shear velocity U_τ is defined as $(\tau_w/\rho)^{1/2}$, ρ is the fluid density, and ν is the kinematic viscosity. The wall shear stress τ_w is obtained through the measurement of pressure drop. The solid line in Figure 5.21 is the theoretical velocity profile of water flow between the parallel plates, which could be described by:

$$u^+ = \frac{1}{0.41}\ln(y^+) + 4.69 \tag{5.6}$$

Coles (1956) described the velocity profile by combining the log-law and a wake function:

$$u^+ = \frac{1}{K}\ln(y^+) + B + \frac{\Pi}{K}W\left(\frac{y}{0.5b}\right) \tag{5.7}$$

in which the constant K and B are determined by using the data measured in the region $y/(0.5b)<0.15$ and the wake coefficient Π is calibrated with the data in the outer flow. Here, we will use Equation 5.7 to describe the velocity profile of turbulent fiber suspension flow. As was found from Figure 5.21, the velocity profiles of fiber suspension flow overlap with those of water flow in the inner wall region. Therefore, we can assume that the value of K and B will be the same as that of water flow, which is 0.41 and 4.69, respectively. In the outer wall region, however, the profiles deviate from Equation 5.6 and the magnitude of the deviation can be described by the third term in Equation 5.7.

From Figure 5.21, it is easy to find that the deviation is the function of fiber concentration (nl^3), Reynolds number (Re), and positions (y^+). Figure 5.22 shows the deviation from

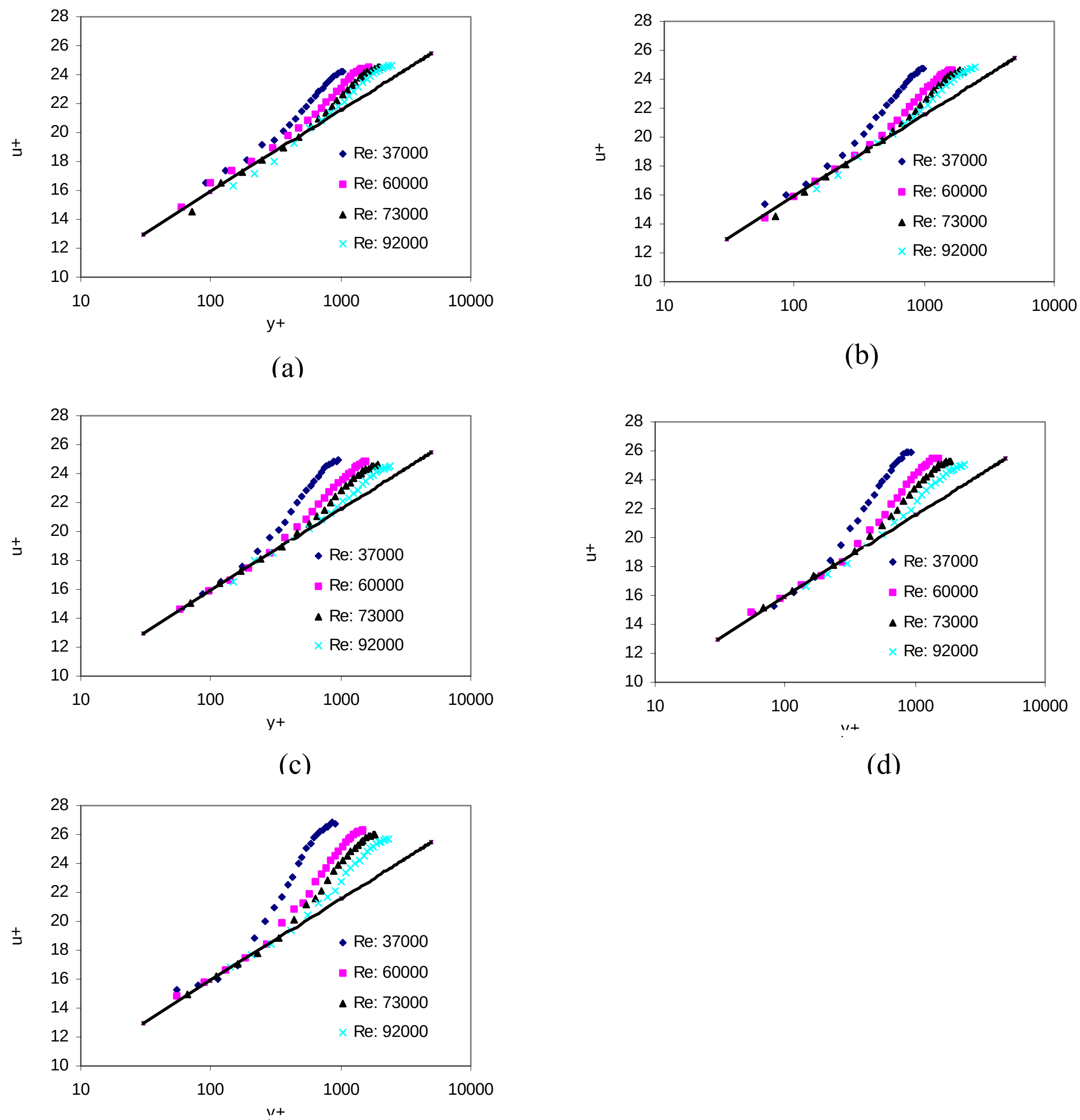

Figure 5.21. The reduced velocity profiles. (a) $nl^3 = 1.0$, (b) $nl^3 = 2.0$, (c) $nl^3 = 3.3$, (d) $nl^3 = 5.0$, (e) $nl^3 = 6.7$

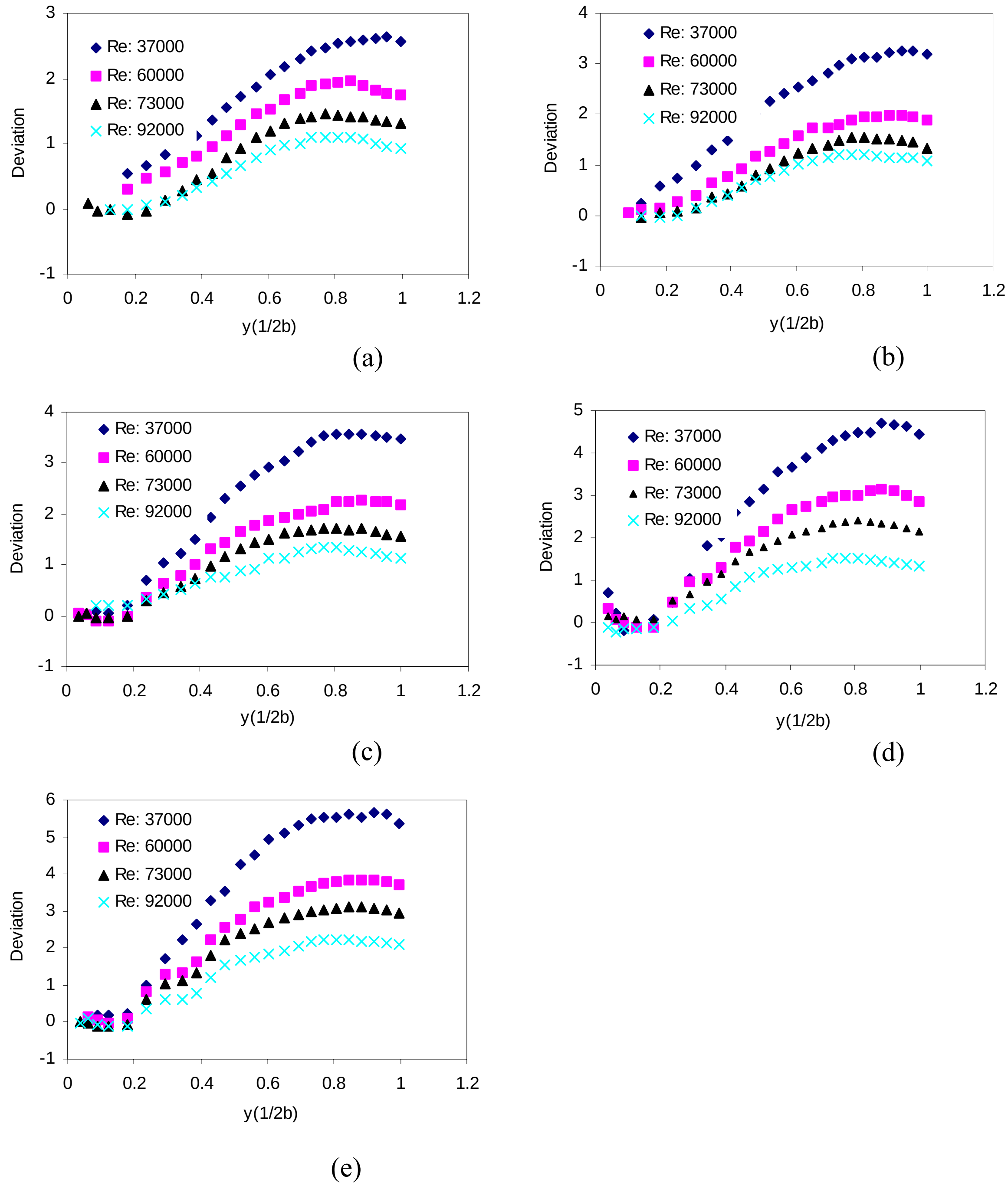

Figure 5.22 The deviation of velocity profile of fiber suspension flow from log-law at different fiber concentrations and Reynolds numbers. (a) $nl^3 = 1.0$, (b) $nl^3 = 2.0$, (c) $nl^3 = 3.3$, (d) $nl^3 = 5.0$, (e) $nl^3 = 6.7$.

law at different Reynolds numbers and fiber concentrations. Since the maximum deviation happens at y/(0.5b) = 0.9 in most of the velocity profiles, we use the following function to perform curve fitting for the deviation curve in Figure 5.22:

$$f(\mathrm{Re}, nl^3, \frac{y}{0.5b}) = \frac{\Pi}{\mathrm{K}} \mathrm{W}(\frac{y}{0.5b}) = \frac{2\Pi}{\mathrm{K}} \sin^2(\frac{\pi}{2} \frac{\mathrm{y}}{0.5\mathrm{b}} \frac{1}{0.9}) \tag{5.8}$$

In the above equation, $\mathrm{W}(\frac{\mathrm{y}}{0.5\mathrm{b}})$ is a universal function and its value will not change with Reynolds number and fiber concentration. Π will be the function of Reynolds number and fiber concentration and its value can be obtained through curve fitting for the deviation curve in Figure 5.22. Figure 5.23 presents the value of Π at different Reynolds numbers and fiber concentrations.

In order to describe Π in terms of Reynolds number and fiber concentration, the following equation was used do curve fitting for the data points in Figure 5.23:

$$\Pi = \mathrm{k}_1 \exp(\mathrm{k}_2 * (\mathrm{nl}^3) - \mathrm{k}_3 * \mathrm{Re}) \tag{5.9}$$

Here, k_1, k_2, and k_3 are constant and could be obtained through curving fitting. Rewrite the equation in the following form:

$$\ln\Pi = \ln(\mathrm{k}_1) + \mathrm{k}_2 * (\mathrm{nl}^3) - \mathrm{k}_3 * \mathrm{Re} \tag{5.10}$$

It can be found from Equation 5.10 that there is linear relation between ln(Π) and nl^3 and Re. The values of k_1, k_2 and k_3 were obtained through linear regression for the data points in Figure 5.22: k_1 =0.98, k_2 =0.14, and k_3 =1.9*10^{-5}.

The solid line in Figure 5.23 gives the predicted value of Π at different fiber concentrations and Reynolds numbers using Equation (5) and above constant values. As we can find from the graph, the predicted Π value fits quite well with the experimental data.

Combining Equations 5.8, 5.9 and 5.10, the velocity profile of fiber suspension flow could be rewritten in the following equation:

$$u^+ = \frac{1}{0.41}\ln(y^+) + 4.69 + \frac{\Pi}{0.41}\sin^2\left(\frac{y}{0.9b}\pi\right) \tag{5.11}$$

where

$$\Pi = 0.98\exp(0.14(nl^3) - 1.9*10^{-5}*\mathrm{Re}) \tag{5.12}$$

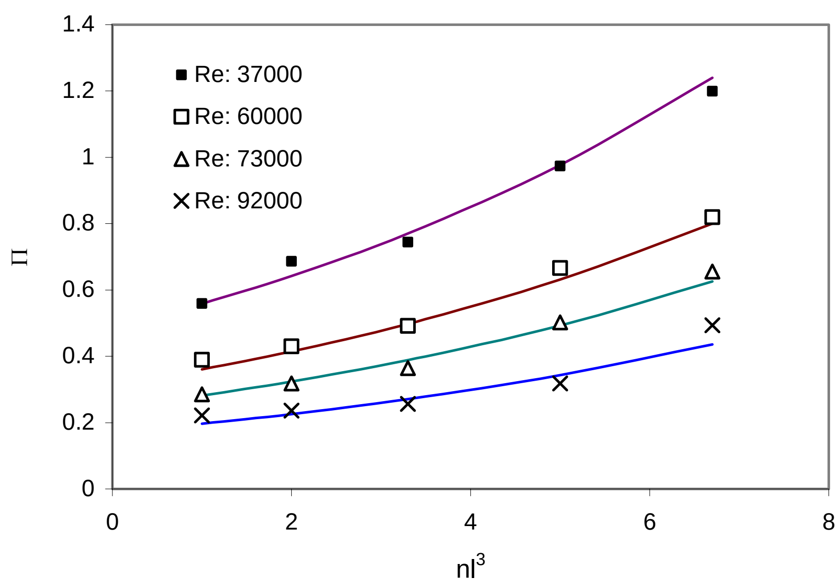

Figure 5.23 The value of Π at different fiber concentrations and Reynolds numbers. The solid line is obtained using Equation 5.12.

Figure 5.24 gives an example of the reduced velocity profile at different Reynolds number (nl^3 =5.0), where the predicted velocity profile based on Equation 5.11 and Equation 5.12 are shown in the solid line. As shown in Figure 5.24, the predicted velocity profiles correlate with experimental data quite well. Therefore, the velocity profile of turbulent fiber suspension flow can be described by Equation 5.11 and 5.12.

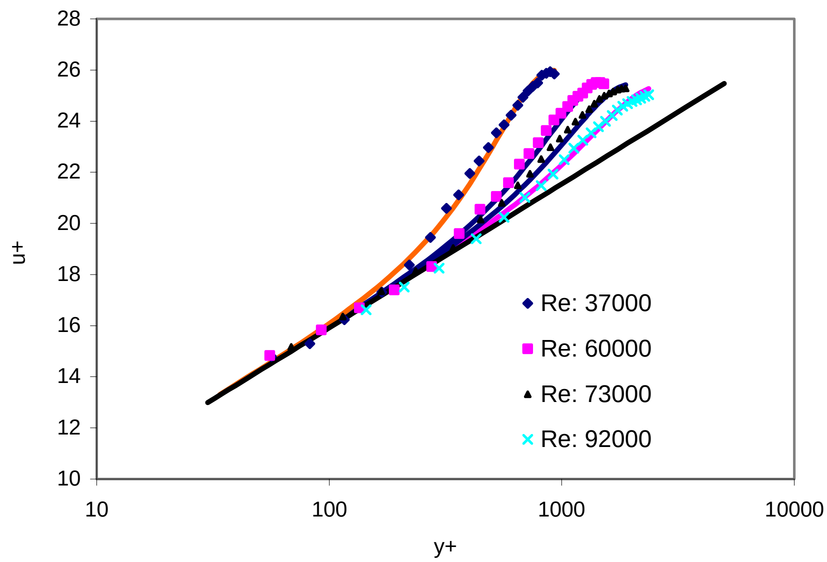

Figure 5.24 The reduced velocity profile at nl^3 =5.0. The dotted line is the experimental data and the solid line is the predicted velocity profile based on Equations 5.11 and 5.12.

5.6 Mechanisms of Turbulent Fiber Suspension Flow

In the fiber suspension flow, fibers tend to entangle with each other, forming flocs and networks. In a turbulent fiber suspension flow, the amount of flocculation is determined by a dynamic equilibrium between the growth of flocs by collision processes and their breakdown by shear stresses. Fiber dispersion is found to be promoted by increasing the velocity gradient and by decreasing fiber concentration (Robertson and Mason 1957). Robertson and Mason (1957) measured flocculation in a turbulent fiber suspension and found that the average size of fiber flocs decreased as shear rate increased and there was a progressive decrease in flocculation with an increase in velocity and a decrease in concentration. In our experiments, we observed that increasing fiber concentrations and decreasing Reynolds numbers have similar effects on the changes of velocity profiles. Therefore, flocculation may have a large effect on the suspension flow.

It has been found in early studies that fiber flocs affect momentum transfer in two opposing ways: they tend to lower it by damping the turbulence of the suspending phase and they also tend to enhance the momentum transfer by providing a solid link between adjacent fluid layers. Because the local shear stress is related to the local velocity gradient through the local momentum transfer, changes in the velocity gradient at different positions offer an insight on the changes in the relative importance of inter fiber transfer and turbulence transfer.

In Type 1 flow, because of the high shear stress and turbulent stress, it is difficult for fibers to interlock with each other and there is less flocculation. In this flow regime, the turbulence is dominated by momentum transfer and the fiber addition has less effect on the turbulence intensity, as proved in the previous measurements (Figure 5.16 D). Therefore, the flow follows Newtonian behavior and the velocity profiles obtained are the same as those of water.

In Type 2 flow, part of the fibers in the suspension will interlock and form flocs with an increase of fiber concentrations or a decrease in Reynolds numbers as observed by Robertson and Mason (1957). The presence of fiber and formation of flocs will reduce the momentum transfer through decreasing turbulence intensity (as shown in Figures 5.16 A, B, C) and, on the other hand, increase momentum transfer through fiber interlocking. The overall momentum transfer will be determined by combinations of these two effects. At this flow regime, when compared to water flow, the reduction of momentum transfer caused by turbulence is higher than the gain of momentum transfer caused by the fiber interlocking. Therefore, the total momentum transfer is less than that of water flow, which leads to a sharper velocity profile compared with the velocity profile for water.

With the increase of fiber concentration or decrease of Reynolds numbers, in Type 3, the contributions to the momentum transfer by fiber interlocking increase. The evidence of this change is that the central part of the velocity profile becomes blunter with the increase of fiber concentration or decrease of Reynolds number. This transition begins at the center of the velocity profile, where turbulence is low and flocs form easily, and extends to the wall region progressively with the increase of fiber concentrations or decrease of Reynolds numbers. Although turbulence momentum transfer is dominated in both Type 2 and Type 3 flow, the trend of how two different momentum transfer mechanisms contribute to the overall momentum transfer changes. In Type 2 flow, the reduction rate of turbulence momentum transfer is higher than the increasing rate of fiber interlock momentum transfer. Therefore, the velocity profile becomes sharper with the increase of fiber concentrations or decrease in Reynolds numbers. In Type 3, the reduction rate of turbulence momentum transfer is lower than the increasing rates of fiber interlock momentum transfer (which begins at the center of the channel and then extends to the wall region). This explains why the center part of the velocity profiles becomes blunter again with the increase of fiber concentrations or decrease of Reynolds numbers.

In Type 4 flow, because of the low turbulence and shear stress, a fiber network forms in the center of the channel and provides a solid link between adjacent fluid layers. In this part of the flow regime, momentum transfer is dominated by the fiber interlocks. Outside the fiber network region, there is a layer of turbulent fiber suspension area although the turbulence intensity has been suppressed greatly (Figure 5.16 A).

5.7 The Drag Reduction of Fiber Suspension Flow

To further study the flow behavior of fiber suspension flow, the pressure loss for fiber suspension flow has been determined at different fiber concentration levels (0%, 0.15%, 0.3%, 0.5%, 0.75%, 1.0%). The relations between pressure loss and Reynolds number at different fiber concentrations are listed on Appendix V.

Friction factor data calculated from the pressure gradient and bulk Reynolds number measurements on pure water are plotted in Figure 5.25. Here, the friction factor f and Reynolds number Re are defined as:

$$f = \frac{2D\ \Delta P}{\rho U^2 x} = \frac{8\tau_w}{\rho U^2} \tag{5.13}$$

$$Re = \frac{DU}{\nu} \tag{5.14}$$

where

D = hydrodynamic diameter of channel, m

P = pressure, Psi

x = length in channel length direction, m

U = bulk flow velocity, m/s

τ_w = wall shear stress, N/m^2

ρ = fluid density, kg/m^3

ν = kinematic viscosity, m^2/s

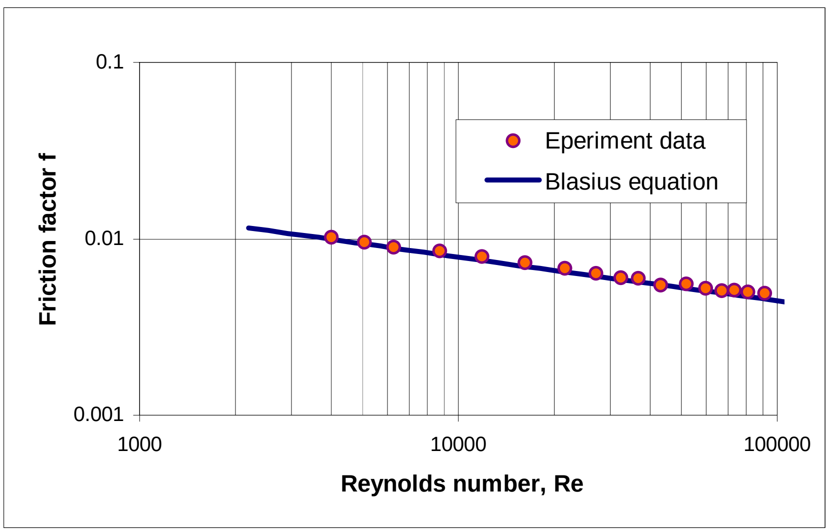

Figure 5.25 Relationship between friction factor and Reynolds number for pure water.

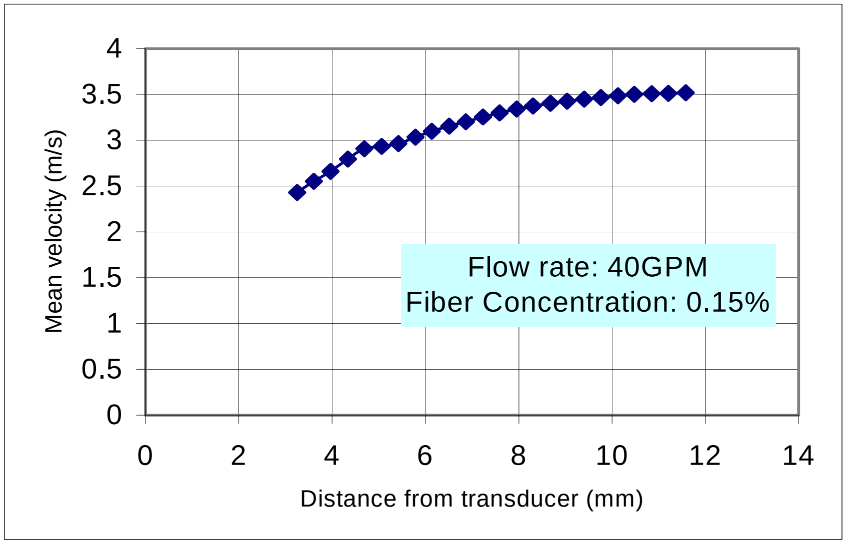

Figure 5.26 Friction factor vs. Reynolds number at fiber concentration of 0.15 and 0.3%.

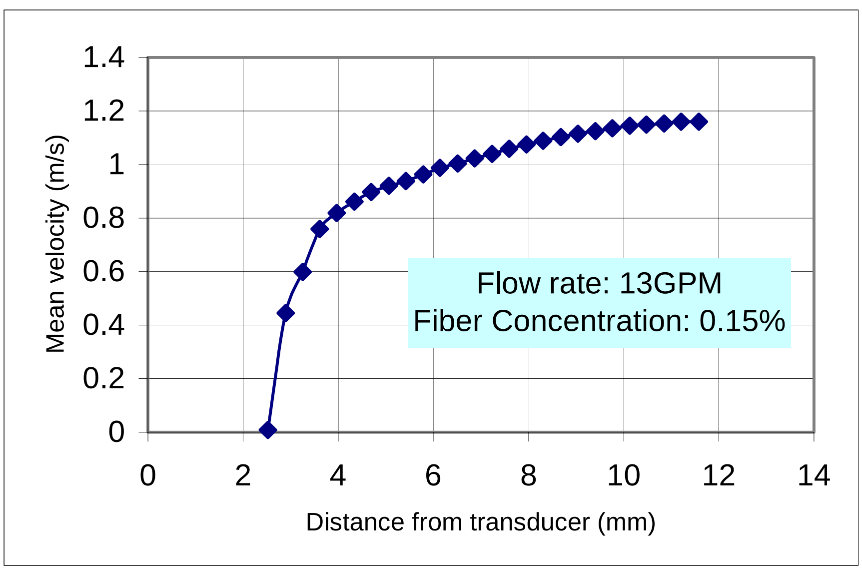

Figure 5.27 Friction factor vs. Reynolds number at fiber concentrations of 0.5, 0.75, and 1.0%.

The agreement of these pure water data with the established Blasius equation (the solid line in Figure 5.25) indicates that the measuring techniques and the general condition of the flow system are acceptable for smooth channel friction factor determinations up to a Reynolds number of at least 10^5.

The experimentally determined friction factor-Reynolds number curves for the fiber suspensions are plotted in Figure 5.26 for fiber concentrations of 0.15 and 0.3% and in Figure 5.27 for fiber concentrations of 0.5, 0.75 and 1.0%. Here, we chose to plot the friction factor as a function of the Reynolds number rather than the mean velocity to compare these curves with that of water. The value of viscosity used to calculate the Reynolds number was taken as that of pure water at the temperature of suspension. The friction factor curve for pure water is shown in the plots as a dashed line.

The Reynolds number-friction factor correlation exhibits certain qualitative characteristics that have consistently been observed in past investigations. First, in the flow regime of AB (Figure 5.27), the fraction factors of fiber suspension (consistency 0.75 and 1.0%) are greater than that of pure water at same Reynolds number. However, with increased Reynolds number, the suspension friction factor value drops below that of pure water (BC and CD regime). A rational and generally accepted explanation of the low suspension friction value in these regimes is that the presence of fiber networks and flocs in the water suppresses the development of turbulence and, hence, reduces the level of momentum transport due to turbulence. In the turbulent layer near the wall, where turbulence is the principal mechanism of momentum transport, this reduced momentum transfer results in a lower velocity at the outer edge of the laminar sublayer, a lower shear gradient through this laminar layer, and consequently, a low friction factor (Mih and Park, Robertson and Mason 1957, Daily and Bugliarello 1958).

Secondly, in regime BC, the suspension friction factor increases with increasing fiber concentration. In regime CD, the friction factor decreases with increasing concentration. This can be explained in the same argument as above. When the momentum transfer is controlled by the transfer through the rigid fiber network or flocs in the flow, a relatively high velocity is developed at the boundary of the laminar sublayer and a relatively high friction factor is developed. However, when momentum transfer by means of turbulence prevails, the greater suppression of turbulence at the higher fiber concentration yields a lower friction factor. It was also observed that, at low concentrations and high Reynolds numbers (Figure 5.26, DE), the friction factors appear to be approaching the Newtonian values as reported by Seely (1968).

5.8 The Formation and Disruption of Plug

Velocity profiles measured in this investigation have provided conclusive evidence that at low turbulent Reynolds numbers a coherent fiber plug exists at the center of the channel. The size of the plug decreases with increasing velocity and decreasing concentration. The existence of the plug is presumed to be a consequence of the fiber network which has a finite yield stress.

One of the advantages of PUDV is that the measuring time is short (a few ms) and all the local velocity data can be obtained in a single measurement. It is, therefore, easy to observe the velocity profile changes as Reynolds number changes and understand the formation and disruption of plug.

Figure 5.28 gives two examples of velocity profile changes with Reynolds numbers for fiber concentrations of 0.3 and 1.0%. It is easy to discover that the plug size decreases with increasing Reynolds number. However, it is hard to determine an exact Reynolds number when the plug disappears with the increasing Reynolds number. With the reduction of plug size as Reynolds number increases, the velocity profile changes smoothly from mixed flow to turbulent flow.

Values for the plug size were obtained from velocity profiles for fiber suspensions at concentrations of 0.3, 0.5, 0.75, and 1.0%. Here, the plug size is defined as the flat region in the center of the plug, although it is difficult to define precisely from the velocity profiles because the transition from the flat region in the center to the sharp region near the wall occurs over a small radial distance. The plug size, bulk velocity, plug velocity, ratio of plug size to channel thickness, and calculated shear stress at plug boundary are presented in Table 5.3. The changes of plug size with the bulk velocity at different fiber concentrations are shown in Figure 5.29.

A disruptive shear stress model has been widely accepted to describe the size of a coherent fiber plug in pipe shear flow. This model was developed on the assumption that a fiber suspension has a disruptive shear stress τ_y, and that the plug surface corresponds to the location of some critical level of stress operating on the plug. The mean shear stress acting on the plug τ_p is assumed equal to the disruptive yield stress of the plug τ_y. The mean stress at any point τ in channel flow can be calculated from the wall shear stress τ_w, the distance from the wall y, and the channel height b:

$$\tau = \tau_w \frac{y}{1/2b} \tag{5.15}$$

Values for τ_y calculated from the data of this investigation by using Equation 5.15 have been presented in Table 5.3. An intuitive expectation is that the yield stress value would be independent of the Reynolds number and depend solely on concentration, since τ_y is a suspension property. This is not the case, however, as can be seen from Figure 5.30, which shows the stress at the surface of the plug against bulk velocity for fiber suspensions with different concentrations. The stress level that the network can support increases with increasing concentration. It also increases with increasing Reynolds number. Mih and Park (1967), Duffy (1972), and Powell (1996) have used similar methods to obtain values for τ_p and thus values for τ_y of fiber suspensions. All the above authors found in most cases that there was a progressive increase in the calculated τ_y for the fiber plug as the plug radius decreased. This variation in yield stress with Reynolds number has been attributed to two potential mechanisms. One explanation is that radial concentration gradients exist in the flowing suspension. Another explanation is that Reynolds stresses arising from velocity fluctuations above the average have a disproportionate role in the breakup of fiber networks (Mih and Parker 1967, Duffy 1978).

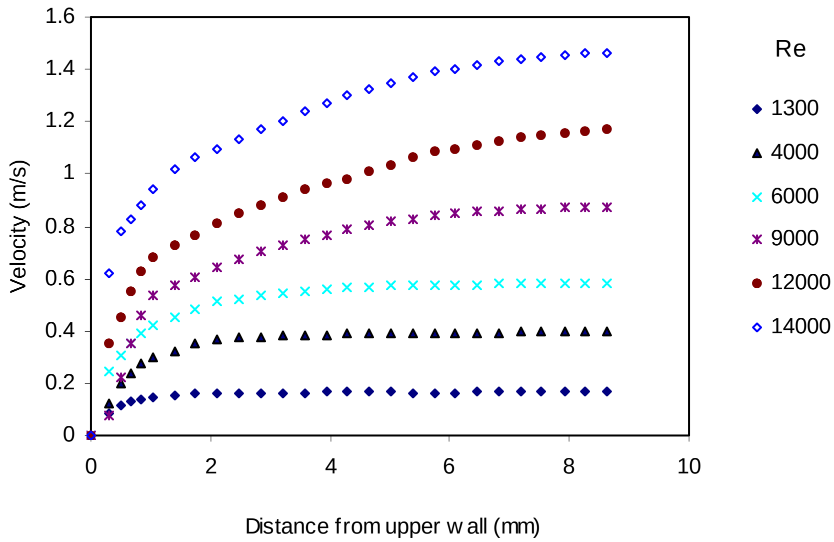

(A)

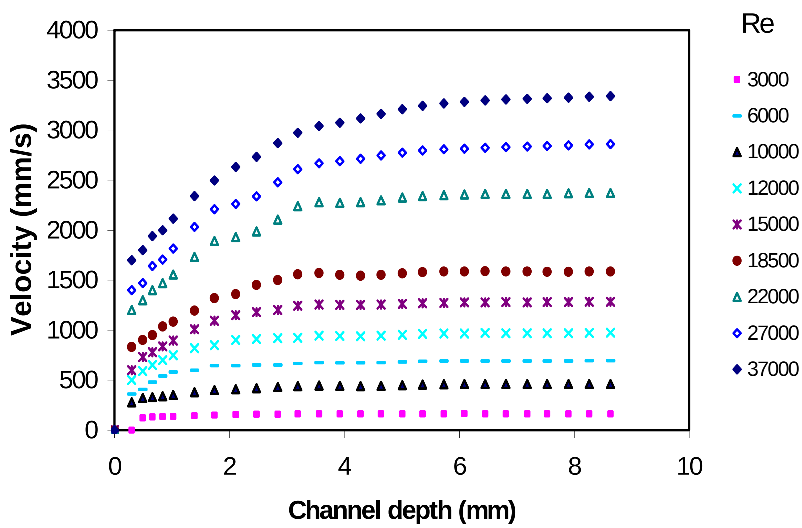

(B)

Figure 5.28 The change of velocity profiles with Reynolds numbers.
(A) Concentration: 0.3%; (B) Concentration: 1.0%.

Table 5.3 Data for plug size and disruptive shear stress calculated from velocity profile and pressure drop data.

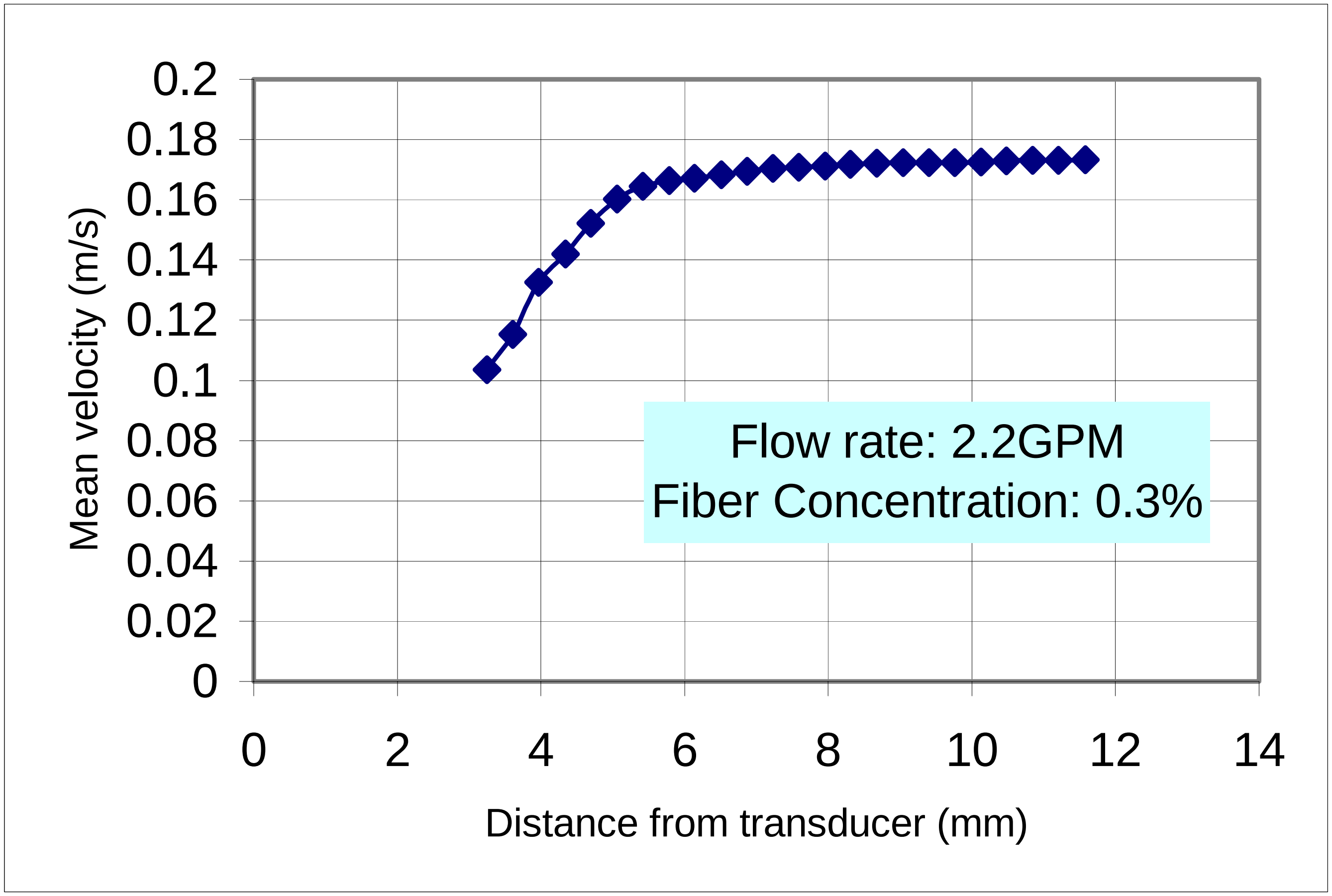

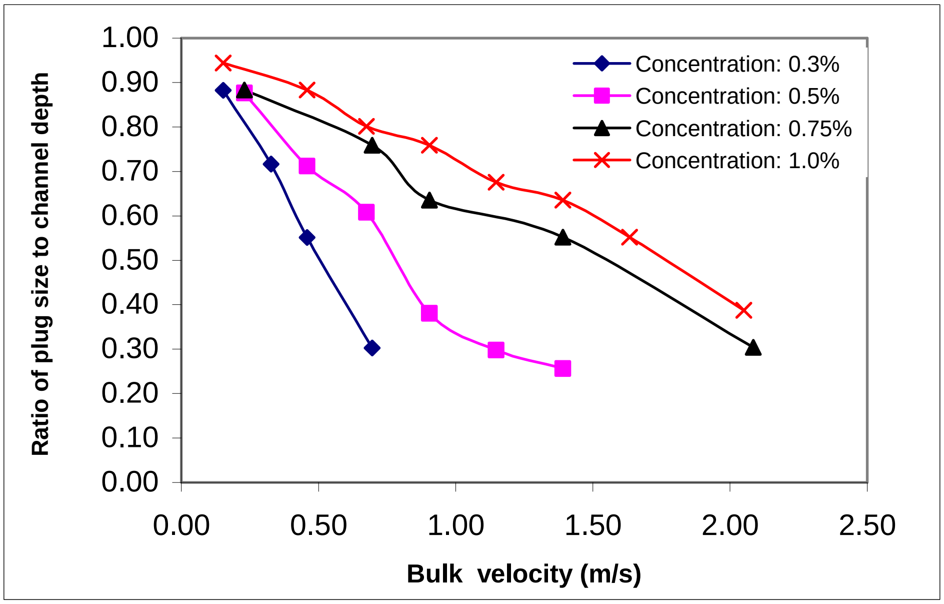

Figure 5.29 The ratio of plug size to channel depth versus bulk velocity.

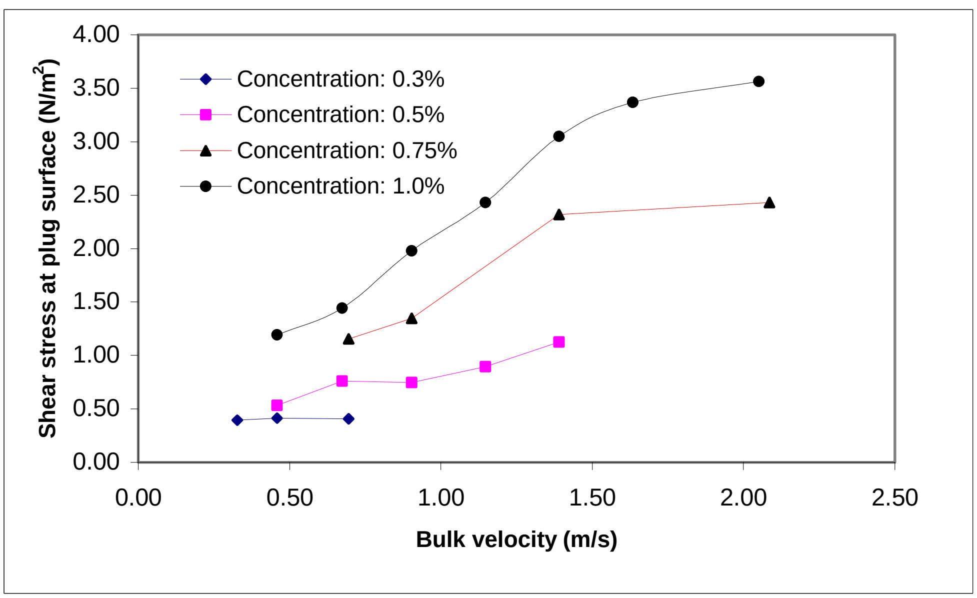

Figure 5.30 Bulk velocity vs. the shear stress at the surface of the plug for various concentrations of fiber suspensions.

5.9 Summary

Pulsed Ultrasonic Doppler Velocimetry in conjunction with pressure drop measurements has been used to investigate the characterization of dilute fiber suspension flow. The following conclusions are drawn from the results of this investigation.

1 Five types of flow exist in the fiber concentration-Reynolds number space. In Type 1 flow, the flow behavior and velocity profiles are similar to that of Newtonian fluid. The shape of the velocity profile does not change with fiber concentration and Reynolds number. In Type 2 flow, the velocity profile will become sharper with the increase of fiber concentration and/or the reduction of Reynolds number. With further increase of fiber concentration and/or decrease of the Reynolds number, in Type 3 flow, velocity profile becomes blunt again. In Type 4 flow, a central plug will be formed in the center of channel. At very high consistency and low Reynolds number, in Type 5 flow, the plug can fill all flow regions.

2 The velocity profile of turbulent fiber suspension can be described by $u^+ = \frac{1}{0.41}\ln(y^+) + 4.69 + \frac{\Pi}{0.41}\sin^2(\frac{y}{0.9b}\pi)$, where b is the height of the channel, Π is the wake constant and it is a function of fiber concentration nl^3 and Reynolds number Re, and $\Pi = 0.98\exp(0.14nl^3 - 1.9 * 10^{-5} * \mathrm{Re})$.

3 Fiber addition can affect the momentum transfer in two ways. It will reduce the turbulence and thus reduce the momentum transfer. On the other hand, the fibers will interlock with each other and increase the momentum transfer.

4 Data from velocity profile measurements indicate that turbulence intensity decreases with increasing fiber concentration. This effect becomes stronger at low Reynolds numbers than at high Reynolds numbers. After the plug forms, the turbulence intensity in the plug region is greatly reduced.

5 Addition of fibers to the flow will cause drag reduction. In the mixed flow regime, the suspension friction factor increases with increasing fiber concentration; in the turbulent flow regime, the suspension friction factor decreases with increasing fiber concentration.

6 The size of the plug will increase with increasing fiber concentration and decreasing Reynolds number. There was a progressive increase in the shear stress for disrupting the fiber plug as the plug radius decreased.

6 DIRECT MEASUREMENT OF THE FORMING JET VELOCITY PROFILE BY PULSED ULTRASONIC DOPPLER VELOCIMETRY

6.1 Introduction

The forming jet velocity profile has a significant impact on the physical properties of finished paper. It is believed that slight variations in the velocity profile can strongly affect fiber orientation, forming table streaks and other properties. Typically, in order to achieve a desired jet-to-wire ratio, the forming jet velocity is controlled using feedback from a pressure transducer in the headbox and the jet velocity is calculated using Bernoulli's streamline equation. However, with high levels of turbulence in the headbox, the total head at the point of the pressure measurement includes a non negligible velocity head that varies with the flow rate. Thus the equation for the total head of a free jet at a nozzle must include a term accounting for the significant pressure losses resulting from the turbulent flow through the nozzle. These losses vary for different headbox designs, flow rates, and slice openings and the head-loss equations must be determined empirically. In practice it is difficult to obtain jet velocity measurements with accuracy better than two percent.

To better characterize the impact of forming hydrodynamics on the physical properties of a sheet, accurate measurements of the jet velocity profile are required. Several techniques have been developed to measure the jet velocity as an aid to papermaking, e.g., the headbox jet-speed profiling system (Nielsen 1997), the jet-velocity measurement system

(Franzen 1987, Loewen 1991), and Surface Pattern Image Velocimetry (Ono et al. 2001). All of these techniques, however, are based on analyzing the optical signal from the surface of the forming jet and therefore can only measure the velocity at the surface of the jet.

The objective of this chapter is to apply PUDV to ZD (direction perpendicular to the jet plane) velocity profile measurement for forming jet in a pilot paper-machine headbox. Section 6.2 introduces the preliminary study results, where the velocity profile for a jet issued from a rectangular channel is measured and the repeatability and sensitivity of the measurement are studied. Section 6.3 introduces the experimental setup for forming jet ZD velocity profile measurement. A theoretical analysis is provided to obtain the local velocities and flow directions at the measuring point by performing two PUDV measurements with different inclination angles. Section 6.4 presents the measuring results of ZD velocity profile for a forming jet issued from a headbox. An example is given to demonstrate how to obtain the jet velocity profile through two PUDV measurements at different inclination angles.

6.2 Preliminary Study

In order to measure the velocity profiles of a forming jet issued from a pilot paper-machine headbox, a preliminary study was carried out in the lab to measure the jet velocity from an open channel. The channel used in the previous study was modified by removing the top wall at the end of the channel as shown in Figure 6.1. The length of the open region is 7 cm. The ultrasound transducer was installed under the bottom channel wall and its inclination angle can be adjusted by the X-Y-Z-rotation positioner through the attached adapter. In all the velocity profile measurements, the fiber concentration is 1.0%.

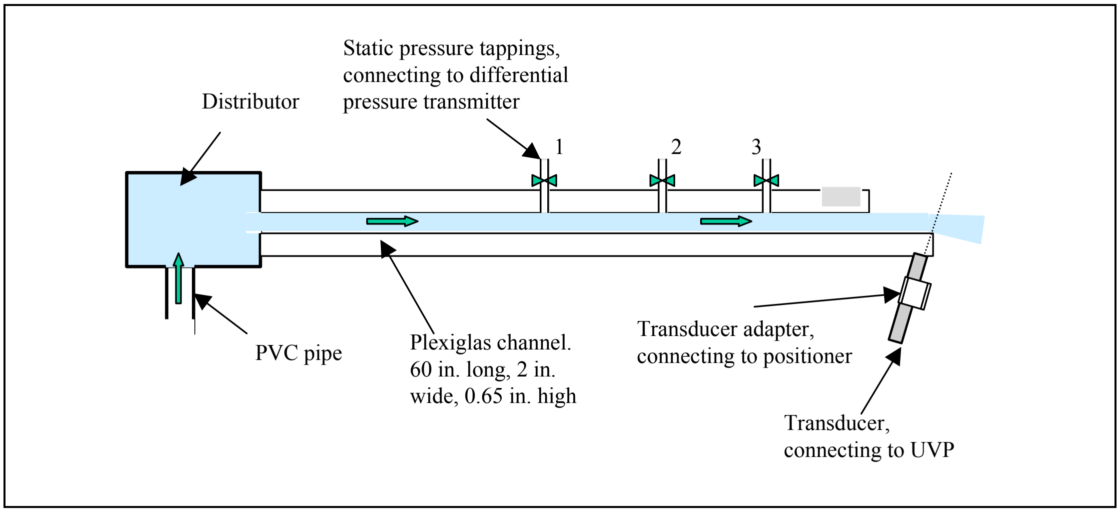

Figure 6.1 The installation of an ultrasound transducer for jet velocity profile measurements in an open channel.

The jet velocity profiles of fiber suspension flow at the exiting point of the channel were measured at mean velocity of 4.6 m/s, 5.6 m/s, and 6.3 m/s. During the measurement, the inclination angle between the transducer and the suspension flow direction was set at 80°. Figure 6.2 shows the velocity profile measured at each flow rate.

The repeatability of the PUDV measurement of jet velocity profiles is shown in Figure 6.3 where velocity profiles of fiber suspension at a flow rate of 65 gpm are measured three times. Similar to the observation in Section 4.4, the difference within the mean velocity profiles for three independent measurements is almost invisible.

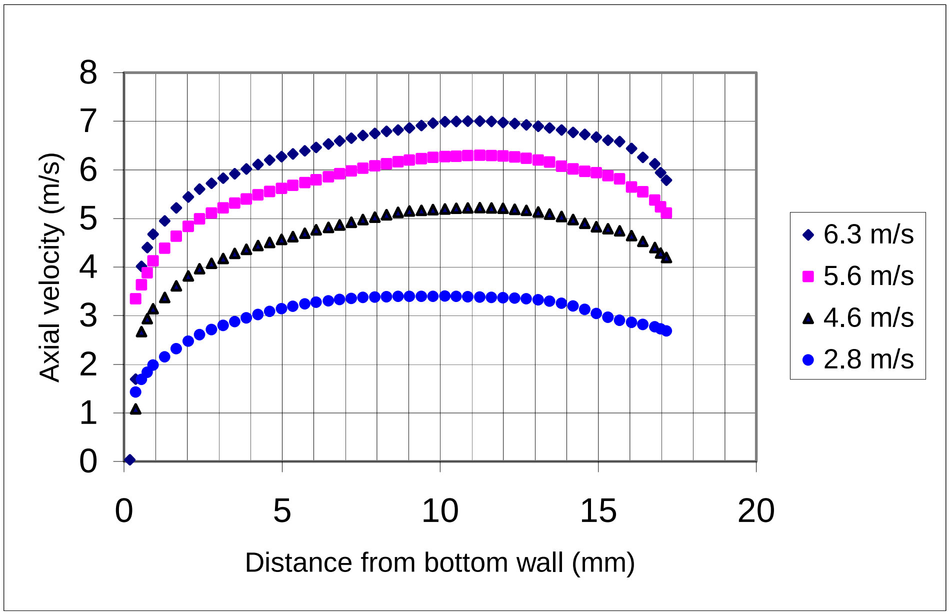

Figure 6.2. Jet velocity profile of fiber suspension measured at the end of the open channel.

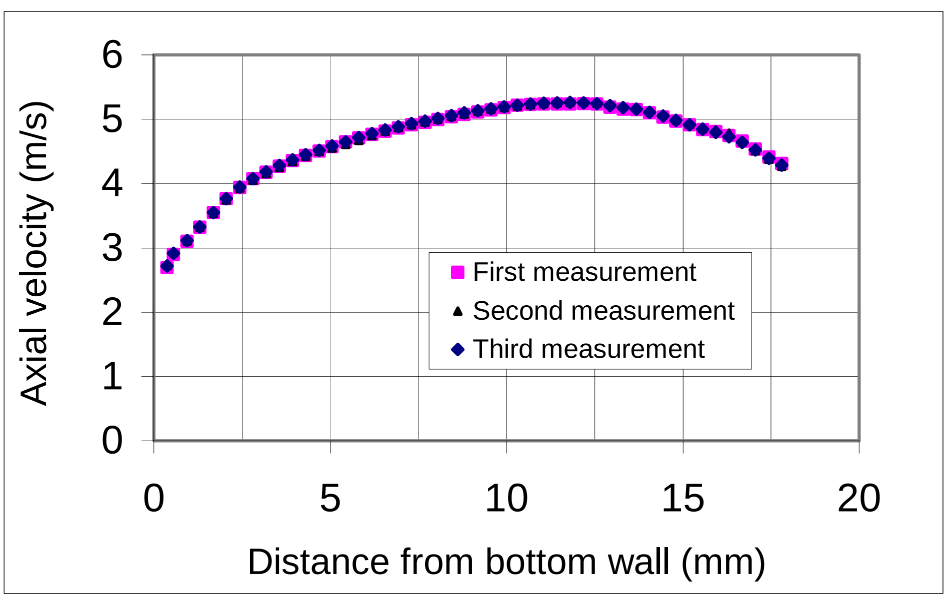

Figure 6.3 Repeatability of jet velocity profile measurement at 4.6 m/s.

As a further test of the velocity profile measurement, the sensitivity of the PUDV measurement to flow rate changes was studied. After measuring the jet velocity profile at a mean velocity of 4.6 m/s, the flow rate was increased or decreased about 1% and the velocity profile was measured again. Figure 6.4 shows the jet velocity profiles before and after the change of flow rate. As seen in Figure 6.4, this small change is reflected in the velocity profiles and a small difference between three velocity profiles is discernible. By integrating the area under the velocity profile, the measured mean velocity changes can be obtained. In this experiment, the mean velocity change obtained through the velocity profile measurement was very close to that of changes obtained from the flowmeter. When the flow rate decreased 0.91%, the measured mean velocity decreased 0.81%; when the flow rate increased 1.08%, the measured mean velocity increased 0.94%.

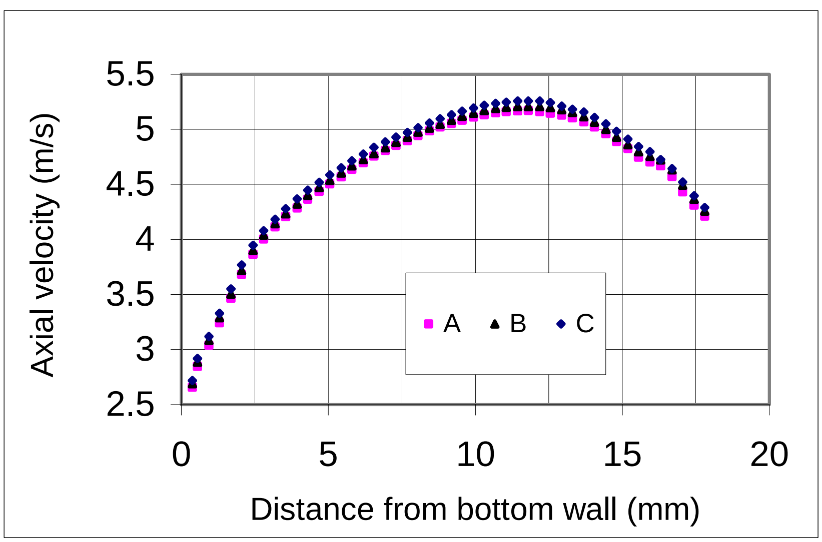

Figure 6.4 The sensitivity of PUDV for jet velocity profile measurement A: flow rate decrease 0.91%; B: 4.6 m/s; C: flow rate increase 1.08%.

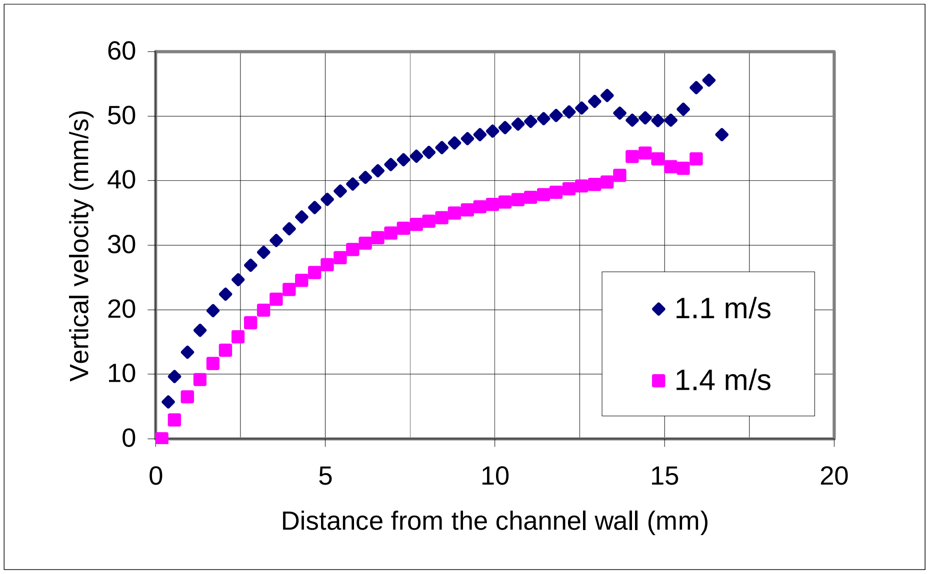

Figure 6.5 Vertical velocity components as jet leaves the channel.

Another preliminary study performed in the lab was to check if PUDV can detect a small velocity component of the flow. It is observed that the depth of the suspension in the open channel region decreased as suspension exited from the closed channel and a small velocity component was created in the vertical direction. In order to test if PUDV can measure this small velocity component, the transducer was installed perpendicular to the channel wall (inclination angle at 90°). Figure 6.5 shows the vertical velocity components at mean velocity of 1.4 m/s and 1.1 m/s. It should be noted that these vertical velocity components are not proportional to the flow rate. In this experiment, the vertical velocity component at 1.1 m/s is higher than that at 1.4 m/s. Also, there is a large velocity fluctuation in the surface of the flow. This velocity fluctuation is caused partially by the ripple formed at the surface of the flow and partially by the ultrasound signal reflecting from the interface between the water and air. It is clear from the above experiment that PUDV can be used to detect the small velocity component of a large flow rate.

6.3 Experimental Setup

6.3.1 Pilot paper machine

The pilot paper machine for this experiment is basically a small fourdrinier forming table, which has been utilized to produce wet webs of products ranging from fine paper to fiber sheets (sheet basis weight range: 50 to 400 g/m^2 with slurry consistencies of 0.3 to 1.5%). The former is generally operated in one of two basic consistency configurations: (1) for a conventional headbox, 0.3~1.3%; (2) for a high-consistency headbox, 1.5~3.5%. The slice width is twelve inches, and maximum wire speed is 1969 feet per minute. The water flow system is schematically shown in Figure 6.6. Since the flow rate is affected significantly by the water level in the machine chest at a fixed pump speed, a second water supply was used. By keeping the machine chest full all the time during the operation, a stable flow rate can be achieved at a fixed pump speed.

Figure 6.7 shows the side view of the headbox used in this study. The slice opening can be adjusted by the knife, which is attached at the end of the slice. The total length of the converging channel is about 20 inches. The top and side walls of the headbox are made of 0.75-inch clear acrylic plastic and the bottom plate is made of aluminum with a polished surface. The whole headbox is placed on an adjusted table. The headbox position and jet angle can be finely adjusted by setting the table at the desired position and angle.

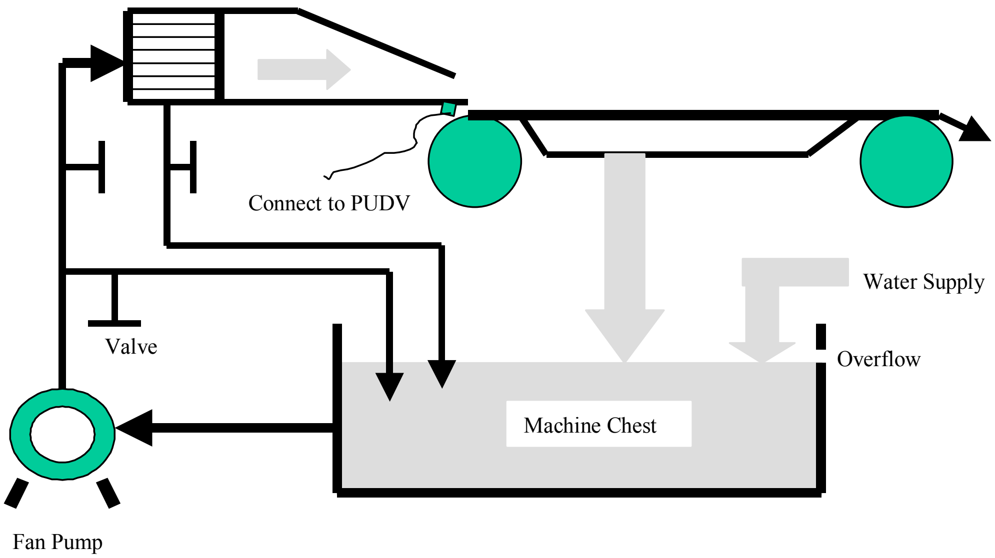

Figure 6.6 Flow system of pilot paper machine.

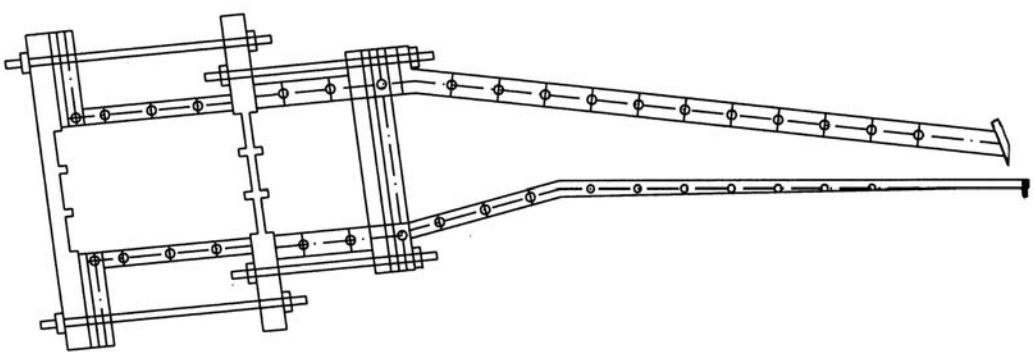

Figure 6.7 The side view of designed headbox.

6.3.2 Installation of transducer

In order to measure the velocity profiles of the forming jet as it leaves the slice of the headbox, a 4 MHz ultrasound transducer was installed underneath the bottom plate of the headbox. The transducer is 8 mm in diameter and 10 mm in length. The effective size of the ultrasound beam is 5 mm in diameter.

Figure 6.8 shows schematically the installation of the ultrasound transducer. Three holes (A, B, C) were drilled in the edges of the slice with one hole in the center; the distance between holes is 3 inches. The difference among these three holes is that each hole has a different inclination angle with the bottom plate. The value of inclination angle α for hole

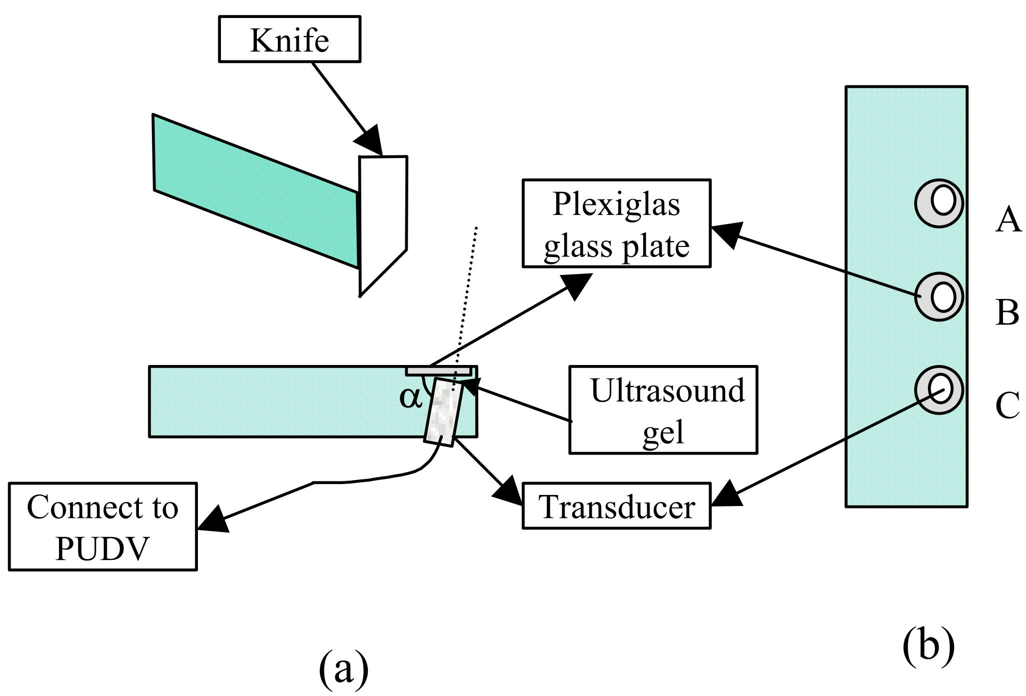

Figure 6.8 Installation of ultrasound transducer. (a) side view, (b) top view

A, B, and C is 70, 75, and 80 degrees, respectively (Figure 6.8). In order to avoid contact between jet and transducer, a circular Plexiglas film, which is 2 mm thick and 20 mm in diameter, is used to cover the hole. The transducer is inserted into one of these holes during the measurement. The ultrasound gel is used to fill the gap between the transducer and the Plexiglas glass film so that the ultrasound can transmit to the liquid easily.

6.3.3 Determining jet velocity and direction

As introduced in Chapter 2, the basic principle of PUDV is to measure the Doppler shift frequency in the ultrasound transmission direction. From the Doppler shift frequency, the velocity component in the ultrasound transmission direction can be calculated and then, if the angle between the flow direction and ultrasound transmission is known, the velocity of the flow can be obtained. Based on the above principle, one of the basic requirements of PUDV measurement is that the angle between the ultrasound transmission direction and the flow direction is known.

In the channel flow, there is only one velocity component in the channel length direction. Therefore, we can assume the angle between the ultrasound transmission direction and the channel direction is equal to the angle between the ultrasound transmission direction and the flow direction. However, this assumption will not be correct in a jet because another velocity component was created in the direction perpendicular to the channel bottom wall as shown in Figure 6.9. Therefore, we cannot assume the flow direction is parallel to the bottom plate for a jet issued from the headbox. In order to measure the jet velocity, the flow direction should be determined during the measurement. In this section, we will propose a method to obtain the flow direction and velocity by performing two PUDV measurements with different inclination angles.

Refer to Figure 6.9 and assume a particle P is moving in an unknown direction with an unknown velocity V_0. In the first measurement, the inclination angle between ultrasound and the bottom plate of the headbox is α_1 and the velocity component in the direction of AC is V_1, which can be measured by PUDV. The relationship between V_0 and V_1 can be expressed in the following equation:

$$V_1 = V_0 \cos(\beta_1) \tag{6.1}$$

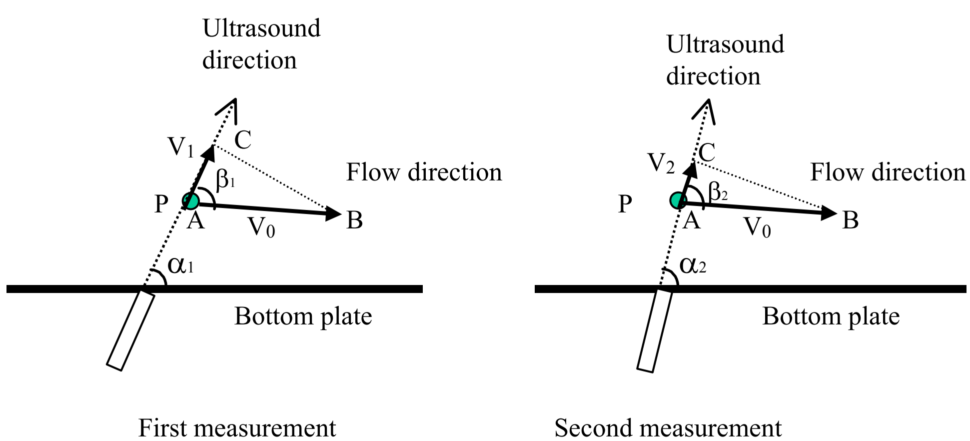

Figure 6.9 Measuring jet velocity and flow direction through two PUDV measurements.

In the same way, the relationship between V_0 and V_2 can be obtained in the second measurement:

$$V_2 = V_0\cos(\beta_2) \tag{6.2}$$

In addition, the relationship between β_1 and β_2 is:

$$\beta_1 - \alpha_1 = \beta_2 - \alpha_2 \tag{6.3}$$

In Equation 6.1, 6.2, and 6.3, α_1 and α_2 are known variables and $V_1$and V_2 are given by two measurements. By solving these three equations, V_0, $\beta_{1,}$ and β_2 can be obtained:

$$\beta_1 = \operatorname{arctg}\left[\frac{\cos(\alpha_1 - \alpha_2) - V_1/V_2}{\sin(\alpha_1 - \alpha_2)}\right] + \alpha_1 - \alpha_2 \tag{6.4}$$

$$\beta_2 = \operatorname{arctg}\left[\frac{\cos(\alpha_1 - \alpha_2) - V_1/V_2}{\sin(\alpha_1 - \alpha_2)}\right] \tag{6.5}$$

$$V_0 = \frac{V_2}{\cos\left(\operatorname{arctg}\left[\frac{\cos(\alpha_1 - \alpha_2) - V_1/V_2}{\sin(\alpha_1 - \alpha_2)}\right]\right)} \tag{6.6}$$

From Equation 6.4, 6.5, and 6.6, the actual flow direction β (the angle between the flow direction and the bottom plate) and the velocity component in the direction perpendicular ($V_{\perp}$) and parallel ($V_{//}$) to the bottom plate can be obtained:

$$\beta = \operatorname{arctg}\left[\frac{\cos(\alpha_1 - \alpha_2) - V_1/V_2}{\sin(\alpha_1 - \alpha_2)}\right] - \alpha_2 \tag{6.7}$$

$$V_{\perp} = V_2 \frac{\sin\left(\operatorname{arctg}\left[\frac{\cos(\alpha_1 - \alpha_2) - V_1/V_2}{\sin(\alpha_1 - \alpha_2)}\right] - \alpha_2\right)}{\cos\left(\operatorname{arctg}\left[\frac{\cos(\alpha_1 - \alpha_2) - V_1/V_2}{\sin(\alpha_1 - \alpha_2)}\right]\right)} \tag{6.8}$$

$$V_{//} = V_2 \frac{\cos\left(\operatorname{arctg}\left[\frac{\cos(\alpha_1 - \alpha_2) - V_1/V_2}{\sin(\alpha_1 - \alpha_2)}\right] - \alpha_2\right)}{\cos\left(\operatorname{arctg}\left[\frac{\cos(\alpha_1 - \alpha_2) - V_1/V_2}{\sin(\alpha_1 - \alpha_2)}\right]\right)} \tag{6.9}$$

6.4 Measuring the Forming Jet Velocity Profile with PUDV

To verify the feasibility of measuring the forming jet velocity profile with PUDV, the experiments are performed in a pilot headbox described in Section 6.3. In this section, an example will be given to demonstrate how to obtain the velocity profile of a forming jet.

During the experiment, the headbox slice opening is fixed at 20 mm and the bulk flow rate is controlled at 215 gpm. In the first measurement, the inclination angle between the ultrasound transducer and the bottom plate of the slice is set at 75°, while in the second measurement, the inclination angle is set at 70°. Figures 6.10 and 6.11 present the measured velocity components in the ultrasound transmission directions. From the velocity profiles, it is easy to find that the top surface of the jet is located at 18 mm from the bottom plate.

As shown in Figures 6.10 and 6.11, the projected velocity component in the ultrasound transmission direction is affected significantly by the inclination angle of the transducer. Referring to Figure 6.9, it is easy to find that the projected velocity component (V_1 or V_2) will not only be affected by the magnitude of velocity (V_0) but also by the angle (β_1 or β_2) between the ultrasound transmission direction and flow direction. The larger the inclination angle, the smaller the velocity components in the ultrasound transmission direction. In this experiment, β_1 and β_2 are not constant inside the jet. Both of them increase from the bottom to the surface of the jet. This explains the velocity profiles observed in Figure 6.10, where the velocity component in the ultrasound transmission direction decreases from the bottom to the surface of the jet.

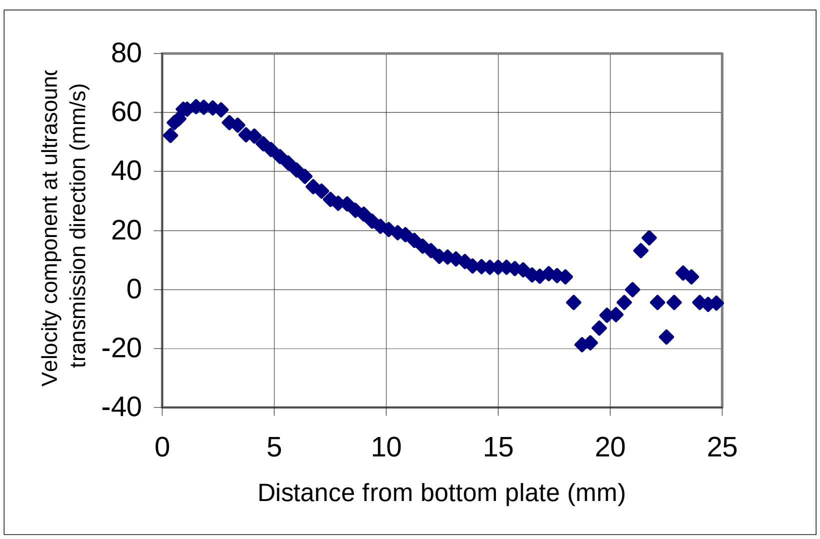

Figure 6.10 Velocity component of a forming jet in the ultrasound transmission direction at inclination angle of 75°.

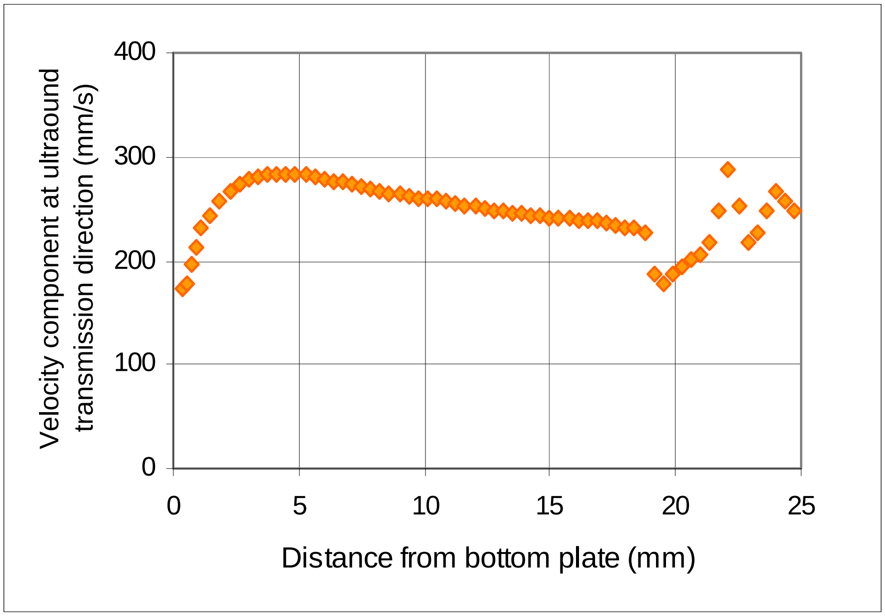

Figure 6.11 Velocity component of a forming jet in the ultrasound transmission direction at inclination angle of 70°.

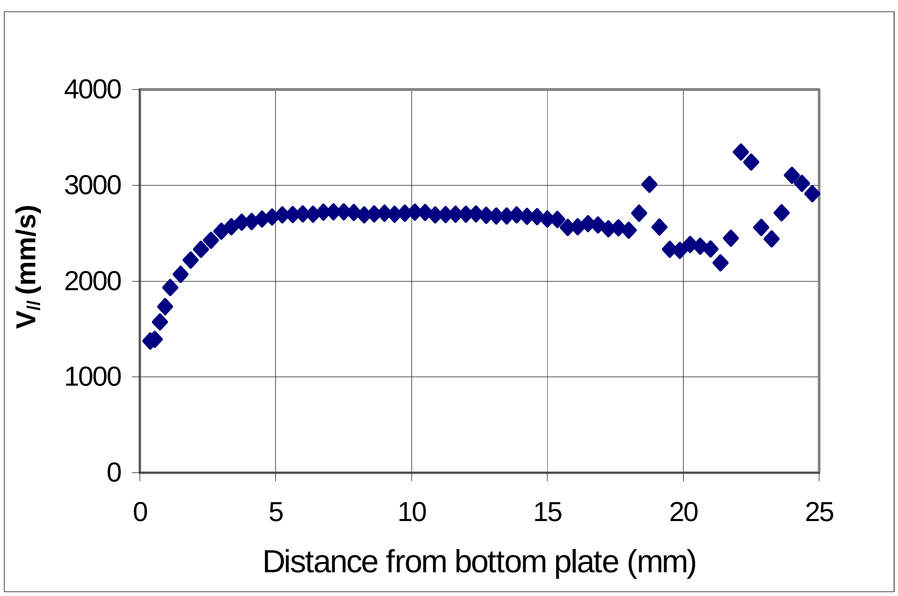

Figure 6.12 Velocity component in the direction parallel to the headbox bottom plate.

From these two measurements, the unknown parameters needed to calculate the value $V_{//}$ (Equation 6.8) and $V_{\perp}$ (Equation 6.9) are obtained. In this example, α_1 is 75°, α_2 is 70°, and V_1 and V_2 can be obtained from Figures 6.10 and 6.11 respectively. Figure 6.12 and Figure 6.13 present the calculated jet velocity profiles in the direction parallel and perpendicular to the headbox bottom plate, respectively. The boundary between the jet and air at the top of the jet surface can be found easily from the profiles. In Figures 6.10 and 6.11, it is located at a point about 18 mm from the bottom plate, beyond which the random data points caused by the noise signal appear.

It should be noted that the velocity component in Figure 6.12 and Figure 6.13 is measured not in a line perpendicular to the bottom plate, but in the center line of the circular ultrasound beam, which has an inclination angle of 75° and 70°, respectively, to the bottom plate. Because the flow is not fully developed at the measuring point, it is possible that a small velocity change exists in the flow direction. However, because the deflection is smaller than the size of the ultrasound beam (5 mm in diameter), this change in velocity can be neglected.

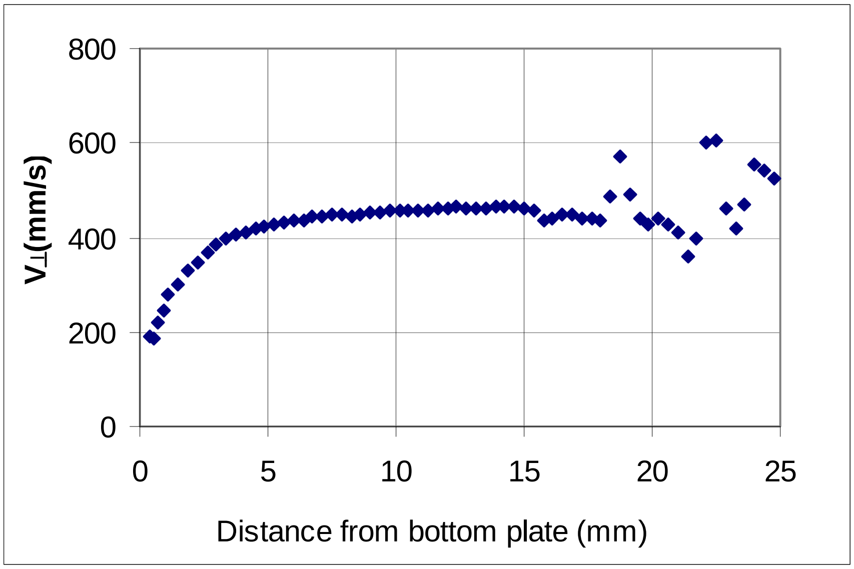

Figure 6.13 Velocity component in the direction perpendicular to the headbox bottom plate.

6.5 The Accuracy of Jet Velocity Profile Measurement

In Section 4.3.2, the accuracy of PUDV measurement has been evaluated through the comparison between the PUDV measuring results and the LDA measuring results. It was found that the relative errors for the average velocity between PUDV and LDA measurements are less than 2%. To evaluate the accuracy of the forming jet velocity profile measurement through PUDV, several tests are performed at different slice opening and flow rates. The details of each test are shown in Table 6.1. Figure 6.14 to Figure 6.22 present the velocity components in different directions at each test condition.

Table 6.1 Test conditions and relative errors for forming jet velocity profile measurement.

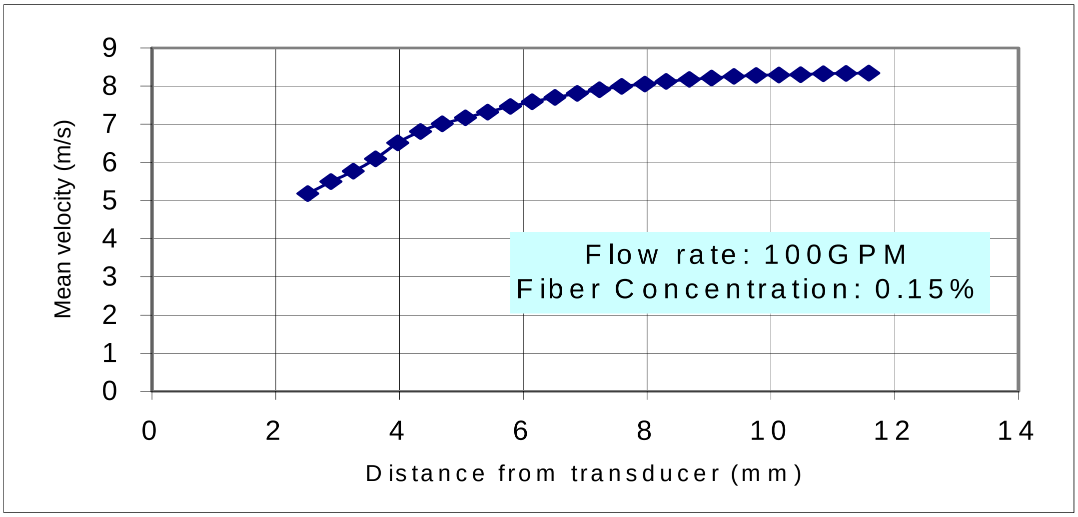

Based on the measured velocity profile, the jet flow rate can be obtained. Table 6.1 presents the comparison between the flow rate from flowmeter reading and flow rate calculated from measured velocity profiles. The relative errors between these two types of measurements are also shown in Table 6.1.

It is obvious from Table 6.1 that the magnitude of the relative error is related to the slice opening. When the slice opening is 20 mm, the relative errors are less than 2.0% in all three measurements. When the slice opening reduces to 15 mm and 10 mm, the relative errors increase accordingly. These larger relative errors come from the jet thickness measurement. In PUDV measurement, the position resolution is 0.36 mm in the ultrasound beam direction. This resolution may lead to higher relative errors if the jet thickness is low. For example, the maximum relative error of the jet thickness measurement could be as high as 6.0% when the slice opening is 10 mm (the jet thickness is about 6 mm), while it is only 2.0% when the slice opening is 20 mm (the jet thickness is about 18 mm).

In a real paper machine, the thickness of the forming jet is normally 20 mm or higher. Therefore, the relative error in jet thickness measurement will be lower than 2.0%. As it is shown in Table 6.1, it is possible to measure the jet velocity with accuracy better than two percent.

6.6 Summary

PUDV has been applied to jet velocity profile measurement. Preliminary studies shows that PUDV can be used to measure the velocity profile of a jet issued from a rectangular channel. The measurements have high repeatability and are also sensitive to the small flow rate changes. By installing an ultrasound transducer underneath the apron, it is possible to obtain the forming jet ZD velocity profile through two measurements with different inclination angles. The accuracy of jet thickness measurement is dependent on the position resolution of PUDV measurement. When the thickness of the forming jet is more than 20 mm, it is possible to measure the average forming jet flow rate with accuracy better than two percent.

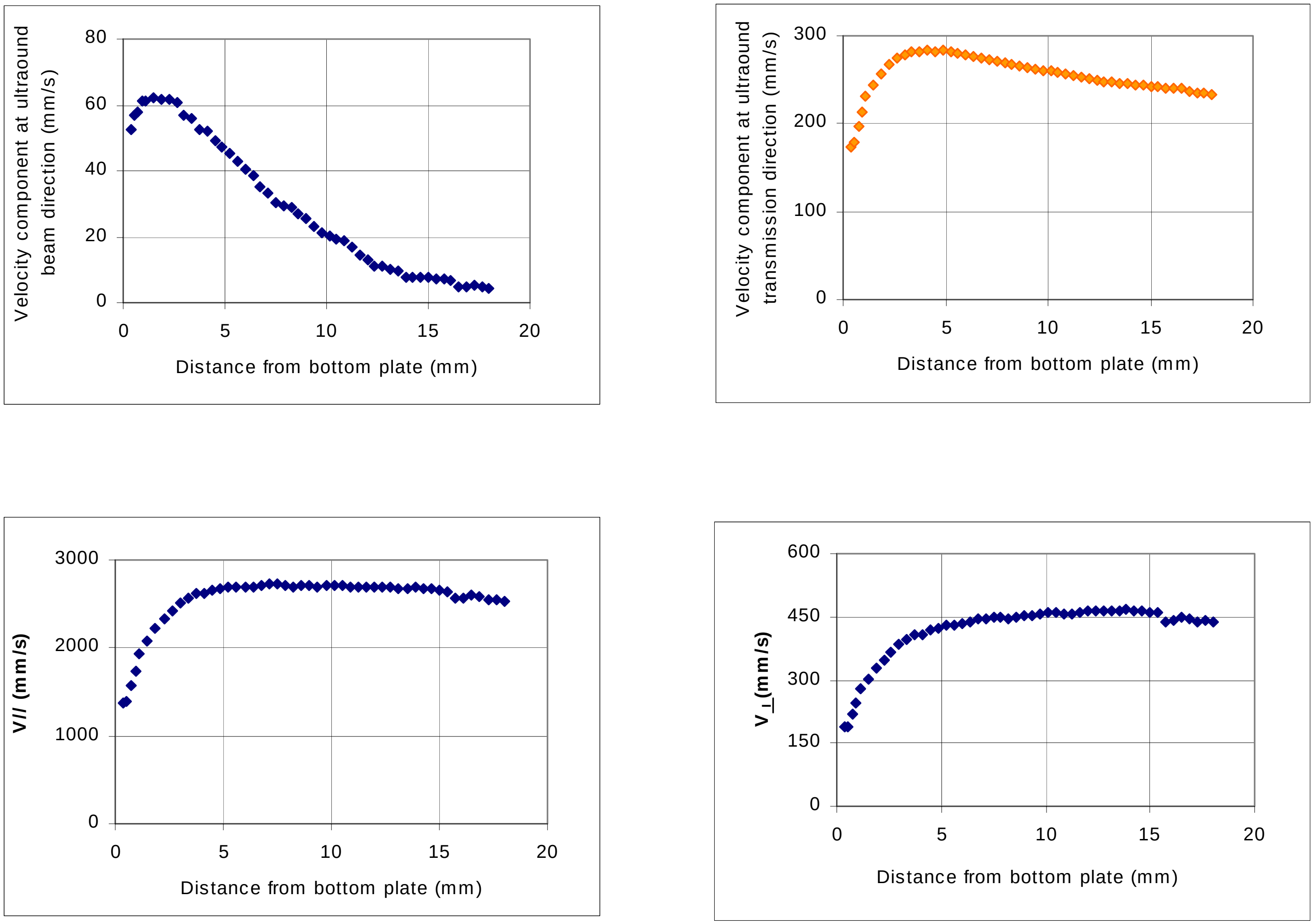

Figure 6.14 Velocity profiles of forming jet (slice opening: 20 mm, flow rate: 215 gpm).

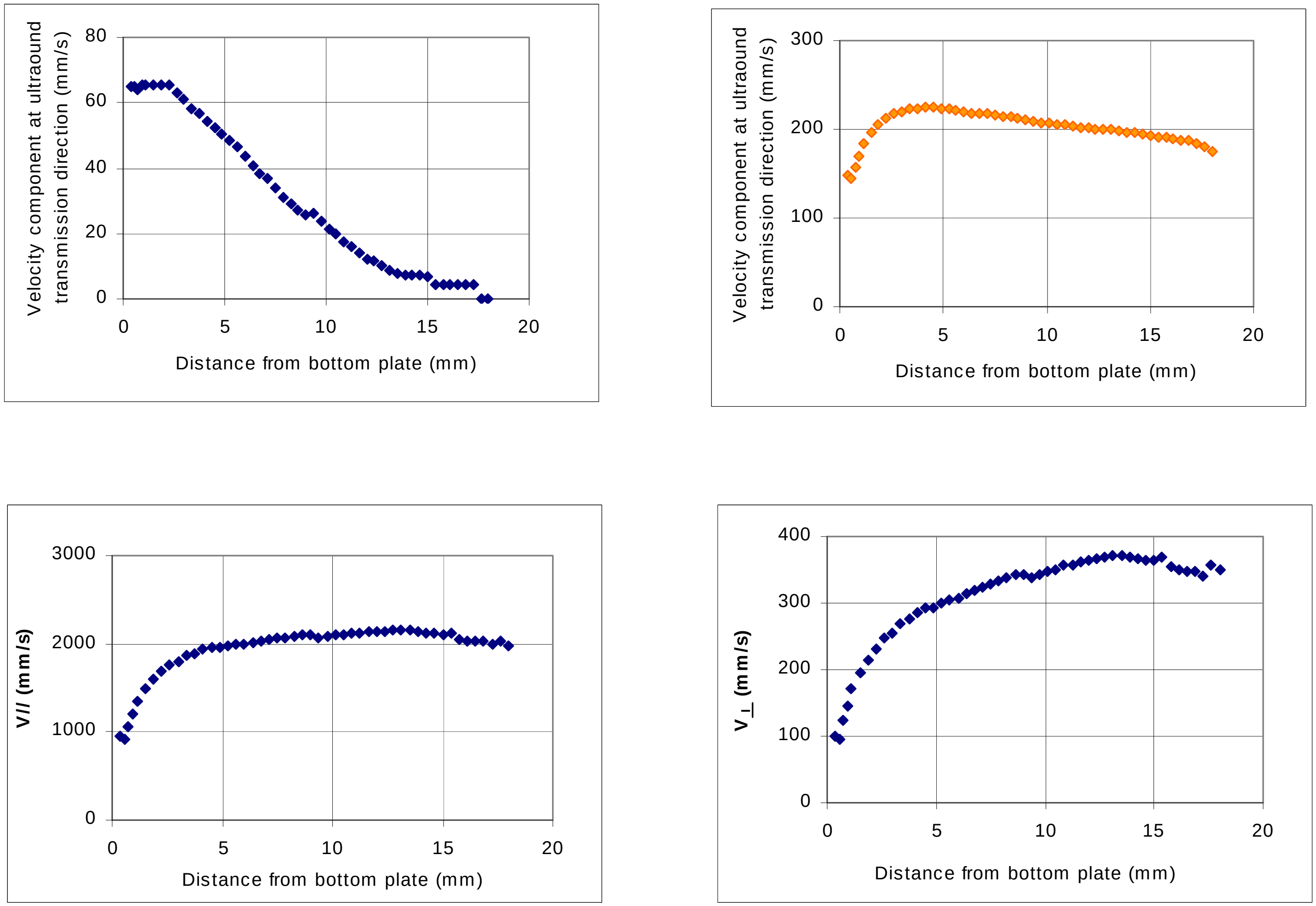

Figure 6.15 Velocity profiles of forming jet (slice opening: 20 mm, flow rate: 168 gpm).

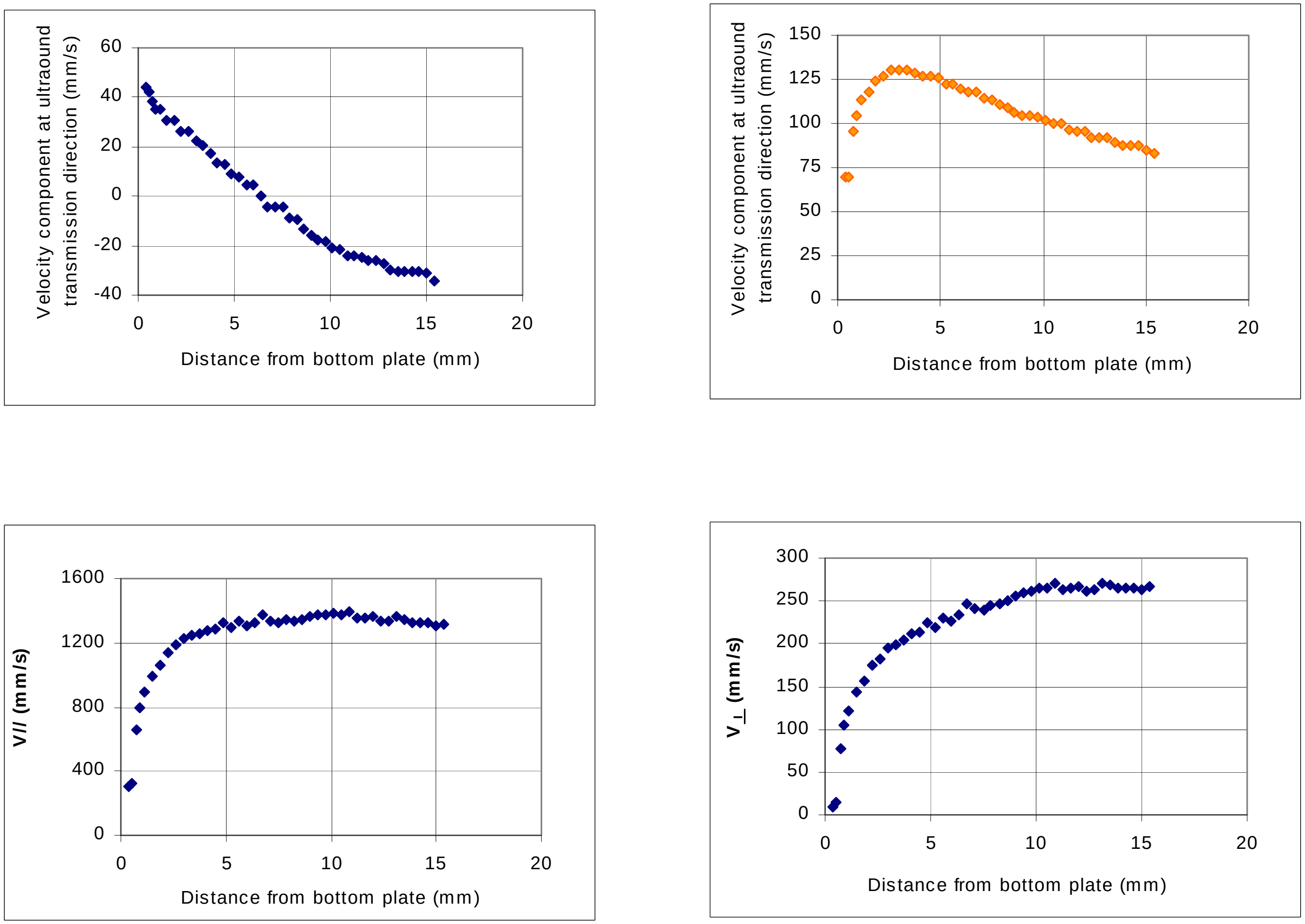

Figure 6.16 Velocity profiles of forming jet (slice opening: 20 mm, flow rate: 125 gpm).

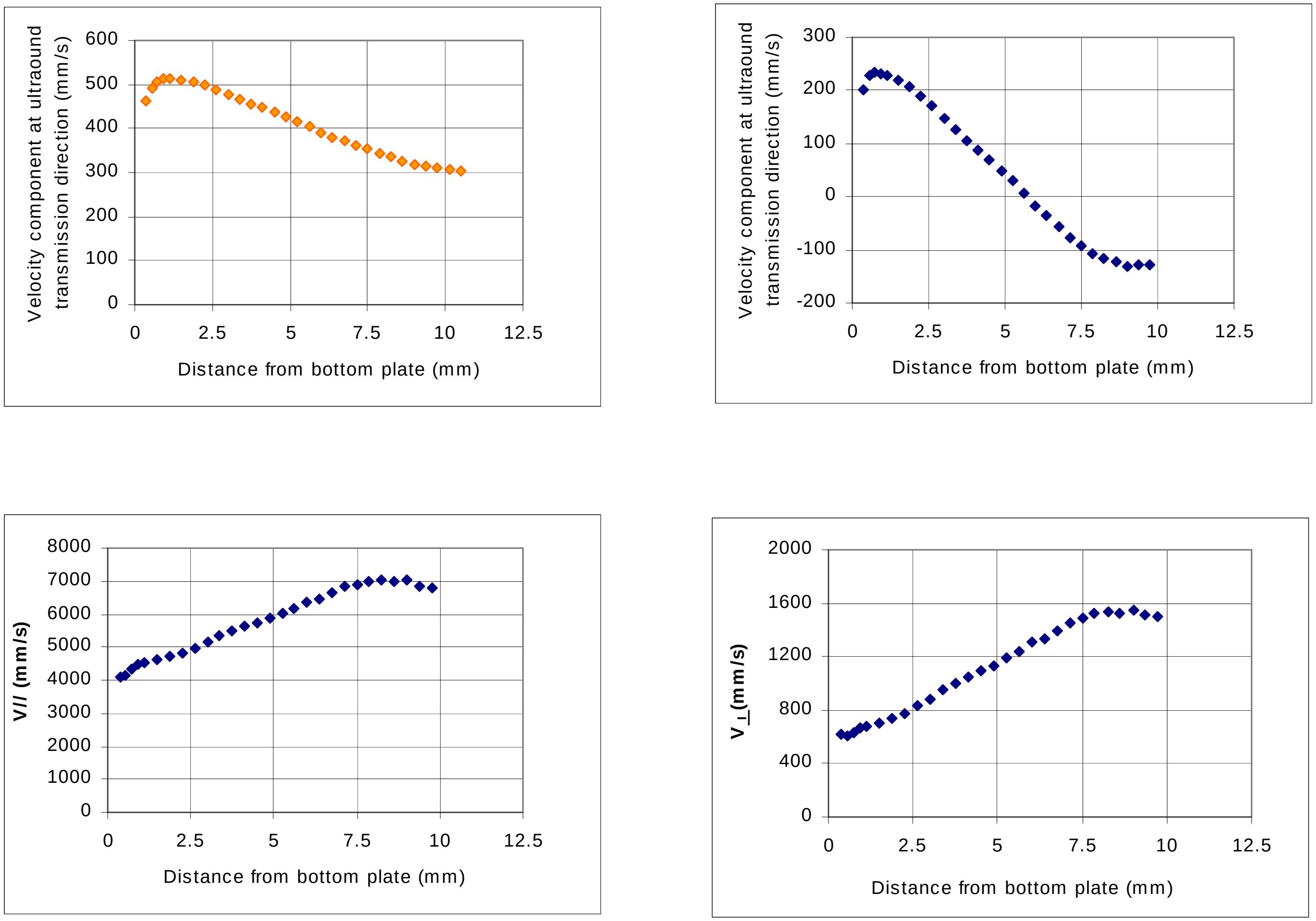

Figure 6.17 Velocity profiles of forming jet (slice opening: 15 mm, flow rate: 300 gpm).

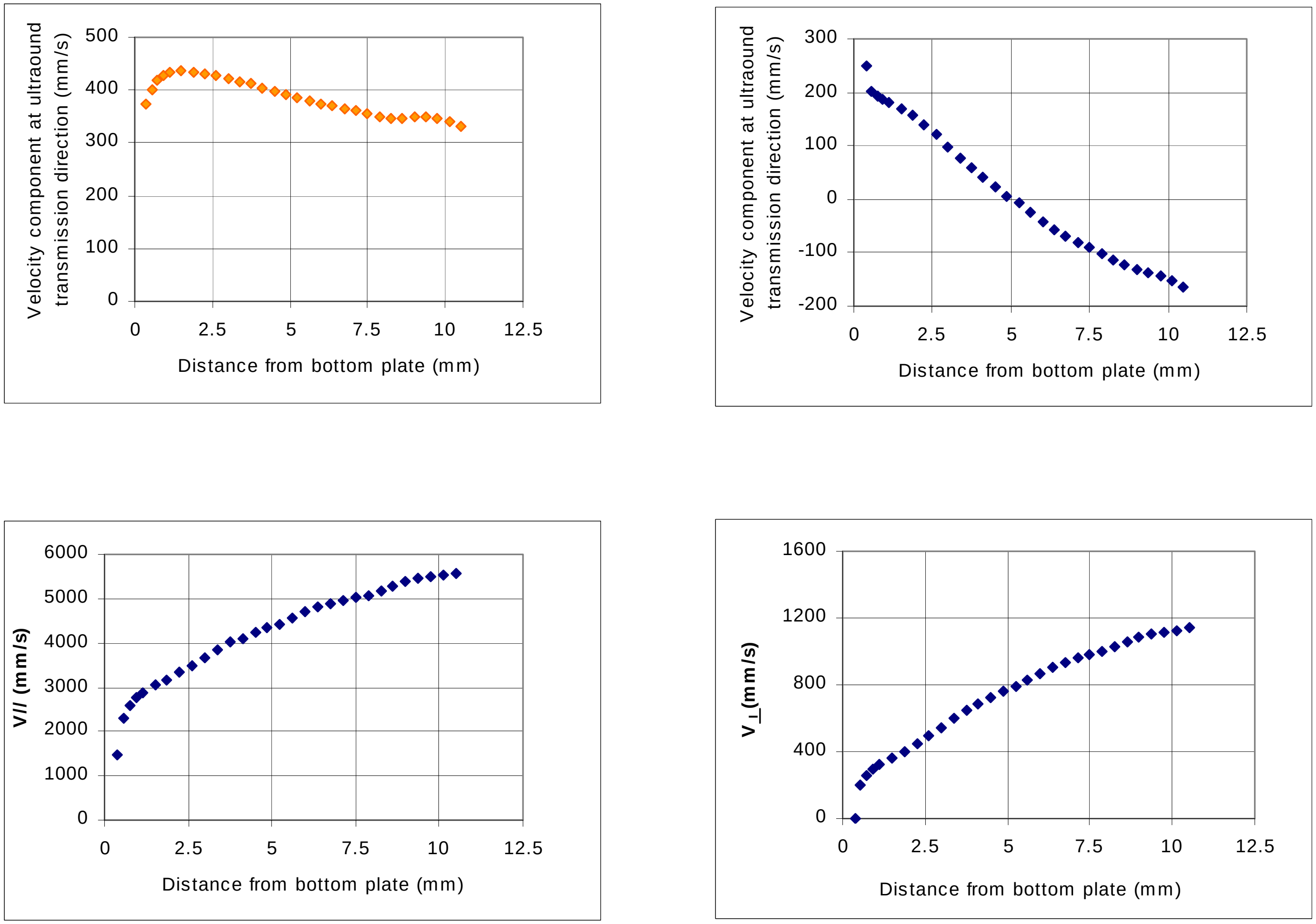

Figure 6.18 Velocity profiles of forming jet (slice opening: 15 mm, flow rate: 200 gpm).

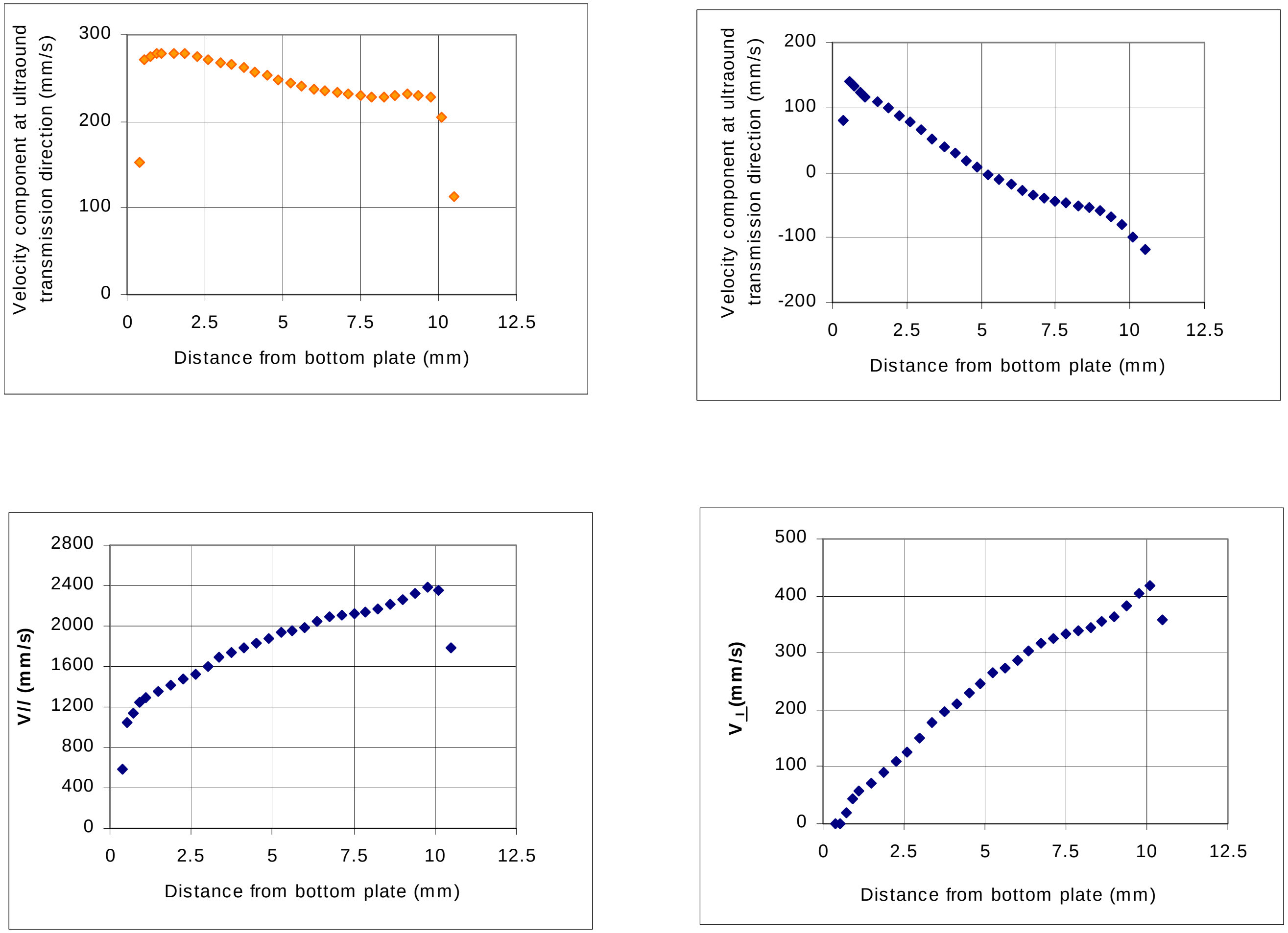

Figure 6.19 Velocity profiles of forming jet (slice opening: 15 mm, flow rate: 90 gpm).

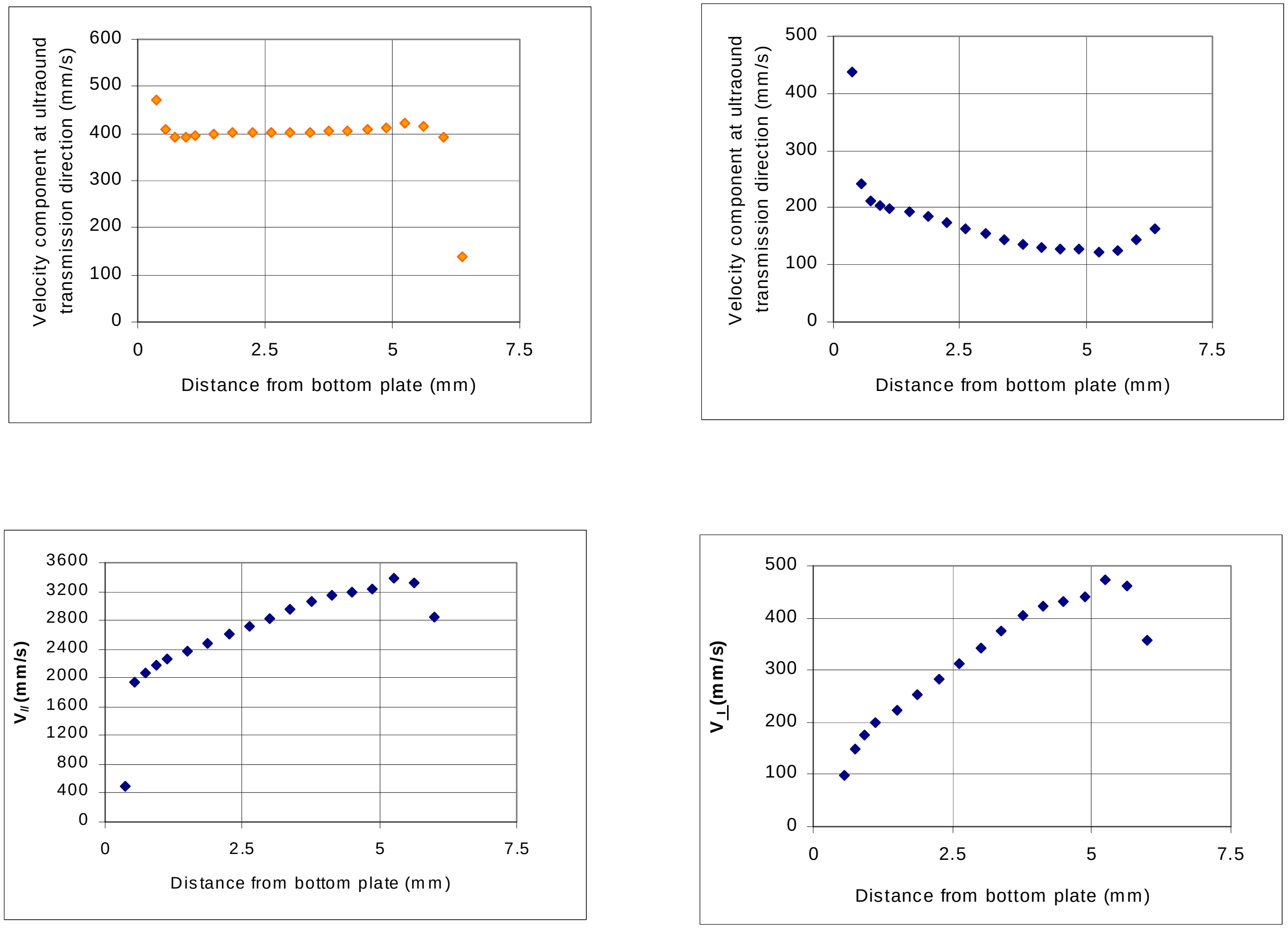

Figure 6.20 Velocity profiles of forming jet (slice opening: 10 mm, flow rate: 75 gpm).

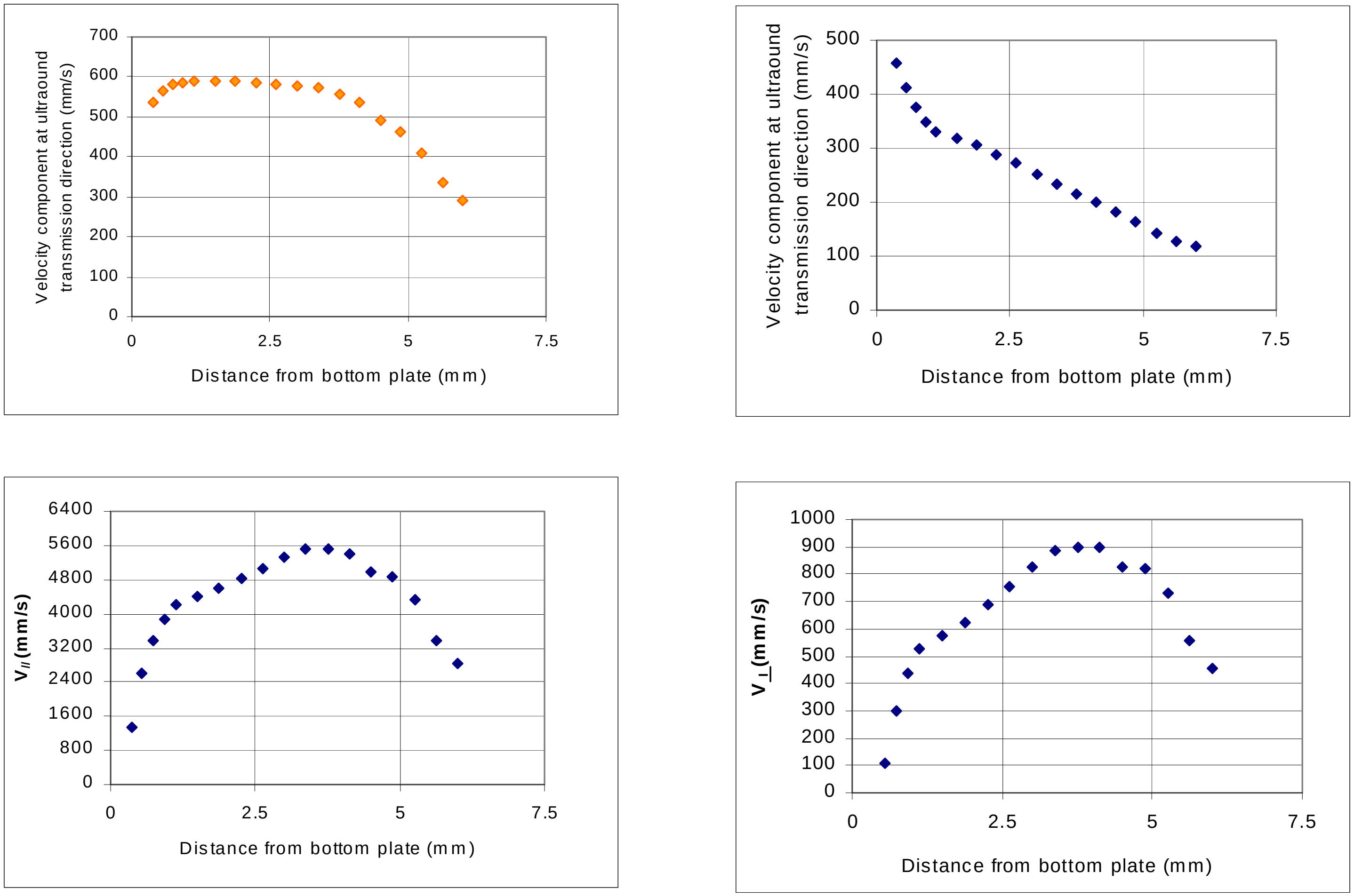

Figure 6.21 Velocity profiles of forming jet (slice opening: 10 mm, flow rate: 120 gpm).

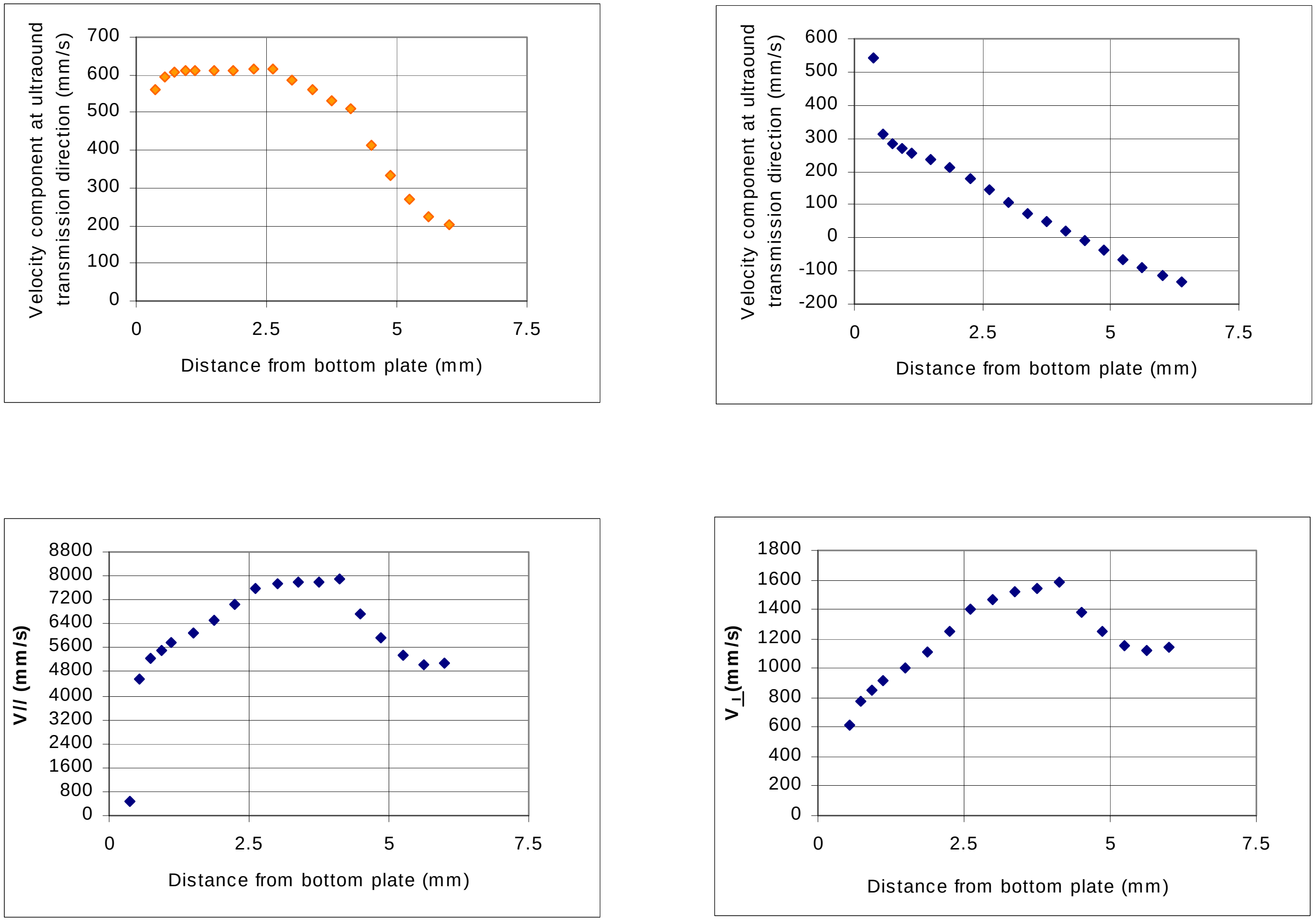

Figure 6.22 Velocity profiles of forming jet (slice opening: 10 mm, flow rate: 180 gpm).

7. CONCLUSIONS

The significant conclusions from this project are:

1. Pulsed Ultrasonic Doppler Velocimetry is an effective technique for the velocity profile measurement of fiber suspension flows. To avoid the static error caused by local velocity fluctuation during PUDV measurement, it is recommended that a sampling number higher than 256 should be used. PUDV measurement has ahigh repeatability and sensitivity.

2. In PUDV measurement, the selection of measuring parameters may affect the measuring results. Pulse repetition frequency (PRF) has a significant effect on the maximum measurable velocity. To reduce measurement errors, it is recommended that a suitable PRF be selected so that the measured velocity is comparable to the scale of maximum measurable velocity. At low flow rate, parameter "sensitivity" should be set at "high" so that the low strength signal will not be nullified. The inclination angles have no effect on the velocity profiles after position adjustment.

3. The maximum measurable depth and velocity of PUDV measurement are determined by pulse repetition frequency, inclination angles, and ultrasound frequency. By selecting suitable measuring parameters, PUDV can measure fiber suspension flow up to a velocity comparable to the papermaking process.

4. Fiber concentrations and flow rates will affect the shape of velocity profiles of fiber

suspension flow in straight rectangular channels. With the changes of fiber concentrations and flow rates, five types of flow exist in the fiber concentration-Reynolds number space. In Type 1 flow, the flow behavior and velocity profiles are similar to that of Newtonian fluid. The shape of the velocity profile does not change with fiber concentration and Reynolds number. In Type 2 flow, the velocity profile will become sharper with the increase of fiber concentration and/or the reduction of Reynolds number. With further increase of fiber concentration and/or decrease of the Reynolds number, in Type 3 flow, velocity profile becomes blunt again. In Type 4 flow, a central plug will be formed in the center of channel. At very high consistency and low Reynolds number, in Type 5 flow, the plug can fill all flow regions.

5. The velocity profile of turbulent fiber suspension can be described by $u^+ = \frac{1}{0.41}\ln(y^+) + 4.69 + \frac{\Pi}{0.41}\sin^2(\frac{y}{0.9b}\pi)$, where b is the height of the channel, Π is the wake constant and it is a function of fiber concentration nl^3 and Reynolds number Re, and $\Pi = 0.98\exp(0.14nl^3 - 1.9*10^{-5}*\mathrm{Re})$.

6. Addition of fiber to the suspension will affect the momentum transfer in two different ways. It will reduce the turbulence and thus reduce the momentum transfer. On the other hand, the fibers will interlock with each other and increase the momentum transfer. Data from velocity profile measurements indicate the turbulence intensity decreases with increasing fiber concentration. After the plug forms, the turbulence intensity in the plug region is greatly reduced.

7. Addition of fibers to the flow will cause drag reduction. In the mixed flow regime, the

suspension friction factor increases with increasing fiber concentration; in the turbulent flow regime, the suspension friction factor decreases with increasing fiber concentration. The size of the plug will increase with increasing pulp consistency and decreasing flow rate. There was a progressive increase in the shear stress for disrupting the fiber plug as the plug radius decreased.

8. Preliminary studies show that PUDV can be used to measure the velocity profile of a jet issued from a rectangular channel. The measurements have high repeatability and are sensitive to small flow rate changes.

9. By installing an ultrasound transducer underneath the apron, it is possible to obtain the forming jet ZD velocity profile through two measurements with different inclination angles. The accuracy of jet thickness measurement is dependent on the position resolution of PUDV measurement. When the thickness of the forming jet is more than 20 mm, it is possible to measure the average forming jet flow rate with accuracy better than two percent.

A number of important findings are addressed in this thesis. The PUDV has been demonstrated to be an excellent non intrusive method for the fiber suspension flow measurement and more importantly, this technique can be applied to the forming jet ZD velocity profile measurement. The five types of flow behaviors observed in this study resolve the contradiction results reported in the literature on how fiber concentration and flow rate affect the velocity profiles. A mathematical model based on the fiber concentration and Reynolds number was proposed to predict fiber suspension flow velocity profile in the turbulent flow regime. In addition, the change of turbulence intensity with the fiber concentration confirms the results reported by other authors. The velocity profile measurements and turbulence intensity measurements provide an insight in understanding the turbulent structure and flow mechanisms of fiber suspension flow.

SUGGESTIONS FOR FUTURE RESEARCH

There is room for a considerable amount of additional work on the application of PUDV to the study of fiber suspension flow behavior, to the forming jet velocity profile measurement, and to other applications in the pulp and paper industry.

1. In the current study, the diameter of the ultrasound is 5 mm in most of the measurements. To reduce the size of sample volume, a transducer with small diameter or a focus transducer can be used. By reducing the lateral size of sample volume, the accuracy of the measurement may increase further.

2. The position resolution in the ultrasound beam direction is 0.36 mm in this study. With such a resolution, it is hard to obtain the velocity distributions in the boundary layer if the channel depth is 37 mm. If a larger channel is used, it will be possible to measure the velocity distribution inside the boundary layer. This information will help us to understand the fiber suspension flow behavior significantly.

3. The different types of flow regimes observed in this study are based on the velocity profile measurements for an unbleached kraft pulp. However, the flow behavior of fiber suspension flow is also dependent on the characteristics and species of fibers. Fibers with different characteristics and species should be used in future studies to confirm the observations.

4. In the forming jet velocity profile measurement, ultrasound gel was used to increase the transmission of ultrasound. This type of gel will shrink and harden with time after the organic components evaporate, which will affect ultrasound transmission. If we want to apply PUDV

for online measurement, a new type of coupling medium should be selected. Another method is to integrate the transducer with the apron together during manufacture of the transducer.

5. In the current study, the forming jet velocity profiles are obtained based on the two measurements at different inclination angles. After the first measurement, the transducer was moved to another location with a different inclination angle. This method is not suitable for online measurement. Fortunately, velocity profiles can be obtained simultaneously from different locations through multiplex, which is a device that collects the velocity information from different transducers and then sends it to PUDV. It is recommended to use multiplex to measure the velocity profile at different locations simultaneously.

6. In this research, we focused on the forming jet velocity profile measurement in the ZD direction. However, it should be noted that the flow in the CD direction could also be measured using PUDV.

7. In addition to velocity profile measurements of fiber suspension flow, it is also possible to apply PUDV in other areas of pulp and paper industry. For example, the strength of echo ultrasound may be used to obtain information about the fiber concentrations (Figure 4.1). By applying PUDV to the black liquor flow measurement, the viscosity of black liquor can be obtained based on the measured velocity profiles.

NOMENCLATURE

c: ultrasound speed in the medium

b: channel height

d: transmitting constant in Piezoelectric effect

d: diameter of the fiber

D: hydrodynamic diameter of channel, m

f: friction factor

f_0: ultrasound frequency of the transducer

f_d: Doppler shift frequency

f_g: frequency of the ultrasound waves perceived by the target

f_r: frequency of the ultrasound waves received by transducer

f_{max}^{D}: maximum detectable Doppler frequency

g: receiving constant in piezoelectric effect

K: von Kármán constant

l: fiber half length

L: fiber length

n: number of the particle per unit volume

x: channel length

P: pressure inside the channel

PRF: pulse repetition frequency

PRF_{max}: maximum pulse repetition frequency

r: radius of the particle or pipe

r: aspect ratio

R: the distance between the transducer and the measuring point

Re: Reynolds number

R_{max}: the maximum measurable depth of PUDV

S_l: the sample volume length

t: time delay between the start of the pulse and its reception

t_b: ultrasound burst duration

U: bulk flow velocity

u: mean streamwise velocity

U^+ : reduced velocity

U_{max}: velocity at the center of the channel

U_τ : wall shear velocity

$V_{//}$: velocity component in the direction parallel to the bottom plate

v: particle moving velocity

$V_\perp$: velocity component in the direction perpendicular to bottom plate

V_0: velocity inside a forming jet

V_1: projected velocity component in the ultrasound transfer direction

V_2: projected velocity component in the ultrasound transfer direction

V_{max}: maximum detectable velocity

y: distance from channel inner wall

y^+ : reduced position

α: inclination angle between ultrasound and the bottom plate of the headbox

β: the angle between the jet and ultrasound transfer direction

ν : kinematic viscosity

Π : wake coefficient

θ: angle between the ultrasound wave transfer and particle moving direction

ρ: fluid density

τ: shear stress in the flow

τ_p: stress acting on the plug

τ_w: wall shear stress

τ_y: disruptive shear stress

ε: dielectric constant

ϕ: volume fraction of fibers in the suspension

LITERATURE CITED

Abbot, J. R., Tetlow, N., Graham, A.L. et al., 1991. Experimental observations of particle migration in concentrated suspensions: Couette flow. J. Rheol. Vol 35, 773.

Aidun, C.K., 1996. Hydrodynamics of streaks on the forming table, Tappi Journal, 155(8):80 (1996)

Aidun, C.K., 1997. A fundamental opportunity to improve paper forming, Tappi Journal, 55(6):79.

Andersson, O., 1966. Some observations on fiber suspensions in turbulent motion. Svensk Papperstidning, 69(2), p 23.

Andersson, S. R., Rasmuson, A., 2000. Flow measurement on turbulent fiber suspension by Laser Doppler Anemometry. AIChE J., 46(6):1106-1119.

Aritomi, M., Zhou, S., Nakajima, M., Takeda, Y., Yoshioka, Y., 1996. Measurement system of bubbly flow using ultrasonic velocity profile monitor and video data procesing unit, J. Nucl. Sci. Technol, 33:915-923.

Baker, D.W. and Watkins, D., 1967. A phase coherent pulse Doppler system for cardiovascular measurement. Proceedings of 20th annual conference on engineering medical biology. 27:2.

Baker, D.W., 1970. Pulsed Ultrasonic Doppler Blood-Flow Sensing, IEEE Trans. Sonics Ultrason., Su-17:170.

Baker, D.W., Campau, D.N., 1973. Characteristics and mathematical modeling of the pulsed ultrasonic flowmeter. Medical and Biological Engineering, July.

Batchelor, G.K., 1971. The Stress Generated in a Non-Dilute Suspension of Elongated Particles by Pure Straining Motion. J. Fluid Mech. Vol. 46, pp. 813-829.

Beyer-Portner, N.A., Decesare, G., Schleiss, A., Boillat, J.L., 1998. Erosion and sedimentation in mountainous environment - physical and numerical modeling, Proceedings of Humid Tropics' 98, Pangkor Island, Malaysia, November 1998.

Blakeney, W.R., 1966. The viscosity of suspension of straight, rigid rods. Journal of Colloid and Interface Science, 22, 324.

Bobkowicz, A. J., Gauvin, W. H., 1967. The effects of turbulence on the flow characteristics of model fiber suspensions. Chemical Engineering Science 22:229.

Bobkowicz, A. J., Gauvin, W. H., 1972. Canadian Journal of Chemical Engineering, 43:87.

Bodenheimer, V.B., 1969. Channeling in bleach toners and friction losses in pulp stock lines. Southern pulp and paper manufacturer. 32(9):42.

Borner, T., Durst, F., and Manero, E., 1986. 3rd international symposium on Application Laser Anemometry to fluid mechanics, Lisbon, Portugal, P. 4.3.

Brecht, W., Heller, H., 1950. A study of the pipe friction losses of paper stock suspensions. Tappi 33(9):14A.

Cellino, M. and Graf, W.H., 2000. Experiments on suspension flow in open channels with bed forms. Journal of Hydraulic Research, 38(4): 289-298.

Carter, L.F., 1967. A study of the rheology of suspension of rod-shaped particles in an N-S fluid, Ph.D. thesis, University of Michigan.

Chuang, S.C., 1982. Microturbulence generation in a paper machine headbox. Proceedings of Tappi Engineering Conference, P205, San Francisco, CA.

Daily, J. W., Bugliarello, G., Troutman, W. W., 1959. M.I.T. Hydrodynamics Lab. Tech. Report No. 35.

Daily, J., Bugliarello, G., 1958. "The Effect of Fibers on Velocity Distribution, Turbulence and Flow Resistance of Dilute Suspensions," M.I.T. Hydrodynamics Laboratory Report, No. 30, Cambridge, Mass., Massachusetts Institute of Technology.

Daily,J., and Bugliarello, G.,1961. Tappi 44:497.

Deininger, A., Gurthert, F.W., Widerer, P.A. 1996. The influence of Currents on circular secondary clarifier perfomance and design, 18th IAWQ Biennial Conference on Water Quality, Conference Prepring Book 3, Singapore.

Dong, S., Feng, X., Salcudenan, M., Gartshore, I., 2003. Concentration of pulp fibers in 3D turbulent channel flow. *Int. J. Multiphase Flow* 29, 1-21.

Duffy, G.G., Titchener, A.L., Lee, P.F.W., and Moller, K., 1976. The mechanisms of flow of pulp suspension in pipes. Appita 29 (5):363.

Ek, R., 1979. Int. Symp. of Paper Machine Headboxes. McGill University, Montreal, Canada.

Flaherty, J.J., Strauts, E.G., 1969. Ultrasonic pulsed Doppler instrumentation. Proceedings 8th international conference on medical biology engineering. 10-10.

Forgacs, O.L., Robertson. A.A., Mason, S.G., 1958. The hydrodynamic behavior of paper-making fibers. Pulp Paper Mag. Can., 59(5), 117-128.

Fry, J.F., 1978. Ultrasound: its application in medicine and biology. Elsevier Scientific Publishing Company, New York.

Franzen, M. F., 1987. Direct measurement of jet velocity as an aid to papermaking. Tappi Journal 70, No. 7:63-67.

Fry, J.F., 1965. Recent developments in ultrasound at the biological research laboratory and their application to basic problems in biology and medicine. Ultrasonic Energy, Kelly E., Ed., University of Illinois press, Urbana.

Goldstein, S.,. 1935. Cambridge Phil. Soc. 31(2):232(1935), as referenced in Lee 1976b.

Gore, R. A., Crowe, C. T., 1989. Effect of particle size on modulating turbulent intensity. Int. J. Multiphase Flow 15(2):279-285.

Gore, R.A., Crowe, C.T., 1991. Modulation of turbulence by dispersed phase. Trans. ASME I: J. Fluid Engng 113, pp 304-307.

Hand, J.H., 1982. Laser penetration in fiber suspensions, Beloit Corp., Research and Development, Rockton, IL.

Harlen, O.G., Koch D.L., 1992. Extensional flow of a suspension of fibers in a dilute polymer solution. Phys. Fluids A 4, pp 1070-1073.

Hinch, E.J., Leal, L.G., 1976. Constitutive equations in suspension mechanics. Part 2. Approximate forms for a suspension of rigid particles affected by Brownian rotations. J. Fluid Mech. 76, 187.

Hirsuimaki, O., 1978. Determination of radial velocity profile and flow disturbance of pulp suspension by ultrasonic echo correlation. Paperi Puu, 60(2):95.

Hirsuimakr, O., Karkonen, E., Karras, M., et al.,1982. Pulp suspension flow measurement using ultrasonic and correlation. IEEE Ultrasonics Symp. (San Diego) Proc. Vol. 2: 915.

Hookham, P. A., 1986. Concentration and velocity measurement in suspensions flowing through a rectangular channel. PhD thesis, California Institute of Technology.

Hueter, T.F. and Bolt, R.H., 1955. Sonics. John Wiley & Sons, inc., New York.

Hutchinson, P., Hewitt, G., Dukler, A. E., 1971. Deposition of liquid or solid dispersion from turbulent gas streams: a stochastic model. Chemical Engineering Science 26:419-439.

Ilmoniemi, E., Kli-Kokko, E., 1986. The Role Of Headbox Turbulence Generators In Grammage Uniformity, 39:36.

Kallio, G.A., Reeks, M.W., 1989. A numerical simulation of particle deposition in turbulent boundary layers. *Int. J. Multiphase Flow* **15**, 433–446.

Kerekes, R. J. E., 1970. Turbulent Drag Reduction in Pipe Flow of Ideal Fiber Suspensions. Doctoral Dissertation, McGill University, Canada.

Kerekes, R.J., Garner, R.G., 1982. Trans.Tech. Sect., CPPA 8, 3, TR 53.

Kerekes, R.J.E., Douglas, W.J.M., 1972. Viscosity properties of suspensions at the limiting conditions for turbulent drag reduction. Canadian Journal of Chemical Engineering. 50:228.

Koch, D.L., Shaqfeh, S.G., 1990. The Average rotation rate of a fiber in the linear flow of a semidilute Suspension. Phys. Fluids A Vol. 2, pp. 2093-21-02.

Koh, C. J., Hookham, P., Leal L. G., 1994. An experimental investigation of concentrated suspension flows in a rectangular channel. J. Fluid Mech., 266:1-32.

Kroger, C., Drossinos, Y., 2000. A random-walk simulation of thermophoretic particle deposition in a turbulent boundary layer. *Int. J. Multiphase Flow* **26** , 1325–1350.

Kulick, J.D., Fessler, J.R., Eaton J.K. 1994. Particle response and turbulence modification in fully developed channel flow. J. Fluid Mech., Vol. 27, pp 109-134.

Lee, P. F. W., Duffy, G. G., 1975. Models for the drag reducing regime of pulp suspension flow. TAPPI Engineering Conf. Proc. :137-142.

Lee, P. F. W., Duffy, G. G., 1976. An analysis of the drag reducing regime of pulp suspension flow. TAPPI J. 59(8):119-122.

Lee, P. F. W., Duffy, G. G., 1976a. An analysis of the drag reducing regime of pulp suspension flow. TAPPI J. 59(8):119-122.

Lee, P. F. W., Duffy, G. G., 1976b. Velocity profiles in the drag reducing regime of pulp suspension flow. Appita 30(3):219-226(1976 b).

Lee, P. F. W., Duffy, G. G., 1976c. Relationships between velocity profiles and drag reduction in turbulent fiber suspension flow. AIChE J. 22(4):750-753.

Lee, P. F. W., Duffy, G. G., 1977. Paper presented at Appita Conference, Queensland, March, 1977.

Lhermitte, R., Lemmin, U., 1996. Open-channel Flow and Turbulent Measurement by High-resolution Doppler Sonar, J. Atmos., & Oceanic Technol. 11, 1296-1308.

Li, T.Q., Powell, R.L. etc., 1994. Velocity measurements of fiber suspensions in pipe flow by nuclear magnetic resonance imaging method, Tappi Journal, 77:145.

Li, T.Q., Powell, R.L., 1995. Flow of pulp suspension through a 4:1 continuous conical contraction studied by NMR imaging technique, Tappi Engineering Conference.

Liljegren, L. M., Vlachos, N. S., 1990. Laser velocimetry measurements in a horizontal gas solid pipe flow. Experiments in Fluids 9:205-212.

Loewen, S. R., Buttler, R. L., 1991. Laserspeed Measurement of Forming-Section Flow Properties. CPPA Annual Meeting 77a: A349-352.

Maneval, J.E., McCarthy, M.J., 1991. NMR flow measurements in fibrous suspensions, Tappi Proceedings, Engineering Conference.

Mason, S.G., Nawab, M.A., 1958. J. Phys. Chem., 62, 1248.

McComb, W. D.; Chan, K. T. J., 1985. Laser-Doppler anemometer measurements of turbulent structure in drag-reducing fiber suspensions. J. Fluid Mech. 152:455.

McComb, W.D., 1991. The Physics of Fluid Turbulence, Oxford Science Publications, Oxford.

Meyers, W.T., 1962. Ph.D. thesis, Institute of Paper Chem., Appleton, June 1962.

Mih, W., Parker, J., 1967. Velocity profile measurement and a phenomenological description of turbulent fiber suspension pipe flow, Tappi 50(5):237.

Moller, K., 1976. A correction of pipe friction data for paper pulp suspensions, Industrial and Engineering Chemistry -- Process Design and Development, 15 (1): 16-19.

Nakamura. H., 1996. Simultaneous Measurement of Liquid Velocity and Interface Profiles of Horizontal Duct Wavy Flow by Ultrasonic Velocity Profile Meter. First International Symposium on Ultrasonic Doppler Methods in Fluid Mechanics and Fluid Engineering, Villigen PSI, Switzerland.

Nielsen, C., 1997. Automatic Jet-Speed Profiling System. International CD Symposium' 97: Cross-Direction Web Measurements, Controls, and Actuator Systems in Paper Machines.

Norman, B.G., Moller, K., Ek, R., Dufffy, G.G., 1977. Hydrodynamics of papermaking fibers in water suspension. Trans. BPBIF Symp. Fiber-water Interactions, p 195.

Ogawa, K., Yoshgikawa, S., Ikeda, J., et al., 1990. Pressure loss and velocity profile of pulp flow in a circular pipe. Tappi Journal, 73(4): 217.

Ono, K., Xu, H.J., Park, C., etc., 2001. Forming jet surface velocity profile measurement with high speed digital camera, Tappi Journal, March, 2001.

Park, J. T., Mannheimer, R. J., Grimley, T. A., Morrow, T. G., 1989. Pipe flow measurements of a transparent non-Newtonian slurry. J. Fluids Engineering 111:331-336(1989).

Parker, D.J., Hawkesworth, M.R., 1995. Emission Tomography. In: Williams R.A. and Beck M.S Eds., Process Tomography: principles, techniques and applications, Butterworth Heinemann Ltd, Oxford.

Pernnneau, P.A., Leger, F., 1969. Doppler Ultrasonic pulsed blood flowmeter. Proceedings 8th International Conference on Medical Biology Engineering. 10-11.

Powell, R., Weldon, M., Ramaswamy, S., McCarthy M., 1996. Characterization of pulp suspension. In: Tappi Engineering Conference, p525.

Radin, I., Zakin, J. L., Patterson, G. K. 1975. Drag reduction in solid-fluid systems. AIChE J. 21:358-371.

Rahnama, M., Koch, D., Shaqfeh, S.G., 1995a. The effect of hydrodynamic interactions on the orientation distribution in a fiber suspension subject to simple shear flow. Phys. Fluids, 7(3):487-506.

Rahnama, M., Koch, D.L. and Cohen, C. 1995. Observation of Fiber Orientation in Suspension Subjected to Planar Extensional Flows. Phys. Fluids, Vol. 7, pp. 1811-1817.

Rahnama, M., Koch, D.L., Shaqfeh, S.G., 1995. The Effect of Hydrodynamic Interactions on the Orientation Distribution in a Fiber Suspension Subject to Simple Shear Flow. Phys. Fluids, Vol. 7, pp. 487-506.

Raij, U., and Wahren, D., 1964. An experimental investigation of paper pulp stock flow in a straight pipe, Svensk Paperstidning, 67(5):186-195, March 15, 1964.

Ricker, N.F. and Forster, F.K., 1985. Pulse Doppler ultrasonic velocity measurement in aqueous pulp fiber suspensions. Tappi Journal. 68(1): 79-82.

Reiner, L., Wahren, D., 1971. The Characterization of Flow From The Headbox Of A Paper Machine. Svensk Paperstidn, 74, 225.

Robertson, A. A., Mason, S.G., 1967. The flow characteristics of dilute fiber suspensions. Tappi 40 (5):326 (1957).

Rolland, T., Lemmin, U., 1996. Acoustic Doppler velocity profilers: application to correlation measurement in open-channel flow. First International Symposium on Ultrasonic Doppler Methods in Fluid Mechanics and Fluid Engineering, Villigen PSI, Switzerland.

Rolland, T., Lemmin, U., 1997. A two-component acoustic velocity profile for use in turbulent open-channel flow, J. Hydraulic Res., 35, 545-561.

Sanders, H. T., 1970. An Investigation of Fiber Consistency Distributions in Turbulent Tube Flow. Doctoral Dissertation, IPC.

Sanfors, L., 1976. Characteristics of Flow from A Two-Dimensional Nozzle with Multiple-Tube Inlet. In: Proceedings Of 1976 Engineering Conference, 159.

Sawada, T., Kikura, H., 1996. Kinematic characteristics of magnetic fluid sloshing in a rectangular container subject to non-uniform magnetic field, Exp. In Fluids, Vol 26, p 215.

Seely, T., 1968. Turbulent tube glow of dilute fiber suspensions. Doctoral Dissertation, IPC, Appleton, Wisconsin.

Shaqfeh, E.S.G., Fredrickson, G.H., 1990. The hydrodynamic stress in suspension of rods. Phys. Fluids A Vol. 2, pp. 7-24

Shaqfeh, E.S.G., Koch D.L., 1988. The effect of hydrodynamic interactions on the orientations of axisymmetirc particles flowing through a fixed bed of spheres or fibers. Phys. Fluids 31, 728.

Shaqfeh, S.G., Koch, D.L., 1990. The effect of hydrodynamic interactions on the orientation of axisymmetric particles flowing through a fixed bed of spheres or fibers. Phys. Fluids, Vol 31, p 728-743.

Shauly, A., Averbakh, A., Nir, A., Semiat, R., 1997. Slow viscous flows of highly concentrated suspensions ----- Part II: Particle migration, velocity and concentration profiles in rectangular ducts. In. J. Multiphase Flow, 23(4), 613-629.

Shimizu, T., 1992. Computer Simulation and Measurement of Flow in A Headbox. Proceedings of Pan-Pacific Pulp Paper Technology Conference, Part A:157.

Sinton, S. W., Chow, A. W. 1991. NMR flow imaging of fluids and solid suspension in Poiseuille flow. J. Rheol. 35, p 735.

Sommerfeld, M., 1992. Modelling of particle-wall collisions in confined gas-particle flows. Intl J. Multiphase Flow 18, p 905-926.

Steen, M., 1989. On turbulence structure in vertical pipe flow of fiber suspensions. Nordic Pulp Paper Res. J., 4:236.

Steen, M., 1990. Turbulence and Flocculation in Fiber Suspensions. Doctoral Dissertation, University of Trondheim, Norway.

Steen, M., 1989. On turbulence structure in vertical pipe flow of fibers suspensions. Nordic Pulp Paper Res. J. 4(4):244-252.

Stover, C.A., Koch D.A., Cohen C., 1992. Observations of fiber orientation in simple shear flow of a semi-dilute suspension. J. Fluid Mech. 238, p 227.

Takeda, T., 1986. Velocity Profile Measurement By ultrasound Doppler Shift Method. International Journal Of Heat And Fluid Flow, 7(4):313.

Takeda, Y., 1990. Development of ultrasound velocity profile monitor. Nucl. Eng. & Design, 126:277.

Takeda, Y., Samcc, K., Kobayashi, K., 1991. Experimental measurements of 2D velocity vector field using ultrasonic velocity profile monitor (UVP), ASME FED- Vol. 128:p47.

Takeda, Y., 1995. Velocity Profile Measurement by Ultrasonic Doppler Method. Experimental Thermal and Fluid Science, 10:444.

Uriev, B., Koller, S., Windhab, E., Baltes, H., Brand, O., 1998. Foodstuff rheology Microsensor, Prpc. MINAST conference, Second Annual Convention, p102, April, 1998, Bern.

Vaseleski, R. C., Metzner, A. B., 1974. Drag reduction in turbulent flow of fiber suspensions. AIChE J. 20:301-306.

Virk, P. S., 1975. Drag reduction fundamentals. AIChE J. 21:625-656.

Wachter, P. 1996. Application of the Ultrasound Velocity Measuring Technique to Stirred Vessel Flows with Multi Elements Stirrers. First International Symposium on Ultrasonic Doppler methods in Fluid Mechanics and Fluid Engineering, Villigen PSI, Switzerland.

Wells, P.N.T., 1977. Biomedical Ultrasonics, Academics press.

Woodcock, J.P., Ultrasonics. Adam Hilger Ltd, Thchno House, 1979.

Yamamoto, S. , Matsuoka, T., 1994. Viscosity of dilute suspensions of rod like particles: a numerical simulation method. *J. Chem. Phys.* 100 , 3317–3324.

Zhu, J.Y., 1996. Laser Doppler Velocimetry for flow measurements in pulp and paper research. IPST technical paper series, 618.

ACKNOWLEDGEMENTS

I would like to thank the Institute of Paper Science and Technology and its member companies for providing the financial support to conduct this research in a truly unique environment.

I am grateful to my thesis advisory Committee, comprised of Dr. Cyrus Aidun, Dr. Seppo Karrila, Dr. Junyong Zhu. Their guidance, comments and suggestions during my work on this thesis have made the endeavor both challenging and successful. I would especially wish to express my gratitude to my advisor, Dr. Aidun, for his assistance, guidance and time provided on a continual basis.

I would like to extend my appreciation to Electronic and Machine Shop for their assistance during the development of the experimental apparatus and the construction of the flow loop. Many thanks go to Jerry Kloth, Jerry Nunn, Brent Minter and Juan Chevere.

Finally, I wish to thank my family for their sincere encouragement and emotional support.

APPENDIX I BLUEPRINTS FOR THE DISTIBUTOR AND CHANNEL

This appendix contains the blueprints of the computer aided drawings obtained using the program Pro Engineering. The blueprints include:

(1) Images of distributor and channel;

(2) Distributor side wall (Figure 1 of 5);

(3) Distributor back wall (Figure 2 of 5);

(4) Distributor bottom wall (Figure 3 of 5);

(5) Distributor front wall (Figure 4 of 5);

(6) Distributor top wall (Figure 5 of 5);

(7) Channel top wall (Figure 1 of 3);

(8) Channel bottom wall (Figure 2 of 3);

(9) Channel side wall (Figure 3 of 3)

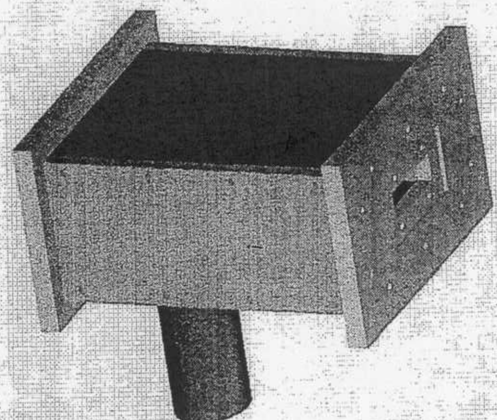

Distributor dimensions (inside):

8” × 5” × 2.25”

Material: 0.5 inch Plexiglas

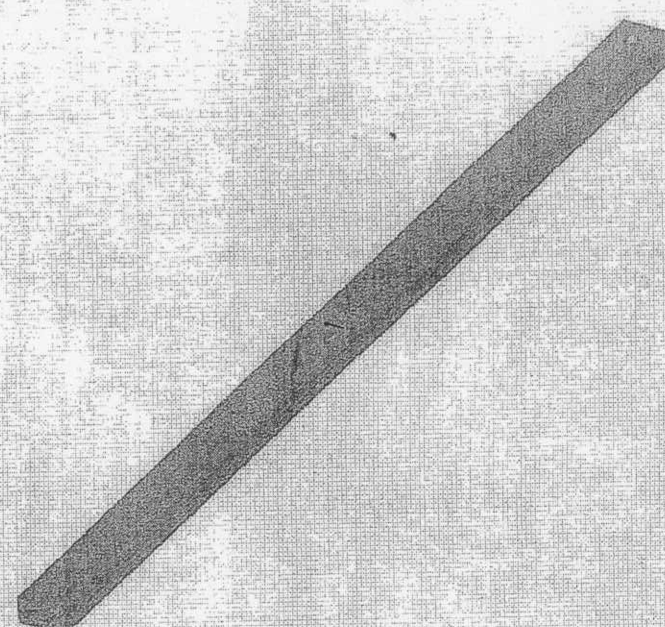

Channel dimensions (inside):

60” × 2” × 0.65”

Material: 0.5 inch Plexiglas

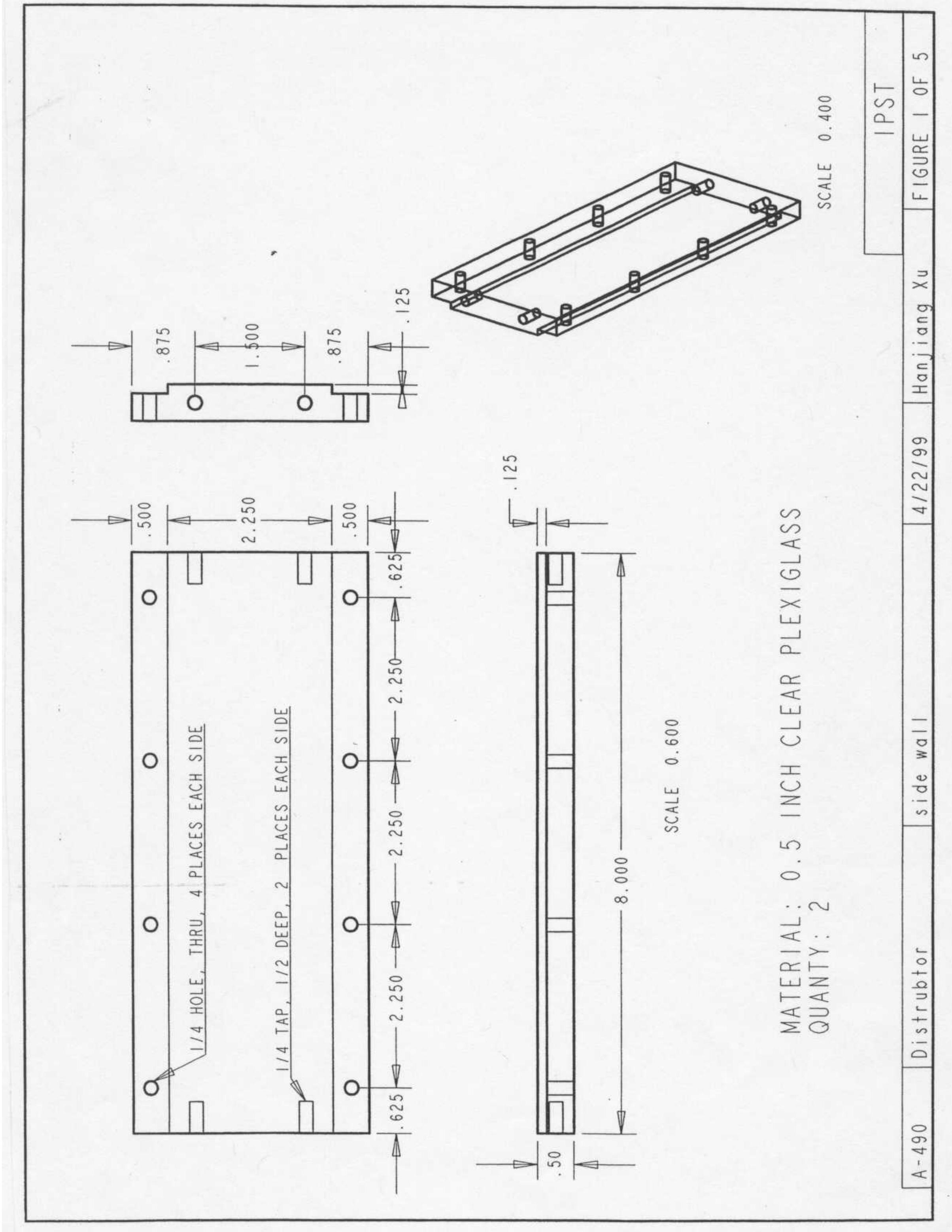

1/4 HOLE, THRU, 4 PLACES EACH SIDE
1/4 TAP, 1/2 DEEP, 2 PLACES EACH SIDE
.500
2.250
.500
.625
2.250
2.250
2.250
.625
.125
8.000
.50
.875
1.500
.875
.125
SCALE 0.600
SCALE 0.400
MATERIAL: 0.5 INCH CLEAR PLEXIGLASS
QUANTY: 2
A-490
Distrubtor
side wall
4/22/99
Hanjiang Xu
FIGURE 1 OF 5
IPST

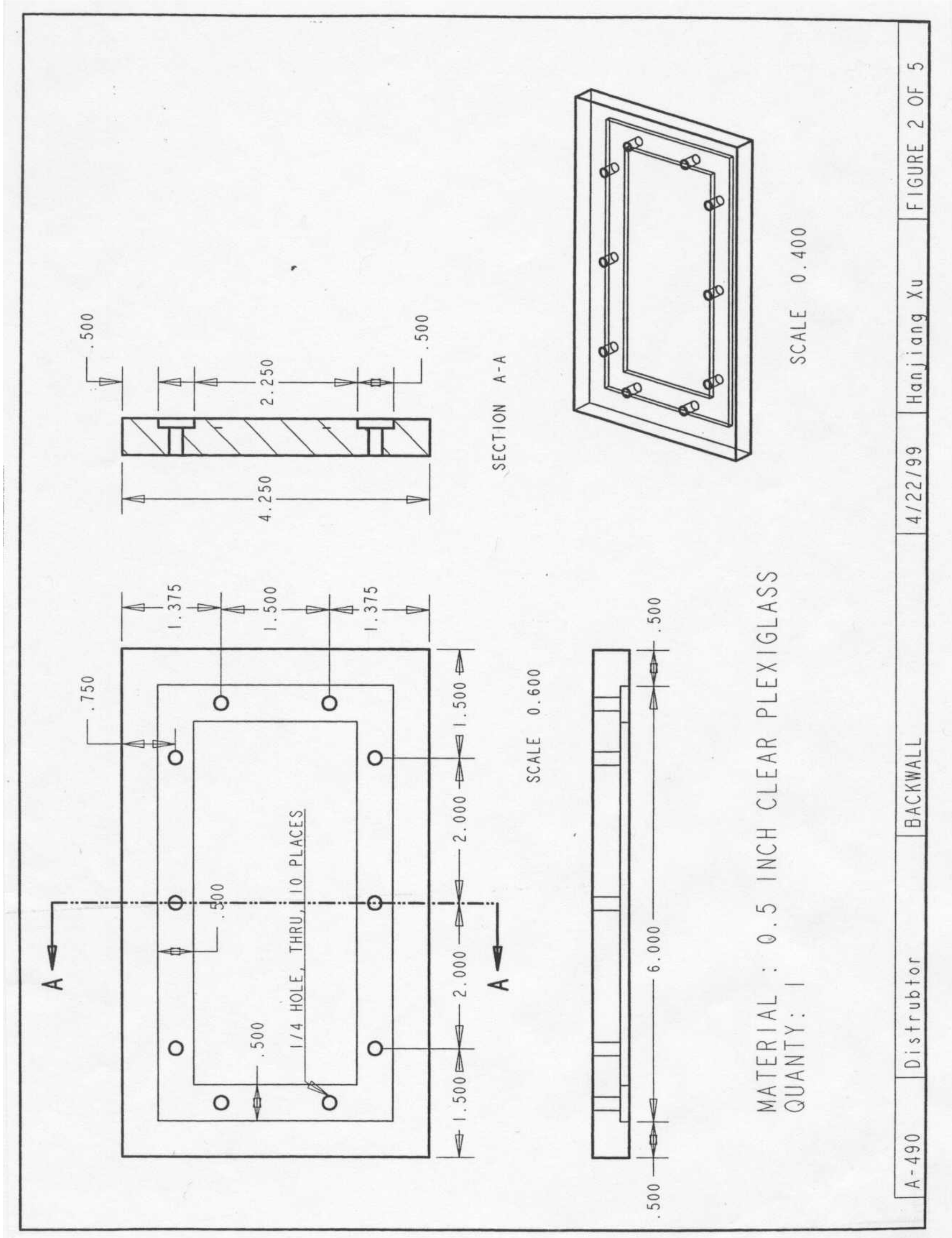
MATERIAL : 0.5 INCH CLEAR PLEXIGLASS
QUANTY: 1
1/4 HOLE, THRU, 10 PLACES
SCALE 0.600
SECTION A-A
SCALE 0.400
A-490
Distrubtor
BACKWALL
4/22/99
Hanjiang Xu
FIGURE 2 OF 5

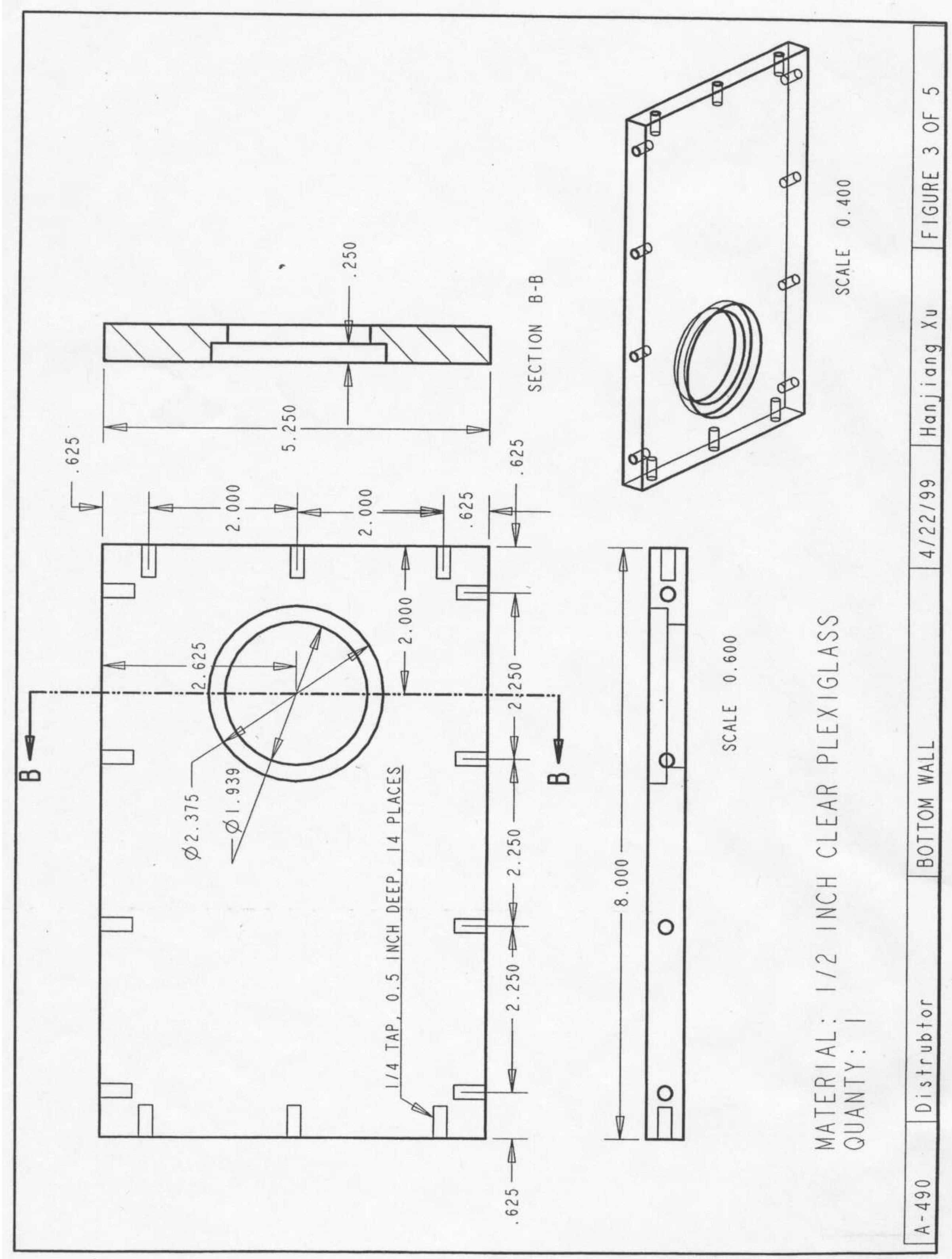
MATERIAL: 1/2 INCH CLEAR PLEXIGLASS
QUANTY: 1
A-490
Distrubtor
BOTTOM WALL
4/22/99
Hanjiang Xu
FIGURE 3 OF 5
SECTION B-B
SCALE 0.600
SCALE 0.400
1/4 TAP, 0.5 INCH DEEP, 14 PLACES
Ø2.375
Ø1.939
B
B
.625
2.000
2.000
.625
.625
5.250
.250
2.625
2.000
2.250
2.250
2.250
.625
8.000

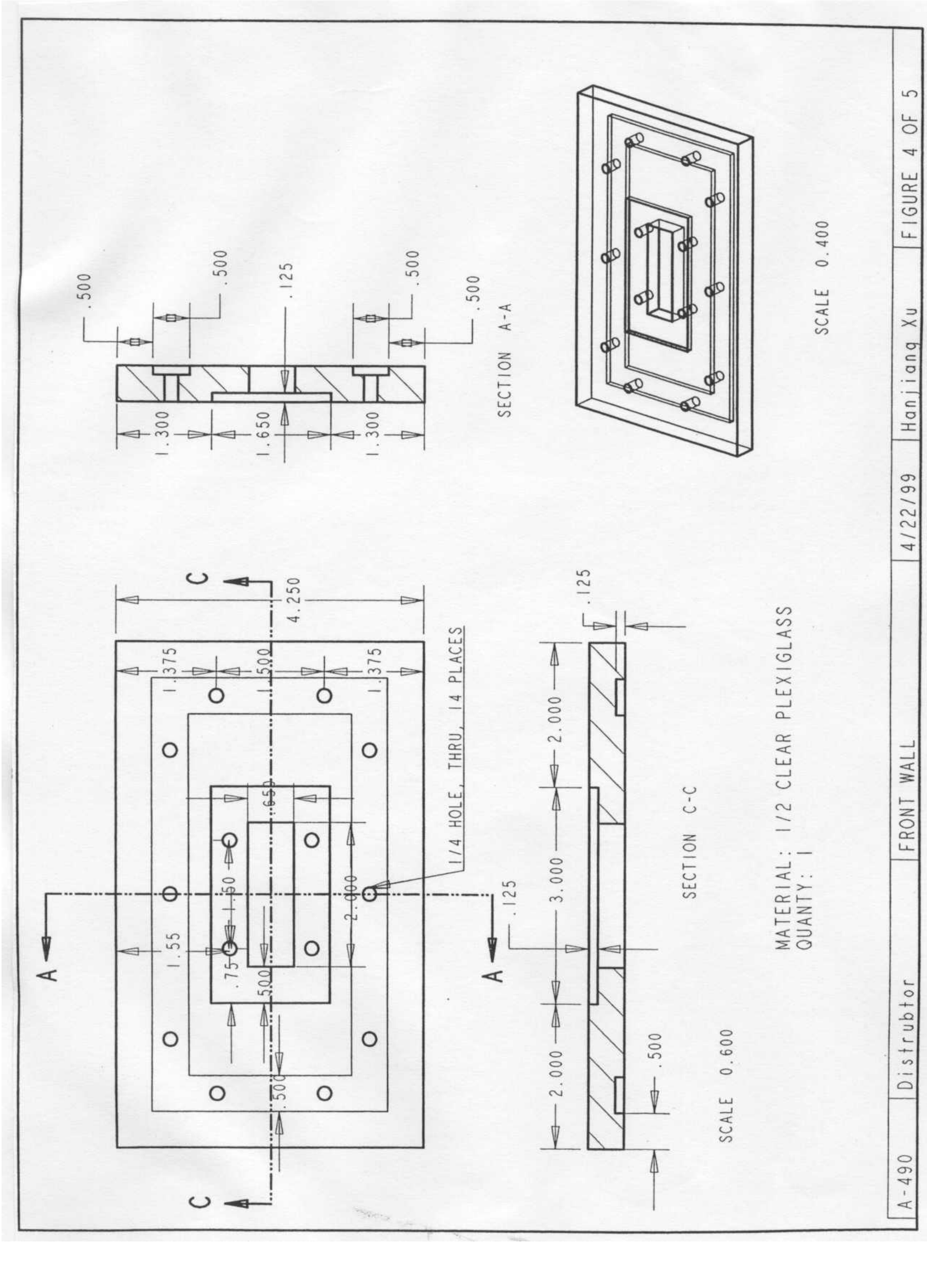
1/4 HOLE, THRU, 14 PLACES
SECTION A-A
SECTION C-C
SCALE 0.600
SCALE 0.400
MATERIAL: 1/2 CLEAR PLEXIGLASS
QUANTY: 1
A-490
Distrubtor
FRONT WALL
4/22/99
Hanjiang Xu
FIGURE 4 OF 5

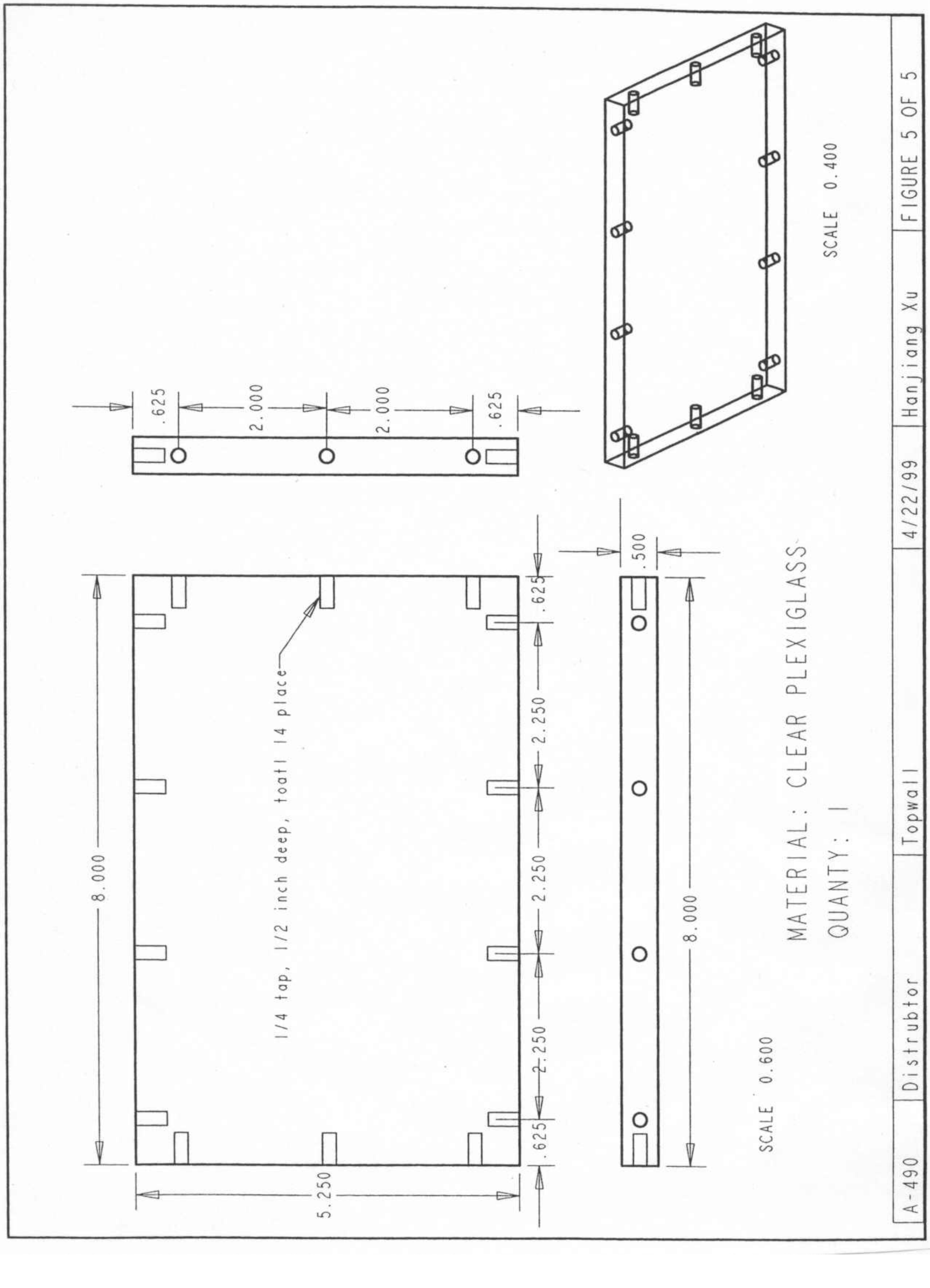

.625
2.000
2.000
.625
.500
8.000
8.000
.625
2.250
2.250
2.250
.625
5.250
1/4 tap, 1/2 inch deep, toatl 14 place
MATERIAL: CLEAR PLEXIGLASS
QUANTY: 1
SCALE 0.600
SCALE 0.400
A-490
Distrubtor
Topwall
4/22/99
Hanjiang Xu
FIGURE 5 OF 5

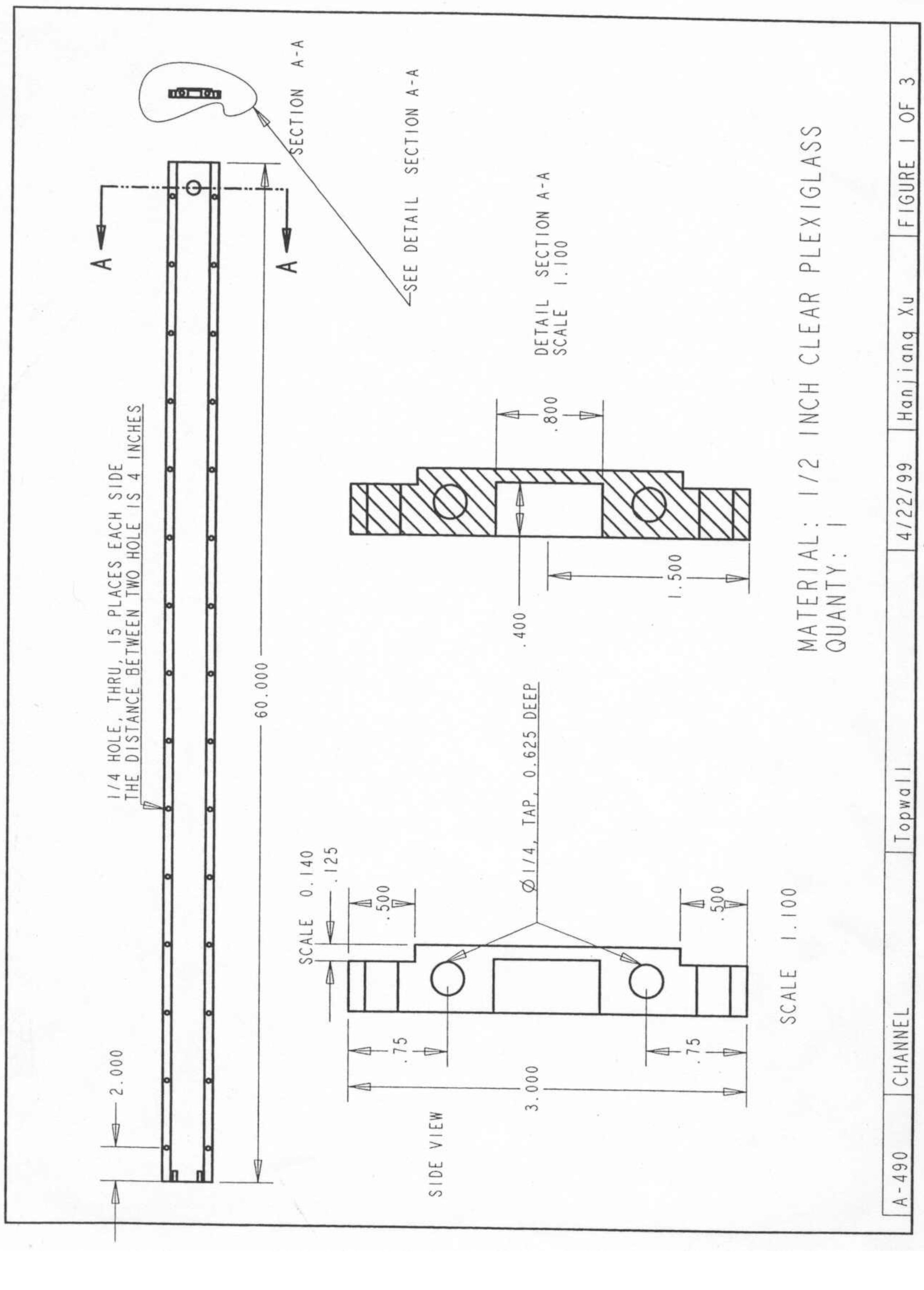

1/4 HOLE, THRU, 15 PLACES EACH SIDE
THE DISTANCE BETWEEN TWO HOLE IS 4 INCHES
A
A
60.000
2.000
SECTION A-A
SEE DETAIL SECTION A-A
DETAIL SECTION A-A
SCALE 1.100
.800
.400
1.500
Ø1/4, TAP, 0.625 DEEP
SCALE 0.140
.125
.500
.500
.75
.75
3.000
SIDE VIEW
SCALE 1.100
MATERIAL: 1/2 INCH CLEAR PLEXIGLASS
QUANTY: 1
A-490
CHANNEL
Topwall
4/22/99
Hanjiang Xu
FIGURE 1 OF 3

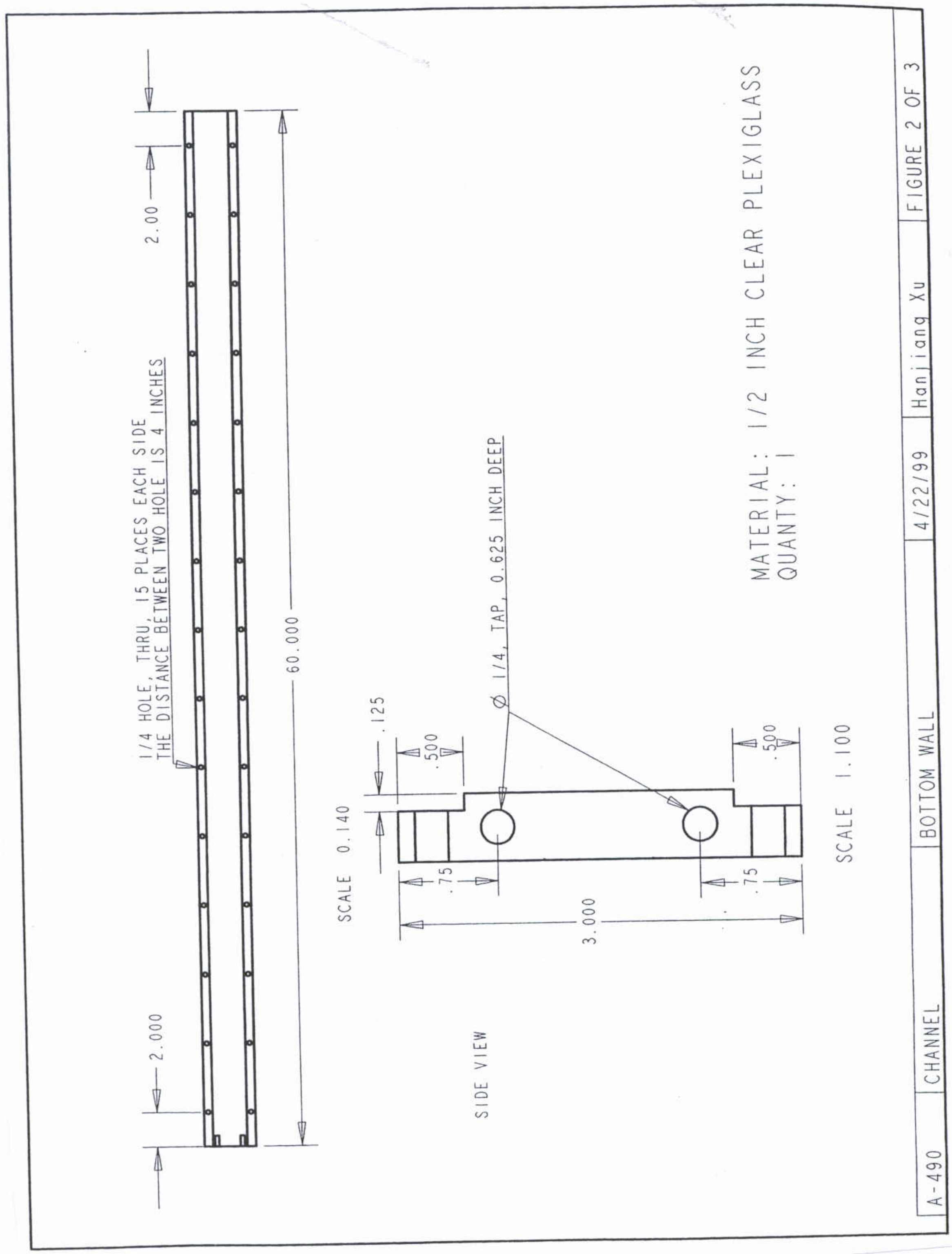
1/4 HOLE, THRU, 15 PLACES EACH SIDE
THE DISTANCE BETWEEN TWO HOLE IS 4 INCHES
2.00
2.000
60.000
SIDE VIEW
SCALE 0.140
.125
.500
Ø 1/4, TAP, 0.625 INCH DEEP
.75
.75
.500
3.000
SCALE 1.100
MATERIAL: 1/2 INCH CLEAR PLEXIGLASS
QUANTY: 1
A-490
CHANNEL
BOTTOM WALL
4/22/99
Hanjiang Xu
FIGURE 2 OF 3

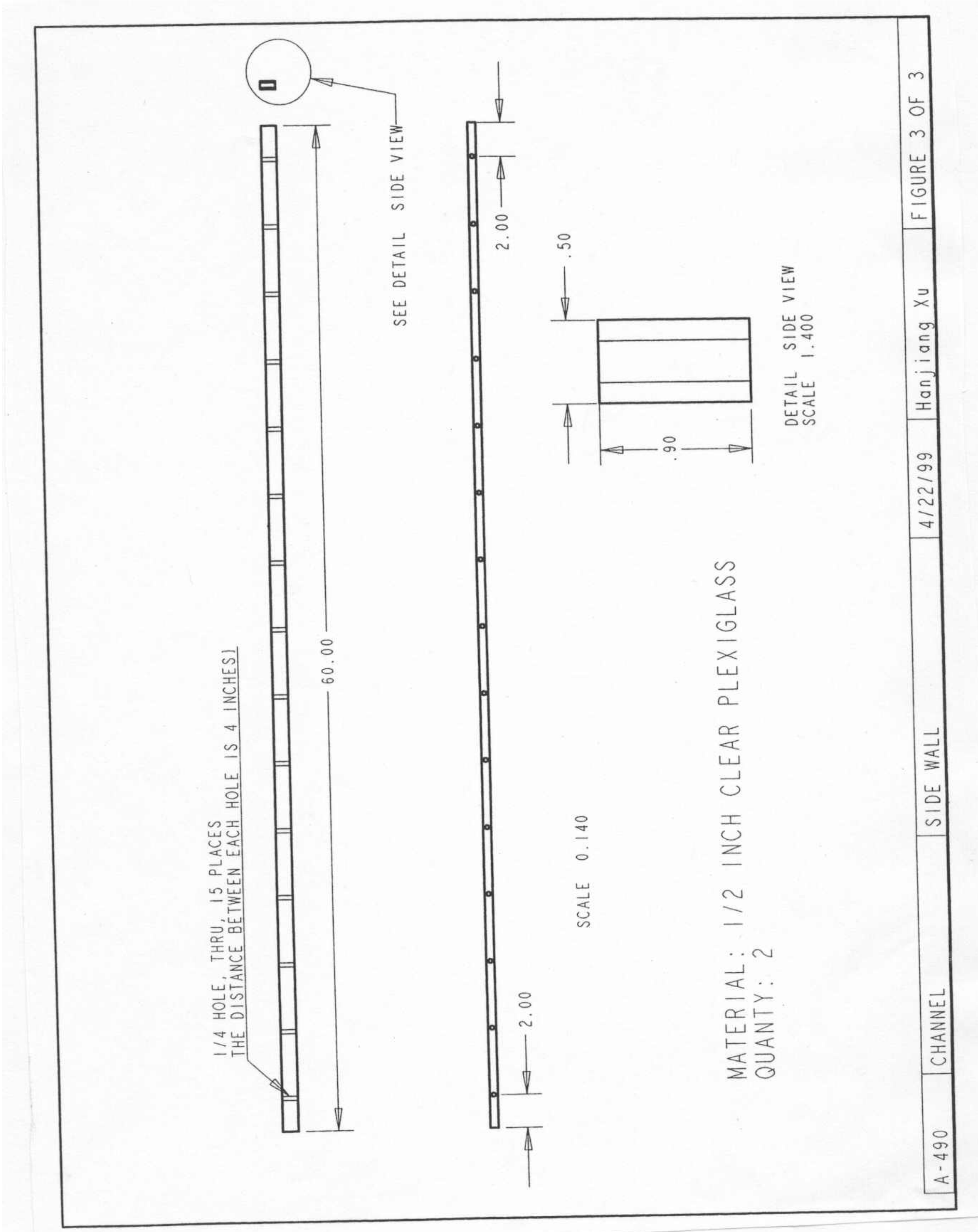
1/4 HOLE, THRU, 15 PLACES
THE DISTANCE BETWEEN EACH HOLE IS 4 INCHES)
60.00
SEE DETAIL SIDE VIEW
2.00
2.00
.50
.90
DETAIL SIDE VIEW
SCALE 1.400
SCALE 0.140
MATERIAL: 1/2 INCH CLEAR PLEXIGLASS
QUANTY: 2
A-490
CHANNEL
SIDE WALL
4/22/99
Hanjiang Xu
FIGURE 3 OF 3

APPENDIX II POSITION CORRECTIONS FOR THE VELOCITY PROFILES

For PUDV measurement, the position information is determined by the time delay between the emission and receiving of the ultrasound signal. The position of each sample volume is located in the center of the sample. However, when part of the sample volume is located inside the channel wall, this position will not reflect the actual measuring position, which is shown in the following figure.

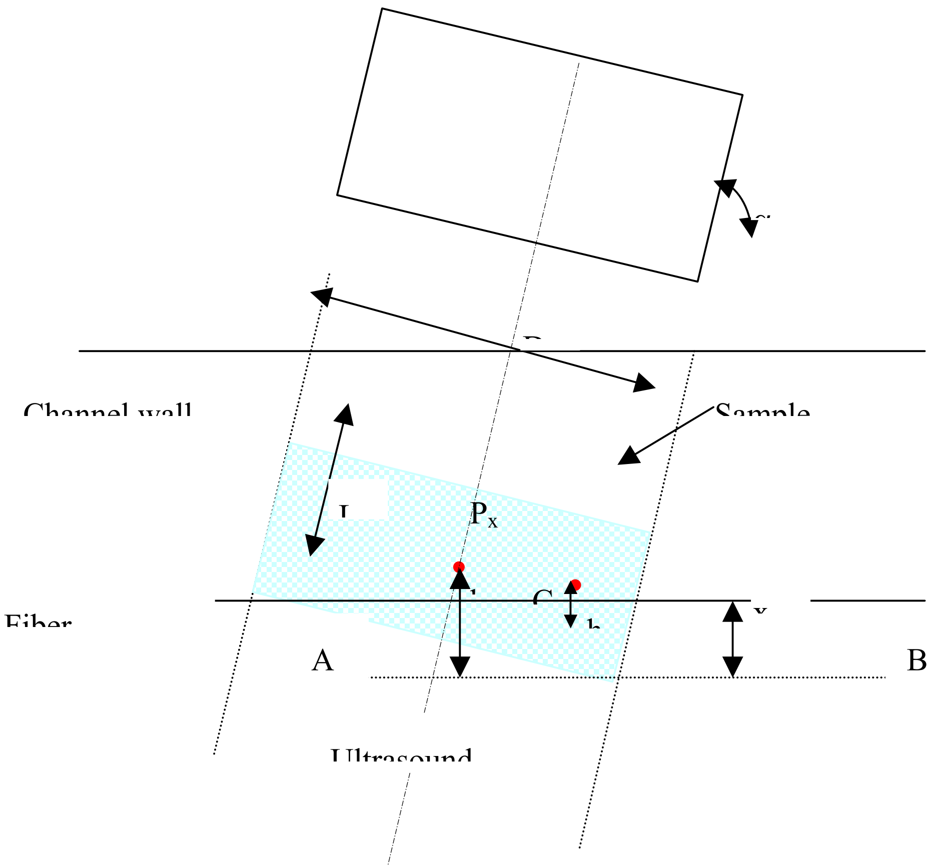

Position correction of sample volume

In the above figure, L is the length of sample volume; D is the ultrasound diameter; α is the ultrasound attack angle; P_x is the measurement sample position, C_x is the actual position. Here, we define the position of C_x as being at the midpoint of sample volume in the fluid.

From the geometry calculation, it can be found:

$$h_1 = (L\sin\alpha + D\cos\alpha)/2$$

$$h_2 = x/2$$

Therefore, the correction distance between Px and Cx is:

$$\Delta h = h1 - h2 = (L\sin\alpha + D\cos\alpha - x)/2$$

The following table gives the Δh value for the different probes used in this study.

Data point		1	2	3	4	5	6	7	8
x value		0.36	0.72	1.08	1.44	1.8	2.16	2.52	2.88
Correction values	4 MHz probe, D = 5mm, L=0.9mm	0.9	0.72	0.54	0.36	0.18	0		
	2 MHz probe, D = 8mm, L=0.9mm	1.29	1.11	0.93	0.75	0.57	0.39	0.21	0.03

APPENDIX III ULTRASOUND INTERACTION WITH CHANNEL WALL AND FIBERS IN THE FLUID FIELD

The interfaces reflect and modify the acoustic field. The intensity of the acoustic field received in a point inside the liquid depends on the material, the shape and the number of these interfaces. This intensity is most of the time very difficult to evaluate. This lack of knowledge does not allow a precise determination of the size of the measuring volume. These interfaces may generate, in certain situations, artifacts and induce modifications in the velocity profiles as presented in the figures 1 and 2 below.

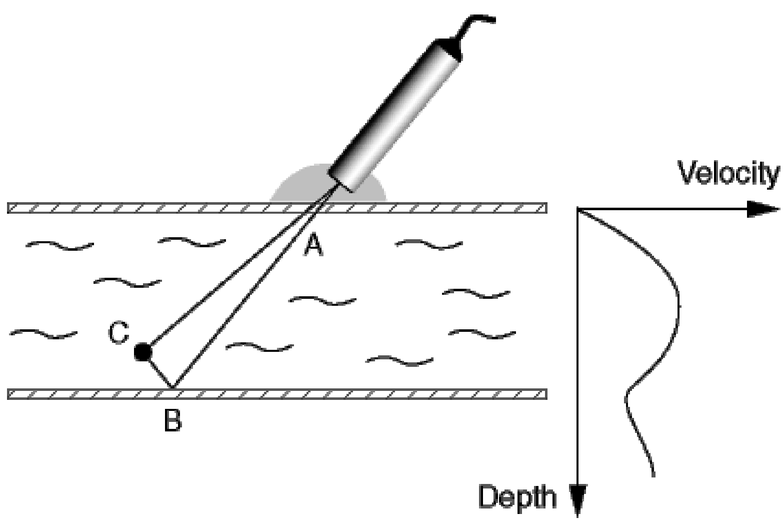

Figure 1

The ultrasonic beam BC reflected by the far interface of the figure 1 transforms this interface in a transmitter. The same particles contained in the liquid will backscatter a second time energy in the direction to the transducer. The depth associated to the path ABC is located outside the flowing liquid. Imaginary velocity components are added to the real velocity profile. The measurement of velocities near the far interface is affected by this phenomena. The size of the ultrasonic beam determines mainly the level of this artifact.

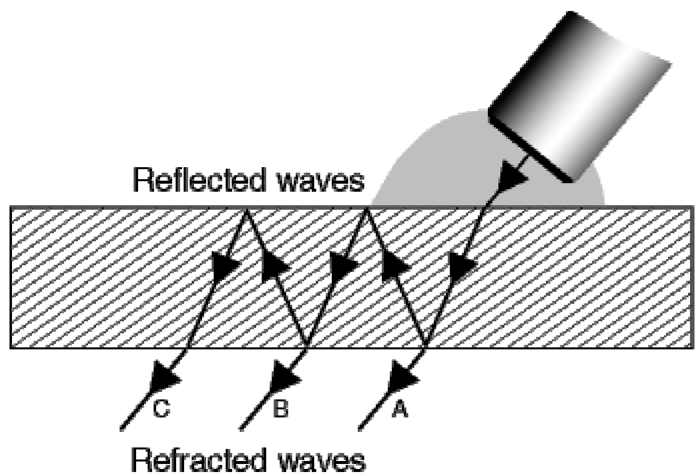

Figure 2

The figure 2 displays another situation. The reflected ultrasonic waves inside a wall enlarge the ultrasonic beam inside the liquid and modify its shape. These reflections disturb the determination of the size and the shape of the measuring volume. The thickness, the acoustical impedance and the attenuation coefficient of the interface determine the level of this phenomena. This situation appears when measuring for instance through steel walls.

The ultrasonic waves generated by the transducer are more or less confined in a narrow cone.

As they travel in this cone they may be reflected or scattered when they touch a particle having a different acoustic impedance. The acoustic impedance is defined by:

$$Z = \rho \cdot c$$

where r is the density and c the sound velocity.

If the size of the particle is bigger than the wavelength, the ultrasonic waves are reflected and refracted by the particle. In such a case the direction of propagation and the intensity of the ultrasonic waves are affected. But if the size of the particle is much smaller than the wavelength an other phenomena appears, which is named scattering. In such a case, a very small amount of the ultrasonic energy is reflected in all direction. The intensity and the direction of propagation of the incoming waves are practically not affected by the scattering phenomena. PUDV needs therefore particles smaller than the wavelength.

For the application of fiber suspension flow measurement in this thesis, the basic frequency of ultrasound is 4 MHz and the ultrasound speed in the fiber suspension is about 1500m/s. Therefore, the wavelength of the ultrasound is about 0.4 mm. Since the fiber diameter is about 40 μm, only a small amount of the ultrasonic energy is reflected in all direction when the ultrasound hit the fibers in the sample volume. The intensity and the direction of propagation of the ultrasound will be not affected by the presence of fiber.

Different types of fiber may have different density and dimensions. However, different types of fiber will not affect the measuring results once its impedance is different with water and its diameter is less than 0.4 mm.

APPENDIX IV VELOCITY PROFILES AT DIFFERENT FLOW CONDITIONS

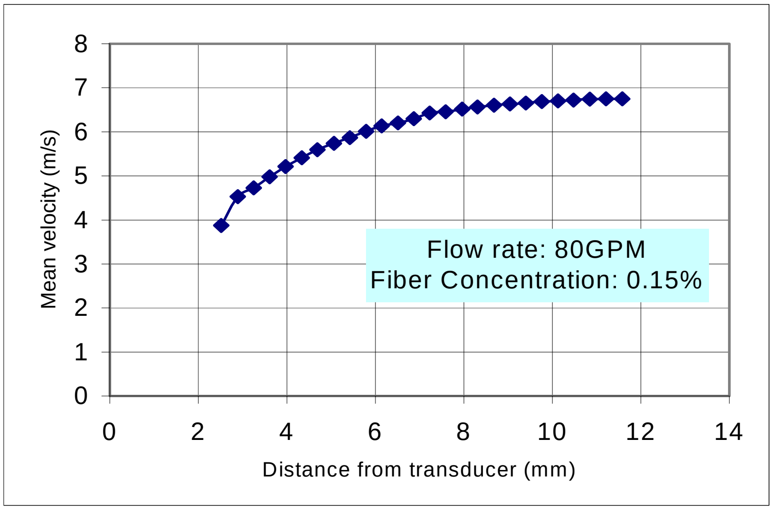

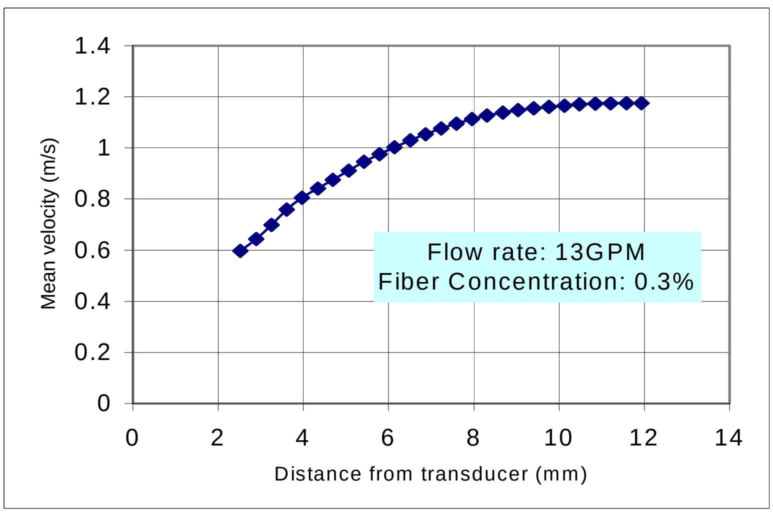

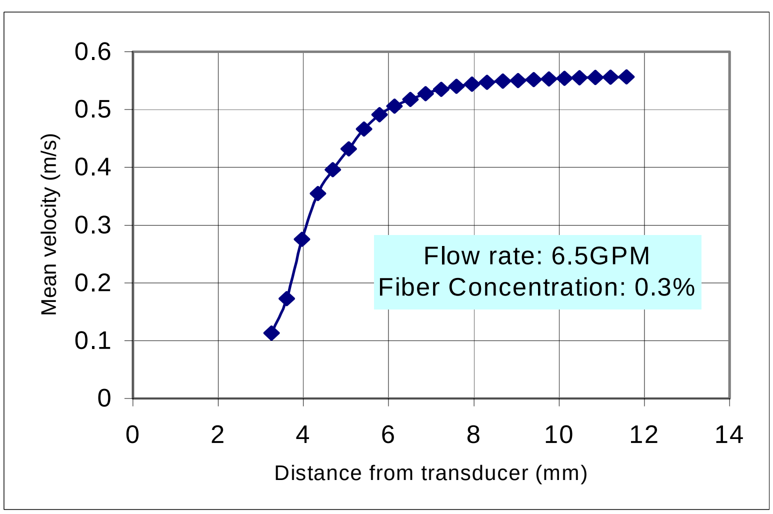

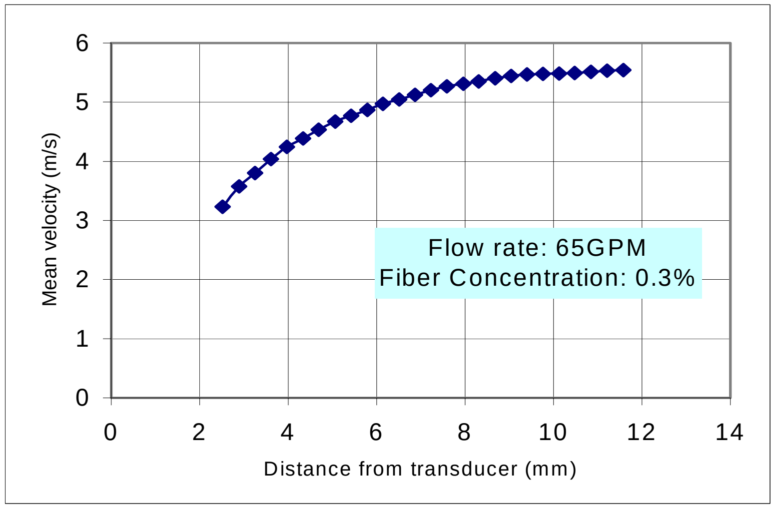
Flow rate: 65GPM
Fiber Concentration: 0.3%
Mean velocity (m/s)
Distance from transducer (mm)
0
1
2
3
4
5
6
0
2
4
6
8
10
12
14

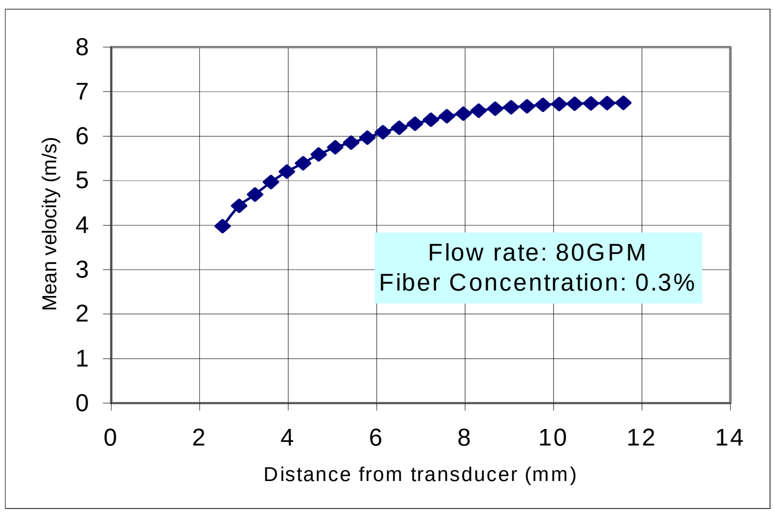
Flow rate: 80GPM
Fiber Concentration: 0.3%
Mean velocity (m/s)
Distance from transducer (mm)
0
1
2
3
4
5
6
7
8
0
2
4
6
8
10
12
14

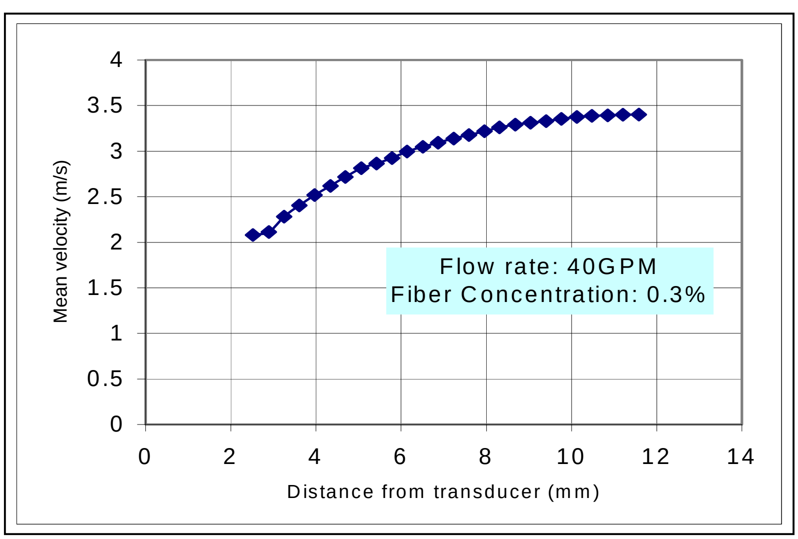
Flow rate: 40GPM
Fiber Concentration: 0.3%
Mean velocity (m/s)
Distance from transducer (mm)
0
0.5
1
1.5
2
2.5
3
3.5
4
0
2
4
6
8
10
12
14

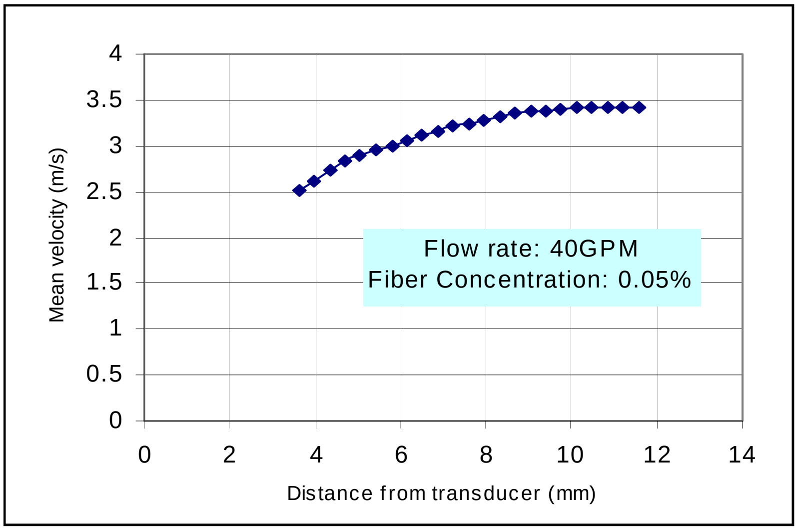
Flow rate: 40GPM
Fiber Concentration: 0.05%
Mean velocity (m/s)
Distance from transducer (mm)
0
0.5
1
1.5
2
2.5
3
3.5
4
0
2
4
6
8
10
12
14

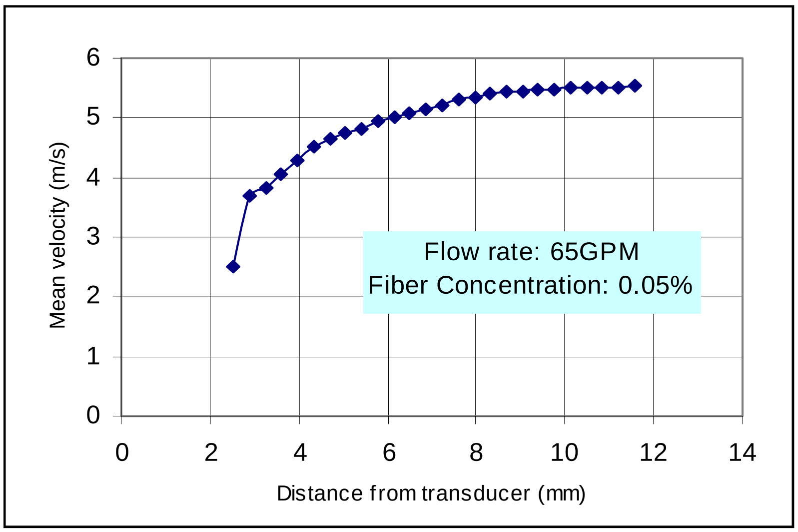
Flow rate: 65GPM
Fiber Concentration: 0.05%
Mean velocity (m/s)
Distance from transducer (mm)
0
1
2
3
4
5
6
0
2
4
6
8
10
12
14

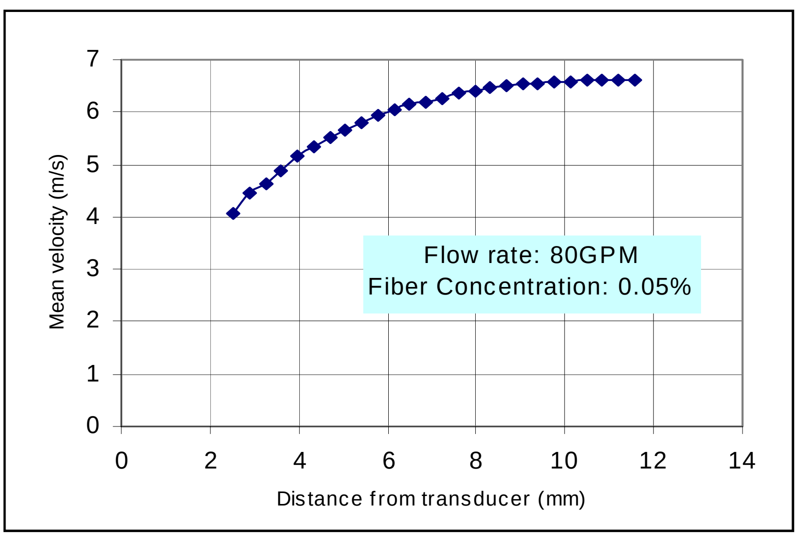
Flow rate: 80GPM
Fiber Concentration: 0.05%
Mean velocity (m/s)
Distance from transducer (mm)
0
1
2
3
4
5
6
7
0
2
4
6
8
10
12
14

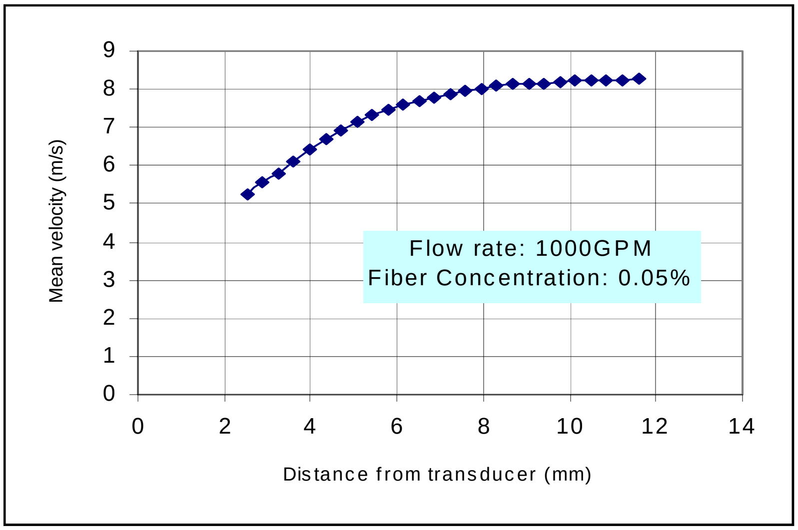
Flow rate: 1000GPM
Fiber Concentration: 0.05%
Mean velocity (m/s)
Distance from transducer (mm)

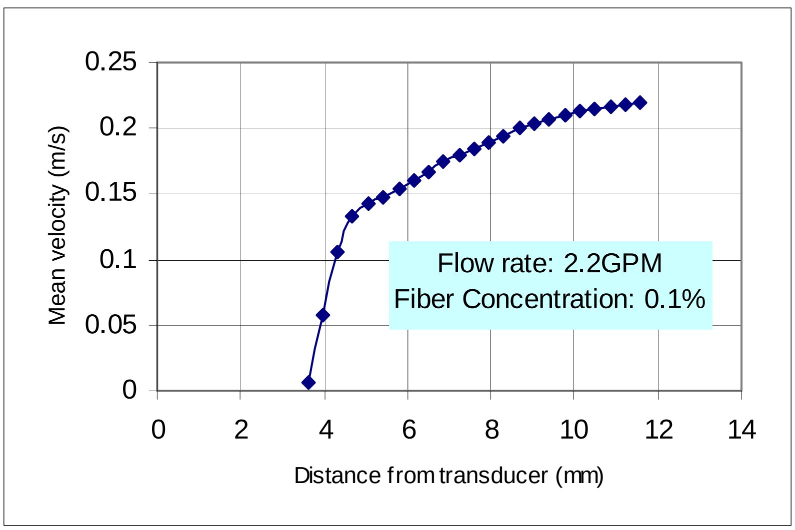
Flow rate: 2.2GPM
Fiber Concentration: 0.1%
Mean velocity (m/s)
Distance from transducer (mm)

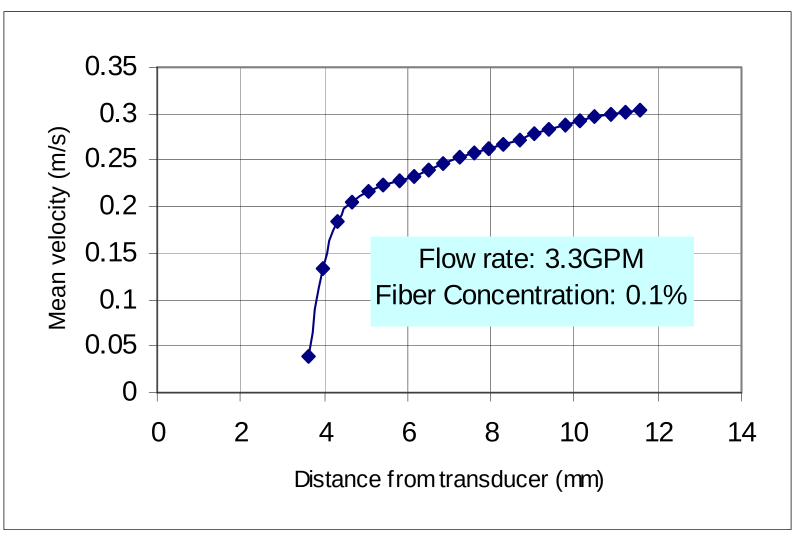
Flow rate: 3.3GPM
Fiber Concentration: 0.1%
Mean velocity (m/s)
Distance from transducer (mm)

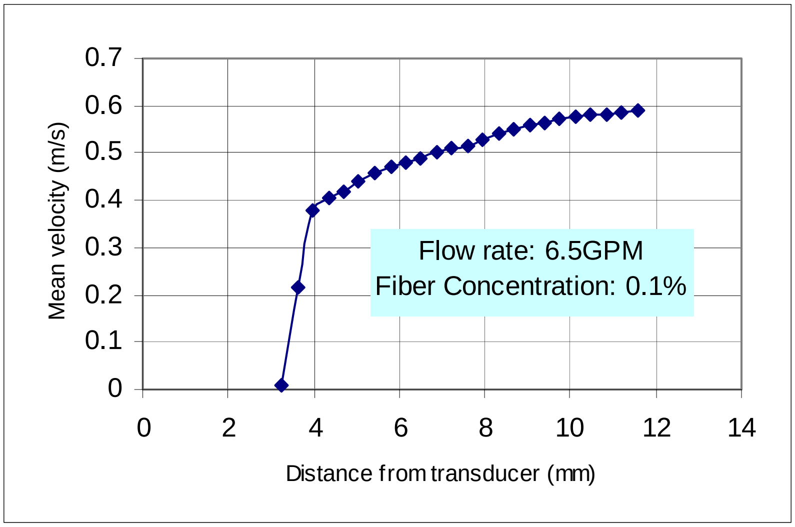
Mean velocity (m/s)
0.7
0.6
0.5
0.4
0.3
0.2
0.1
0
0 2 4 6 8 10 12 14
Distance from transducer (mm)
Flow rate: 6.5GPM
Fiber Concentration: 0.1%

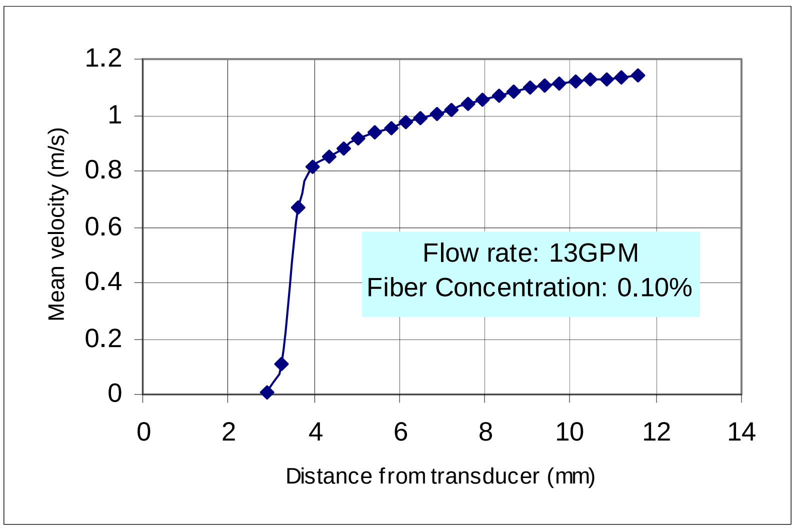
Mean velocity (m/s)
1.2
1
0.8
0.6
0.4
0.2
0
0 2 4 6 8 10 12 14
Distance from transducer (mm)
Flow rate: 13GPM
Fiber Concentration: 0.10%

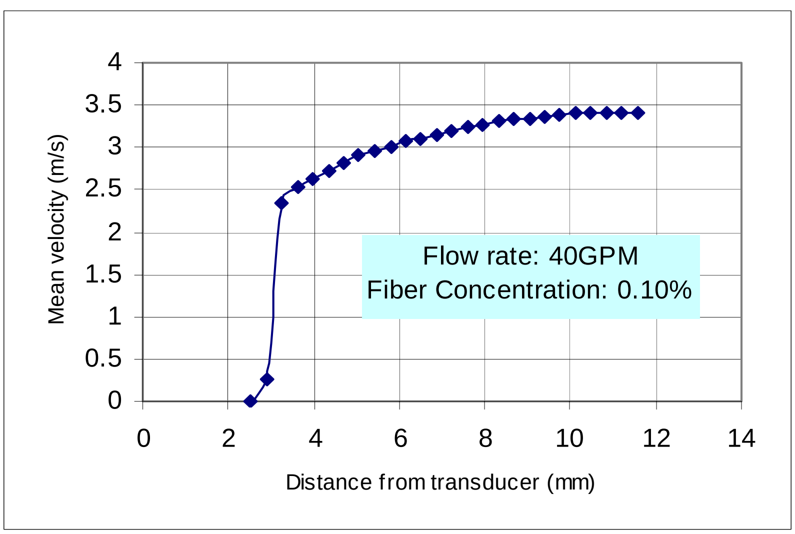
Mean velocity (m/s)
4
3.5
3
2.5
2
1.5
1
0.5
0
0 2 4 6 8 10 12 14
Distance from transducer (mm)
Flow rate: 40GPM
Fiber Concentration: 0.10%

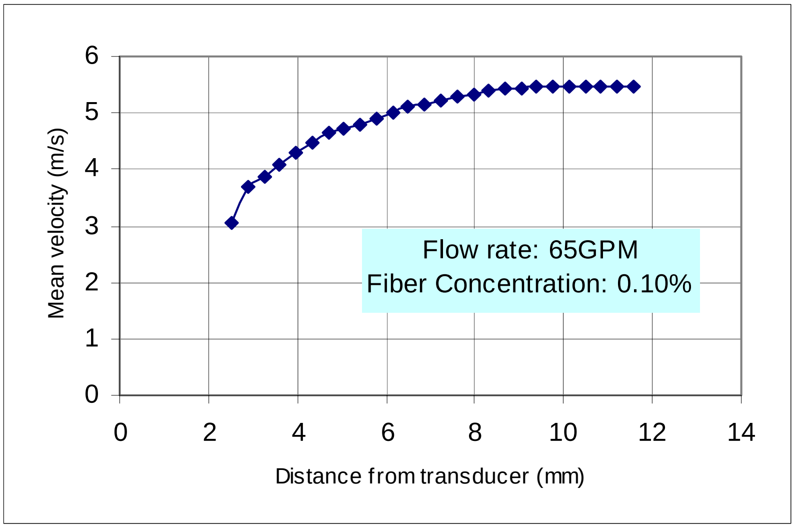
Flow rate: 65GPM
Fiber Concentration: 0.10%
Mean velocity (m/s)
Distance from transducer (mm)

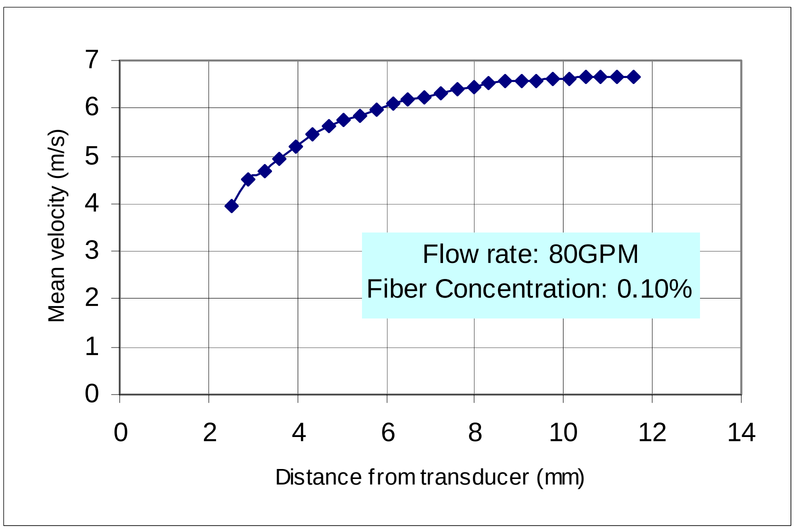
Flow rate: 80GPM
Fiber Concentration: 0.10%
Mean velocity (m/s)
Distance from transducer (mm)

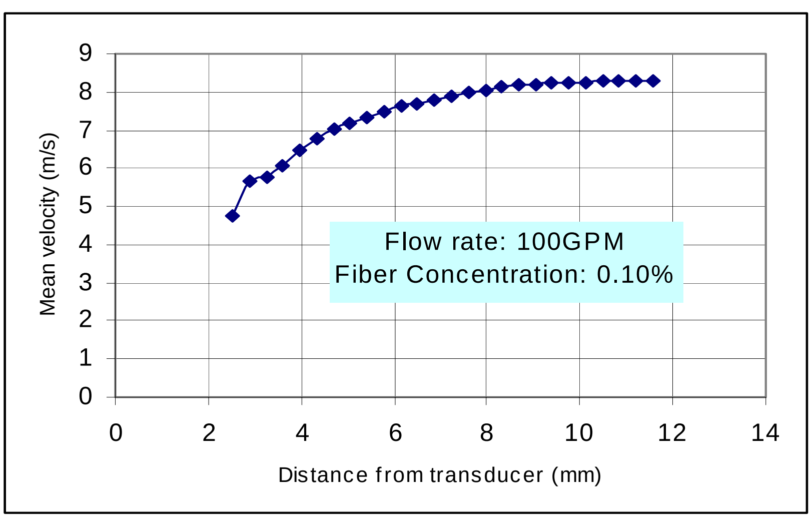
Flow rate: 100GPM
Fiber Concentration: 0.10%
Mean velocity (m/s)
Distance from transducer (mm)

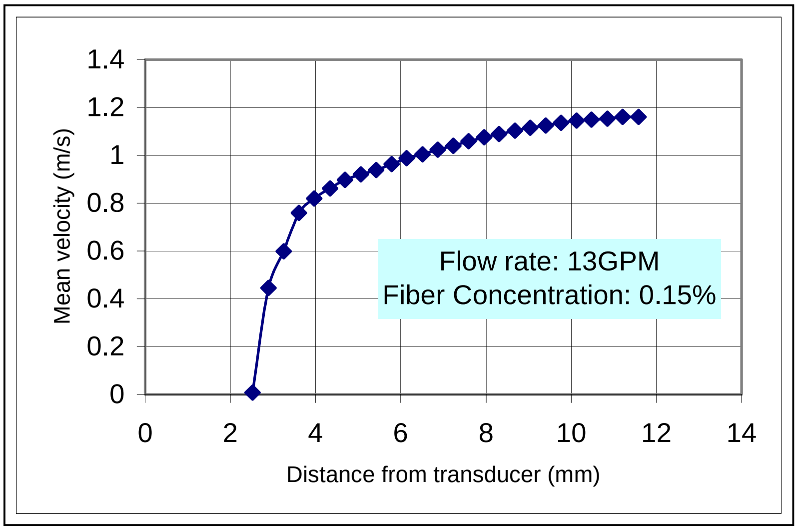
Flow rate: 13GPM
Fiber Concentration: 0.15%
Mean velocity (m/s)
Distance from transducer (mm)

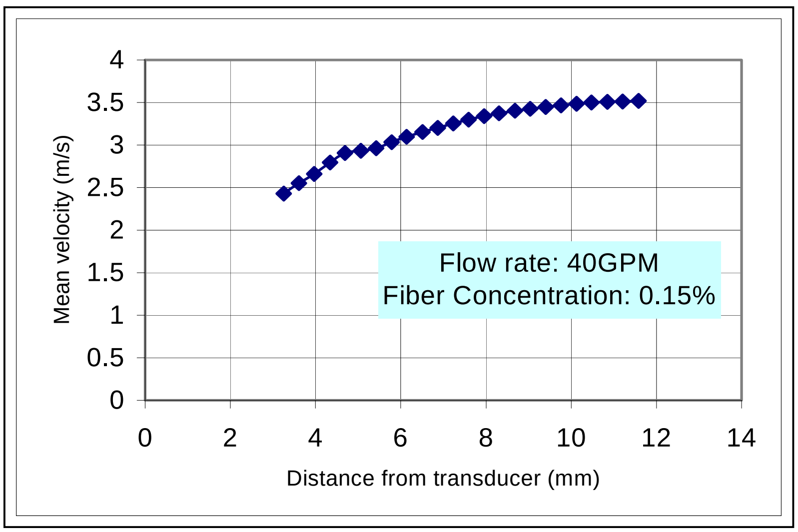
Flow rate: 40GPM
Fiber Concentration: 0.15%
Mean velocity (m/s)
Distance from transducer (mm)

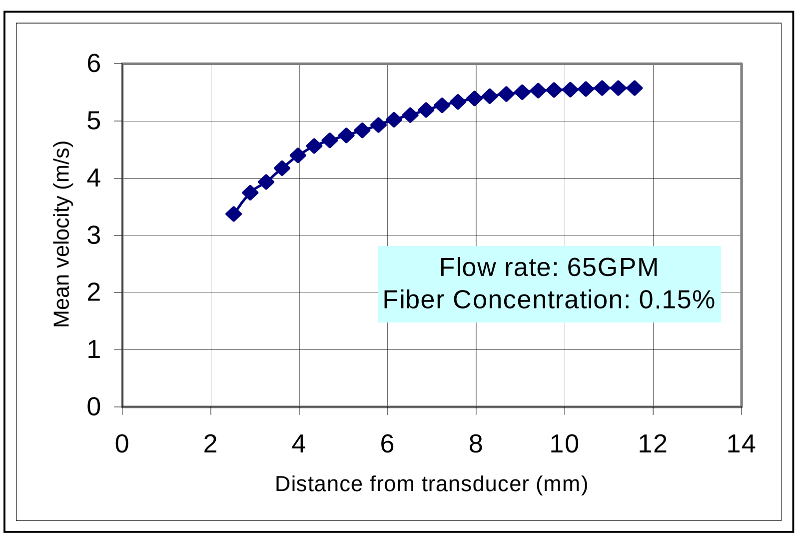
Flow rate: 65GPM
Fiber Concentration: 0.15%
Mean velocity (m/s)
Distance from transducer (mm)

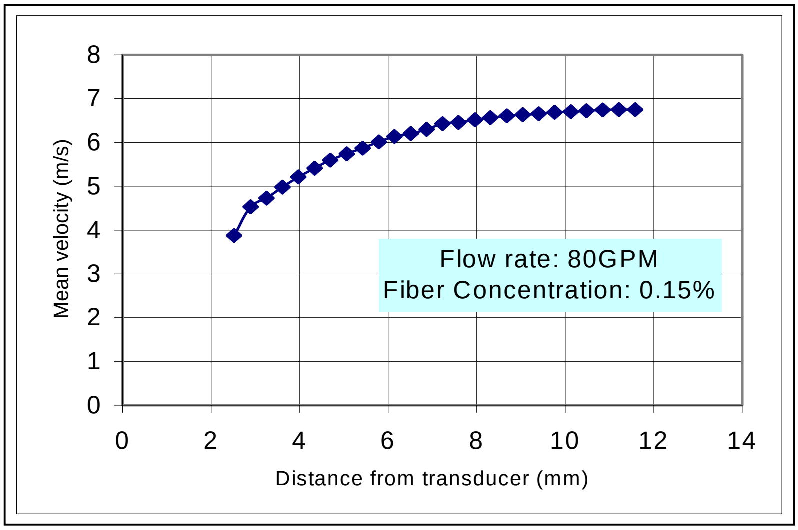
Mean velocity (m/s)
8
7
6
5
4
3
2
1
0
Flow rate: 80GPM
Fiber Concentration: 0.15%
0
2
4
6
8
10
12
14
Distance from transducer (mm)

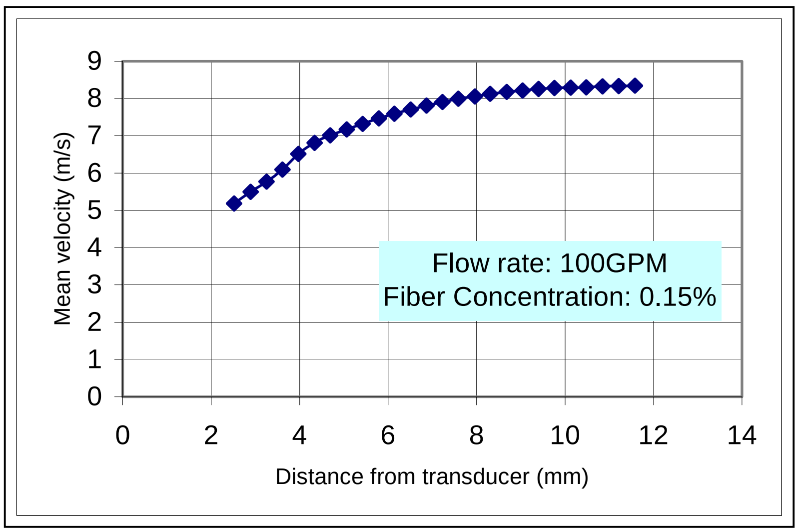
Mean velocity (m/s)
9
8
7
6
5
4
3
2
1
0
Flow rate: 100GPM
Fiber Concentration: 0.15%
0
2
4
6
8
10
12
14
Distance from transducer (mm)

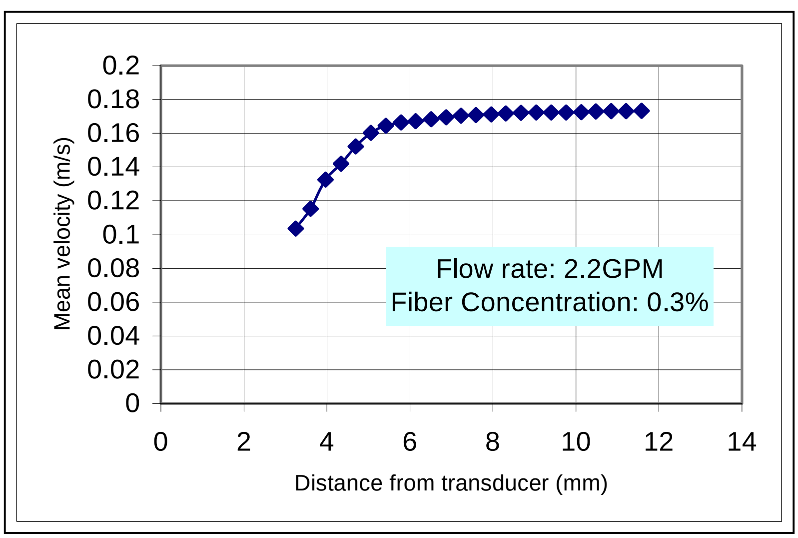
Mean velocity (m/s)
0.2
0.18
0.16
0.14
0.12
0.1
0.08
0.06
0.04
0.02
0
Flow rate: 2.2GPM
Fiber Concentration: 0.3%
0
2
4
6
8
10
12
14
Distance from transducer (mm)

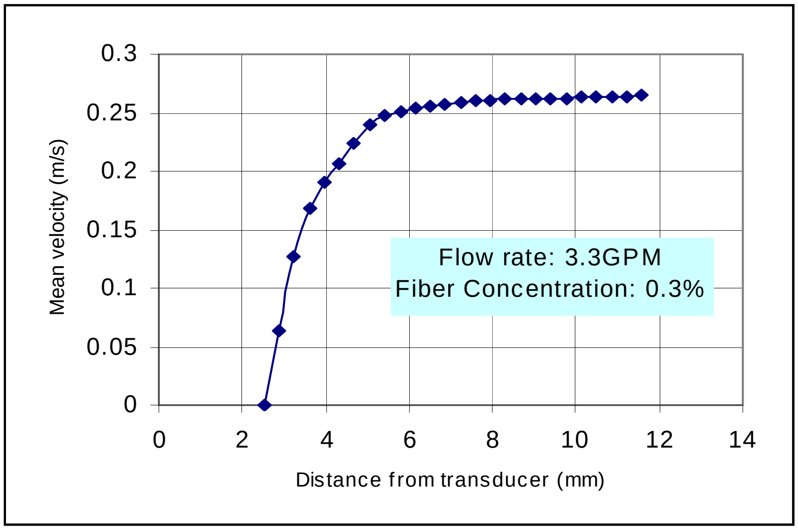
Mean velocity (m/s)
0.3
0.25
0.2
0.15
0.1
0.05
0
Flow rate: 3.3GPM
Fiber Concentration: 0.3%
0
2
4
6
8
10
12
14
Distance from transducer (mm)

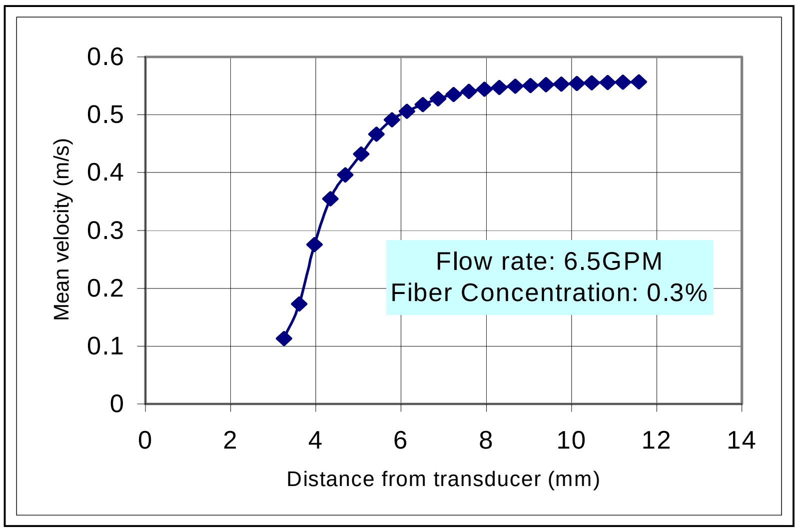
Mean velocity (m/s)
0.6
0.5
0.4
0.3
0.2
0.1
0
Flow rate: 6.5GPM
Fiber Concentration: 0.3%
0
2
4
6
8
10
12
14
Distance from transducer (mm)

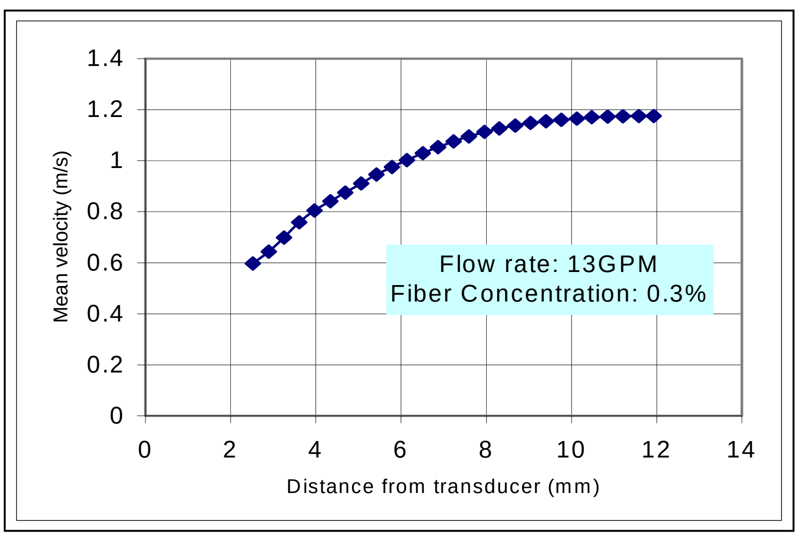
Mean velocity (m/s)
1.4
1.2
1
0.8
0.6
0.4
0.2
0
Flow rate: 13GPM
Fiber Concentration: 0.3%
0
2
4
6
8
10
12
14
Distance from transducer (mm)

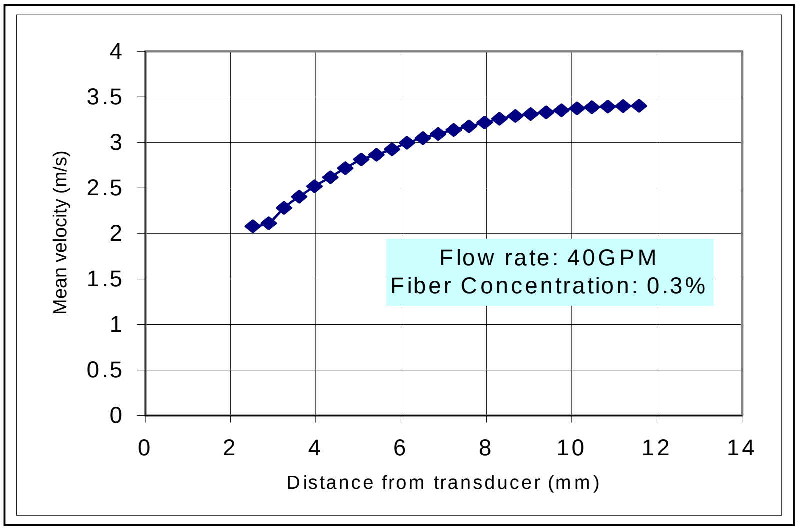
Flow rate: 40GPM
Fiber Concentration: 0.3%
Mean velocity (m/s)
Distance from transducer (mm)

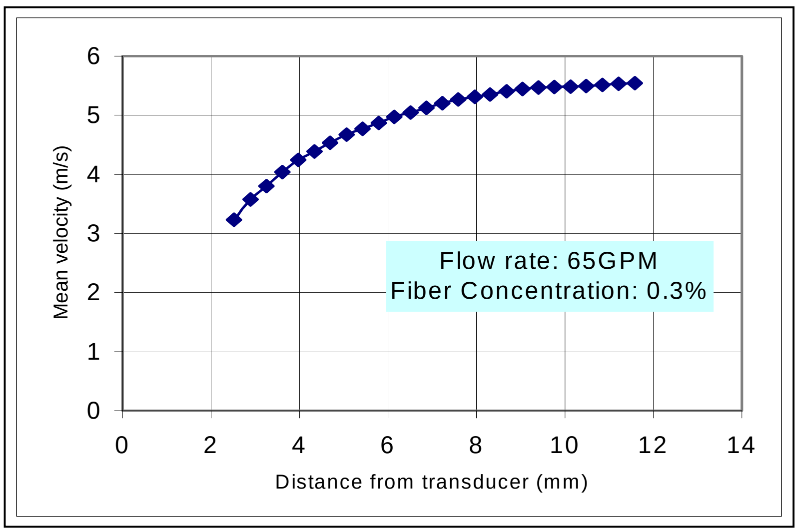
Flow rate: 65GPM
Fiber Concentration: 0.3%
Mean velocity (m/s)
Distance from transducer (mm)

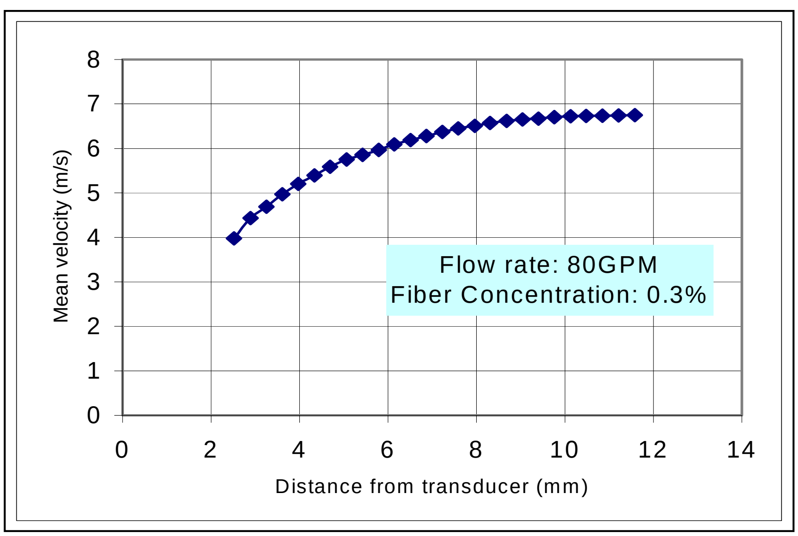
Flow rate: 80GPM
Fiber Concentration: 0.3%
Mean velocity (m/s)
Distance from transducer (mm)

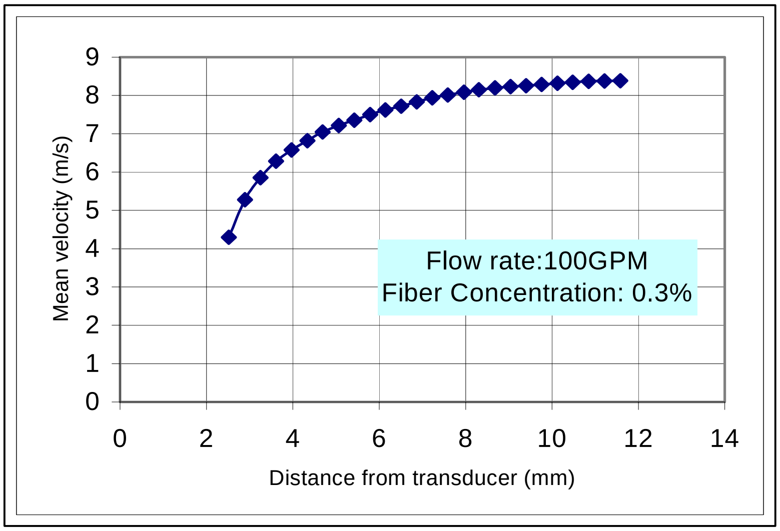
Flow rate:100GPM
Fiber Concentration: 0.3%
Mean velocity (m/s)
Distance from transducer (mm)
0
1
2
3
4
5
6
7
8
9
0
2
4
6
8
10
12
14

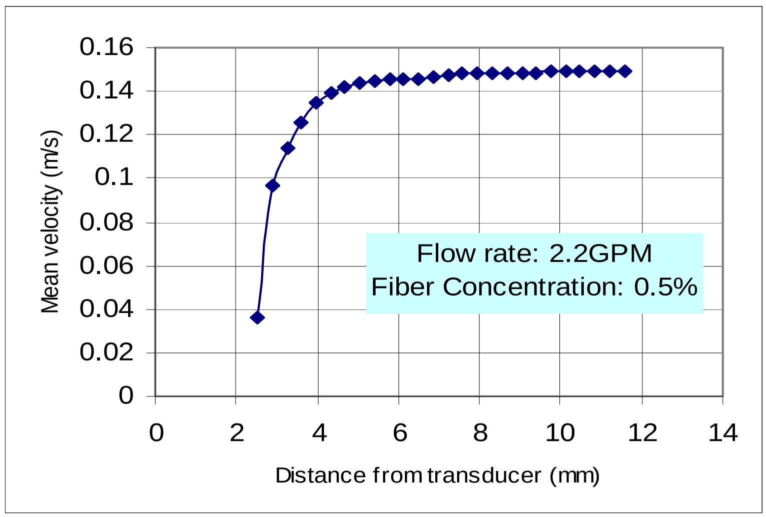
Flow rate: 2.2GPM
Fiber Concentration: 0.5%
Mean velocity (m/s)
Distance from transducer (mm)
0
0.02
0.04
0.06
0.08
0.1
0.12
0.14
0.16
0
2
4
6
8
10
12
14

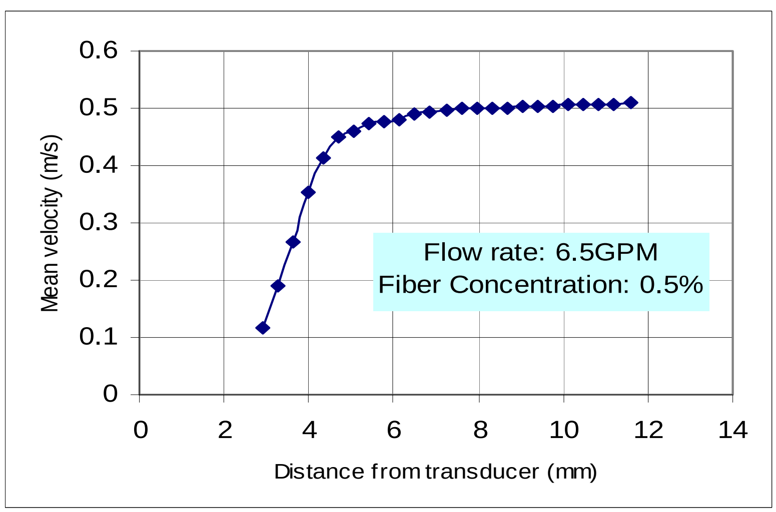
Flow rate: 6.5GPM
Fiber Concentration: 0.5%
Mean velocity (m/s)
Distance from transducer (mm)
0
0.1
0.2
0.3
0.4
0.5
0.6
0
2
4
6
8
10
12
14

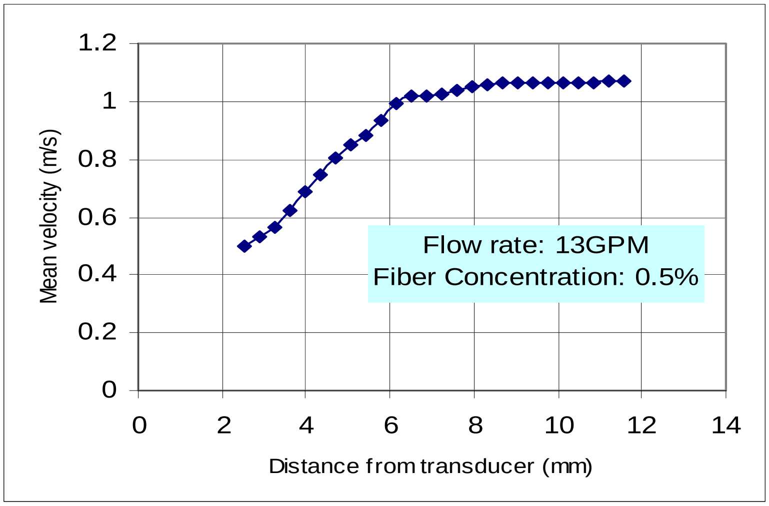
Mean velocity (m/s)
1.2
1
0.8
0.6
0.4
0.2
0
0
2
4
6
8
10
12
14
Distance from transducer (mm)
Flow rate: 13GPM
Fiber Concentration: 0.5%

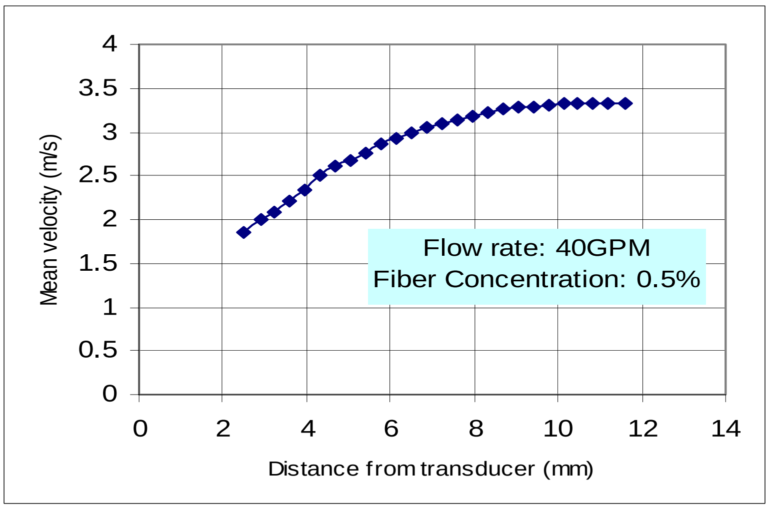
Mean velocity (m/s)
4
3.5
3
2.5
2
1.5
1
0.5
0
0
2
4
6
8
10
12
14
Distance from transducer (mm)
Flow rate: 40GPM
Fiber Concentration: 0.5%

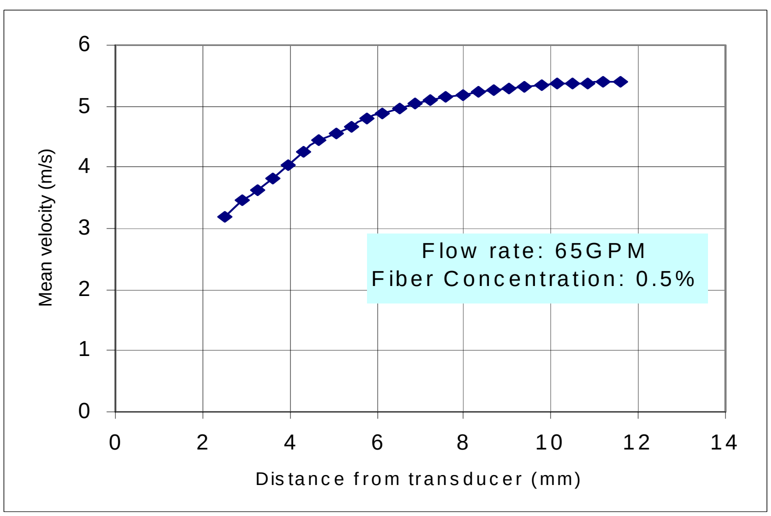
Mean velocity (m/s)
6
5
4
3
2
1
0
0
2
4
6
8
10
12
14
Distance from transducer (mm)
Flow rate: 65GPM
Fiber Concentration: 0.5%

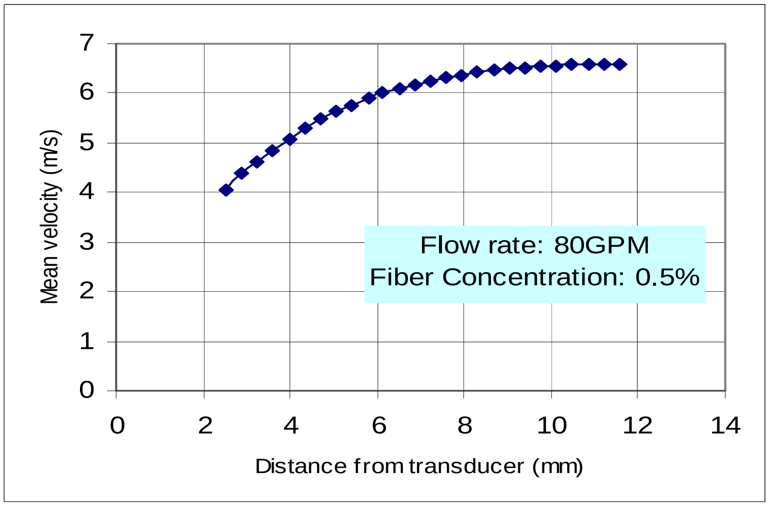

Mean velocity (m/s)
Distance from transducer (mm)
Flow rate: 80GPM
Fiber Concentration: 0.5%

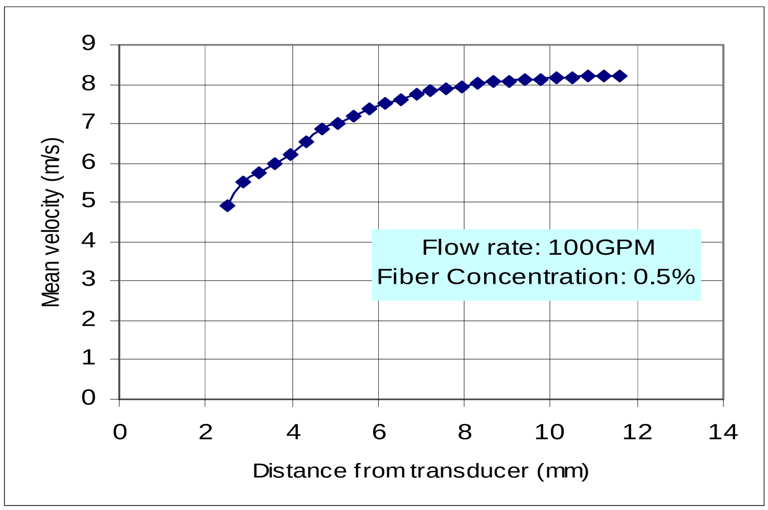

Mean velocity (m/s)
Distance from transducer (mm)
Flow rate: 100GPM
Fiber Concentration: 0.5%

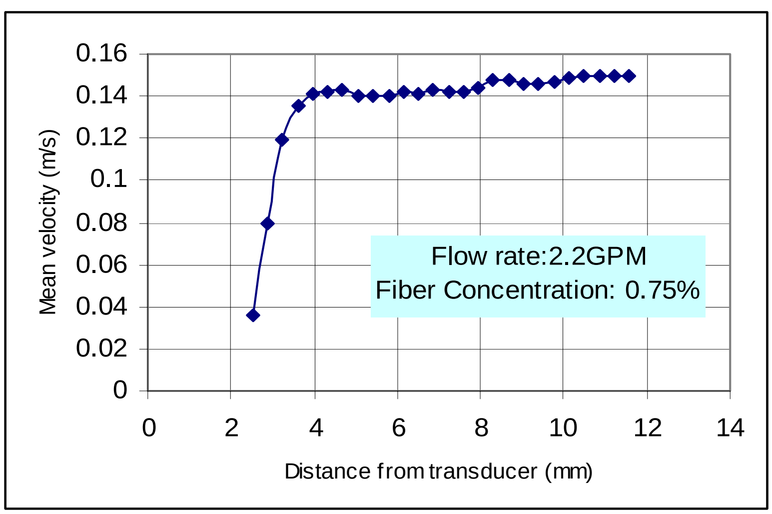

Mean velocity (m/s)
Distance from transducer (mm)
Flow rate:2.2GPM
Fiber Concentration: 0.75%

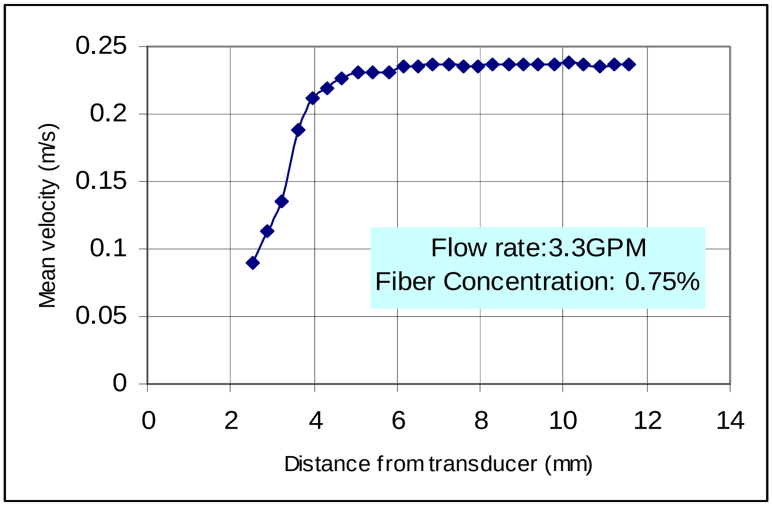

Mean velocity (m/s)
0
0.05
0.1
0.15
0.2
0.25
0
2
4
6
8
10
12
14
Distance from transducer (mm)
Flow rate:3.3GPM
Fiber Concentration: 0.75%

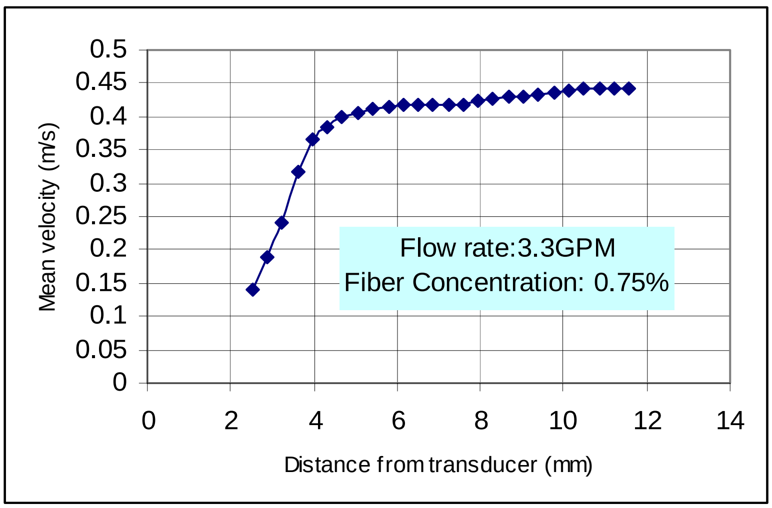

Mean velocity (m/s)
0
0.05
0.1
0.15
0.2
0.25
0.3
0.35
0.4
0.45
0.5
0
2
4
6
8
10
12
14
Distance from transducer (mm)
Flow rate:3.3GPM
Fiber Concentration: 0.75%

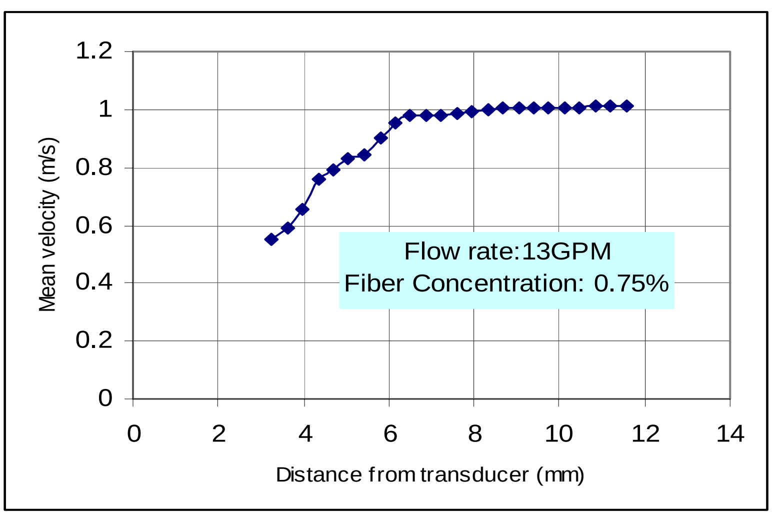

Mean velocity (m/s)
0
0.2
0.4
0.6
0.8
1
1.2
0
2
4
6
8
10
12
14
Distance from transducer (mm)
Flow rate:13GPM
Fiber Concentration: 0.75%

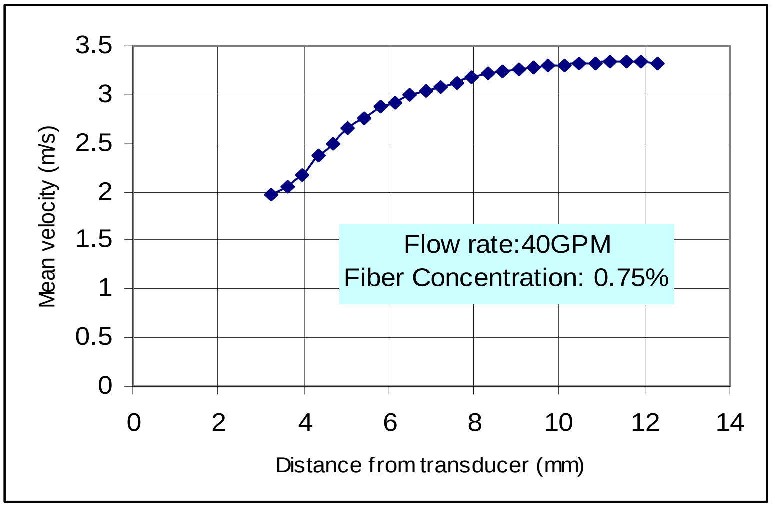

Flow rate:40GPM
Fiber Concentration: 0.75%
Mean velocity (m/s)
Distance from transducer (mm)

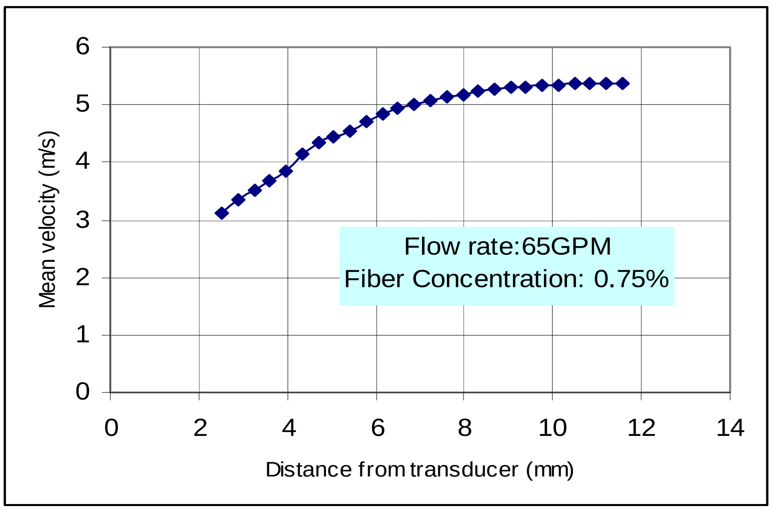

Flow rate:65GPM
Fiber Concentration: 0.75%
Mean velocity (m/s)
Distance from transducer (mm)

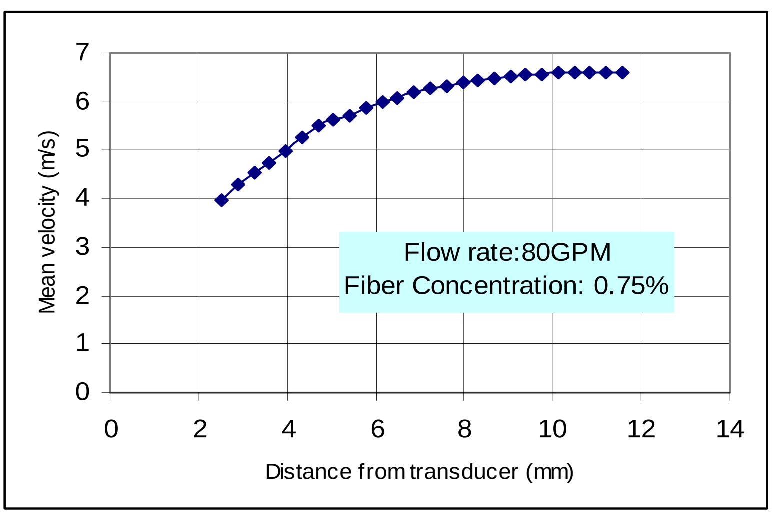

Flow rate:80GPM
Fiber Concentration: 0.75%
Mean velocity (m/s)
Distance from transducer (mm)

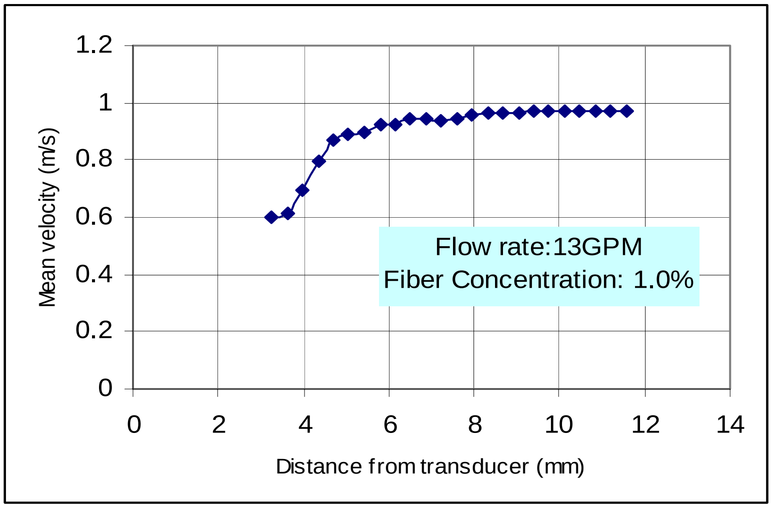
Flow rate:13GPM
Fiber Concentration: 1.0%
Mean velocity (m/s)
Distance from transducer (mm)

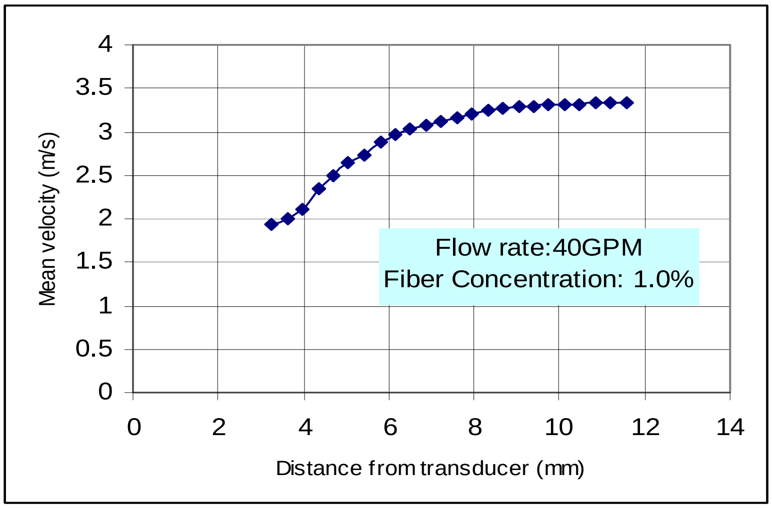
Flow rate:40GPM
Fiber Concentration: 1.0%
Mean velocity (m/s)
Distance from transducer (mm)

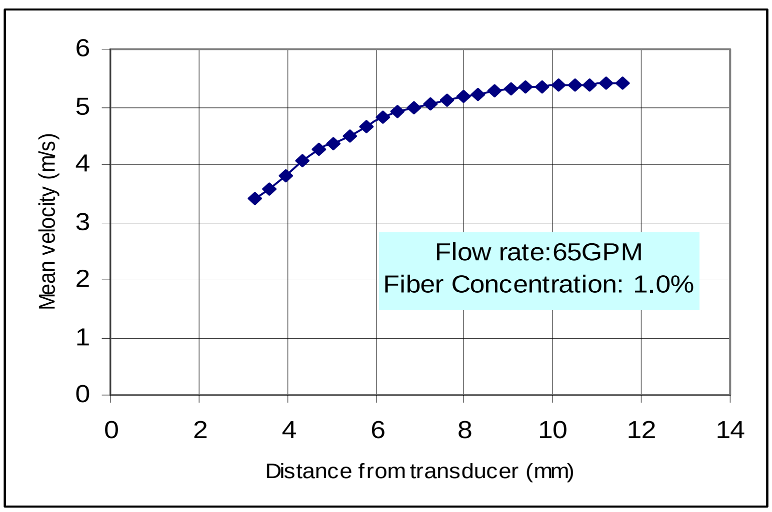
Flow rate:65GPM
Fiber Concentration: 1.0%
Mean velocity (m/s)
Distance from transducer (mm)

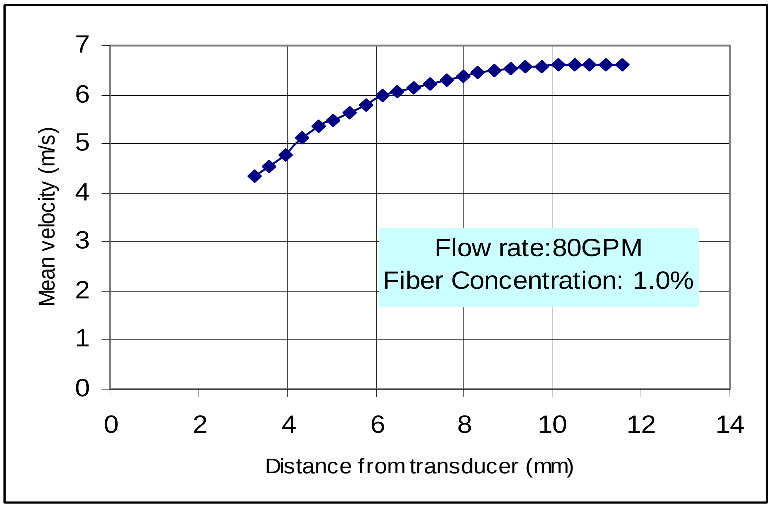
Flow rate:80GPM
Fiber Concentration: 1.0%
Mean velocity (m/s)
Distance from transducer (mm)
0
1
2
3
4
5
6
7
0
2
4
6
8
10
12
14

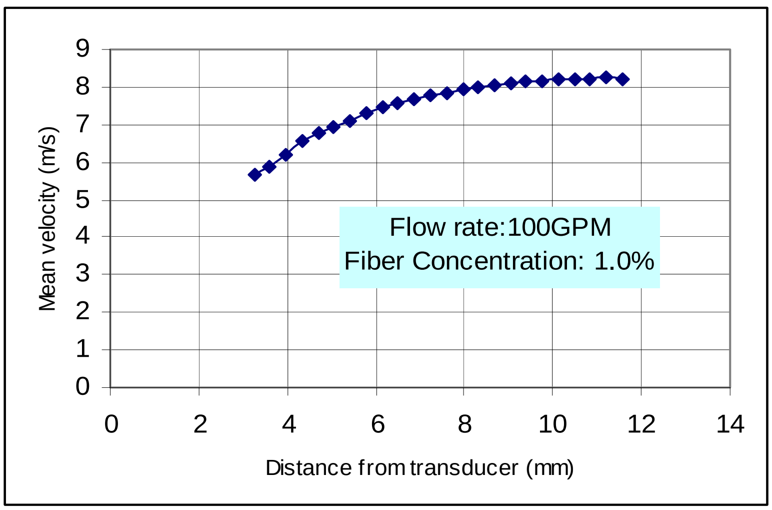
Flow rate:100GPM
Fiber Concentration: 1.0%
Mean velocity (m/s)
Distance from transducer (mm)
0
1
2
3
4
5
6
7
8
9
0
2
4
6
8
10
12
14

APPENDIX V PRESSURE DROP DATA

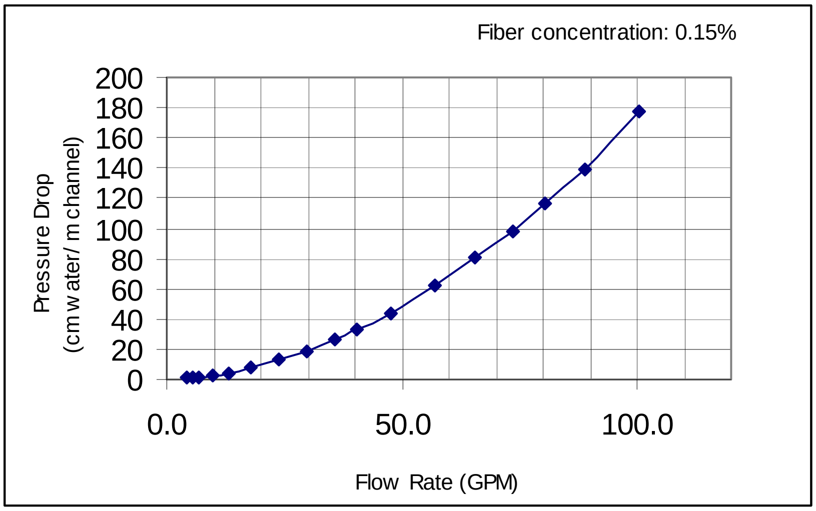

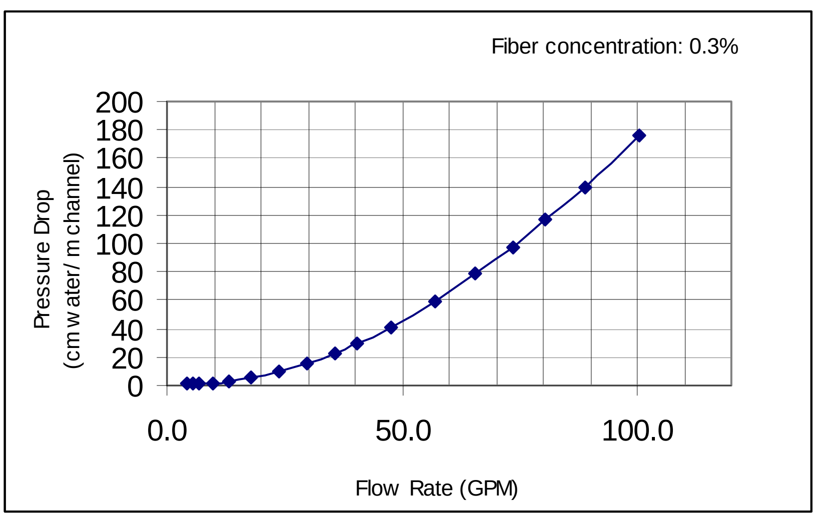

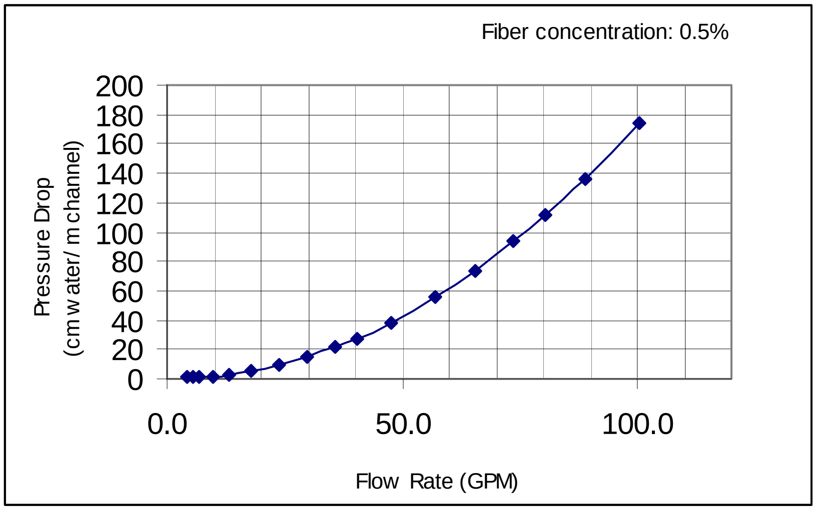
Fiber concentration: 0.5%
200
180
160
140
120
100
80
60
40
20
0
Pressure Drop
(cm water/ m channel)
0.0
50.0
100.0
Flow Rate (GPM)

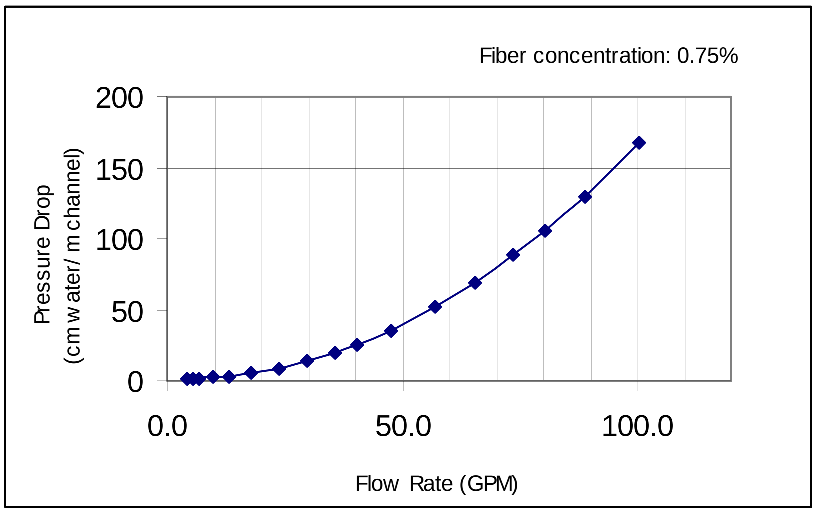
Fiber concentration: 0.75%
200
150
100
50
0
Pressure Drop
(cm water/ m channel)
0.0
50.0
100.0
Flow Rate (GPM)

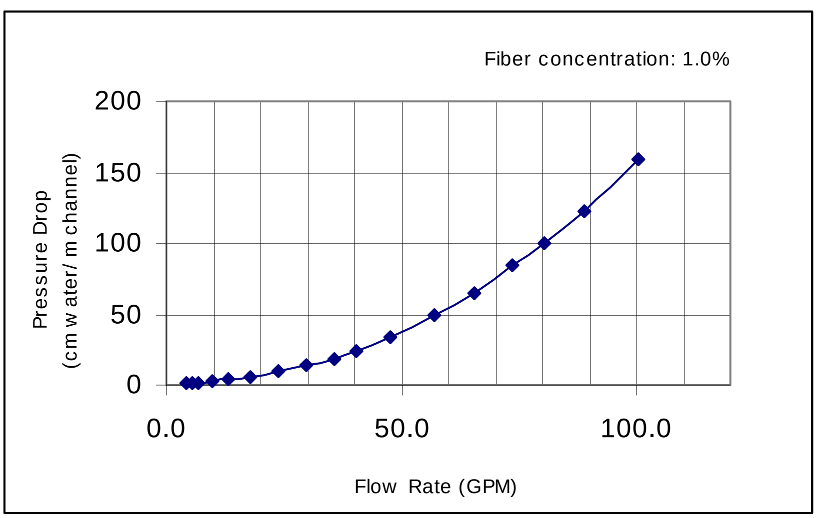
Fiber concentration: 1.0%
200
150
100
50
0
Pressure Drop
(cm water/ m channel)
0.0
50.0
100.0
Flow Rate (GPM)